ITY OF THE PELOPONNESE
NT OF HISTORY, ARCHAEOLOGY
RAL RESOURCES MANAGEMENT

NATIONAL CENTER
FOR SCIENTIFIC RESEARCH
"DEMOKRITOS"

NATIONAL
OBSERVATORY
OF ATHENS

Master of Science in
«Cultural Heritage Materials and Technologies»

STELIOS - KESIDIS
(R.N. 1012201802002)

DIPLOMA THESIS:

Multi-Analytical Study of Two Western European Canvas Paintings from The Series Stations of The Cross

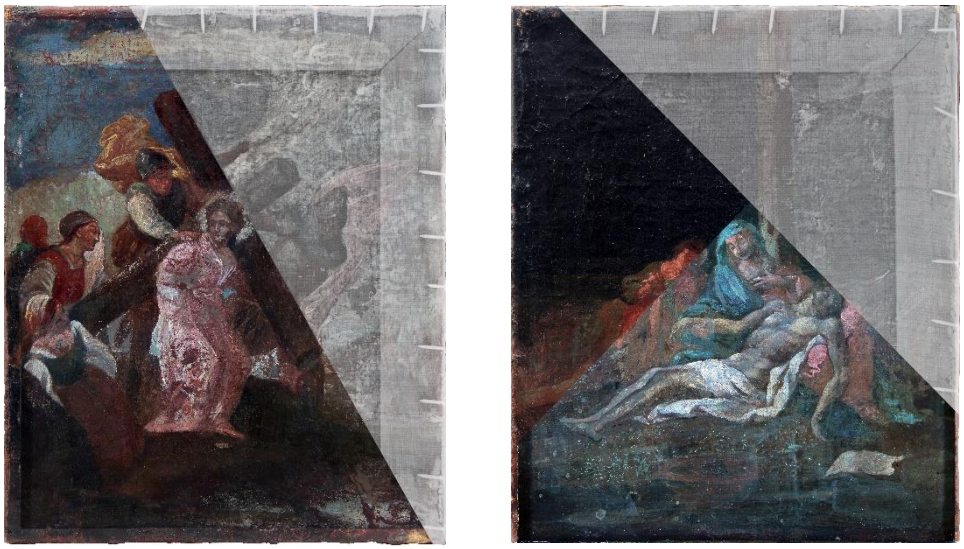

SUPERVISING COMMITTEE:
- **Dr. Eleni Kouloumpi**
- **Dr. Andreas-Germanos Karydas**
- **Prof. Dr. Nikolaos Zacharias**

EXAMINATION COMMITTEE:
- **Dr. Eleni Kouloumpi**
- **Dr. Andreas-Germanos Karydas**
- **Prof. Dr. Nikolaos Zacharias**

ΚΑΛΑΜΑΤΑ, OCTOBER, 2020

Acknowledgements

During this "journey" there were many people, without their valuable help this dissertation would not have been possible. I would like to thank the following people for their substantial help.

Dr. Eleni Kouloumpi, Conservation Scientist at the Laboratory of Physicochemical Research of the National Gallery – Alexandros Soutzos Museum and Chief Supervisor of my dissertation. Her help in choosing the topic of the dissertation, her guidance, patience and support throughout this project, but also the final editing of the dissertation text, make her a cornerstone of the course of this dissertation.

Dr. Andreas-Germanos Karydas, Research Director of the XRF Laboratory of the Institute of Nuclear and Particle Physics of the National Center of Scientific Research “Demokritos” and second supervisor of my dissertation, for carrying out the μ-XRF analyses and his valuable help and guidance in interpreting the results.

Professor Dr. Nikolaos Zacharias, Director of the MSc CultTech Program and third supervisor of my dissertation for the permission to use the SEM/EDS of the Archaeometry Laboratory of the Department of History, Archaeology and Cultural Resources Management of the University of Peloponnese, and his guidance and trust throughout this dissertation.

Professor Dr. Demetrios Anglos, Professor of the Department of Chemistry, University of Crete and Associate Researcher and Head of the Laboratory of Applied Spectroscopy at IESL-FORTH, for his assistance in determining the research protocol and for the permission to use the required equipment for performing μ-Raman, Diffuse reflectance and LIF analyses.

Dr. Sophia Sotiropoulou, research associate at IESL-FORTH and Ms. Marilena Konstantinou, chemistry student at the University of Crete for conducting the diffuse reflectance spectroscopy analyses on both paintings, for the

interpretation of the data and for their overall help during my visit to IESL-FORTH.

Dr. Olga kokkinaki, Post-Doctoral Fellow at IESL-FORTH and Ms. Vasiliki Straganioti and Ms. Evaggelia Kapourani, chemistry students at the University of Crete for the conduction of the laser-induced fluorescence spectroscopy analysis on both paintings, for the interpretation of the data and for their overall help during my visit to IESL-FORTH.

Dr. Anna P. Moutsatsou, Conservation Scientist at the National Gallery - Alexandros Soutzos Museum for the conduction of the multispectral imaging technique on both paintings, her valuable help on the interpretation of the data, and for patiently answering all my questions related to the technique.

Dr. Eleni Palamara, Post-Doctoral fellow at the University of Peloponnese for conducting the SEM/EDS analysis on all four samples, for the elaboration of the data acquired, her help on their interpretation, and most importantly her continuous support and trust.

Dr. Aggelos Fillipidis, Post-Doctoral Fellow at IESL-FORTH and Maria Spanoudaki, chemistry student at the University of Crete for conducting the Raman analyses on both paintings, the interpretation of the data received and for their overall help during my visit to IESL-FORTH.

MSc Agni-Vasileia Terlixi, Conservation Scientist of the National Gallery - Alexandros Soutzos Museum, for the conduction of the sampling procedure, for the preparation of the samples, for the conduction of the Optical Microscopy and her essential help on the interpretation of the microscopy observations.

Ms Melesanaki Kristalia, Art Conservator and Staff Member of IESL-FORTH for her help on the interpretation of the multispectral imaging data, her help on the conduction of all the spectroscopic techniques held on the IESL-FORTH and for her overall help during my visit to IESL-FORTH.

Mr. Panagiotis Rompakis, Conservator at the National Gallery - Alexandros Soutzos Museum for the conduction of digital photography on both paintings, for the editing of the photos and his valuable help on their interpretation.

Mr. Theodoros Panou, Special Technical and Laboratory Personnel of the Sector of Radiology and Radiotherapy of the Department of Biomedical Sciences of the University of West Attica for the conduction of the X-Ray Radiography analysis on both paintings.

Dr. Georgios Mastrotheodoros, Post-Doctoral researcher at Nanoscience and Nanotechnology Institute of NCSR "Democritos" for his help on the interpretation of the XRF data and for the valuable discussion on historic pigments and artistic practices.

Ms. Michelle Hicks, co-student at the MSc CultTech Program and a great friend, for her immense help on the language-editing of this Dissertation, while writing her own Dissertation. Without her help, the completion of this Dissertation wouldn't have been possible.

Ms. Aggeliki-Christina Vedinoglou, Art Conservator, currently a post-graduate student on the MSc "Protection, Maintenance and Restoration of Cultural Monuments" Program and a wonderful friend for her help on editing all the imaging data of this Dissertation, for her continuous support and trust throughout the duration of this project.

MSc Kalliopi Tsampa, Staff Member of the XRF Laboratory of the Institute of Nuclear and Particle Physics of the National Center of Scientific Research “Demokritos” for her great help on elucidating the Artax, Origin and PyMca programs and her immediate response on any problem occurred during the interpretation of the XRF data.

Ms. Celia Valadu, Staff Member of the University of Peloponnese, co-student at the MSc CultTech Program and a great friend, for her help and support throughout the duration of my studies on the MSc Program.

Mr. Patrick Layton, Paper Conservator, co-student at the MSc CultTech Program and a great friend, for his help on editing parts of my Dissertation, his support and encouragement throughout the duration of this project and his help on deciding the topic of this Dissertation.

Finally, to my family and friends for their continuous support, patience and encouragement throughout the duration of this project. Without their substantial help, this Dissertation wouldn’t have been possible.

ABSTRACT

Two Western canvas paintings from the series “Stations of the cross”, which is part of a private collection in Athens, Greece, is going to be studied. Despite their importance as cult objects of Catholic Church and their long history, they have not received due attention, as there are no published studies of archaeometric interest on canvas paintings from the Stations of the Cross. This study aims to investigate the manufacturing technology of the two paintings, their preservation state and the later interventions and finally to determine, if possible, the relative date of production.

The research protocol emphasized on the use of mainly non-invasive and non-destructive, state-of-the-art analysis methods, such as digital photography, multispectral imaging, X-ray radiography, OM, SEM/EDS, μ-XRF, μ-Raman, LIF and Diffuse reflectance spectroscopy. The application of imaging techniques revealed, inter alia, extensive overpaintings, and hidden features of the underlying painting layers. The stratigraphic techniques recorded that the paintings have a thick, complex and multi-layered stratification. The original preparation layer, based on gesso and red bole, is typical of the 16th to 18th c., while the detected overpainting layers seem to have been applied after the second half of the 19th c. since the preparation layer of the overpainting was based on a mixture of lithopone, red or yellow ochre and silicon typical of the period. And finally, through the application of spectroscopic techniques, a great variety of pigments was identified. Of high interest was the results obtained from the identification of selected pigments, which leads to conflicting conclusions, as the presence of some pigments is not chronologically consistent with the presence of others. Thus, combining data from microscopy techniques and spectroscopic techniques, it appears that the initial phase of the painting can be dated to the end of the 18th century (red preparation + presence of azurite), with the overpainting being carried out after the second half of the 19th century (zinc white + lithopone) and possibly early 20th century interventions (manganese blue + titanium white).

Regarding the preservation state of the painting, the physicochemical analysis confirmed its poor condition, which is due to the lining, patching interventions and the extensive overpaintings. Subsequent restoration interventions, such as grouting and filling, were also detected.

The physicochemical study of the two works brought to light a wealth of information about the techniques and materials used to manufacture them. Giving the impetus for the more intense study of this type of paintings. Also, by clarifying the preservation state of the two objects, the questions about their history were answered and their importance was demonstrated.

TABLE OF TABLES & FIGURES

INTRODUCTION

The present dissertation will deal with the analysis of two canvas paintings from the series "Stations of the Cross" from an archaeometric perspective. The two works, which come from a private collection based in Athens, Greece, were bought in the second half of the 20th century in Germany, while it is rumored that they originate from France. Specifically, the objects to be analyzed are the painting "Statio VIII Jesus and the Women of Jerusalem" and the painting "Statio XIII Lamentation".

The motivation for choosing this theme was the realization that despite their importance as cult objects, but also their long history, there are no published studies on canvas paintings from the series "Stations of the Cross". This study aims to expand the technical details of this category of objects, but also to examine, for the first time, the changes that have taken place over time. In order to fulfill the above objectives, the manufacturing technology of the objects, their preservation state will be examined and finally an attempt will be made to indirectly date them, through a series of innovative, state-of-the-art analytical techniques.

In the first chapter of the dissertation, there will be an extensive report on the historical development of the series "Stations of the Cross", as well as the iconographic description of the paintings to be analyzed. It contains very important information about the evolution of the series "Stations of the Cross", the reasons that led to its creation, but also the path that followed until it reached its current form.

The next chapter provides a bibliographic overview of the materials and methods used in canvas paintings between the 18th and 20th centuries, with references to each layer of a painting. This information will help in order to better evaluate the manufacturing technology of the two paintings and to draw conclusions about their relative date of production.

The third chapter contains an extensive report on the physicochemical methods used for the study. In more detail, the principles of operation of each method and their applications in the study of canvas paintings are mentioned, along with their advantages and disadvantages. In addition to the reference to the methods of analysis used in the study, mention was also made to new, innovative technologies used in the science of cultural heritage.

The fourth chapter presents the research objectives set by this dissertation. Specifically, the study of the techniques and materials used in the production of the two paintings, the evaluation of their state of preservation and finally, the drawing of indirect conclusions regarding the date of their production. The chapter also contains the research protocol followed, which was created based on the use of new, innovative and mainly non-destructive methods of analysis.

The next chapter presents the results from the application of the research protocol on the two paintings. Where, through the citation of the information obtained from each method separately, it is possible to better interpret them, but also to draw rich conclusions. This is followed by a discussion about the paintings, where information is compiled from different methods to answer research questions. Finally, there is a comparison of the two objects in terms of their similarities and differences and an attempt to clarify the possibility that the two works belong to the same artistic ensemble.

Finally, the sixth chapter presents the conclusions that emerge after the completion of the analysis techniques and the combination of information obtained from the literature reviews, as well as targeted proposals for future research, concerning either answering questions that were not part of the present study, or questions that arose during the study.

1. THE TWO PAINTINGS

1.1. Stations of the Cross and their Historical Evolution

Stations of the Cross, also called Way of the Cross or Via Crucis, are a group of fourteen scenes from the life of Jesus Christ, depicting his way from the hall of Pilate to his entombment. Traditionally they take the form of reliefs or sculptures made of stone, wood or metal, or the form of paintings. (Jutras, 2017) Their devotional character constitutes the way with which religious people understand the sufferings and the death of their Savior and follow him to his entombment.

The Stations as they have evolved up to present day (Gillman, 2011) are: (1) Jesus is condemned to death, (2) Jesus receives the cross, (3) Jesus falls the first time, (4) Jesus is met by his Mother, (5) The Cross is laid on Simon of Cyrene, (6) Veronica wipes Jesus' face with her veil, (7) Jesus falls the second time, (8) Jesus speaks to the women of Jerusalem, (9) Jesus falls the third time, (10) Jesus is stripped of his garments and receives gall to drink, (11) Jesus is nailed to the Cross, (12) Jesus dies on the Cross, (13) Jesus' body is taken down from the cross, and (14) Jesus is laid in the Sepulchre.

The devotions of the Stations of the Cross were initiated by the effort of the church and clerics to make this part of the life of Jesus Christ understandable by the faithful. The number of people that actually had the opportunity to visit the sacred lands of Palestine was very small. The pilgrimage of the Stations of the Cross made the faithful feel more connected with the passions of their Lord and made this devotion easier for everyone to attend without the need for a dangerous expensive overseas journey. (Thurston, 1914, p. 2) The first references about the stations came only after the middle ages, although there are many examples of pious people that had visited the holy places some years after the death of Christ, aiming at recreating His last journey. The earliest narrative from the holy places belongs to Lady Egeria c. 380 AD, in which, she does not refer to the Stations of the Cross. Through the centuries people continued to visit the Holy Land, documenting their visits, in a similar way as

that of Lady Egeria, trying to share their experiences with those that did not have the opportunity to visit these places. (Thurston, 1914, pp. 4-7) For the next centuries, visitors, after their return, were creating replicas of the Holy Places, by constructing oratories devoted to stops, like Golgotha, the Mount of Olives and the Holy Sepulchre. Although, they do not resemble with today's known Stations of the Cross. (Thurston, 1914, pp. 12-13) The first reference to the "way of the cross" was made by Phillippus Brusserius Savonensis at 1285-1291 AD, in which, he refers to stops devoted to the actual places from where Christ Ascended carrying his cross. However, they belong to a larger group of places that people visit, of which, the actual stations are only a small part. (Thurston, 1914, p. 21) After the occupation of the Holy places by the Turks, and due to strict restrictions, pilgrimages were conducted by Franciscans of Mount Sion during the night. Their visit started from the Holy Sepulchre and then, "before dawn", was continued to the streets of Jerusalem. Considering the fact that the pilgrimage started from Calvary down and not the reverse, gives information that by the end of the 14th century there was no adequately established idea of the route of Jesus on his last journey. (Thurston, 1914, p. 22) Both narratives and pilgrims' journeys were conducted in a way that could explain the reversed way that Franciscans showed the Holy places. One such example is the narrative of Felix Fabri at the end of the 15th century (Thurston, 1914, p. 23, 26). Over time, the path, from which Jesus was thought to have ascended, carrying his cross towards his crucifixion, changed many times, with "Stations" or "Statio", as William Wey first describes the stops of the devotions, to be added and subtracted (Brown, 2003, p. 500).

The arrangement of the Stations of the Cross had been reversed from the way they are conducted today, towards Calvary, for the first time in the pilgrimage of Torkington (1517 AD). Thurston notices that "there are no mentions of the way of the cross to be conducted from Calvary eastwards". (1914, p. 55) The faithful in their efforts to describe and reenact as accurately as possible the events concerning Christ's journey to Calvary employed the practice of measuring the steps from the Praetorium to the place of the crucifixion. Although during the passing of time the roads and building of Jerusalem had been changing, having as a consequence, the faithful could only guess the

exact steps in various points of the journey, a detail that leads to references with very big deviations. (Thurston, 1914, pp. 57-58) One of the first and most known sets of Stations of the Cross was made by Adam Krafft in Nuremberg in 1507-1508 AD. They were seven in number and made out of stone. Underneath each depiction there is an inscription that states the title of the Station and the steps from Pilate's house. This set of stations, with some differences between them, due to their focus on Christ during his journey to Calvary, have been named "The Seven Falls". (Thurston, 1914, pp. 63-34) Another important early set of the Seven Falls is that made by Peter Sterckx (Peter Potens) at Louvain (1505 AD.). The importance of this set is due to its influence in the arranging of Stations of the Cross as they are today. (Thurston, 1914, pp. 65-66) The pilgrimage of John Pascha with the title "*Gheestelyck Strass*", edited by Peter Calentyn, at Louvain, in 1563, due to the volume of information and detailed references to places as well as detailed measurements of distances between stations, was considered as an almost scientific work. Excluding the facts that Pascha's stations are greater in number and have different starting point, they have the exact order of today's stations. (Thurston, 1914, pp. 82-86) Many later writers, having as template the Gheestelyck Strass, wrote their own pilgrimages. One such example is the pilgrimage of Adrichomius, published in 1584. In this pilgrimage, the first twelve stations are the same as today's conducted stations. Adrichomius who, although he never visited Holy Lands himself, borrowed preexisting information from Pascha's Pilgrimage, in which in some cases extra information was arbitrarily added, with the last two stations not mentioned. (Thurston, 1914, p. 87) Adrichomius' pilgrimage "*Jerusalem sicut Christi tempore floruit*" prevailed globally over the other versions of the Stations of the Cross due to the circulation of his book. (Thurston, 1914, p. 93)

All the above lead to the conclusion that Stations of the Cross as they are conducted today have their roots in Louvain and not Jerusalem. As a consequence, and after the aforementioned analysis, the authenticity of the stations is considered uncertain as it relies on erroneous data. (Thurston, 1914, p. 127)

Until the fifteenth century, it was believed that only those who visit the actual Stations of the Cross could gain the indulgences of this devotion (Thurston, 1914, p. 162). However, this was changed by Pope Innocent XI, on September 5, 1686, when he declared, by an apostolic decree, that those who make the devotion of the Stations of the Cross in a church, gain the same indulgences with those actually visiting the real Stations. (Bouvier, 1848, p. 101) The final form of the Stations of the Cross was established by Pope Clement XII, by apostolic decree, in 1731. (Gillman, 2011)

The devotional aspect of the Stations of the Cross has changed many times through the years of its existence. As it was mentioned, the original effort of the faithful to convey every detail of Christ's journey carrying the Cross resulted in the adoption of a dedication that would be more appealing to the world, turning it from an attempt to clarify the truth to a fully symbolic devotion (Thurston, 1914, p. 136)

Pope Benedict XIV, by apostolic decree, in January 16, 1741, gave to every priest of the General order of the Friars of Minor the permission to erect Stations of the Cross, under the condition that there had to be a request, by the priest of the church, who has written consent granted by the Bishop. (Bouvier, 1848, p. 143) The priest, who erects the Stations has to bless the crosses that are fastened on the top of each Station, because, they are the part of the station to which, the blessing attaches. The crosses must be wooden. It is emphasized that the sculpture figures or paintings can be replaced as long as the crosses are intact. (Thurston, 1914, p. 175) After successive changes by earliest Popes, Pope Pius VI decided to allow the Stations erected to be not only in churches but even in houses. (Bouvier, 1848, p. 144) Those decisions made the devotion of the Stations of the Cross very easily accessible to the faithful, making them gain more popularity.

Today, the reenactment of the Stations of the Cross takes place on a smaller scale every Friday afternoon throughout the year (Thurston, 1914, p. 127) and every Good Friday. (The Editors of Encyclopaedia Britannica, 2018)

1.2. Statio VIII "Jesus and the Women of Jerusalem"

1.2.1. Historical Evolution

During his journey to Calvary, carrying the cross, Jesus met with the women, or, as they also were called, the daughters of Jerusalem. According to the set of Stations, established by Pope Clement XII, this scene is the eighth and happened between the second and third fall of Jesus. Luke in his gospel, 23:27-31, writes *"A large number of people followed him, including women who mourned and wailed for him. Jesus turned and said to them, "Daughters of Jerusalem, do not weep for me; weep for yourselves and for your children. For the time will come when you say, 'Blessed are the childless women, the women that never bore and the breasts that never nursed!' Then "'they will say to the mountains, "Fall on us!" and to the hills, "Cover us!"' For if the people do these things when the tree is green, what will happen when it is dry?"* (Anon., 1993) This Station is referred, by almost all the pilgrims, since the thirteenth century (Thurston, 1914, p. 183). However, up until today, its order between the Stations of the Cross, and also, the exact site in which it is believed this incident occurred, has changed many times. As mentioned before, the incident with the women of Jerusalem, as it is honored today, occurred between the second and third fall of Jesus. However, the faithful of earlier ages had associated the incident with the meeting of Jesus and Simon of Cyrene (Thurston, 1914, p. 183). Both Fabri and Wey place the meeting with the Women before that with Simon, while Sir Richard Guylforde and Surius Bernardine place it after Simon. Those references from pilgrims, whose writings came from different epochs, show the differentiations between them but also with todays established system of stations (Thurston, 1914, pp. 60-61). The first set of stations in which the incident with the women is referred between the second and third fall of Jesus is in the set of Peter Sterckx. (Thurston, 1914, p. 65)

As regards the order of the incident between the other Stations, Wey refers to it as the Fifth Station, *"Locus ubi mulieres flebant propter Christum"* (Thurston, 1914, p. 51), Sir Richard Guylforde places it fourth, while, in his set of Stations, Adam krafft, places it third (**Figure 1.1**) (O'Neill, 1986, p. 72). John Pascha

mentions it as the Ninth Station in order, which is “872 feet” from the previous Station, in this case, the meeting with Veronica. (Thurston, 1914, p. 84) Finally, Adrichomius, whose contribution has been mentioned before, mentions it as eighth (Thurston, 1914, p. 118). Also important is the exact site in which it is believed this incident occurred. Many writers through the ages placed the meeting in different spots in Jerusalem. (Thurston, 1914, pp. 105-107) In contrast, Adrichomius mentions that the incident occurred outside of Jerusalem (Thurston, 1914, p. 117).

Figure 1.1 3rd Station, Jesus meets the women of Jerusalem, carving made by Adam Krafft in 1508 at Nuremberg. The original artifact is kept in the National Museum of Germany. Derived from: link

1.2.2. Pictorial Description

The work to be analyzed is a painting on canvas depicting Jesus' meeting with the women in Jerusalem (**Figure 1.2**).

Figure 1.2 VIII STATIO Jesus meets the women of Jerusalem (Photo Credits: Panagiotis Rompakis, National Gallery-Greece)

Starting from the frame, it consists of six separate sections. The four are the main frame. They are dark brown and have three equal decreasing gradients towards the inside of the frame, with the last to be gold. The next section is located on the top of the main frame. Its dominant feature is the inscription, "VIII. Statio.” painted in black on a white background. The right and left sides of the section end up in, two gold acanthus-shaped leaves, s-scroll type. The last section of the frame

is a gold cross, on the top of the frame. The particular cross is a variant of Cross pattée (Koch, 1955, p. 15) a Teutonic cross, used by the Teutonic order until 13th c. The Teutonic order was a group of German Knights, which was militarized by the German Princes and Bishops along with King Amalric II of Jerusalem, in 1197. The order was reestablished in 1834, as an ecclesiastical institution, by the Austrian Emperor. (Lepage, 2005, pp. 193-201)

Figure 1.3 VIII STATIO, unframed, depicting a multifaceted representation (Photo Credits: Panagiotis Rompakis, National Gallery-Greece)

The painting's dimensions are 29.2 cm long, 24.1 cm wide and 1.8 cm high. Starting with the background, it consists of a cloudy, blue sky (**Figure 1.3**). The color of the sky varies from point to point but generally is vibrant blue. Its extent is small, as the rest of the background is covered by thick grey clouds. Clouds start from the ground level and end in the upper left corner of the canvas. The ground on which all the figures of the scene are found is brown with some points of it in either green or light red color. On its left side, it has a big dark brown rock. The ground is tilted to the right, which is also the way the scene moves. The dominant figure of the multifaceted scene is the barefooted Jesus, carrying the cross with his left hand. Jesus is located in the center of the painting, wearing a crimson-colored garment. He has a halo on his head, while, he is also wearing a thorny wreath. The cross which he is carrying is brown with some points of it having different shading than others. His head is turned to the right, looking at the woman who is kneeling. The kneeling woman has her body tilted in an expression of sadness. She wears a red skirt, a white blouse, and over it a sleeveless dark blue vest. On her head, she wears a white semi-transparent hair scarf. Although her body shows strong emotions, there are very few details of her face, with only the basic characteristics shown. Right behind the woman stands another figure, who is also looking towards Jesus.

She wears a white blouse and over it a red sleeveless shirt. On her head, she wears a grey-blue colored hair scarf. The face of the woman is very expressive, with many details. On her right, exists a white area, while on the left, a black area with no clear purpose. Behind the woman is located a figure of a man who is wearing a vibrant green garment. His head is red colored and has no details drawn. On the left side of Jesus stands one of the two soldiers that led him towards Calvary. His movements are intense, as the gestures of his hands show. With his right-hand, he holds the right shoulder of Jesus, while with the left, he is holding a sword and shows the way towards Calvary. He is clothed in soldier's armor which includes a metallic helmet, breastplate, and a yellow cape. The second soldier standing on the left side of Jesus has his body tilted to the right. With his right hand, he seems to drag Jesus, while in his left-hand, he holds a big light-red flag. The soldier's armor includes a metallic helmet, breastplate and blue scarf. The scene is completed by three figures on the right. Those figures seem to have a secondary role to the scene since they are drawn in a smaller scale and with very few details.

As can be concluded from the above, the painter uses clothing that is not time-consistent with those of the time of Jesus. Jesus is the only figure wearing clothes from his contemporary epoch, all the other figures wear clothes referring to working classes of the 17th century (Laver, 1969, p. 120). This information could indicate details about the dating in which the painting was made.

1.3. Statio XIII "Lamentation"

1.3.1. Historical Evolution

Lamentation is one of the most important scenes of Christianity. According to the set of Stations, established by Pope Clement XII, this scene is the thirteenth. John in his gospel, 19:32-35, 38, writes, *"The soldiers therefore came and broke the legs of the first man who had been crucified with Jesus, and then those of the other. But when they came to Jesus and found that he was already dead, they did not break his legs. Instead, one of the soldiers*

pierced Jesus' side with a spear bringing a sudden flow of blood and water. The man who saw it has given testimony, and his testimony is true. He knows that he tells the truth, and he testifies so that you also may believe. Later, Joseph of Arimathea asked Pilate for the body of Jesus. Now Joseph was a disciple of Jesus, but secretly because he feared the Jewish leaders. With Pilate's permission, he came and took the body away." (Anon., 1993, pp. 160-161) The earliest references of the lamentation of Christ as a Station of the Cross come from Adam Krafft's carvings in 1508, where he includes a carving with the title "Jesus laid in the arms of his Blessed Mother" (**Figure 1.4**)

Figure 1.4 7th Station, Jesus laid in the arms of his Blessed Mother, carving made by Adam Krafft in 1508 at Nuremberg. The original artifact is kept in the National Museum of Germany. Derived from: link

Thurston, states that the last four Stations, including the descent from the cross, are already established, as part of the Stations of the Cross, by the 16th c. (1914, p. 154) While, John Pascha mentions it as the fourteenth station of the fifteen stations in total. (Thurston, 1914, p. 85)

Although all gospels refer to Joseph of Arimathea and Nicodemus as the two that were present during the deposition of Christ's body from the cross, and the fact that there is no reference to the lamentation after the deposition, the well-established template of lamentation includes the Virgin Mary, which holds the body of Jesus, St. John, the three Marys, Joseph, and Nicodemus. (Hazzikostas, 1998, p. 368) A common feature of the subject is the addition of symbolic objects, such as a ladder, skull, and other. (Shefer, 1998, p. 225)

1.3.2. Pictorial Description

The work to be analyzed is a painting with a painting on canvas depicting the lamentation of Jesus dead body by Mary the Virgin and St. John. (**Figure 1.5**) The frame of the painting consists of five separate sections. Four are the main frame. They are dark brown and have three equal decreasing gradients towards the inside of the frame, with the last to be gold. The next section is located on the top of the main frame. Its dominant feature is the inscription, “XIII Statio”, painted in black on a white background. The right and left sides of the section end up in, two gold acanthus-shaped leaves, s-scroll type. The frame in its initial state was completed by a cross on the top of the frame, which had been detached.

Figure 1.5 XIII STATIO Lamentation of Christ (Photo Credits: Panagiotis Rompakis, National Gallery-Greece)

The painting’s dimensions are 29.2 cm long, 24.1 cm wide and 1.8 cm high. The background consists of mountains at different distances, and a dark black sky (**Figure *1.6***). The ground, where all forms of the scene are found, is brown with some areas having different shades, and some areas that are green or light red. The ground has some elements, such as the plate, with a human skull inside, a thorny wreath, an inscription and some plants. The three figures of the subject, Jesus, Virgin Mary and St. John, stand in the center of the painting. Right behind them stands the cross, which is turned about ¾ to the left. The right arm, as also the upper arm of the cross is not shown in the painting. Jesus is placed on a white linen cloth (Anon., 1993, p. 47), while the upper part of his body rests on the body of the Virgin. Jesus' body, which is positioned in profile, follows the kinesiology of a dead body, with his head positioned backward. His left hand falls down, while the right hand is held by the Virgin. The Virgin stands kneeling next to Jesus' body, looking down, as a sign of sadness. With her right hand, she holds Jesus' hand while the other is on her chest. She wears a blue himation, a red-violet under-tunic, and a yellow shawl. Next to her, St. John is

found, who stands kneeling, having his hands in a prayer position and looking down, as an indication of sadness. He wears a red himation and a green under-tunic.

As can be concluded from the above, the painter uses clothing similar to those which had been worn in biblical times, with no reference to any, contemporary to the painter, subject or item. As mentioned before, the lamentation scene consists of Jesus' dead body, the Virgin Mary, St. John, the three Marys, Joseph, and Nicodemus. However, this scene differs from the iconographic model, as it only presents Jesus, the Virgin and St. John.

Figure 1.6 XIII STATIO, unframed, depicting the three central figures (Photo Credits: Panagiotis Rompakis, National Gallery- Greece)

2. MATERIALS AND METHODS

2.1. Canvas Painting Stratigraphy

The term painting describes a work of art depicting images and symbols through color (Kouloumpi, 2007, p. 22). The basic components of a painting are the substrate, the ground layer, the paint layers, and the layer of varnish (Kouloumpi, et al., 2012, p. 362). In more detail, the substrate used, varies according to the time and era of the production of the painting. The materials used as substrates can be wood, canvas, stone, paper, metal, even glass. This study will focus on canvas painting stratigraphy (**Figure 2.7**).

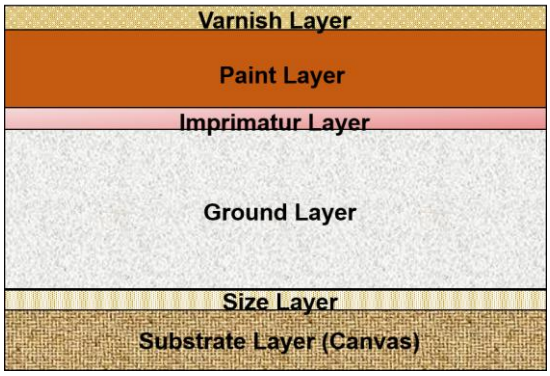

Figure 2.7 Schematic representation of a canvas painting stratigraphy (digital processing by St. Kesidis)

Wood was the most common material used as a substrate until the end of 15th century when canvas paintings prevailed (Alexopoulou - Agoranou & Xrysoulakis, 1993, p. 19). In order to help the substrate accept the subsequent layers, the application of size, a glue of organic origin, was necessary to eliminate absorbance (Taft & Mayer, 2000). Then, several thin layers of ground cover the substrate. The ground layer produces a fine surface with the desirable properties, such as absorbency, hardness, and color, for the paint to be applied. The most common ground layer used is gesso, a mixture of animal glue, calcium carbonate, sometimes including, the addition of a white pigment (Mastrotheodoros, 2016, p. 23). After the application of the ground layer and before the application of the paint layers, a thin layer of color is applied, called imprimatura. Imprimatura reduces the absorbance of the ground layer and acts as a toned ground (Taft & Mayer, 2000, p. 5). The paint layers consist of pigments dispersed in a binder. Pigments are very fine-grained powders, and can be categorized by their origin as: mineral, synthetic/artificial, and natural organic pigments (Mastrotheodoros, 2016, p. 24). Binders are used as a dispersive medium for the pigments,

however, when they get solidified, they act as binding media, holding the pigments in position (Kouloumpi, 2007, p. 26). In Europe, during the middle ages, egg yolk was the prevailing binder, until 15th century when it gradually was replaced by drying oils, which came to be used universally (Mayer, 1970, pp. 23-24). Another component, which is not always present in the paint layer, is the vehicle or diluent. Its presence leads to paint with a lower viscosity during its application, and also to faster drying of the paint layer, due to the evaporation of the diluents (Taft & Mayer, 2000, p. 3). The completion of a painting happens when the varnish layer is applied. Varnishes are transparent liquids of natural or artificial origin, used for the protection of the sensitive paint layers and the vibrancy enhancement they offer to the paint (Mastrotheodoros, 2016, p. 26).

2.2. Materials and Manufacturing Technologies of Western Easel Paintings from the 18th to the 20th Century

2.2.1. Support

Canvas, as mentioned above, prevailed as the most common painting support after the 15th century. Fabrics considered as canvases are coarse, tightly woven fibers (Mayer, 1970, p. 250). The fiber types used as painting support most often between the 18th and the 20th centuries are mainly hemp, linen and cotton (Young, 2012, p. 139). In the 18th century the most common fiber-type used by artists was hemp, with only a few to use linen as painting support. At the end of the 18th and the beginning of the 19th century, the transition from hemp to linen canvases was initiated. Due to the increased industrialization of fabric making, the majority of the 19th century artists were using machine woven linen, which, in many occasions, the first size layer had already been applied. Linen was considered by the artists of the time to represent the most suitable material for canvas making, but its high price made it eligible only for very significant works (Laurie, 1926, pp. 65-66). In the late 19th century the gradual use of cotton fiber was introduced, as a substrate material. Initially, cotton was combined with linen, but in the beginning of the 20th century the price of linen

was considerably higher than that of cotton, so canvases made of pure cotton began to be preferred (Vanderlip de Carbonnel, 1981, pp. 16-19).

2.2.2. Ground

The ground layer consists of an inert material, such as chalk, gypsum or others, and an organic binder, such as animal glue or drying oil (Kouloumpi, et al., 2012, p. 364). The most traditional ground historically used as preparation for paintings (panel & canvas) was gesso, as it was described by Cennino Cennini in his treatise “Il Libro dell’ Arte”, where he also mentions the procedure of sizing (Tambroni, 1821, pp. 67-69). Gesso is comprised of calcium sulfate or calcium carbonate and an organic binder (glue), such as rabbit skin glue or casein (Mastrotheodoros, 2016, p. 37).

Depending on the technological developments, the aesthetical preferences of each period, and even the subject of the painting, the characteristics of the ground layer would change (Stols-Witlox, 2012, p. 169).

Although white grounds, like gesso, were the most popular during the Middle Ages, this changed in the 16th century when colored ground layers began to be used more often. In the 17th century the use of darker preparation layers prevailed. With the examination of paintings from this period, grounds of grey, reddish, and brown hues have been observed (Stols-Witlox, 2012, p. 172). According to Groen (2011, p. 82), one of the prime reasons for the widespread use of colored grounds was the ease they offer in achieving the effect of chiaroscuro, as it functioned as the middle tone. Especially as concerned the reddish or brown grounds, there was one more reason of a financial nature. The pigments used for achieving the desired hues had large economic differences. The main pigment used for grey grounds was the expensive lead white, while for reddish or brown grounds red earth was used which is abundant in nature (Groen, 2011, p. 87). Additionally, dark-colored grounds were employed for their effect in the final color of the painting, giving a warmer look (Grygar, et al., 2003, p. 1155).

During the first half of the 18th century, some painters began to use lighter tonalities for their grounds. Hence in Dutch paintings of this period, white or light grey grounds are observed. In the second half of the 18th century painters started to express concerns regarding colored grounds (Stols-Witlox, 2012, p. 176).The frequency of greyish and brownish grounds decreased in order to be replaced by light hues, such as cream, light yellow, light pink or white (Stols-Witlox, 2015, pp. 174-175). It had already been observed that paintings with colored grounds in the passage of time get darker and transparent, for this reason the use of pure white grounds was recommended (Hiller, 1945, p. 104).

During the 19th century, even though painting treatises describe the procedure for the stretching and “priming” of canvases, the majority of painters were buying ready-made and pre-primed canvases (Stols-Witlox, 2012, p. 178). Most commercial primings had a composition of lead white and chalk in linseed oil, with the addition of silicates (Townsend, 1994, p. 149). However, complaints had been expressed due to the inclusion of plasticizers, additives and siccatives, which resulted in canvases of low quality (Stols-Witlox, 2012, p. 178). For the aforementioned reasons but as well as financial ones, non-commercial primings were also produced (Townsend, 1994, p. 149). To counter the effect of excess oil on their works, painters by the end of the 18th and the beginning of the 19th century began to use grounds of higher absorbency. Reviewing works of earlier great masters, like Rubens, the view was adopted that the reason for their greatness and resilience was the high absorbent white grounds employed (Abendschein, 1906, p. 64). By the end of the 19th century Impressionists experimented with new materials and recipes for their grounds, introducing the categories of absorbent and semi-absorbent grounds. The experimentation went beyond inert materials, as different binding media, like casein, starch, even egg (Stols-Witlox, 2012, pp. 179-181; Townsend, 1994, p. 150).

In the 20th century the recipes from the previous century continued to be used. However, the two most important developments that occurred in this century were the introduction of acrylic dispersion grounds and alkyd grounds (Ormsby & Gottsegen, 2012, p. 185).

Acrylic grounds, which were introduced in the mid-1950s, are composed by an acrylic dispersion resin binder, such as ethyl acrylate/methyl methacrylate (EA/MMA) or butyl acrylate/methyl methacrylate (BA/MMA) copolymer resin, while the pigment used is titanium white. During the manufacturing procedure many stages must be followed for the completion of the ground. The three most significant advantages of acrylic dispersion grounds are their flexibility, the fact that they dry fast, and that they get discolored (yellowing) less than their competitors (Ormsby & Gottsegen, 2012, pp. 185-186).

Alkyd grounds, which were introduced in 1960, are composed of a polybasic acid and a polyhydric alcohol. The oils used as modifiers were drying or semi-drying oils, such as sunflower, castor, linseed, and others, while the pigment used is titanium white. Alkyd grounds replaced oil grounds, as they offer similar working properties and have less disadvantages (Ormsby & Gottsegen, 2012, pp. 186-188).

2.2.3. Paint Layer

The paint layers, as mentioned in §2.1, consisted of pigments dispersed in a binder, and after a certain period, the addition of a new vehicle was observed. The following are brief definitions of the above elements and their evolution over the centuries.

Pigment is a very fine colored substance which gives its color effect to another material (Mayer, 1970, p. 32). They can be classified according to their color, composition, origin, and other characteristics (Goffer, 2007, p. 67).

Binder is the liquid responsible for the dispersal of the pigment powder for the formation of a homogeneous mass. However, when it solidifies, it acts as binding medium, holding the pigments in position (Kouloumpi, et al., 2012, p. 365).

Vehicles were materials used as binder modifiers by the painters in an effort to achieve optical characteristics from the Old Masters' paintings and to remove any undesirable effects (Carlyle, 1990, p. 76).

These paragraphs will deal with pigments used from the 18th to the 20th century, however, it should be noted, that the majority of the most common pigments are used since antiquity (Eastaugh, et al., 2012, p. 203).The industrial revolution of the 18th century (1760-1840) caused many upheavals and changes (Britannica, 2019). These changes have led to the rapid growth of new materials. One of the areas that benefited from this development was the area of pigments used by artists. Consequently, as the pigments were produced industrially with controlled quality characteristics, artists gradually stopped producing their colors and started buying commercially-made paints. Some of the most important pigments discovered in 18th century were Prussian blue (1706), cobalt (1735), and chromium (1791) (Eastaugh, et al., 2012, pp. 205-206). However, the industrialization of pigment production also had disadvantages. Pigment producers, in search of higher profits, began to adulterate their products; this practice was observed in both the 18th and the 19th century (Carlyle, 1993, p. 56).

In the 19th century, artists started to be concerned about more things, like the stability of pigments, the harmful substances that some pigments include and the substitution of toxic materials with other non-toxic ones (Eastaugh, et al., 2012, p. 205). One such example was the gradual substitution of the toxic lead white with the newly investigated white pigments, barium sulfate (1830) and zinc white (early use at the end of the 18th century; more frequently encountered in the early 19th century) (Eastaugh, et al., 2004, pp. 39, 406). Other important pigments introduced in the 19th century were cadmium sulfate pigments (1817), magenta, synthetic alizarin and Perkin's Mauve (middle 19th century) (Eastaugh, et al., 2012, p. 206).

The key changes that occurred in the 20th century were the introduction of titanium dioxide white (1930s) and the phthalocyanine blues and greens (1935) (Eastaugh, et al., 2012, p. 206; Eastaugh, et al., 2004, p. 364. 312).

Concerning medium binders, the most commonly used drying oil was linseed oil, with walnut and poppy oil also being used, but not as frequently. Additionally, during this period, artists used different drying oils for different pigments (Hermens & Townsend, 2012, p. 210). Carlyle mentions that drying oils were treated with driers in order to speed the drying time (1999, p. 71). Drier or siccative is a material used to enhance the drying properties of oil; the most commonly used were metallic compounds, pigments with metallic compounds or varnishes which were included in the commercial-made painting oils. Some driers used in the 18th and early 19th century were leaded-glass, lead acetate, and smalt, while later litharge, zinc, verdigris, manganese compounds, cobalt-based driers were also employed (Carlyle, 1999, pp. 70-71).

Painting manuals of the 18th and 19th century instruct painters to use resinous and waxy vehicles as a mixture with their oil pigments for three main reasons; (1) for the dilution of stiffly-ground colors to make them suitable for brushing, (2) for better manipulation, and (3) for transparency in shadows and color enrichment (Carlyle, 1990, p. 77).There were three main types of vehicles, the gelled mediums, the waxy mediums and the emulsion mediums.

The most common vehicles were the gelled mediums, which were thixotropic gels formed of drying oil and varnish known as *megilp*. The most common recipe for megilp was the mix of a drying oil and mastic varnish, although other varnishes, such as copal, were also used. Other forms of gelled mediums have been found to contain albumen, and animal glues.

Mediums containing wax was another popular vehicle type during the 19th century. The most common wax used was beeswax and its most important feature was the reduction of the viscosity of the paints.

Finally, emulsion mediums were a mix between gelled and wax mediums, and they were popular in the first half of the 19th century. One such medium is the

‘Grecian’ encaustic medium which consisted of gum Arabic, water, mastic resin, and wax, mixed with pigment (Carlyle, 1990, p. 77).

2.2.4. Varnish

According to their diluents, varnishes can be divided in three main categories; oil/resin, solvent based and water-based varnishes.

The oil/resin varnishes are mixtures of a resin with a drying oil and they were produced by thermal treatment (Phenix & Townsend, 2012, p. 252). The varnish results from the oxidation and polymerization of oil, which creates a permanent film (Varella, 2013, p. 11). The most common mixtures used were of linseed oil with hard or fossilized resins (sandarac, copal and shellac). Their use started to decline in the early 17th century and they were replaced by solvent-based varnishes (Ioakimoglou, 2004, p. 168).

The solvent-based varnishes (spirit varnishes) are mixtures of tree resins (colophony, sandarac and mastic in a volatile solvent, such as alcohol. They were formed by the evaporation of their solvent (Phenix & Townsend, 2012, p. 253).

The third category of varnishes are water-based varnishes. These types of varnish began to be applied in the 19th century for contemporary applications. Phoenix and Townsend mention that in 19th century Britain, egg white (glair) was commonly used as a varnish (2012, p. 253).

The traditional varnishes used in the 18thup to the 20th century is mainly mastic, dammar, shellac, amber and copal varnishes.

Mastic is derived from the tree *Pistachialentiscus L.* (Ioakimoglou, 2004, p. 174). From the 16th to the 19th century, it was used extensively in Europe as a painting varnish, replacing oil/resin varnishes (Ioakimoglou, 2004, p. 175). Moving onwards, mastic varnish was used mostly as a finishing layer above a copal varnish layer; its tendency to darken fast, along with the fact that it could

be removed easily without any harm to the underlying layer made it the most replaceable coating (Speed, 1873, p. 227; Phenix & Townsend, 2012, p. 259; Van der Goltz, et al., 2012, p. 650).

Dammar is a triterpenic resin, which is collected from various plant species of the *Dipterocarpaceae* family and is indigenous to tropical climates (Ioakimoglou, 2004, p. 177). The dammar varnish was first described in Germany in the early 19th century by Lucanus, who describes is as superior to mastic for its optical properties (Phenix & Townsend, 2012, p. 260). The use of dammar varnish began in the early 19th century in Europe but it was widely accepted as paint varnish at end of the century (Colombini & Modungo, 2009, p. 17; Ioakimoglou, 2004, p. 178).

Shellac is secreted by the scale insect *Lacciferlacca Kerr*, which lives as host to plants indigenous to India and Thailand (Goffer, 2007, p. 305).The use of shellac as a varnish began in Europe in the16th century for paintings, furniture, musical instruments, wooden and metal artifacts (Ioakimoglou, 2004, p. 185). The methods of total decolorizing of shellac were perfected in the 19th century, although examples of shellac used as a varnish in the 19th century are rare (Phenix & Townsend, 2012, p. 260). Toward this direction lead, the high sensitivity to moisture, which destroys the varnish and this also had as a result the darkening of the color and the insolubility to alcohol (Ioakimoglou, 2004, p. 185).

Amber, on the other hand, is a fossilized resin that derives from an extinct coniferous tree, *Pinitessuccinifer* (Mills & White, 1987, p. 96). The use of amber as a varnish seems to begin in the 16th or 17th century and it was known to produce very dark-colored varnishes (Mayer, 1970, p. 195; Ioakimoglou, 2004, p. 180).

Finally, copals are semi-fossilized or fossilized resins derived from various trees of Latin America and Africa (Ioakimoglou, 2004, p. 166). Copals were first introduced in the 18thcentury, with the escalation of their use starting to occur in the second half of the 19thcentury (Phenix & Townsend, 2012, pp. 258-259).

The varnish can be produced with both, oil/resin and spirit varnish recipes but the most common recipes were the ones of oil/resin copal mixtures (Church, 1890, pp. 100-101; Phenix & Townsend, 2012, p. 259). The reasons that copal varnishes were so popular during that period were the toughness and hardness of the varnish layer (Church, 1890, p. 105). Artists wanted to protect their paintings from different decay factors, such as the extreme atmospheric pollution of the cities but also with factors related with the appearance of their artworks after the appliance of the varnish, such as the paint cracking, the darker hues of colors due to oxidation and also from the effects of the restoration (Phenix & Townsend, 2012, pp. 258-259). So, the idea of two different resins in separate layers was often used for the final varnishing (Carlyle, 1990, p. 79). Predominant resins used for this purpose were copal, as the first layer and mastic or dammar as second "sacrificial" layer of varnish[1] (Van der Goltz, et al., 2012, p. 650). Artists of this period admired the protectiveness that copal varnish offered through its aforementioned properties. However, the two main limitations of copal varnishes were the discoloration when ageing and the poor removability (Phenix & Townsend, 2012, p. 259).

In the 18th and early 19thcentury the practices of previous centuries with the same staple materials prevailed. The major changes that occurred in the 18th century was the experimentation with some copal and amber varnishes and the establishment of the role of colourman[2] (Phenix & Townsend, 2012, p. 257).

The artists in the 19th century changed their preferences for how to apply the varnish layer and the materials used to produce their artistic style. Academies

[1]This practice was widely adopted during the late 19th century. In their effort to prevent the danger of a "conservator" damaging the painting surface, during a varnish removal treatment, artists used to seal the painting surface with a durable varnish, like copal, and apply a second layer of varnish with different physical and chemical properties, like mastic or dammar. Consequently, when the upper varnish layer had been oxidized, it could be removed safely, causing no harm to the painting surface laid under the copal varnish layer (Van der Goltz, et al., 2012, p. 650; Phenix & Townsend, 2012, p. 259).

[2]Colourmen, firstly encountered in the 18th century, were professionals who produced and supplied materials for artists, such as canvases, boards, stretchers, pigments, mediums and varnishes. Colourmen used to label their products, for promotion purposes, with stickers, stamps and stencils (Phenix & Townsend, 2012, p. 257; National Gallery of Victoria, n.d.).

of art, had a dominant role in the development of the artistic approaches of those centuries, favoring the concept of “dutifully finished work” (Swicklik, 1993, pp. 157-159). According to this concept, favorable for public exhibition were the paintings with a highly polished surface (Swicklik, 1993, p. 159).

Jean François Léonore Mérimée, a French academic with strong acceptance from the academy, recommends the combination of oil and varnish in the paintings medium, which leads to a greater brilliance and transparency of color. He was the first to recommend the use of the two different layer varnishes, of copal and mastic. However, his instructions were not followed by all painters (Swicklik, 1993, p. 160). Those who opposed the academic style and wanted to experiment had to find their own ways of surviving outside of the academy (Swicklik, 1993, p. 161).

In the second half of the 19th century, the application of a thin layer of varnish seems to be preferred, as a possible reaction of the progressive style painters against the determined protocol of academic paintings (Phenix & Townsend, 2012, p. 258).

Moving towards the end of the 19th century the techniques of the independent artists tend to be more radical in comparison to those of the academic style (Swicklik, 1993, p. 165). The varnishing practices of this period differ from artist to artist and from period to period of an artist’s career (Mayer & Myers, 1993, p. 134). It is this period that, for the first time, the varnish is not an integral part of a painting (Phenix & Townsend, 2012, p. 261). In the 20th century the practice is observed of intentional local application of varnish in an effort to achieve variations of surface gloss (Phenix & Townsend, 2012, p. 263).

3. REVIEW OF ANALYTICAL METHODS

The first application of science in the analysis of historical paint occurred in the 18th century along with the rise of the science of chemistry (Nadolny, 2012, p. 337). Of great importance was the conception, that art studies should be based on the examination of objects, not texts, which was the prevailing method until then (Nadolny, 2003, p. 39). The techniques that scientists employed in their first attempts were the addition of various reagents, the application of heat and flame and the observation of reactions, smell, and other. Very popular, although in many cases destructive, was the method of wiping tests. This practice included the wiping of the painting surface with different types of solvents in an attempt to characterize its composition by its solubility characteristics. (Nadolny, 2003, p. 40)

During the 19th century, scientific experts began to be involved in restoration matters. This led to the progression of the techniques employed in the analysis of works of art, beyond the aforementioned methods (Nadolny, 2012, p. 337). One of the catalytic factors of this progress was the use of microscopes in the analysis of paint samples (Nadolny, 2003, p. 42). Photographic documentation of cross-sections was first printed in 1910, while in 1953 colored photographs of cross-sections were used for the first time (Nadolny, 2012, p. 339).

In the early 20th century the number of publications related to the analysis of paintings grew. Scientists and conservators began to better understand the potentials and benefits of analysis, which led to the advancement of contemporary methods and the application of pre-existing methods for the first time in the analysis of paintings, such as UV and IR radiation, and X-rays. (Nadolny, 2012, p. 339) Ultraviolet radiation (UV) discovered in 1801 by Johann Wilhelm Ritter, however, for the analysis of paintings was first used in the decade of the 1920s (MacBeth, 2012, p. 294). Infrared radiation (IR) discovered in 1800 by Sir William Herschel, however, infrared photography became possible in the early 20th century (MacBeth, 2012, p. 296). Infrared reflectography (IRR) was first used in the decade of the 1960s, by J. R. J. van Asperen de Boer (MacBeth, 2012, p. 297). X-rays were discovered by Wilhelm

Conrad Rontgen in the late 19th century, with their early use in the analysis of paintings occurring in 1938 (MacBeth, 2012, p. 300). From the second half of the 20th century onwards, the progress of analytical methods was rapid. In the decade of the 1960s, lasers were invented and very quickly used for the analysis of paintings, while scanning electron microscopes started to be used in 1970. (MacBeth, 2012, p. 345)

Nowadays, the use of scientific methods constitutes an inseparable part of the study and conservation of works of art. Scientific articles and books of the late 20th and early 21st century dedicated to the analysis of paintings show the progress and the abundance of analytical methods available (Schneider, 1990; Casoli, et al., 1995; Anglos, et al., 1997; Janssens & van Grieken, 2004; Kouloumpi, et al., 2007; Artioli, 2010; Bastidas & Cano, 2018).

Easel paintings on canvas are, as it is been mentioned in chapter 2 of this thesis, very complicated and multileveled works of art. The data obtained by the analytical procedure can be divided in the groups of

- morphological information, such as measurements of physical, chemical and other parameters of an object,
- physical information, such as physical, mechanical and optical properties of the object, that help in the interpretation of its use and its method of manufacturing,
- chemical and mineralogical information, qualitative and quantitative data regarding the chemical composition of the object and the aggregation of the chemical elements into crystalline or amorphous phases; this information helps to understand the object's history, its raw components, manufacturing techniques, and its alterations.
- dating and authentication information, (Domenech-Carbo, et al., 2009, pp. 3-6) (Artioli, 2010, p. 24).

The optimum characteristics that an analytical method employed in cultural heritage field should have are

- to be non-invasive or to require small sample quantities for the analysis,
- to produce reproducible, precise, accurate, and useful information with low detection limits, and
- to be easily accessible to the user community (Artioli, 2010, p. 104).

For the design of the research protocol, one has to set into consideration a number of rules. (a) A fundamental parameter in the design of the research protocol has the analysis questions. (b) Also, the understanding that the principles of each technique lead to the proper selection of methods. Such principles comprise the type and depth of information taken, the necessity of a sample and its amount, the accuracy and precision, and the detection limits of the techniques. (c) The availability and cost of the methods. (d) the selection between non-invasive and invasive methods and if invasive methods are applied, it's of high importance to have knowledge of the number of samples that can be taken. And finally, (e) the level of difficulty in the comparison of the results with available literature data and databases. (Artioli, 2010, pp. 106-107)

Considering the complexity and the multi-parametricity of the above rules for the design of the research protocol it becomes clear that to answer some analytic questions more than methods may be needed. The combination of methods is used in order to cover a broader spectrum of answers. (Artioli, 2010, p. 111)

Equally important remains the decision between the use of invasive or non-invasive methods. As mentioned earlier, it is optimum to utilize non-invasive or at least micro-destructive methods. However, either due to the unavailability of specific methods, either due to high cost it is sometimes necessary to employ invasive techniques. (Artioli, 2010, p. 113)

The scientific methods utilized in heritage science can be divided in three groups; the examination or imaging methods, which use different parts of the electromagnetic spectrum to give information invisible to the naked eye, the analytic methods, which are divided into atomic, molecular and separation techniques, and finally dating methods. (Lahanier, 1991, p. 246)

3.1. Imaging Techniques

Imaging techniques are those employing different types of radiation and record their interactions with matter and create a visual image of the component's

distribution from the simultaneous measurement of spectra and spatial information (Kozaris, 2013, p. 38). These interactions are diffusion, reflection, scattering and absorption (Kouloumpi, et al., 2012, p. 368). The required instrumentation is composed by a radiation source to react with the sample, a sample which will interact with the radiation, and a detector.

Radiation can be divided into particulate and electromagnetic radiation. The particles used in particulate radiation are electrons, positrons, protons, neutrons, and alpha particles, while, electromagnetic radiation (**Figure *3.8***) is photons. (Kozaris, 2013, pp. 38-40) Photons are uncharged energy particles obeying the rules of quantum mechanics. Due to the wave-particle dualism of light, the energy of photons is calculated by the formulas:

$$\boldsymbol{E = hv}$$

$$\boldsymbol{v = \frac{c}{\lambda}}$$

where E = energy of the photon, v = frequency of light wave, λ = wavelength, h = Plank's constant (Artioli, 2010, p. 17).

The type of interaction observed depends on the nature of radiation and on the structure of the atoms. Radiation can be ionizing and non-ionizing. Ionizing radiation utilizes sufficient energy to liberate an electron from an atom. For radiation to be characterized as ionizing, its energy must exceed 10 eV. Non-ionizing radiation is radiation with sufficient energy to excite an electron to a higher energy state. (Kozaris, 2013, pp. 38-40)

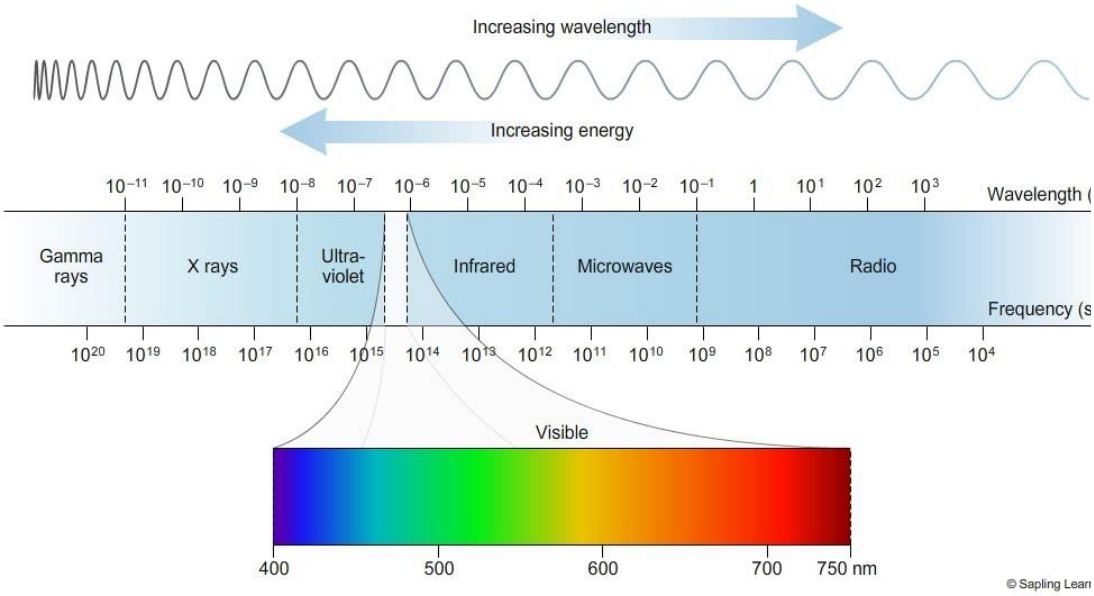

Figure 3.8 The Electromagnetic spectrum (derived from: link)

The way photons interact with matter is of great importance for a better understanding of potentials that any imaging method may have. The depth that a photon will penetrate in matter depends on its energy and on the material properties of the medium that will penetrate. When a photon interacts with matter it can penetrate with or without any interaction, it can interact and lose its energy completely by absorption, and it can interact and be scattered or deflected and lose part of its energy. (Kozaris, 2013, p. 40)

As regards the way photons are detected, there are three main types of interactions that are of great interest, that provide differentiation according to the energy of the incident photon and the atomic number of the interacting material. At low energies and high atomic numbers, the predominant interaction is the photoelectric effect. At intermediate energies and low atomic numbers, the main interaction is Compton scattering, and at high energies the main interaction is pair production. (Kozaris, 2013, p. 41)

3.1.1. X-Ray Radiography

X-ray radiography (XRR) is a non-invasive, non-destructive imaging technique which is employs X-rays of wavelength 10^{-8}-10^{11} m (**Figure *3.8***). (Stuart, 2007,

p. 77) The penetrating abilities of X-rays on opaque objects was first observed by Rontgen in 1895, while the first radiograph of a painting was made by Faber in 1913 (Mairinger, 2004).

The interactions occurring when X-ray photons hit matter are transmission, absorption, and scattering leading to the attenuation of the incident beam (Mairinger, 2004, p. 55). XRR is based in the recording of the attenuated transmitted photons registered by analog or digital means (Alfeld & Broekaert, 2013, p. 225). Thus, the understanding of the attenuation laws is of great importance for the interpretation of X-ray radiographs. The attenuation is dependent on the thickness of the object, the quality of radiation, and the atomic number of the absorbing material. The absorption and scattering are the interactions causing the attenuation, and the level of attenuation is dependent on the atomic number and the wavelength. So, the wavelength used, the chemical composition, the thickness and the density of the object determine the radiation contrast. (Mairinger, 2004, p. 57) The readability of radiographs, which is dependent on the contrast and scatter, is secured by employing the optimum voltage for the analysis of paintings, which is <100 kV, the current (mA) and the amount of exposure time (Stuart, 2007, p. 78; MacBeth, 2012, pp. 301-302).

The information gained by XRR extends to all components of an easel painting. The information regarding the stretcher concerns manufacturing methodologies and joining techniques. Information about the textile support can be obtained by the negative impression of the ground layer. This effect is crucial for relined paintings, where the first canvas is covered. Through this characteristic the borders of the first canvas can be located (Alfeld & Broekaert, 2013, p. 226). The physical characteristics, the structure and density of the yarn and the weave can lead, if enough information exists, to the characterization of the artistic period or even the attribution to an artist. Another important feature observed is the cusping of the canvas; the absence or not of the symmetric wavy structure may indicate the alteration or not of the dimensions of the painting (Gavrilov, et al., 2014, p. 346; Mairinger, 2004, pp. 63-64). The interpretation of the painting layer can be difficult on occasions. The information

concerning this layer comes from a thin film, which is affected by the information of the underlying layers. Since XRR is a technique that presents its information through contrast, the difference between the atomic number of the pigments and the underlying layer has to be enough for sufficient contrast to be achieved. In the opposite situation, pigments will be invisible to X-rays. (Alfeld & Broekaert, 2013, p. 226) In regard to the above, XRR can give information about the pentimenti of the artist, hidden changes below the upper paint layer and compositional mapping of the pigments of heavy elements. Also, the detection of damage, cracks, ageing, later alterations, and grouts. (MacBeth, 2012, p. 302; Mairinger, 2004, p. 64; Stuart, 2007, p. 79; Alfeld & Broekaert, 2013, p. 225)

Despite the extended use of XRR in the analysis of easel painting, there are some limitations in its performance and the type of information obtained:

- the information obtained concerns mostly the heavy element pigments,
- the lighter elements are in many cases obscured when heavy elements in great concentrations are present,
- in paintings on which the ground layer consists of a heavy element such as Pb, an overall absorbance background is presented
- and, the wide spectrum of X-rays used is reducing the contrast. (Janssens , et al., 2010, pp. 815-816)

To counter the above limitations, scientists employ state of the art techniques as alternatives to the classic XRR. Such techniques are the group of tomographic techniques. The basic principle of tomography is the acquisition of a set of multiple radiographs by rotating the object perpendicular to the source-detector axis. Later, through mathematical reconstruction a virtual 3D rendition is created of the object's shape and inner "stratigraphy". (Janssens , et al., 2010, p. 816) The tomographic technique employed in the examination of canvas paintings is the computed laminography (CL) (Alfeld & Broekaert, 2013, p. 227). Additionally, the use of synchrotron radiation (SR), with its high intensities and narrow spectrum leads to high contrast and detailed images (Janssens , et al., 2010, p. 816).

3.1.2. Multispectral Imaging

Multispectral Imaging (MSI) is a non-invasive non-destructive technique that utilizes well defined optical bands of the electromagnetic spectrum (**Figure *3.8***) from Ultraviolet (UV) to Infrared (IR) for the optical diagnosis, the identification of materials, technical construction, and the indirect dating of an object (Kouloumpi, et al., 2012, p. 369; Alexopoulou, et al., 2018, p. 444). The employment of MSI to the examination of cultural heritage objects began in the decade of the 1990s (Liang, 2012, p. 310). The reason that this technique is established as a part of the routine in the examination of cultural heritage objects is due to its unique characteristics, such as its non-invasive non-destructive nature, its quick in situ application, the ability to examine and map the entire surface of an object, and the absence of expensive consumables (Alexopoulou, et al., 2018, p. 444). Commercially available multispectral systems offer several operation modes, with each one of them offering different information about the object (Kouloumpi, et al., 2012, p. 369). Such modes are visible imaging, UV imaging in Reflectance and Fluorescence mode, and IR imaging in Reflectance, Transmission, and False Color mode. The development of these setups serves the purpose of utilization of all the aforementioned modes with the same equipment, however, a drawback in these setups is that the detectors can detect a small part of the infrared region, only up to 1000 nm. However, systems that focus on the exploitation of the infrared region exist, such as InGaAs detectors that are sensitive from 900 to 1700 nm. (Alexopoulou, et al., 2018, p. 444)

3.1.2.1. UV Imaging

In this technique the ultraviolet (UV) portion of the electromagnetic spectrum is utilized. The ultraviolet region of electromagnetic spectrum can be divided in four bands; the near or long-wave ultraviolet (320-400 nm), middle ultraviolet (280-320 nm), far or short-wave ultraviolet (200-280 nm) and vacuum ultraviolet (200-10 nm). Only the near or long-wave ultraviolet is useful for examining paintings. This band of UV is also called as UVA (MacBeth, 2012, p. 294).

Due to its wavelength, UVA radiation is mostly absorbed by the upper layers of the painting (Gavrilov, et al., 2014, p. 343). For this reason UV imaging is used for the examination of the top layers, and surface characteristics invisible in the visible portion of the electromagnetic spectrum (Mairinger, 2004, p. 45). As mentioned above UV imaging is used in reflectance and fluorescence modes, however UV reflectance is not used in the examination of paintings.

On the other hand, UV fluorescence (UVF), which is used for the study of art objects since the 1920s, constitutes a very important technique (Kubic, 2007, p. 205). This technique exploits the property of many organic and non-organic materials to fluoresce and the differentiations that arise since not all materials fluoresce in the same way. Fluorescence is the outcome of the re-emission of the reduced initial radiation after its absorption by the painting (Mairinger, 2000, p. 64). The identification of materials is not reliable since even the same element can produce different fluoresce depending on the deposit. (Mairinger, 2004, p. 47).

By the use of UVF, as mentioned above, the varnish layer can be studied. Different kinds of varnishes exhibit different glow when irradiated by UV (Gavrilov, et al., 2014, p. 343). The fluorescence of the varnish gets intensified by the oxidation process. This feature helps with the clarification of the varnish distribution on the surface, providing information on the treatment history of the painting. Since later alterations and additions exhibit different fluorescence intensities or they don't exhibit any at all. (MacBeth, 2012, pp. 294-295) Areas of later restorations, retouching, and over-paintings are very easy to track. They appear as dark spots or areas over the greenish fluorescence of the varnish. However, later alterations that have been made before 80-100 years develop fluorescence, a fact that makes their localization difficult (Mairinger, 2000, p. 65). Concerning the paint layer, they can also be examined by UVF. Pigments added in the top layers of the painting that were sensitive to light and were invisible in the visible spectrum can be tracked (MacBeth, 2012, p. 295). Also, some pigments exhibit strong fluorescence and the comparisons of

differentiation between pigments' fluorescence can lead to semi-qualitative data (MacBeth, 2012, p. 296).

3.1.2.2. Visible Imaging

Visible imaging techniques constitute the basic and first steps towards the examination of a work of art. The positioning of the visible light source and the detector in different angles emphasize different characteristics of the surface of a painting. The positioning of the light source at 45^{o} degrees to the painting reduces reflection, and make this method suitable for the imaging of pictorial characteristics of the painting. The positioning of the light source at 90^{o} degrees to the painting induces differences in the reflectivity of surface materials. (Kouloumpi, et al., 2012, p. 369; Stuart, 2007, pp. 43-44) The positioning of the light source at 10^{o} degrees towards the painting surface highlights textural characteristics, such as distortions, cracks, later additions, and flaking in the paint surface and support. Additionally, any artistic characteristics of the painter may be visible, such as impasto. (MacBeth, 2012, p. 293; Kouloumpi, et al., 2012, p. 369)

3.1.2.3. Infrared Imaging

In this technique the infrared (IR) portion of the electromagnetic spectrum (**Figure *3.8***) is utilized. The infrared region can be divided into three bands; the near-infrared (NIR, 750-1000 nm), short-wave infrared (SWIR, 1000-2500 nm), and mid-infrared (MWIR, 2500-15000 nm) (Alfeld & Broekaert, 2013, p. 221).

The degree of opacity of a paint layer is determined by the absorption of light by the pigment and the binder, and the scattering of light by the pigment and the binder. Pigments absorb different amounts of light, depending on their nature, while the refraction coefficients of both pigment and binder regulate the level of scattering. (Gavrilov, et al., 2014, p. 344) Because of its energy, which is lower than visible radiation, IR can penetrate layers that are opaque in the visible portion of the spectrum. While when it interacts with molecules it excites only vibrational and rotational states whereas no electronic transitions occur.

(Mairinger, 2000, pp. 40-41; Mairinger, 2004, p. 50). As mentioned previously, IR imaging is used in Reflectance, Transmission, and False Color mode.

Infrared reflectography (IRR) as the reflectance mode of IR imaging is referred to as an established technique for the examination of paintings since the 1960s (Gavrilov, et al., 2014, p. 344; MacBeth, 2012, pp. 297-298; Janssens , et al., 2010, p. 821). NIR (750-1000 nm) is used for the examination of works of art through IRR (Kubic, 2007, p. 206). Since most pigments are transparent to IR radiation, IRR is used for the study of underdrawings. Underdrawings are more clearly observed in paintings dated from the 16th c. and before. The paintings of these periods have strongly reflecting chalk or gypsum grounds and the underdrawings are made of strongly IR absorbing materials like carbon-based black pigments. After the 16th c. painters used less absorbent grounds and made the underdrawings with materials that are transparent to IR. (Alfeld & Broekaert, 2013, p. 222) IRR is used for the detection of pentimenti and other touch-ups that were invisible with the naked eye (Kubic, 2007, p. 206). Pigments become transparent in different wavelengths, so the examination of paintings with a multi band system such as MSI can give semi-quantitative data about the distribution of pigments in the paint layer. (MacBeth, 2012, p. 299; Kubic, 2007, p. 206)

Another mode of IR imaging is the false color infrared (FCIR). Areas of the painting which produce the same color in visible, are made of different materials (Kouloumpi, et al., 2012, p. 369). Researchers use false color imaging to better visualize differences between photos acquired from various wavelengths (MacBeth, 2012, p. 299). FCIR images are created by the assignment of different single-wavelength IR or VIS images to each of the red, green and blue channels of an RGB image and displaying them simultaneously (Fischer & Kakouli, 2006, p. 8; MacBeth, 2012, pp. 299-300; Faries, 2005, p. 109). By superimposing all the different spectral images, it is possible to observe the unique features offered by each. The proper choice of spectral images to the color composite image leads to the emphasis of the results, rendering clear the interrelations between images, and visually enhances the differentiated

features across the wavelengths. (Daffara & Fontana, 2011, p. 692; Delaney, et al., 2016, p. 7)

Finally, the mode of transmittance IR imaging (IRT) is used with the same equipment as IRR with the difference being the point of the illuminating source. According to Kushel (1985, p. 2), a transmittogram offers information which in many cases both IRR and XRR cannot obtain. The IRT is used for the study of underdrawings and underpaintings in canvas paintings (Alexopoulou, et al., 2018, p. 458). Also, it has been used for the revelation of hidden inscriptions and labels in the back of lined paintings. The effectiveness of this mode is based on its ability to penetrate pigments, such as lead white, which remain unpenetrated in IRR. Finally, IRT is useful for the study of paintings with low reflectivity or little contrast in IRR, such as paintings with dark grounds. (MacBeth, 2012, p. 300)

3.1.3. Other Techniques

In this subchapter a number of new state-of-the-art imaging techniques will be briefly discussed. In more detail, reference will be made to Terahertz imaging, Optical Coherence Tomography, and Photoacoustic Imaging.

Terahertz (THz) imaging is a non-invasive non-destructive depth-profiling technique. The THz radiation region has frequencies from 15 μm to 3 mm wavelength or 20 to 0.1 THz (Alfeld & Broekaert, 2013, p. 224). THz rays show great penetrating ability in dielectric materials, which surpasses the penetrating ability of IRR. THz imaging operates in reflectance, transmittance, and reflectance/transmittance modes. (Picollo, et al., 2015, p. 74; Janssens , et al., 2010, p. 823) The object is illuminated by short, focused THz pulses and focuses on the study of interfaces between the various paint layers and of the canvas-ground interfaces. (Janssens , et al., 2010, p. 823) The technique allows the creation of a two-dimensional view of the layer of interest or a map which highlights the presentation of a specific material. Because of the characteristic “fingerprint” of many materials, the distinction between materials is in many cases possible. (Picollo, et al., 2015, p. 74) Additionally, THz imaging

is a very promising technique for the visualization of underdrawings. (Tserevelakis, et al., 2017, p. 2) However, the images acquired can be used only for qualitative analysis (Picollo, et al., 2015, p. 79). Heritage scientists in the last years develop THz databases for a more reliable identification of compounds (Alfeld & Broekaert, 2013, p. 224).

Optical Coherence Tomography (OCT) is a scanning interferometric technique, which is most usually employing partly coherent, polychromatic light from the NIR region (Janssens , et al., 2010, p. 822; Alfeld & Broekaert, 2013, p. 223). The NIR light probed at the object gets absorbed or reflected. The reflected light is analyzed by the interferometer. Through the interferometric analysis, differences in the absorption/scattering characteristics of the materials composing the object, as well as the depth in which the reflection took place, is apparent. The depth profiling data permits the mapping of the distribution of materials and material interfaces in 3D volumes, acquired in the form of perpendicular or parallel cross sections. (Alfeld & Broekaert, 2013, p. 223; Janssens , et al., 2010, p. 823) The advantages of OCT over other techniques providing stratigraphic information is its non-invasive non-destructive character, which permits the investigation of areas where sampling would be impossible (Elias, et al., 2011, p. 339). The applications of OCT to the examination of paintings applies to the imaging of secondary layers, and the acquisition of data concerning the build-up of the varnish and paint layers, and the identification of overpainting layers (Iwanicka, et al., 2018, p. 55). Though, it has to be mentioned that the depth resolution obtained is highly dependent on the nature of pigments present. OCT cannot penetrate thick opaque paint layers which are not transparent to IR radiation (Tserevelakis, et al., 2017, p. 2; Janssens , et al., 2010, p. 823).

Photoacoustic (PA) Imaging is based on the property of materials to produce acoustic waves when irradiated by time-variable (laser pulse) light (Tserevelakis, et al., 2017, p. 2). The characteristics of these waves, such as speed, phase, amplitude, transmission, and reflection, are depended on the properties of the medium (object’s materials) to which they are propagated. When the propagated light faces discontinuities in the material, a partial

reflection and transmission occurs. The speed of the received wave is dependent on the mass density and the elastic properties of the medium. The comparison of the propagated and the received wave makes possible the estimation of the internal structure of the medium. (Gavrilov, et al., 2014, p. 347) The high sensitivity and contrast of PA imaging results in accurate results in the study of underdrawings made by graphite and covered by different opaque paints (Tserevelakis, et al., 2017, pp. 3-6). However, because acoustic waves cannot propagate adequately throughout gases, a liquid (distilled water or gels) coupling was employed (Amanatiadis, et al., 2018, p. 475). In their study, Tserevelakis et al. (2019, p. 95) use air-coupling transducers, solving the invasive nature of PA imaging, and render it as a non-invasive non-destructive technique for the inspection of inner structures. The biggest advantage of PA imaging is that by the adjustment of the wavelength of the emitted light the inspection of different materials is possible. (Tserevelakis, et al., 2017, p. 7)

3.2. Microscopy Techniques

Microscopic techniques have been used since the first half of the 20th c. for the examination of paintings (Kouloumpi, et al., 2012, p. 372; Eastaugh & Walsh, 2012, p. 307). Scientists use microscopy in order to examine cultural heritage objects in larger scale (Pavlidou, 2013, p. 47). Through them, they can acquire information regarding the “history” of the painting, like the original preparatory layers and paint structure, the presence of varnish layers, any later alterations and additions, like overpaintings and compensations (Wolbers, et al., 2013, pp. 334-335). Some of the microscopy techniques most widely used for the examination of works of art are the optical microscopy (OM), the scanning electron microscopy (SEM), and the transmission electron microscopy (TEM). These techniques belong to the branch of invasive methods for the examination of works of art, because they require a sample for the analysis. (Pavlidou, 2013, pp. 47-48; Wolbers, et al., 2013, p. 326) The procedure of sampling consists of the steps of: sectioning, mounting, grinding, and polishing (Leng, 2008, p. 15).

The objective of sampling is to take the smallest representative samples possible form areas of interest (Wolbers, et al., 2013, pp. 327-328). The samples must be taken under a stereomicroscope with a suitable instrument, such as a micro-scalpel, a fine needle. The documentation of the sampling procedure must be detailed with information such as the name of the object, the color of the sample's surface, relevant physical characteristics, the location of the sample, and finally general observations regarding the location of sampling. (Eastaugh & Walsh, 2012, p. 314) The conservation ethics dictate the samples to be taken from the edges of damaged areas, such as cracks or losses. (Wolbers, et al., 2013, p. 328) Samples in powder form are placed on a microscope slide, which has a small bead of solidified thermoplastic resin. Subsequently, the slide is placed on a hot plate for the bead to become fluid. Finally, the cover-slip is placed. After this the sample is ready for examination. (Eastaugh & Walsh, 2012, p. 314) Regarding cross section samples, next is the step of mounting, which refers to the embedding of the sample in a mounting material. The samples are embedded in synthetic resin. (Kouloumpi, et al., 2012, p. 373) Next is the step of grinding and polishing the sample. During the procedure of grinding, the excess resin and any damages on the examination surface of the sample are removed. The grinding is performed by hand with a grinding machine with the use of a sequence of abrasive paper of increasing grit number. (Leng, 2008, p. 19) Finally, in the procedure of polishing, damages on the sample's surface caused by grinding will be removed, generating a flat surface with no scratches (Leng, 2008, p. 22).

3.2.1. Optical Microscopy

The optical microscope (OM) consists of one of the basic methods for the examination of cross section samples (Pavlidou, 2013, p. 51; Leng, 2008, p. 1; Berrie & Thoury, 2019, p. 119). It has been widely used for the examination of paintings for the characterization of pigments and the painting technique. It is based on the principle that light which interacts with a specimen is magnified through glass lenses. (Pavlidou, 2013, p. 49) The basic parts of an optical microscope are: illumination system, objective lens, eyepiece, photomicrographic system, and specimen stage (Leng, 2008, p. 8). The

illumination of the specimen can be done in reflection and transmission mode. The main difference between the two modes is the illumination system. In reflection or epi-illumination mode variations in the surface topography and reflectivity caused by grain orientation, distinct phases, and boundary regions lead to the observation of the various regions of the sample. In transmission mode, the sample must be in the form of a thin slice for the light to be able to transmit through it. The information gained is due to the differentiation of the absorption coefficient of the various regions of the sample. (Pavlidou, 2013, p. 49; Leng, 2008, p. 21) Optical microscopes are divided into low and high-power microscopes. Low-power microscopes offer magnifications of the order 60x or 100x, while, high-power microscopes can magnify a sample at 100x to 1000x (Pavlidou, 2013, p. 51). The resolution of an optical microscope is controlled by the diffraction of light. The resolution of the optical microscope is dependent on the wavelength whereby decreasing the wavelength the resolution rises. The optimum resolution of optical microscopes is estimated at 0.2 μm. (Leng, 2008, pp. 3-5) As highlighted, the difference in the wavelength of light (amplitude) affects the resolution and general observations of a sample. Based on that conclusion, several examination modes have been developed. The two most commonly used are bright-field and dark-field imaging. In bright-field imaging the specimen is illuminated evenly by the light source. (Leng, 2008, p. 25) The observed image is the result of the reflected light collected in the aperture of the objective. Scattered light that does not fall into the aperture of the lens is lost and areas of the specimen which scatter part of the incident light appear as dark. (Brandon & Kaplan, 2008, pp. 139, 151) Dark-field imaging is used when, under bright-field imaging, topographic differentiations appear faint. In dark-field imaging the specimen is illuminated by oblique light rays with the diffusely scattered light to be collected in the objective (Leng, 2008, p. 26; Brandon & Kaplan, 2008, p. 139). Additionally, the deflection of the condenser system enhances the topographical information, due to the illumination from one side only.

Another type of microscopy is polarized light microscopy (PLM) (Eastaugh & Walsh, 2012, p. 306). PLM is applicable to materials exhibiting optical anisotropy (Leng, 2008, p. 30). Anisotropic materials compose 90% of the solid

materials (Stuart, 2007, p. 82). Optical anisotropy is the property of a material in which the refractive index of the light is a function of the direction of propagation (Brandon & Kaplan, 2008, p. 157). PLM is one of the most widely applied methods for the identification of pigments (Kouloumpi, et al., 2012, p. 373; Stuart, 2007, pp. 84-85). The identification is based on the observation of color in transmitted and reflected light, particle shape, particle surface characteristics and inclusions, diaphaneity, pleochroism, refractive index measurements, isotropy/anisotropy, birefringence, elongation, etc. However only some features are present in each particle type. (Eastaugh & Walsh, 2012, p. 315)

The spectrum of the optical microscopy method variations is completed with Ultraviolet fluorescence microscopy (UVFM). The differentiation with optical microscopy is the illuminating source, which in the case of UVFM is a UV light source, and the filter used for the reduction of the wavelength range reaching the objective lens (Eastaugh & Walsh, 2012, p. 317; Berrie & Thoury, 2019, p. 123). UVFM is performed both in reflectance (epi-illumination) and transmittance mode, however, epi-illumination has more advantages due to smaller losses of exciting light (Berrie & Thoury, 2019, p. 123; Leng, 2008, p. 37). UVFM is used for better distinction of micro-stratigraphic structure (Kouloumpi, et al., 2012, p. 373). Many of the materials composing a painting, like pigments, dyes, lakes, proteins, gums, and some inorganic complexes emit fluorescence when illuminated by UV light. The level of fluorescence, on the sample materials, is also dependent on their aging and degradation products. The aforementioned properties result in the visualization of characteristics not visible by optical microscopy. (Berrie & Thoury, 2019, p. 126; Kouloumpi, et al., 2012, pp. 373-374)

3.2.2. Scanning Electron Microscopy – Energy Dispersive X-ray Spectroscopy

Scanning electron microscopy (SEM), was invented in 1938 by Von Ardenne and today is the most widely used type of electron microscopy (Leng, 2008, p. 121; Akhtar, et al., 2018, p. 114). As mentioned in §3.2.1, the resolution of an

optical microscope is limited to about 0.2 μm, which is related to the wavelength of the light source used (400-700 nm). Thus, radiations of shorter wavelength can produce higher resolution images. (Calvo Del Castillo & Strivay, 2012, p. 86) However, by taking advantage of wave-particle duality, particles, specifically electrons, can be used as the medium to interact with the specimen. The wavelength of the electrons is dependent on their momentum, which can be changed by acceleration. (Inkson, 2016, p. 18)

The use of SEM offers many advantages to the researcher. The most important of these is the very high resolution that goes down to 1 nm (Akhtar, et al., 2018, p. 117). Also, the magnification range of SEM ranges from 10-500.000 times, with the effective/sufficient magnification for applications related to cultural heritage artefacts to be up to 20.000 times (Inkson, 2016, p. 19; Leng, 2008, p. 123; Calvo Del Castillo & Strivay, 2012, p. 87). Another key advantage of SEM application is the signals generated through the use of electrons. Because of their size and wavelength, electrons interact strongly with atoms resulting in a wide range of phenomena. The detection of these phenomena leads to the creation of structural and chemical images of the specimen. (Inkson, 2016, p. 19; Akhtar, et al., 2018, p. 114)

On the other hand, the application of SEM has some disadvantages too. The size of the object under analysis must be small to be placed in the specimen chamber, or else the analysis requires a sample, which requires further preparation. (Calvo Del Castillo & Strivay, 2012, p. 87) Furthermore, the analysis in SEM is conducted under a vacuum, because electrons do not travel far through air. Thus, the samples used must be vacuum tolerant. Another disadvantage of SEM application is its micro-destructive nature. The accelerated electrons used for the analysis transfer their kinetic energy to the sample causing damages or destruction to a part of its surface. (Pavlidou, 2013, p. 51; Inkson, 2016, p. 19; Adriaens & Dowsett, 2004, p. 74)

A SEM system consists of (a) an electron source (or electron gun), producing a large and stable electron beam of varying energies depended on the need, which is accelerated down the column (Akhtar, et al., 2018, p. 125; Pavlidou,

2013, p. 51); (b) a series of lenses (condenser and objective) and coils (scanning coils and stigmator coils) that control the diameter of the beam and its focus on the specimen; (c) apertures for the refinement of the beam; (d) controls for specimen position; (e) specimen chamber, where occur and are detected the interactions of the electron beam with the specimen. (Akhtar, et al., 2018, pp. 129-131; Pavlidou, 2013, p. 51)

During the interaction of the electron beam with the specimen, several phenomena can occur (Calvo Del Castillo & Strivay, 2012, p. 88). When electrons strike the specimen, three main types of signals are detected: the backscattered electrons, the secondary electrons and X-rays (Pavlidou, 2013, p. 52). These signals are the result of several scattering and absorption events within a teardrop-shaped volume of the specimen, which extends from 100 nm to around 5 μm into the surface, depending on the properties of the specimen and of the beam. Because of these events, there may be an energy loss of the electrons. (Calvo Del Castillo & Strivay, 2012, p. 88; Leng, 2008, p. 130). If an electron, after the encounter with the specimen, has an energy equal to its total kinetic energy, then the collision was *elastic*. While, if an electron, after the encounter with the specimen, has lost part of his kinetic energy, then the collision was *inelastic*. (Pavlidou, 2013, p. 52)

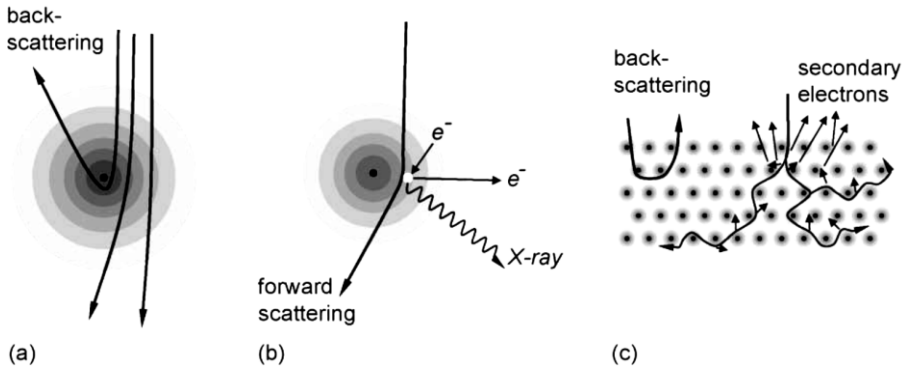

Figure 3.9 Electron scattering and emission. (a) Elastic scattering examples; (b) inelastic scattering; (c) secondary electron emission. Derived from: *(Adriaens & Dowsett, 2004, p. 80)*.

Backscattered electrons (BE) are the result of elastic and inelastic scattering with the atoms of the specimen (**Figure** 3.9 Electron scattering and **emission. (a) Elastic scattering** examples*; (b) inelastic scattering; (c) secondary electron*

emission. Derived from:, and usually retain a large part (greater than 50 eV) of their original energy. (Pavlidou, 2013, p. 54; Calvo Del Castillo & Strivay, 2012, p. 89) Because of their high energy, these electrons can escape from the deepest level of the interaction zone (tear-drop volume) (Leng, 2008, p. 130). Most of the electrons of the primary beam scatter forwards, however, a fraction will be scattered backward and will re-emit from the specimen's surface. (Calvo Del Castillo & Strivay, 2012, p. 89) The fraction of BE depends on the average atomic number of the specimen and increases with the increasing of the atomic number. Considering this feature, the signal of BE can visualize local variations in the atomic number contrast. Thus, on a specimen containing more than one element, those with a higher atomic number, will produce more BE and so will appear brighter, offering compositional contrast. (Brandon & Kaplan, 2008, p. 277; Leng, 2008, p. 133)

Secondary electrons (SE) are produced as a result of the inelastic scattering of the primary electrons with electrons from the specimen, which results in a loss of energy to it. (Pavlidou, 2013, p. 53) The lost energy is transferred to an electron of an atom in the sample, ionizing the atom. If the transferred energy is greater than the energy that bounds the electron to the orbital, then the electron can leave the orbital and eject from the sample's surface as a secondary electron, having energy less than 50 eV. (Calvo Del Castillo & Strivay, 2012, p. 89; Pavlidou, 2013, p. 53; Brandon & Kaplan, 2008, pp. 280-281; Akhtar, et al., 2018, p. 120) The SE because of their low energy can escape from depths of 5-50 nm, thus offer information about the morphology and the topography of the specimen. (Leng, 2008, p. 130; Akhtar, et al., 2018, p. 119)

After the displacement of an electron from the inner shell of an atom, because of the ionization caused by the electron beam, a vacancy is generated. For the re-stabilization of the electron structure, an outer shell electron may fall to the vacancy to occupy it. (Pavlidou, 2013, pp. 54-55) The transition of the energy state of the electron is causing the release of X-rays of specific energy, which is equal to the difference of energy between the two levels. These characteristic X-rays can be attributed to the specific element that produced them, and thus

used for elemental analysis. (Inkson, 2016, pp. 23-24) The X-rays are detected qualitatively and quantitatively by an energy dispersive X-ray (EDS) detector, located in the specimen chamber. EDS detectors performed in vacuum allow the detection of low atomic number elements (Z=6 and onwards). (Inkson, 2016, p. 29; Pavlidou, 2013, p. 55)

The specimens, as in the case of painting cross sections, follow the sampling procedure of optical microscopy, however, after this preparation they must be coated with an electrically conducive material. The coating is done by high vacuum evaporation. This further preparation is necessary for the prevention of static electricity fields accumulating on the specimen, which will result in a blurred image. There is a big variety of coating materials, however, when EDS analysis is to be performed, graphite must be used, in order to not interfere with the elemental data. (Stuart, 2007, p. 94; Calvo Del Castillo & Strivay, 2012, pp. 90-91)

The SEM-EDS has been proven to be a very useful tool for the investigation of cultural heritage related materials. The features of high magnification and the high resolution along with the compositional and topographical data that can be acquired, make SEM-EDS part of the routine examination by invasive methods. (Stuart, 2007, pp. 94-95; Calvo Del Castillo & Strivay, 2012, p. 92)

Considering the examination of painting specimens, by the application of SEM-EDS is possible (a) the study of the stratigraphy of a cross-section, considering the distribution of paint and preparation layers; with much higher detail and magnification comparing to optical microscopy, (b) the observation, and distinction of different materials seeming similar to other techniques, through topographical and compositional information, (c) the acquisition of elemental composition of areas of the specimen with the ability of elemental mapping, through the use of EDS, which give information about the techniques and the materials used by the artist and the observation of any alterations or later additions. (Calvo Del Castillo & Strivay, 2012, pp. 92-93; Townsend & Boon, 2012, pp. 345-346)

3.2.3. Other Techniques

Recent technological developments made possible the coupling of microscopy principles with various spectroscopic techniques; this coupling offers more selectivity and accuracy in the utilization of the spectroscopic techniques. Some of these techniques are Raman microscopy and Fourier transform infrared (FTIR) microscopy, which will be presented in §3.3.2.

3.3. Analytical Techniques

There are many types of analytical techniques, two major categories playing an important role to the analysis of cultural heritage materials are the spectroscopic and the separation techniques (Kouloumpi, et al., 2012, pp. 375-378). According to the information that they can yield, spectroscopic techniques are separated into elemental and molecular techniques (Nevin, et al., 2012, p. 339).

3.3.1. Spectroscopic Techniques

Spectroscopic techniques are employing various parts of the electromagnetic spectrum and yield information through the light-matter interaction with an object/specimen, and provide chemical information of the material under analysis at the atomic and molecular level (Artioli, 2010, pp. 17-19; Anglos, et al., 2009, p. 47). The type of spectroscopic techniques used is determined by the wavelength employed, which leads to electronic, vibrational, or rotational spectroscopy (Anglos, et al., 2009, p. 48; Artioli, 2010, p. 33). Thus by the utilization of different types of spectroscopic techniques different information is yielded, extending the separation to the elemental spectroscopy techniques (Nevin, et al., 2012, pp. 340-346) and molecular spectroscopy techniques (Nevin, et al., 2012, pp. 346-356).

3.3.1.1. Elemental Techniques

For the acquisition of elemental information is necessary to have the interaction of spectroscopic techniques with the nucleus and core electrons of an atom.

The interaction with these parts of the atom will provide qualitative and quantitative information on the nature of the chemical elements presented. (Artioli, 2010, pp. 32-33; Nevin, et al., 2012, p. 340) Several spectroscopic techniques, such as Neutron Activation Analysis (NAA), X-Ray Fluorescence (XRF), Particle-Induced X-ray Emission (PIXE), Laser Ablation Inductively Coupled Plasma Mass Spectroscopy [(LA-ICP)-MS], Laser-Induced Breakdown Spectroscopy (LIBS), and others, are used to obtain information on the elemental composition of the material. (Nevin, et al., 2012, p. 340; Artioli, 2010, p. 33)

In the following sub-chapters, a review will follow of the elemental techniques used by the author on this thesis and a review of the elemental techniques mostly used on the examination of paintings.

3.3.1.1.1. X-Ray Fluorescence Spectrometry

X-Ray Fluorescence (XRF) Spectrometry is a well-established method for qualitative and quantitative elemental analysis. It is based on the ionization of the atoms of the material by an energetic beam of primary X-rays and the record of the produced X-rays from the material under analysis. (Janssens, 2013, p. 80; Donais & George, 2018, p. 1) XRF is the most widely used technique in the analysis of cultural heritage materials because it comprises a set of unique features, such as the non-destructive, non-invasive, multi-elemental nature, simplicity, and the customizability of the technique. (Sokaras, et al., 2009, p. 2199; Gigante & Ridolfi, 2013, p. 96).

XRF spectrometry is based on the interaction of primary X-rays with the electrons of the atoms. According to Bohr's atomic model, each element possesses a specific atomic number (Z), which is the number of protons in its nucleus. The nucleus of an atom is comprised of the positively charged protons and the neutrally charged neutrons. The space around the nucleus of the atom contains negatively charged electrons equal to the number of protons for the accomplishment of a neutral charge for the atom. The electrons of the atom are in shells at specific distances from the nucleus, the atomic orbitals. Each atomic

orbital can be occupied by a specific maximum number of electrons. Because each element has a different number of electrons in its orbitals, their configuration in them is different, resulting in the conclusion that each element has a unique energy signature and pattern. (Donais & George, 2018, pp. 1-2) The electrons, depending on their distance from the nucleus, have different bounding energies. The innermost electron orbital (K shell) is more strongly bound to the nucleus from the following electron orbitals (L shell, M shell etc.). (Donais & George, 2018, p. 2; Polland & Heron, 2008, p. 33) The arrangement of the electrons of an atom is disturbed by its interaction with electromagnetic radiation. This interaction is called the photoelectric effect.

In the case of XRF, a high energy photon from an X-ray source impacts the electrons of the atom. If the energy of the impacting photons is greater than the binding energy of the electron with the atom, the photon gets absorbed by an electron of the atom, resulting in its excitation and ejection from the electron shell. (Janssens, 2013, p. 82; Donais & George, 2018, p. 2) When an electron gets ejected from the inner electronic shell (K shell) of the atom (ionization), it creates a vacancy “hole” (Polland & Heron, 2008, p. 62). For the restoration of stability in the atom, an electron from another shell (L or M shell) fills that vacancy. Because electrons are quantized, during this process, they have to release the excess of energy. The release can occur in two ways; the first is in the form of photon (fluorescence) with characteristic X-ray energy declarative of the element’s identity, the second way occurs when the released energy gets absorbed by another electron, resulting

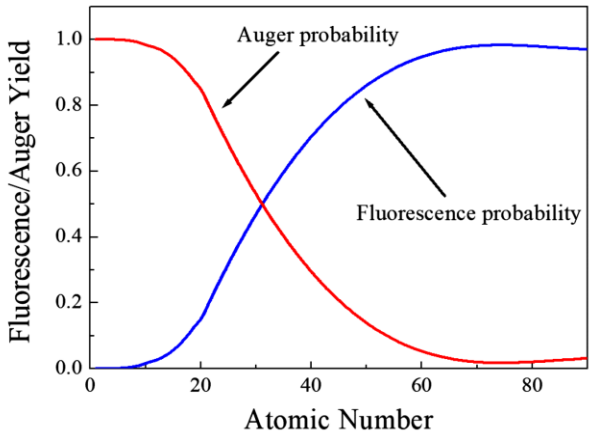

Figure 3.10 Fluorescence and Auger electron yields as a function of atomic number for K shell vacancies (Derived from: *(Kokiasmenou, 2018, p. 15)*.

in its excitation and ejection. This process is called the Auger effect. (Schlotz & Uhlig, 2000, p. 3; Donais & George, 2018, pp. 2-3; Polland & Heron, 2008, p. 34; Karydas, 2007, pp. 419-420) The probability for either of these two processes occurring depends on the energy level of the initial vacancy, and the atomic weight of the atom. These processes are called fluorescence yield and Auger yield respectively. (Schlotz & Uhlig, 2000, p. 3; Polland & Heron, 2008, pp. 34-37) Considering the aforementioned effect, some elements do not produce detectable XRF signals either because they have only one shell of electrons, either due to the fact that the Auger yield in low atomic number elements is greater than the fluorescence yield (**Figure *3.10***). (Donais & George, 2018, pp. 2-3; Janssens, 2013, p. 82)

The energy of the emitted X-ray photon is equal to the difference in the energy levels participating in the procedure to fill the vacancy. (Polland & Heron, 2008, p. 34; Schlotz & Uhlig, 2000, p. 3) Each element produces a number of characteristic lines. Thus, according to the shell from which the second electron will come to fill the vacancy and the shell of the vacancy, the emissions named as shown in **Figure *3.11***. K emissions occur when electrons of the L or M shell fill a K shell vacancy; they are named as Kα and Kβ respectively, L emissions occur when electrons of the M or N shell fill an L shell vacancy; they are named as Lα and Lβ respectively, and so on. (Calvo Del Castillo & Strivay, 2012, pp. 63-65; Schlotz & Uhlig, 2000, p. 4; Janssens, 2013, p. 89)

The emission of the X-ray photons occurs in different depths in the sample. On their way out, the X-ray photons have to travel through the sample, resulting in their reduction according to Beer's Law. The parameters from which the amount of reduction depends are the absorbance of the medium (sample), and the angle on which the photon travels towards the detector. Thus, X-ray photons generated at or greater than a specific depth (escape depth) cannot reach the detector. The escape depth depends on the absorbance of the sample and the energy of the emitted X-ray photons (greater in high Z elements). (Polland & Heron, 2008, pp. 40-41; Donais & George, 2018, p. 7)

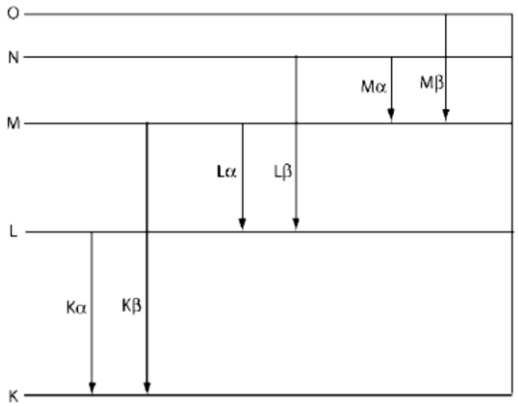

Figure 3.11 X-ray line labeling (Derived from: *(Glascock, 2011, p. 163)*

The detected characteristic lines of each element in the sample under analysis and their intensities are depicted in an XRF spectrum. The XRF spectrum is a bivariate plot of energy in KeV on the x-axis versus signal intensity on the y-axis. (Donais & George, 2018, p. 4) Apart from the characteristic lines of the analyzed materials there are some unwanted or interfering peaks. Such peaks are the Rayleigh and Compton peaks resulting from the material of the cathode of the X-ray source. Also, sum peaks can be observed for high concentration elements.

An XRF spectrometer mainly consists of an excitation source, a filter, transducers, and a multichannel analyzer for data processing (Donais & George, 2018, pp. 13-16; Gigante & Ridolfi, 2013, p. 96). Considering the excitation sources, there have been three main types. The first are the radioisotope sources, which due to safety and inconvenience issues have been replaced by tube sources. The second are synchrotron facilities, which utilize accelerated particle-based X-rays with high spectral purity, high beam intensity and small spot size. However, synchrotron facilities present a set of

disadvantages, such as high cost, and the fact that due to their nature, samples or artifacts to be analyzed have to be transported to the synchrotron facilities. Finally, the most common type of excitation source is the X-ray rube. The X-rays are produced by the impact of electrons against a target. The main parts of an X-ray tube are the filament cathode, the target anode, the tube housing itself, a heater circuit, an accelerator circuit, and the window. The material most often used for the cathode is Tungsten (W), while anodes are made either by Tungsten (W), Rhodium (Rh), Molybdenum (Mo), Chromium (Cr), or Palladium (Pd). (Janssens, 2013, pp. 93-94; Donais & George, 2018, pp. 13-15; Polland & Heron, 2008, pp. 38-39; Schlotz & Uhlig, 2000, p. 4; Liritzis & Zacharias, 2011, p. 111) The X-rays produced by an X-ray tube are the sum of the characteristic lines of the material of the anode and of the *Bremsstrahlung continuum* (Janssens, 2013, p. 93; Polland & Heron, 2008, p. 38)

Filters are used for the optimization of the analysis (Donais & George, 2018, p. 15). The filter produces a low background valley above the filter's absorption. They are thin films made of one or more metals, or plastics. (Shackley, 2011, p. 28) Common materials used for the production of filters are copper (Cu), titanium (Ti), and aluminum (Al) (Donais & George, 2018, p. 16).

The transducers or detectors collect the energy emitted from the sample and convert it to electric signals. There are three main types of transducers; the scintillation counters, the gas-filled detectors, and the semiconductor (solid-state) detectors. (Donais & George, 2018, pp. 16-17; Shackley, 2011, p. 31; Polland & Heron, 2008, p. 43) In wavelength-dispersive spectrometry the first two types of detectors are used, combined in a tandem detector. In the case of energy-dispersive spectrometry semiconductor detectors are used. The two most commonly used semiconductor detectors are lithium-drifted silicon (Si(Li)) and hyper pure germanium (HP-Ge). (Janssens, 2013, p. 95; Donais & George, 2018, pp. 17-18)

There are two instrument design categories used for the XRF spectrometry analysis; the wavelength-dispersive (WD) systems, and the energy-dispersive (ED) systems (Gigante & Ridolfi, 2013, p. 96). In WDXRF systems the X-rays

are separated into bands of different wavelengths, which occurs due to diffraction through a single crystal. The main components of a WDXRF spectrometer are a sample holder, a monochromator, and a transducer. (Janssens, 2013, pp. 95-96; Donais & George, 2018, p. 19) EDXRF systems, on the other hand, measure the energy of the X-ray photons, and count the number of photons with known energies. (Polland & Heron, 2008, p. 42)

Apart from the WDXRF and EDXRF systems developed for laboratory analysis, recent technological developments have resulted in portable XRF (PXRF) systems (Karydas , et al., 2005, p. 28; Gigante & Ridolfi, 2013, p. 97). Portable XRF systems combine a set of unique benefits, such as sensitivity, advanced analytics, small size and weight, and automated and in-situ operations (Liritzis & Zacharias, 2011, p. 110; Donais & George, 2018, p. 21; Janssens, 2013, p. 98; Karydas , et al., 2014, p. 138).

Because the majority of cultural heritage materials have a multi-elemental nature and inhomogeneous composition, an instrument with higher selectivity is necessary for an adequate XRF analysis. (Janssens, et al., 2013, p. 404; Donais & George, 2018, p. 23; Alfeld & Broekaert, 2013, p. 218) The Micro-XRF (μ-XRF) spectrometer is a variant of the EDXRF. The excitation beam focuses on a micro-spot of the sample, providing information about the major, minor, and trace elements. Through μ-XRF it is possible to conduct line or area scanning of a sample. (Janssens, 2013, p. 99; Donais & George, 2018, p. 23; Adriaens, 2005, p. 1505)

While both laboratory and portable XRF systems are non-invasive, non-destructive techniques, they present a series of disadvantages. The data acquired by their application concerns the measuring points of the analysis, thus, changes in the qualitative and quantitative nature of other neighboring areas cannot be excluded. Furthermore, as mentioned before, the data are taken from different depths, or layers of the painting, making the interpretation of the results difficult. (Janssens , et al., 2010, p. 818; Alfeld & Broekaert, 2013, p. 218) These disadvantages are, to some extent, tackled by the utilization of XRF scanners (Sciutto, et al., 2018, p. 277). XRF scanners have been used

extensively in the past, although, because of their non-portable nature and the slow pace on the acquisition of data, it made them insufficient. Recent developments resulted in the manufacture of portable and non-portable XRF scanners, capable of scanning large areas in a few hours. These systems are called Macroscopic X-Ray Fluorescence (MA-XRF) scanners. (Alfeld & de Viguerie, 2017, p. 87) The unique feature of MA-XRF is the production of chemical maps, showing the chemical distribution of elements of the painting (Janssens, et al., 2016, p. 104). Thus, through MA-XRF imaging techniques the visualization is possible of underlying hidden layers of a painting and, the chemical distribution of the pigments used, the detection of any later alterations, the authentication of the painting, and the inspection of its condition (Janssens, et al., 2013, pp. 410-419; Alfeld & de Viguerie, 2017, pp. 87-89; Sciutto, et al., 2018, pp. 279-283).

The majority of XRF analyses on paintings are concerned with the identification of the pigments used by the artist. Pigments are detected through the identification of their key elements. Through this information, one can:

- study the painting techniques and the pallet of the artist,
- trace the provenance of pigments, through the study of trace elements contained in the pigments,
- study the authenticity of the painting, by the detection of key elements with a known production date, like zinc white, or titanium white,
- detect areas where alterations have been made
  (Adriaens, 2005, p. 1504; Janssens & van Grieken, 2004, pp. 195-196; Liritzis & Zacharias, 2011, p. 112).

3.3.1.1.2. Other Techniques

In this subchapter, a number of elemental techniques utilized in the study of paintings will be discussed. The spectrum of elemental techniques, because of significance in the heritage science, is broad. The elemental techniques, applied in a non-invasive way, are used for the identification of the pigments of the artifact. (Siozos, et al., 2017, p. 93) The techniques discussed below will include: Laser Induced Breakdown Spectroscopy (LIBS), X-ray Absorption Spectroscopy, and Particle-Induced X-ray Emission (PIXE).

Laser-Induced Breakdown Spectroscopy (LIBS) is a micro-destructive elemental technique. The application of the technique can be done in situ, while no sampling is required. LIBS can offer qualitative, semi-quantitative, and quantitative data depending on the material on which it is applied. The working principle of LIBS is based on the spectroscopic analysis of a photoemission spectrum in a microplasma, which is generated by means of focusing a nanosecond laser pulse on the surface of the object. (Siozos, et al., 2017, pp. 93-94; Nevin, et al., 2012, p. 340)

X-ray Absorption Spectroscopy (XAS) is a non-destructive technique utilized in combination with Synchrotron Radiation (SR) probes, resulting in Synchrotron Radiation X-ray Absorption Spectroscopy (SR-XAS). The information obtained, by the utilization of XAS, for selected chemical species concerns the quantitative information on the local and electronic structure around the absorber atom. (Bardelli, et al., 2011, p. 3148) The working principle of XAS is based on the absorption of X-rays by the analyzed material near the absorption edge of one of its elements. Through the use of beam-line setups, scanning the surface of the object species-specific maps can be acquired. (Janssens, et al., 2013, pp. 405-406)

Particle-Induced X-ray Emission (PIXE) can be a non-invasive technique, because it can be utilized with an external beam. Despite its advantages, the employment of PIXE is not so widespread, because of the potential risk of damage, caused to the painting surface by the beam. PIXE has many similarities with XRF, although, PIXE uses proton instead of X-rays. (Calligaro, et al., 2015, p. 135) The PIXE techniques are capable of detecting all the elements from sodium (Na) up to uranium (U) (Beck, et al., 2008, p. 1871). There are two different PIXE techniques that are usually utilized in the analysis of paintings; differential PIXE and multiscale PIXE imaging. The differential PIXE technique is used to determine the composition of the paint layers. Due to the increment of the beam energies, data from bigger depths of the paint layers are collected. By the comparison of the different spectra depths, depth profiles of the paint layers can be produced. Multiscale PIXE imaging is a variant of MA-XRF imaging; however, multiscale PIXE imaging has two

advantages compared to MA-XRF. It offers larger X-ray production yield for low atomic number elements, and faster scanning, through the use of magnetic deflection. (Calligaro, et al., 2015, p. 136)

3.3.1.2. Molecular Techniques

Molecular techniques are the techniques providing information about the molecular environments of the material under analysis. This branch of spectroscopic techniques has been used in heritage science since the 1970s for the identification of the chemical composition of the material under analysis, offering information concerning both inorganic and organic materials. (Nevin, et al., 2012, p. 346) The molecular techniques most frequently used are Raman and IR spectroscopies, although many more are gaining space in the analysis of cultural heritage artifacts. Such spectroscopic techniques are the Laser-Induced Fluorescence (LIF), Diffuse Reflectance, Nuclear Magnetic Resonance (NMR), and others.

3.3.1.2.1. Raman Spectroscopy

Raman spectroscopy is an established analytical molecular technique for the investigation of the molecular environment of cultural heritage objects (Vandenabeele, et al., 2007, p. 678; Fotakis, et al., 2007, p. 95; Anglos, et al., 2009, p. 49). The atoms in a molecule or an elemental lattice are connected by chemical bonds. Depending on its complexity (number of atoms composing it), every molecule has a number of vibrational degrees of freedom, called normal vibrations. Each normal vibration corresponds to a frequency, which depends on the atomic mass, the binding forces, the molecular species and the lattice structure. Consequently, each type of molecule has a unique number of bonds and therefore, a specific number of vibrational degrees of freedom. All these properties act as a fingerprint of the molecule and are used for its identification. (Salzer, 2013, p. 66; Larkin, 2011, pp. 8-9; Fotakis, et al., 2007, p. 95) The working principle of Raman spectroscopy is the measurement of vibrational transitions within materials, caused by the inelastic scattering of electromagnetic radiation from molecules (Fotakis, et al., 2007, p. 95).

Scattering can be elastic or inelastic. When an incident monochromatic radiation of given frequency illuminates a sample a portion of incoming photons will interact with the molecule through their oscillating electric field, setting the molecule to a non-stationary (virtual) excited state. As a result of the instability of the virtual state, molecules are decaying instantaneously to the ground state by one of three different processes. (Smith & Clark, 2004, p. 1138; Rai & Dubey, 2018; Fotakis, et al., 2007, p. 99)

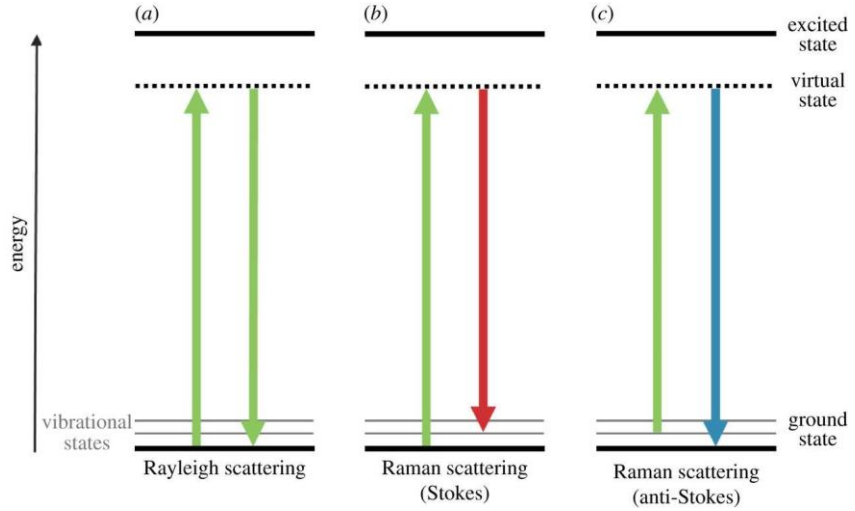

Figure 3.12 Schematic diagram of the energy transitions involved in Rayleigh scattering (a) and Raman scattering (b,c). Raman scattering occurs through the interaction of an incident photon with a molecular vibration mode, gaining (anti-Stokes scattering, blue-shifted) or losing (Stokes scattering, red-shifted) an amount of energy equal to that vibrational mode. Derived from: *(Moura, et al., 2016, p. 3)*.

The majority of the scattered molecules will do so elastically, a phenomenon referred to as Rayleigh scattering (**Figure *3.12*** (a)). In Rayleigh scattering, the excited molecule emits a photon equal to the energy it received by the incident radiation and returns to its ground state. Hence, Rayleigh scattering provides no information about the vibrational energy levels of the molecule. (Smith & Clark, 2004, p. 1138; Fotakis, et al., 2007, p. 99)

For inelastic, or else referred to as Raman scattering to occur, the emitted photon must have lower (Stokes) (**Figure *3.12*** (b)) or increased (anti-Stokes) (**Figure *3.12*** (c)) energy than the Rayleigh photons, thereby generating a set of frequency-shifted Raman photons. However, Raman scattering is far less likely to occur compared to Rayleigh scattering. (Larkin, 2011, p. 17; Smith & Clark, 2004, p. 1138) The Raman spectrum is produced by the spectral

resolving of the scattered light. The Raman spectrum is a plot of the intensity of the scattered light as a function of the frequency difference between the incident and scattered radiation; the frequency difference is called the Raman shift and is expressed in units of wavenumbers (cm^{-1}) (Edwards & Vandenabeele, 2012, p. 52). Not all the vibrational modes of a molecule can be observed through Raman spectroscopy. The modes that change the polarizability of the molecule are Raman active. (Fotakis, et al., 2007, pp. 99-100; Smith & Clark, 2004, p. 1138; Larkin, 2011, pp. 15-18)

Moreover, due to the weakness of the Raman scattering signal, a number of interferences and side-effects occurring can influence it. One such interference is the absorption of the laser light by the sample, reducing thus the number of photons reaching the analyte. This problem can be avoided by the use of a laser source with a different excitation wavelength. (Vandenabeele, 2013, pp. 39-40) Equally important is the interference of the fluorescence. The probability associated with the Raman processes is much lower than the probability of fluorescence emission, which, consequently, can overlap the Raman photons. Therefore, aiming for the solution to this problem several approaches have been applied. One of the most common solutions is the use of a laser with different wavelength, usually of infrared or near-infrared regions, due to the negligible absorption occurring in longer wavelengths. (Fotakis, et al., 2007, p. 101; Vandenabeele, 2013, pp. 40-43)

The analysis of samples employing Raman spectroscopy includes the irradiation of the sample by an excitation source, the collection of the scattered light into a spectrograph, and the recording of its intensity as a function of the wavelength (Fotakis, et al., 2007, p. 102).

The excitation sources are divided into two groups, the continuous wave (CW) lasers, with the most common being the helium-neon, argon, krypton and mixed argon-krypton, utilizing the visible region of the electromagnetic spectrum. (Casadio, et al., 2017, pp. 162-163) Diode lasers, like the gallium, aluminum, and arsenic (GaAlAs) diode, utilizing the near-infrared. When longer wavelengths are necessary a neodymium-doped yttrium aluminum garnet

(Nd:YaG) diode can be employed. (Casadio, et al., 2017, p. 163; Fotakis, et al., 2007, pp. 102-103)

The scattered light is then collected through a microscope. The coupling of a Raman spectrometer with a microscope in 1975 added many advantages to Raman spectroscopy or micro-Raman (μ-Raman) spectroscopy. (Anglos, et al., 2009, p. 50) Apart from the inherent characteristics of Raman spectroscopy, such as molecular specificity, non-destructiveness, high spatial (≤ 1 μm) and spectral (< 1 cm^{1}) resolution, μ-Raman spectroscopy offers the ability for micro-analysis, owing to the very small diameter of the laser beam, which increases the selectivity of the technique. Thereby, the analysis of very heterogeneous samples is possible. (Burgio, et al., 2000, p. 463; Casadio, et al., 2017, p. 164; Smith & Clark, 2004, p. 1140) In addition to micro-analysis, through the focusing of the excitation source, the usage of lower power lasers becomes possible, with the typical excitation power, for very sensitive materials, fluctuating in the range of 0.1 to 5 mW (Casadio, et al., 2017, p. 164; Fotakis, et al., 2007, p. 103). Furthermore, the high numeric aperture of the microscope objectives leads to improvement in the collection of Raman scattering. Additionally, the coupling of the μ-Raman to a motorized stage permits the Raman mapping and imaging. (Casadio, et al., 2017, p. 164) Finally, μ-Raman is a portable technique, therefore permitting the analysis to be conducted in situ (Smith & Clark, 2004, p. 1140; Fotakis, et al., 2007, p. 104).

The analysis of the collected scattered light is done either by a dispersive spectrometer, such as single-channel detectors and multi-channel detectors, either a Fourier-transform (FT-) Raman spectrometer, such as semi-conductor detectors. (Vandenabeele, 2013, p. 62; Casadio, et al., 2017, pp. 164-165) The scattered light, after its collection by the objective lens of the microscope, is filtered for the minimization of the Rayleigh radiation interference, either by an edge, or a notch filter (Fotakis, et al., 2007, p. 103). The interpretation of the Raman spectra is done by cross-checking with spectral reference libraries (Anglos, et al., 2009, pp. 50-51; Casadio, et al., 2017, p. 180). Raman spectroscopy, aside from the qualitative identification of materials, can also produce semi-quantitative data. This can be done by employing mathematical

approaches, such as principal component analysis (PCA) or spectral decomposition. (Casadio, et al., 2017, p. 186)

The contribution of Raman spectroscopy to the analysis of paintings primarily concerns the identification of the pigments present, as well as the binder and varnish (Fotakis, et al., 2007, pp. 106, 111). The analysis of pigments contributes to the understanding of various aspects of a painting. Through the analysis of pigments, the authentication of a painting can be verified. Although most of the pigments used are known since antiquity, some pigments as was mentioned in sub-chapter §2.2.3 were introduced at later dates. (Smith & Clark, 2004, p. 97; Casadio, et al., 2017, p. 190; Fotakis, et al., 2007, p. 106) The identification of such an indicator can lead to a re-estimation of the production age of the painting or prove later additions. Furthermore, the analysis of pigments describes the palette of the artist, which constitutes a very important piece of information, since through the interpretation of the received data the painting technique of the artist can be studied, as well as the potential provenance of the pigments. This information can lead to a better understanding of the techniques used during that period, and of the trade routes of art supplies. (Vandenabeele, et al., 2019, p. 64; Smith & Clark, 2001, p. 98)

Through Raman spectroscopy, inorganic and organic pigments can be identified (Casadio, et al., 2017, p. 189; Fotakis, et al., 2007, p. 106). However, in contrast with inorganic, organic pigments don't produce good quality Raman spectra, since they suffer from the interference of strong fluorescence, making them thus more difficult to be identified (Stuart, 2007, pp. 139-140; Fotakis, et al., 2007, p. 108; Anglos, et al., 2009, pp. 50-51).

A great advantage of Raman spectroscopy is its molecular specificity. As a consequence, through Raman spectroscopy, one can identify and differentiate between materials, and in this case pigments, with the same chemical formula but with different crystalline structures and connectivity. (Smith & Clark, 2001, p. 96; Stuart, 2007, p. 140)

Additionally as concerns the identification of pigments, Raman can also identify the binder and the varnish of a painting (Casadio, et al., 2017, p. 180; Fotakis, et al., 2007, p. 111; Stuart, 2007, p. 158). Although, due to the chemical similarity of many different substances to the same chemical class, such as proteinaceous, polysaccharide, fatty acid, and resinous media, and the fact that they have degraded by aging and environmental conditions, this makes their identification complex (Fotakis, et al., 2007, p. 111).

3.3.1.2.2. Laser Induced Fluorescence Spectroscopy

Laser-induced fluorescence (LIF) is a fluorescence spectroscopic technique employing a coherent monochromatic laser source, in either pulsed or continuous operation (Nevin, et al., 2012, p. 347). Fluorescence spectroscopy is based on the study of fluorophores also called fluorochrome which typically is an organic molecule made up of 20 to 100 atoms. Fluorescent radiation is spontaneously emitted as a consequence of the de-excitation to the ground state of an electronically excited fluorophore (**Figure *3.13***). (Telle & Ureña, 2018, p. 231; Nevin, et al., 2012, p. 347; Atanassova, et al., 2014, p. 5) The technique exploits the fact that each material has a unique fluorescence spectrum through which the identification of the material is made (Atanassova, et al., 2014, p. 5) LIF has wide-spread application in the analysis of cultural heritage materials.

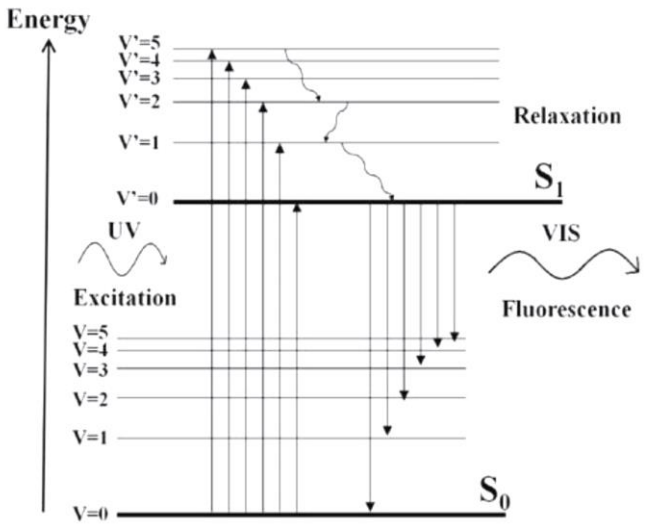

Figure 3.13 Schematic representation of the excitation and de-excitation of a molecule resulting in the emission of fluorescence. Derived from: *(Atanassova, et al., 2014, p. 6)*.

This is due to the analytical advancements of non-destructivity, versatility, selectivity, sensitivity and the ability of real-time analysis (Fantoni, et al., 2013, p. S59). In spite of the different set ups available they all share common components. A typical LIF set up consists of: (1) the light excitation source (laser), (2) the interaction zone of the excitation light with the sample, including light-guiding component, (3) the light analysis components and photon detectors, and (4) the electronic signal acquisition and data analysis system (spectrometer). (Telle & Ureña, 2018, p. 248; Nevin, et al., 2012, p. 347)

The component most usually differentiated between the set ups is the laser source and in more detail its wavelength, with the wavelengths of the laser sources falling in the UV region of the electromagnetic spectrum. (Nevin, et al., 2012, p. 347; Fantoni, et al., 2013, p. S59) According to Anglos et al. (1996, p. 1332) the ability of LIF to employ different excitation wavelengths adds selectivity and versatility to the technique, permitting the utilization of the appropriate wavelength for the analysis of a material, such as varnish or pigments. In addition, the materials of interest in cultural heritage have a broad emission spectrum, leading to the need of detectors with a wide range of detection with most of the usual detectors having a detection range from 200 to 1200 nm and spectral resolution from 0.1 to 10 nm. (Nevin, et al., 2012, p. 347) However, the radiation emitted can be related to the heterogeneities of the sample rather than the specific identification of materials. Furthermore, the absolute identification of materials gets more difficult due to the intrinsic similarities in the emission spectra of many materials. Apart from the difficulty in the absolute identification of materials, LIF is also sensitive to a limited

number of compounds, since not all the materials have a strong fluorescence signal, also the broad emission spectrums, the spectral complexity and the unavailability of databases act cumulatively as disadvantages. (Atanassova, et al., 2014, p. 6; Nevin, et al., 2012, p. 347; Spizzichino, et al., 2020, p. 2)

Despite its disadvantages, LIF with its non-destructive nature, simplicity, speed and the ability to be performed in situ has been used extensively in the study and characterization of cultural heritage materials, since it can give information about the materials used for creating the object (Anglos, et al., 1996; Spizzichino, et al., 2020; Fantoni, et al., 2013; Nevin, et al., 2012).

Concerning its contribution to the analysis of paintings, LIF can give information about the pigments and colorants, the binding medium and the varnish of the painting. LIF can characterize both organic and inorganic pigments. However, in this case, the restriction applies that only fluorescent pigments and colorants can be detected, narrowing in this way the number of identifiable pigments. Some of the pigments emitting intense photons have no very broad spectrum and so are more easily identified include: zinc white (ZnO), titanium white (TiO_2), vermillion (HgS) and cadmium-based yellows and reds. As concerns organic fluorescent pigments commonly detected by LIF, they include: cochineal lakes, sappanwood and hansa yellow. (Nevin, et al., 2012, pp. 348-349)

The binding media of paintings can also be studied by LIF spectrometry, this is due to the fact that some fluorophores associated with protein-based media have been identified. However, the molecular complexity and the difference in the optimum excitation wavelength suggest the need for use of different excitation sources ranging from 300 nm to 700 nm. (Nevin, et al., 2012, p. 350)

The analysis of painting varnishes is usually done by the utilization of the near-UV laser excitation with some exceptions. Among the historical varnishes, only those which are shellac-based can be discriminated easily, since the emissions of the other varnishes have many similarities, not excluding however the identification of other varnishes. (Nevin, et al., 2012, pp. 349-350)

3.3.1.2.3. Diffuse Reflectance Spectroscopy

Diffuse reflectance (DR) spectroscopy is a well-established technique for the analysis of pigments and colorants in works of art (Brunetti, et al., 2017, p. 45; Cosentino, 2014, p. 54; Analytical Methods Committee AMCTB No 75, 2016, p. 5894; Cheilakou, et al., 2009, pp. 114-115; Aceto, et al., 2014, p. 1489). The basic principle of DR is the analysis of the reflected light which has undergone a series of scattering and wavelength-dependent absorption within the material under analysis (Torrent & Barron, 2002, p. 1438). The basic components are a light source, a spectrometer, a probe and two fiber optics and can detect spectra from the near UV (200 nm) to the near IR (1000 nm). (Cosentino, 2014, p. 55) When fiber optics are used the technique is also called Fiber Optics Reflectance Spectroscopy (FORS). However new equipment has greater IR sensitivity permitting the probe of an extended spectral range (up to 2500 nm) (Analytical Methods Committee AMCTB No 75, 2016, p. 5894). The identification of pigments and colorants is done by the analysis of the received spectra and the comparison with spectral databases (Cheilakou, et al., 2009, p. 115). The received spectrum is the result of electronic (in near UV and vis) and vibrational transitions (in near IR) (Analytical Methods Committee AMCTB No 75, 2016, p. 5894; Gulmini, et al., 2013, p. 137). By analysis through DR spectroscopy both qualitative and quantitative data can be produced. However, while the qualitative data can be interpreted easily, the quantitative information is difficult to extract. (Analytical Methods Committee AMCTB No 75, 2016, p. 5895) According to Liang (2012, p. 316), one of the biggest drawbacks of the technique is the lack of comprehensive databases of reference pigments and colorants. The received spectra in most cases describes the diffusely reflected light of a mixture of pigments, rather than single pigments or colorants. Hence, for the identification of pigment mixtures the spectrum has to undergo unmixing to reveal the spectral components of the constituent pigments. (Liang, 2012, p. 316) The spectral unmixing in the case of pigments and colorants is most usually performed by employing the Kubelka-Munk theory which describes the way light transports in a turbid medium (Dupuis & Menu, 2005; Liang, 2012, p. 316; Aceto, et al., 2014, pp. 1490-1491). DR spectroscopy can identify most of the blue, green, white and red pigments, since most yellow and black pigments

are not characteristic enough. Furthermore, in some cases a broad categorization of analyzed binders and varnishes can also be done. (Analytical Methods Committee AMCTB No 75, 2016, pp. 5894-5895)

The advantages that made DR spectroscopy a well-established technique for the analysis of pigments and colorants is the ability to be performed in situ since its lightweight and small equipment size permit easy transportation. Additionally, it is a non-invasive and non-destructive technique adding thus all the advantages of the non-invasive techniques. The analysis requires short acquisition times rendering the technique very fast with good quality spectrum. (Cheilakou, et al., 2014, p. 542; Analytical Methods Committee AMCTB No 75, 2016, p. 5895; Cosentino, 2014, pp. 54-55) Moreover, apart from the point analysis on areas of interest, DR spectroscopy permits the scan of the entire painting offering this way information on the chemical distribution of pigments (Delaney, et al., 2010, p. 584).

Despite its many advantages, DR spectroscopy also has disadvantages. Due to the broad emission of some pigments and colorants in the UV and VIS results to lower fingerprinting ability compared to other molecular spectroscopic techniques (Aceto, et al., 2014, p. 1489; Brunetti, et al., 2017, p. 45). Additionally, studies have proven that the yellowing of the old degraded varnish acts as a yellow filter suppressing the blue reflectance, thus making the identification of blue pigments more difficult. Also, the particle size of the pigments and the presence of dust can affect the position and shape of the reflectance band (Stuart, 2007, p. 160; Liang, 2012, pp. 317-318).

3.3.1.2.4. Other Techniques

In this subchapter, a number of molecular techniques utilized in the study of paintings will be discussed. The spectrum of molecular techniques, because of their significance in heritage science, is broad. The techniques discussed below will be Fourier Transform Infrared (FTIR) spectroscopy and X-Ray Diffraction.

Fourier Transform Infrared (FTIR) spectroscopy is one of the most common molecular spectroscopic techniques employed for the analysis of cultural heritage materials (Stuart, 2007, p. 110). As Raman, FTIR is also a vibrational technique, however, in contrast to Raman for which the active modes require changes in the polarizability have to occur, for FTIR active modes changes have to occur in the dipole moment (Fotakis, et al., 2007, p. 100). Analysis can be conducted in both invasive (depending on the procedure the analysis can be micro-destructive or non-destructive) and non-invasive modes. The analytical procedures in which FTIR can be accomplished are transmission (T), total reflection (TR) and reflection absorption spectroscopy (RAS) (Kouloumpi, et al., 2012, p. 375; Prati, et al., 2017, p. 130). Its major uses in the analysis of paintings concerns the identification of inorganic and organic pigments, binding media, materials of the ground layers and varnishes (Kouloumpi, et al., 2012, pp. 375-376; Stuart, 2007, pp. 126-128; Prati, et al., 2017, p. 130).

X-Ray Diffraction (XRD) spectroscopy has been used extensively for the analysis of cultural heritage materials with crystalline structures (Alfeld & Broekaert, 2013, p. 219; Westlake, et al., 2012, p. 1415). The working principle of XRD is based on the acquisition of constructive interference X-rays which have interacted (diffracted) in the lattice planes of the material under analysis. Constructive interference occurs when the angle of the incident X-rays and the angle of the diffracted X-rays are the same. Consequently, the correlation of this angle with the crystalline material acts as a fingerprint of the specific phase of the material. (Calvo Del Castillo & Strivay, 2012, pp. 95-96; Stuart, 2007, p. 230; Kvick, 2017, p. 649; Janssens, et al., 2013, p. 406; Martin-Ramos, et al., 2017, p. 344) The identification is done through the comparison of the acquired “fingerprint” with databases of already tested crystalline materials (Artioli, 2017, p. 676; Calvo Del Castillo & Strivay, 2012, p. 100). XRD spectroscopy can be conducted both invasively (a sample is required) and non-invasively, providing qualitative and quantitative data concerning crystalline phases of cultural heritage materials (Stuart, 2007, p. 232; Vanmeert, et al., 2019, p. 7154; Cotte, et al., 2018, p. 580; Martin-Ramos, et al., 2017, p. 344).

The applications of XRD spectroscopy on the analysis of paintings is concerned with the identification of inorganic pigments the majority of which is composed of minerals (Stuart, 2007, p. 232; Calvo Del Castillo & Strivay, 2012, p. 100). Through the utilization of XRD the crystalline phase is identified and the lattice parameters and the crystallinity of the pigment are determined. The study of such crystallographic parameters permits the identification of the manufacturing steps of pigments. (Cotte, et al., 2018, p. 580) Furthermore, through XRD spectroscopy the discrimination between materials with the same chemical structure but with different crystalline phases is possible (Stuart, 2007, p. 232; Cotte, et al., 2018, p. 580). Moreover, by the utilization of synchrotron radiation the scanning of areas of the painting's surface can be conducted. Macroscopic X-ray Powder Diffraction Scanning (MA-XRPD) offers direct identification and visualization of crystalline compounds on the painting layers, with its information being complementary to the information extracted by MA-XRF (Alfeld & Broekaert, 2013, p. 219; Vanmeert, et al., 2019, p. 7154).

3.3.2. Separation Techniques

Separation techniques are used for the qualitative and quantitative analysis of complex organic mixtures (Kouloumpi, et al., 2012, p. 377). Among the different separation techniques in existence, mostly the chromatographic techniques (gas chromatography (GC), high-pressure liquid chromatography (HPLC)) and capillary electrophoresis play an important role in archaeometry (Saverwyns & Vanden Berghe, 2012, p. 132; Vieillescazes, et al., 2013, p. 16). The working principle of the chromatographic techniques is based on the distribution of the organic compounds being separated between a stationary phase and a mobile phase (Saverwyns & Vanden Berghe, 2012, p. 132). The stationary phase, which can be of a liquid or a solid nature, is held in the column. The mobile phase, which can be a gas (GC) or a liquid (HPLC), is moving through the column. (Stuart, 2007, p. 296; Saverwyns & Vanden Berghe, 2012, p. 133; Kouloumpi, et al., 2012, p. 377) Depending on the affinity of the organic compounds to the stationary phase, the different compounds are retained to some extent in the column (the retention time of each compound depends on its affinity to the mobile phase), resulting in their separation

(Saverwyns & Vanden Berghe, 2012, pp. 132-133). Chromatographic techniques record the differential retention of the organic compounds of the analyte in the stationary phase. At the end of the column sensitive detectors permit the analysis of the eluded components. (Kouloumpi, et al., 2012, p. 377; Saverwyns & Vanden Berghe, 2012, p. 133; Vieillescazes, et al., 2013, p. 18) Despite the fact that chromatographic techniques are both invasive and micro-destructive, they are characterized by a set of advantages, such as high selectivity, sensitivity and the ability to analyze complex mixtures, which makes them the most common separation techniques employed (Kouloumpi, et al., 2012, p. 377; Saverwyns & Vanden Berghe, 2012, pp. 133-134; Vieillescazes, et al., 2013, p. 22). GC is employed for the identification of lipids, resins, proteins, gums and waxes (Saverwyns & Vanden Berghe, 2012, pp. 136-143; Vieillescazes, et al., 2013, p. 16). While HPLC is employed for the identification of organic colorants and proteins (Saverwyns & Vanden Berghe, 2012, pp. 147-151; Vieillescazes, et al., 2013, p. 16).

Capillary electrophoresis (CE), like chromatographic techniques, is used for the qualitative and quantitative analysis of complex molecules (Stuart, 2007, p. 325; Saverwyns & Vanden Berghe, 2012, p. 151). The working principle of the technique is based on the differential transportation of charged species in an electric field through a conductive medium (Saverwyns & Vanden Berghe, 2012, p. 151). The differential transportation (separation) of the molecules is driven by electrophoretic and electroosmotic forces and depends on their charge and the size of the molecules. CE is an invasive technique although, the required sample volume is very small (0.1-10 nl) (Stuart, 2007, p. 325; Vieillescazes, et al., 2013, p. 26). The type of the detectors at the end of the capillary analyzing the eluded compounds can be optical, electrochemical and mass spectroscopy detectors (Stuart, 2007, p. 325; Vieillescazes, et al., 2013, p. 28). The application of CE in the analysis of cultural heritage materials is limited. However, its advantages, such as the high peak efficiency, the low cost and the few volumes of sample required, make it an excellent technique for the analysis of cultural heritage materials. In the case of paintings, capillary electrophoresis is used for the identification of all chemical classes but waxes, due to their non-ionic nature. In more detail, CE can be used for the

identification of plant gums, animal glues, natural resins and organic colorants (Saverwyns & Vanden Berghe, 2012, p. 152; Stuart, 2007, pp. 326-328; Vieillescazes, et al., 2013, pp. 29-32).

4. Research Methodology

4.1. Goals of Research

The aim of this study is the scientific analysis of two (2) western-European canvas paintings from a series of *Stations of the Cross* to examine their manufacturing technology, to investigate their preservation state, and finally, if possible, to determine their date of manufacture, although it constitutes a secondary aim. The significance of this study lies in the fact that there is no published work on canvas paintings derived from the Stations of the Cross. In addition to the information that will be drawn about the technical details of this category of paintings, such as the materials and techniques used by the artist, the changes that have taken place in later years will be examined for the first time.

In pursuit of specification, clarification and better articulation of the research questions, the specific objectives to be achieved will be outlined below. To fulfill the research aim concerning the manufacturing technology of the two paintings, this study will provide analytical information for each of the painting's layers. In more detail, the questions needing to be answered concerning the manufacturing technology of the two paintings are:

- What is the composition of the varnish?
- What is the composition of the pigments?
- What is the composition of the ground layers?
- Are there any intervention layers?

To achieve the research aim concerning the preservation state of the paintings, this study will provide information regarding the conservation state of the paintings as well as its history in the course of time. The questions needing to be answered concerning the preservation state of the two paintings are:

- What is the preservation state of the paintings?
- Are there any later interventions?
- Are there any later conservation treatments?

Finally, to satisfy the research aim of dating determination, this study will seek and provide information that could be used for the indirect dating of the paintings. The questions needing to be answered concerning the potential determination of the dating of the two paintings are:

- Are there any indirect dating indicators?
- In which chronological periods do the techniques, artistic trends and newer interventions of the two paintings belong?

4.2. Research Protocol

Having established the research goal and the specific objectives required in order to fulfill this aim the next step is to build the research protocol. The main axis of this effort is based on the use of innovative, non-invasive and if possible non-destructive techniques for the analysis of the two paintings. The factors that contributed to the adoption of this type of research are, among others, ensuring the integrity of the object, the exploitation of the ability of these techniques to be applied broadly in various points of the paintings offering thus a plethora of valuable information about the whole objects, the fact that they can be conducted quickly without the need of sample pre-treatment and their versatility.

Since the research questions and the main axis of the research have been set, the next step towards the setting of the investigation protocol is the selection of the analytical techniques to be applied. Initially, it was decided that imaging, elemental and molecular techniques would be used. Through the use of imaging techniques, visible and invisible elements of the paintings will be explored, then, through the use of elemental techniques the inorganic pigments, as well as inorganic elements of the ground layer, which are exposed to the surface of objects will be studied, and finally, through the use of molecular techniques organic materials of the objects such as organic dyes, varnishes and binders will be investigated. In particular, it was decided to use digital photography (DPH), multispectral imaging (MSI), X-ray radiography (XRR), X-ray fluorescence (XRF) spectroscopy, Raman spectroscopy, Laser-induced fluorescence (LIF) spectroscopy and Diffused reflectance (DR) spectroscopy.

However, during the research process it became clear that due to the structural complexity of the objects to be analyzed, which is due to the rich and multi-layered stratification, it would not be possible to draw safe conclusions using only non-invasive techniques. Thus, it was deemed necessary to compliment

the research protocol with a series of non-destructive microscopic techniques. It has to be emphasized that, ideally, the sampling positions should result from the interpretation of the data of non-destructive analysis techniques, which however was not possible due to restrictions on the sampling areas set by the owner and time constraints.

Respecting the principle of non-invasiveness, it was decided to take only two samples from each object that would be used in both microscopic techniques, thus ensuring that as much information as possible is obtained by following non-destructive methods. Through the microscopy techniques, the stratigraphic structure of the samples will be examined in terms of its stratification and the composition of the layers. Drawing conclusions that will help or enable the best interpretation of the data obtained through non-invasive techniques. Therefore, it was decided to use optical microscopy (OM) and scanning electron microscopy coupled with an energy dispersive X-ray detector (SEM-EDS). The following flow chart describes the full investigation protocol (**Figure *4.14***).

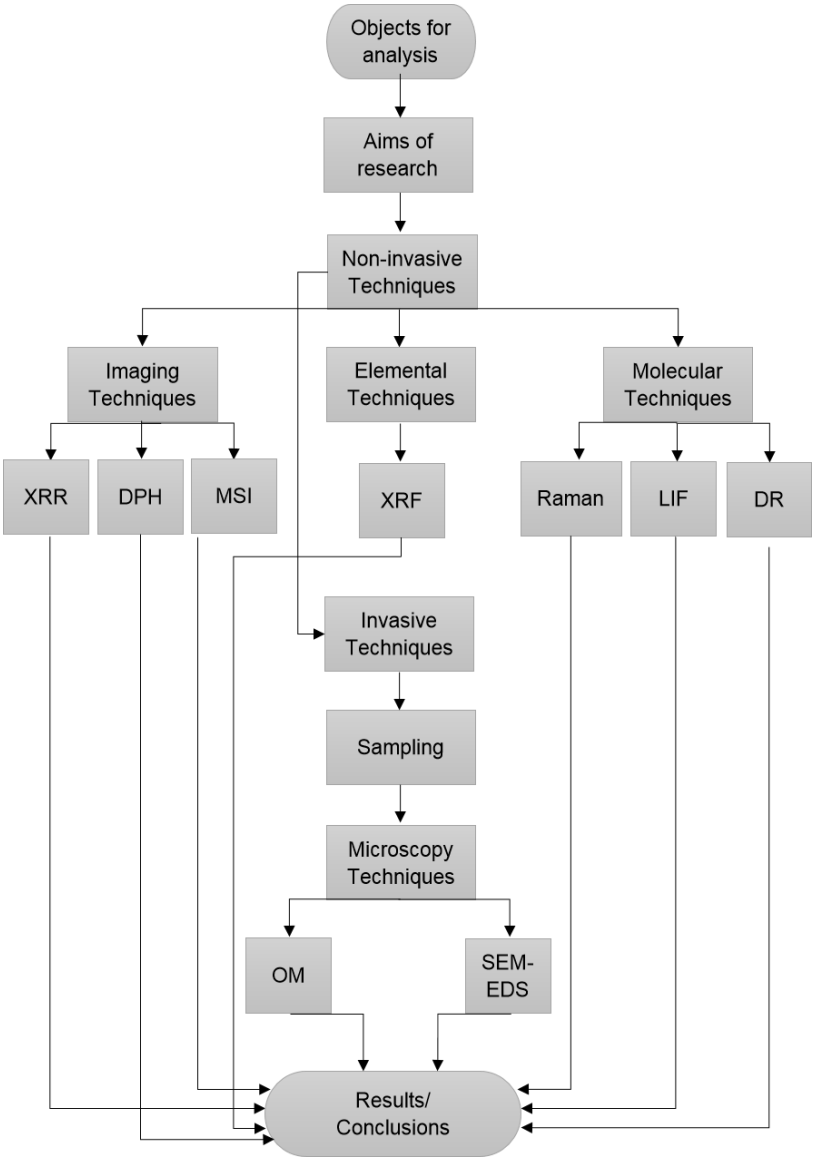

Figure 4.14 The flow chart of the research protocol for the analysis of the two western canvas paintings.

4.3. Digital Photography

Digital photography (DPH) was applied to the two paintings with various apparatus settings and configurations to answer research questions regarding a) the surface characteristics of the paintings b) the composition of the varnish and the pigments and c) the preservation state of the paintings. Through this, artistic details describing the techniques of the artist can be studied, also the preservation state and any later additions can be identified.

The technique was performed in the laboratory of Physicochemical Research at the National Gallery - Alexandros Soutzos Museum in Athens by Panagiotis

Rompakis, Conservator at National Gallery - Alexandros Soutzos Museum. The apparatus for digital photography consisted of a Canon EOS 5D Mark II camera equipped with a Canon EF 24-105 mm f/4 L lens. The operating conditions were: f-stop 4, 11 and 13, ISO-100 and shutter speed from 2.5 to 30 seconds. In the framework of digital photography, ultraviolet (UV) and visible (VIS) spectrum photography were performed. The UV photography was conducted using a UV illumination source (Sylvania Blacklight - Blue, F36W/BLB - T8) at an angle of 45^{o} degrees to the painting. The VIS photography was conducted with two illumination settings, the normal illumination where the light source is positioned at an angle of 45^{o} degrees to the painting, and the tangentially incidental radiation where the light source is positioned at an angle of 5^{o}-10^{o} degrees to the painting. The illumination source for VIS photography was an Osram 64540, 650 W, GX6.35. The final image processing of the acquired photos was carried out using Adobe Photoshop.

4.4. Multispectral Imaging

Multispectral imaging (MSI) was applied on the two paintings in order to answer the questions regarding a) the disclosure of underlying or hidden features of the paintings, such as overpaintings, underdrawings, pentimenti, etc., b) the construction techniques, c) the assessment of the composition of the materials, d) the chemical distribution mapping of the materials and e) the detection of later interventions and past conservation treatments.

The technique was carried out in the National Gallery of Greece Laboratory of Physicochemical Research by Dr. Anna P. Moutsatsou, Conservation Scientist at National Gallery - Alexandros Soutzos Museum. The camera MuSIS™ MS by the Forth Photonics (now DySIS medical) company was used to conduct the multispectral imaging (Forth-Photonics, n.d.). For the process of observation/ analysis using the multispectral camera, the research protocol of the laboratory of physicochemical analyzes of the National Gallery was followed. The protocol includes observation of the object in reflection, transmission mode and in combination of reflection and transmission. The MuSIS™ MS system has spectral responsivity in the range 360 nm (UV) – 1000 nm (NIR) using a CCD

optical detector with seven selectable spectral bands in black & white and colored mode. In particular, the seven spectral bands correspond to the spectra of 390 nm, 500 nm, 600 nm, 700 nm, 800 nm, 900 nm and 1000 nm. Additionally, it provides for the use of the technique of False Color Infrared Imaging (FCIR) in two imaging modes. An FCIR image is a composite image synthesized from combining a color image with an infrared spectral image. In the first mode of FCIR the IR imaging band is 650 - 750 nm, while in the second mode is 750 - 850 nm. The spectral bands are achieved by the use of imaging monochromator and optical filtering. The camera is equipped with a 25 mm lens, capturing images at 1024 × 960 pixel resolution. Since in the context of digital photography an ultraviolet observation was performed, the spectral bands from 500 nm to 1000 nm and the two false-color modes were used. The illumination sources used were two OSRAM Halogen Display/Optic Lamps 650 W with 3400 K color temperature. The camera was controlled by specially developed software through a laptop. The images obtained were later processed through Adobe Photoshop and ImageJ.

4.5. X-Ray Radiography

X-ray radiography was applied to the two paintings to answer research questions regarding a) the invisible technical and artistic characteristics of the paintings, b) the manufacturing techniques of the different layers of the painting, c) their preservation state and d) the presence of later additions and past conservation treatments.

The technique was performed at the laboratories of the Department of Biomedical Sciences of the University of West Attica by Panou Theodoros, Special Technical and Laboratory Personnel of the Sector of Radiology and Radiotherapy. The X-Ray radiography apparatus consisted of the radiological equipment (model CPI-CMP 200 of General Medical Merate SpA) and the digitizer (FCR CAPSULA X of Fujifilm). The settings for analysis of the painting Statio VIII “Jesus and The Women of Jerusalem” were 60 kV high voltage and 6.3 mAs. While the settings for the painting Statio XIII “The Lamentation” were 60 kV high voltage and 7.1 mAs.

4.6. X-Ray Fluorescence Spectrometry

X-Ray Fluorescence (XRF) Spectrometry was applied on the two paintings in order to answer the questions regarding a) the composition of the inorganic pigments and the ground, b) the indirect dating and c) the detection of later interventions and past conservation treatments.

The analysis was conducted at the Institute of Nuclear and Particle Physics of the National Center of Scientific Research “Demokritos”, by Dr. Andreas-Germanos Karydas, Director of Research of the XRF Laboratory. For the μ-XRF analyses a customized model of the ARTAX (Bruker Nano GmbH) portable micro-XRF spectrometer was utilized. The spectrometer probe consists of an X-ray micro focus Rh-anode tube (spot size 50 μm × 50 μm, 50 kV, 0,6 mA, 30 W maximum power consumption with 0,2 mm Be window thickness) and a poly-capillary X-ray lens as a focusing optical element that offers a focal distance of 21.2 mm and a spatial resolution in the range 40 μm – 80 μm, when the unfiltered tube radiation is used as an excitation X-ray beam. The X-ray detection chain consists of a thermo-electrically cooled 10 mm^2 silicon drift detector (X-Flash, 1000 B) with FWHM equal to 146 eV (at MnKα and 10 kcps) coupled with a digital signal processor. The colored CCD camera that is attached to the spectrometer head can offer live documentary images of the analyzed spot, whereas together with a dimmable white LED for sample illumination and a laser beam indicator, the reproducible positioning of the measuring probe with respect to the analyzed surface is guided. Three stepping motors coupled with the spectrometer head allow three-dimensional movement for elemental mapping and precise setting of the analysis spot at the focal distance of the poly-capillary lens. (kantarelou, et al., 2015, p. 1789; Kantarelou, et al., 2011, p. 682) In the analysis of the two paintings, 96 point, 8 linear and 4 area scanning analyzes were performed. The point analyzes were performed at the following operational conditions: high voltage set at 50 kV, current of 600 μA and the collection time for each measurement was 100 seconds. The obtained spectra were later processed and evaluated through the PymCa software (Sole, et al., 2007).

4.7. Raman Spectroscopy

Raman spectroscopy analysis was performed on the two paintings to answer the questions regarding a) the composition of the organic and inorganic pigments, b) the composition of the binding medium, c) the composition of the varnish and d) the identification of later anachronistic additions.

The technique was carried out in the research laboratories of the Division of Laser Interactions and Photonics of the Institute of Electronic Structure and Lasers (IESL) part of the Foundation for Research and Technology-Hellas (FORTH) by the Dr. Aggelos Filippidis, Post-Doctoral Fellow at IESL-FORTH and Maria Spanoudaki, chemistry student at the University of Crete. A mobile Raman micro-spectrometer (JY Horiba HE 785) was employed for the non-invasive analysis of the two paintings. Excitation at 785 nm was provided by a cw (continuous wave) diode laser, coupled with a fiber optic to an optical head. A light-emitting diode (LED) and a high-resolution colour camera (video microscope) offer a very clear view of the area under investigation, necessary for positioning the beam on individual pigment particles or particle aggregates. The scattered radiation was collected through the objective lens, passes through an edge filter that cuts off Rayleigh scattering, and was focussed into an optical fiber that is fed into a compact spectrometer (BWTEK, Exemplar Plus), which provides spectral coverage in the range of 100 - 3360 cm^{-1} at a spectral resolution of about 8-10 cm^{-1}. During analysis the power delivered by the laser beam on the sample surface was adjusted to 8 mW and the objective lens 20x. Typical exposure time was 30 s, and spectra reported corresponded to an average of 2 consecutive scans on the same point. In total, 29 point analyzes were performed.

4.8. Laser Induced Fluorescence Spectroscopy

Laser-Induced Fluorescence Spectroscopy analysis was conducted on the two paintings to answer the questions regarding a) the composition of the

fluorescent organic and inorganic pigments, b) the composition of the binding medium and c) the composition of the varnish.

The technique was implemented in the research laboratories of the Division of Laser Interactions and Photonics of the Institute of Electronic Structure and Lasers (IESL) part of the Foundation for Research and Technology - Hellas (FORTH) by Dr. Olga Kokkinaki, Post-Doctoral Fellow at IESL-FORTH and Vasiliki Straganioti and Evaggelia Kapourani, chemistry students at the University of Crete. A Q-switched KrF Excimer laser beam (at 248 nm) was focused weakly d, perpendicularly, on the surface of the paintings (irradiation area almost 0.08 cm^2) at very low laser fluence (approximately 0.3 mJ cm^{-2}). The paintings were placed on the surface of an optical table and the selection of the irradiation areas was performed manually, by removing the paintings along the x-y axis on the optical table surface (maximum size of the painting to be analyzed is almost 70 cm x 70 cm). The fluorescence emission was collected through a telescopic lens – optical fiber system and transferred into a portable spectrometer (Avaspec 2018L), operating at 172-1100 nm, which was connected to a laptop via USB cables. Data acquisition was controlled via Avaspec software. All the recorded LIF spectra, corresponding to a single point on the painting, resulted from the average of 100 single-shot spectra. In total, 86 point analyzes were performed.

4.9. Diffuse Reflectance Spectroscopy

Diffuse Reflectance Spectroscopy analysis was executed on the two paintings to answer the questions regarding a) the composition of the organic and inorganic pigments, b) the composition of the binding medium and c) the composition of the varnish.

The technique was implemented in the research laboratories of the Division of Laser Interactions and Photonics of the Institute of Electronic Structure and Lasers (IESL) part of the Foundation for Research and Technology - Hellas (FORTH) by Dr. Sophia Sotiropoulou, research associate at IESL-FORTH and Marilena Konstantinou, chemistry student at the University of Crete. A portable

diffuse reflectance spectrometer hybrid instrument (hybrid LMNTII+), developed and constructed at IESL-FORTH, was used for the study of the two paintings. The instrument consisted of two modules that used the same optical bench. An external halogen tungsten lamp (OSRAM DECOSTAR 35, 10 W), was used for illuminating the object surface. The reflection from the surface part with a diameter of 2 mm approximately, was collected by means of a plano-convex lens (f = +75 mm) and transmitted via an optical fiber to the spectrometer unit (Avaspec-2048-USB2, Avantes). To achieve broader spectral coverage a low-resolution spectrometer was utilized, with a detection range from 200 - 1100 nm and a resolution of 1.4 nm approximately. However, the actual usable range of the diffuse reflectance spectra is limited from 380 to 950 nm due to the reduced sensitivity of the detector and the low intensity emission of the lamp in the UV spectral range. The calibration of the spectra was performed using a Spectralon® Diffuse Reflectance Standard. The halogen lamp along with necessary optics and a miniature CCD camera are integrated with a light-weight optical probe head. The probe head of the instrument was mounted on an XYZ translation stage. The camera offers a magnified view of the object surface during analysis and permits accurate aiming at the sample area with the aid of a cross-hair indicator superimposed on the image. The instrument fits in a compact case (dimensions of 46 x 33 x 17 cm^3) and weighs less than 9 Kg. Instrument operation and spectra acquisition are fully controlled via a custom-made software. In total, 54 point analyzes were performed.

4.10. Sampling

The taking of cross-sectional samples was deemed necessary in order to clarify the stratigraphy of the two paintings and the composition of the underlying layers, thus leading to a better interpretation of the analytical results.

The sampling was carried out in the Laboratories of Physicochemical Research of the National Gallery - Alexandros Soutzos Museum, by Agni-Vasileia Terlixi, conservation scientist of the National Gallery - Alexandros Soutzos Museum.

A total of four (4) cross-section were taken from the two paintings, two from each painting.

The samples were taken under a stereomicroscope from already damaged areas on the borders of the surface with the use of a micro-scalpel. At the same time, all samples, were carefully labeled and documented with all possible means (digital recording of the sampling point, photographic recording of the samples and its color were made).

Before observation with microscopic techniques, the samples had to be embedded in the mounting material (polyester resin Neotex). The polishing of the embedded samples was done by means of a Struers polishing wheel (Labopol 5) and successive use of various grit sized (200, 500, 1000 and 1200) silicon carbide papers.

Each sample was used in both microscopic techniques, ensuring in this way the minimum invasiveness.

4.11. Optical Microscopy

Optical Microscopy was applied on the two paintings to answer the questions regarding a) the stratigraphic composition of the paintings (in particular, the exact sequence of the different layers, the thickness of layers, the color/size/shape of the particles and anomalies in stratification, such as layer discontinuities, cracking and losses) b) the painting techniques, c) the preservation state, d) the detection of later additions, such as overpaintings and new varnish layers and e) the indirect dating of the paintings.

The optical microscopy observation was conducted in the laboratories of physicochemical analyzes of the National Gallery - Alexandros Soutzos Museum, by Agni-Vasileia Terlixi, conservation scientist of the National Gallery - Alexandros Soutzos Museum.

The apparatus for Optical microscopy consisted of a Leica DM/LM microscope equipped with a digital infrared camera DC 300 F and an inset high-pressure mercury lamp (500 W)

Observation of the samples using visible (VIS) and ultraviolet (UV) radiation was performed in a reflected light configuration in different magnifications, ranging from X50 to X200. For the application of Ultraviolet Fluorescence Microscopy and the observation of the inherent (primary) fluorescence of the materials used in the various layers of the cross sections, filter cube A of LEICA with excitation at 340 -380 nm and suppression at 425 nm was used (Terlixi, et al., 2010).

4.12. Scanning Electron Microscopy – Energy Dispersive X-Ray Spectroscopy

The application of Scanning Electron Microscopy on the two paintings was implemented to answer the questions regarding a) the stratigraphic composition of the painting samples, b) the elemental composition of all the sample layers, c) the preservation state, d) the detection of later additions and conservation treatments and e) the assessment of the dating of the two paintings.

The SEM-EDS analysis was applied at the Laboratory of Archaeometry of the University of Peloponnese, at the Department of History, Archaeology and Cultural Resources Management in Kalamata by Dr. Eleni Palamara, Post-Doctoral fellow at the University of Peloponnese. The samples were analyzed by a scanning electron microscope (type JEOL SM-6510LV) coupled with an Oxford Instruments Energy Dispersive Spectrometer (type 250 X-ct systems). The analytical data was obtained by INKA software. The point assays were performed in a low vacuum to avoid the effects of the electric charging of the samples, furthermore, by gold or carbon coating the samples, the technique would be described as destructive (Genestar & Pons, 2005, p. 270; Antonopoulou-Athera, et al., 2017). The samples were mounted onto a specimen holder and a double-sided carbon tape was used, which improves

conductivity and permits analysis. The operating conditions were: 20 kV accelerating voltage and with a count time of 60 seconds with the observation and analysis to be performed in various magnifications from X100 to X1500 in back-scattered electron mode. Digital images and spectra emerged from the analysis of the samples. The images were then processed by Adobe Photoshop, while the spectral data normalized to 100% was expressed in elemental weight percentage (wt. %).

5. RESULTS AND DISCUSSION

5.1. Statio VIII “Jesus and the Women of Jerusalem”

5.1.1. Digital Photography

Digital photography provided important and useful information regarding the study of the artist’s techniques and the surface characteristics of the painting which lead to a better understanding of its preservation state, with the detection of later additions or alterations.

Starting with the analysis of the picture taken in the visible part of the electromagnetic spectrum with the illumination positioned at an angle of 45^{o} degrees to the painting (**Figure 5.15**), it is observed that the artist used a wide variety of colours as well as techniques in creating the painting. Moreover, from the way in which the pigments were applied, and also the structure of the painting's scene, with its structural discontinuities, such as its disproportions or the strange proportions or even the absence of body parts of the figures, raise suspicions of overpaintings.

Figure 5.15 Statio VIII “Jesus meets the Women of Jerusalem”, under VIS illumination at 45^{o} (photo credit: Rompakis, Panagiotis, National Gallery - Greece).

The colour of the sky varies in different hues of blue, starting from dark blue on the edges of the painting, reaching very light blue in some areas. However, these changes were abrupt and do not appear to have been intentional or deliberate.

The above observation may be justified with the assumption of the partial removal of the varnish, which would mean that the varnish was removed while the frame was not removed. Also, in the area between the upper arm of the cross and the yellow cape of the left guard, the blue area is more vibrant in some places, especially in the left corner of the upper arm of the cross. Such areas were found scattered in the area of the sky. Another such area is located to the left of the left guard's cape. Finally, there were various areas of the sky that were covered by a golden pigment.

The cloud is the element that occupies most of the composition. Its colour presents very large differentiations and ranges from white, pale-yellow, gray shades, light blue, green and purple. It seems that the area of the cloud had received numerous and widespread over-paintings. Therefore, it is not easy to indicate which of all the shades is authentic. The purple areas next to the flag may be considered as overpaintings, also the greenish areas on both sides. Much of the cloud area is covered by a pale-yellow hue. The fact that in some places the underlying colour is visible but also that it had not been spread evenly (the painter's touches were strongly visible) lead to the conclusion that these may be overpaintings. The blue area to the right of Jesus maybe be considered as a later addition, which supposedly is part of the cloud.

The ground varies in shades from green, brown, red to black. Despite its homogenous appearance, there were many and strong indications of overpaintings. One such indication is the rock on the left of the painting, which covers a big part of the right hand of the kneeling woman. Additionally, the ground in the area where the three small forms were located does not seem to follow the slope and had a different height.

Jesus which is the central figure of the painting seems to have received extensive overpaintings and alterations. His characteristics were not clear and the distribution of colours is not uniform and even, while, the design of His garment cannot be observed. His halo is irregularly shaped and the thorny wreath is only observed partially. The body of Jesus present vivid colour differentiations with no clear indication of the authentic parts. Moreover, Jesus' body present

discontinuities with some body parts missing. In particular, the right palm and sole of Jesus were not shown, while His left palm is vaguely visible. The cross also presents indications of overpaintings and alterations. Its colour presents abrupt changes with some of them which had clear outlines, also the horizontal beam of the cross is larger towards the side facing the ground.

In the same way, the lower part of the tunic of the left soldier is disproportionately high in relation to his body and legs. He also seemed to have two left hands (**Figure 5.16**); the first is the one holding the sword and the second is between the body of the guard and the upper arm of the cross. Concerning the right soldier, a large part of his left hand does not appear, while his left leg does not look natural; it does not harmonize with the lower part of his tunic and seems to overlap by the arm of the cross. Parts of his tunic, such as the two lower sides, seemed to have been overpainted. It could be seen that on both sides the pattern with rhombuses had been erased (**Figure 5.17**), and maybe these overpaintings act as an aesthetical reconstruction. Also, after a closer observation of the flag, becomes apparent that the part of the flag from the elbow of the soldier and above, along with the pole of the flag were overpaintings (**Figure 5.18**). This conclusion leads to the observation of the difference of the application, with the colour of the sky being visible in many cases, and the difference on the texture between these areas. The kneeling woman on the left of the painting had a vivid colour differentiation on her neck and chest, maybe as part of a later alteration, while her blouse had some intense blue touches while the rest of her blouse is darker in colour. These touches seem to be of better quality than the dark blue colour, and so an assumption could be made that the dark blue colour may be an overpainting. The head of the male figure wearing the green garment seemed to not have a paint layer, leaving as the last layer the red-coloured layer of preparation.

Figure 5.16 Statio VIII "Jesus meets the Women of Jerusalem", detail depicting the two left hands of the left soldier (photo credit: Rompakis, Panagiotis, National Gallery - Greece).

Figure 5.17 Statio VIII "Jesus meets the Women of Jerusalem", detail depicting the areas of overpainting on the lower part of the right soldier's tunic (photo credit: Rompakis, Panagiotis, National Gallery - Greece).

Figure 5.18 Statio VIII "Jesus meets the Women of Jerusalem", detail of the flag depicting areas of the sky clearly visible under the flag (photo credit: Rompakis, Panagiotis, National Gallery - Greece).

Figure 5.19 Statio VIII "Jesus meets the Women of Jerusalem", detail depicting (1) the black triangle to the right of Jesus' knee, and (2) the light-blue irregular shape below the right soldier (photo credit: Rompakis, Panagiotis, National Gallery - Greece).

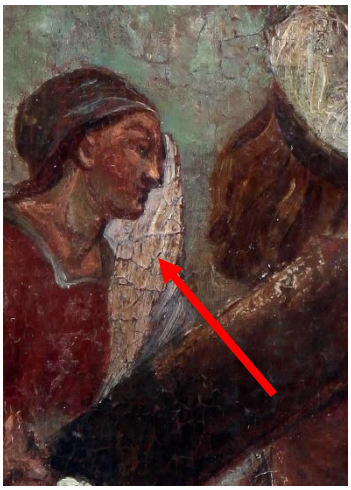

Figure 5.20 Statio VIII "Jesus meets the Women of Jerusalem", detail depicting the white irregular shape to the right of the standing female figure on the left of the painting (photo credit: Rompakis, Panagiotis National Gallery – Greece).

Finally, the three figures on the right side of the painting were depicted with very few details. Their facial characteristics were abstract, while the left side of the tunic of the female figure in the front is brown and the right is light-purple in colour. Apart from these observations, the painting carries some details which cannot be attributed to any figure or the background. Such examples were the black triangle to the right of Jesus' knee, the light-blue irregular shape (**Figure 5.19**) below the right soldier and the white irregular shape (**Figure 5.20**) to the right of the standing female figure on the left of the painting.

As concerns the preservation state of the painting, it is characterized as poor. Starting with the canvas of the painting, at least two different types of canvas were presented; the first on the top left corner and the second on the bottom right corner of the painting. The key difference between them is the weave density and fiber thickness. These results suggest the assumption that the painting was relined. Additionally, both the preparation and the paint layer present many losses. In the first case, they reveal the canvas, while in the second case they reveal the red-coloured preparation layer.

Besides the surface damage, areas, where grouting was done as a previous restoration treatment, were located on the surface of the painting. The first is located to the right of the flag, while the second on the area of the sky right above the upper arm of the cross. Later additions or alteration may also be considered on the area in the bottom right corner.

Figure 5.21 Statio VIII "Jesus meets the Women of Jerusalem", under VIS illumination at 45^{o}, rear view (photo credit: Rompakis, Panagiotis, National Gallery - Greece).

The frame and the backside of the canvas could be observed on the rear view of the painting (**Figure 5.21**). The frame had a good preservation state with only some surface damage. On its right an inscription could be observed, with the number 29 written. However, only the number 2 is clearly visible. The edges of the canvas had many free fibers, while the main body is characterized by intense weave distortions, gaps between the fibers and the presence of a substance resembling wax.

The pictures taken in the visible part of the electromagnetic spectrum with illumination positioned at an angle of 5º degrees to the painting will be studied afterward (**Figure 5.22**). During the study of the painting under tangentially incidental radiation the intense relief, the cracks and the bad preservation state of the surface became apparent.

Figure 5.22 Statio VIII “Jesus meets the Women of Jerusalem”, under VIS illumination at 45º (photo credit: Rompakis, Panagiotis, National Gallery - Greece).

After the analysis of the picture it is observed that the intensity of the relief is limited to the perimeter of the painting due to the stretcher that supports it. Moreover, the differentiation of the crack network indicates the presence of materials of a different nature, of materials applied in a different period (later additions) and the presence of materials added as conservation treatments (groutings).

In more detail, the area of the sky presents an uneven cracking network, with many areas presenting local cracking patterns. The cracking network in the middle of the sky had a lower profile than the sides, with some areas presenting no cracking network. These areas right above the cape of the left soldier and to the right of the upper arm of the cross constitute areas of grouting.

The area of the cloud is characterized by great differentiations on the relief. Starting from the left side, the relief right above the male figure wearing the green garment is very low due to the existence of the stretcher which supports it, continuing to the right, the pattern of the canvas becomes apparent. On the right of the female figure, the relief and the cracking network get more intense, with impasto brush strokes observed on the contact of the cloud with the left soldier. The upper part of the cloud, due to the support of the stretcher, bore a low relief,

with some parts of it having been applied with the technique of impasto. On the center of the painting the cracking network is very intense, with the climax of the relief located on the area where the soldier's sword ends. On the right side, areas without relief were identified, such as in the case of the areas of the sky, which had grouting. In particular, the area to the right of the flag may be considered as a later addition (**Figure 5.23**).

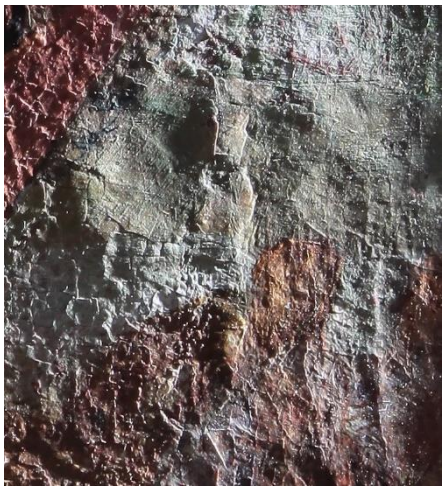

Figure 5.23 Statio VIII "Jesus meets the Women of Jerusalem", detail depicting the area of the sky, where grouting treatment is observed (photo credit: Rompakis, Panagiotis National Gallery – Greece).

The relief of the ground is relatively smooth, while the crackle is characterized by large pieces. The area between Jesus and the kneeling woman, where the cracking network looks similar to that of the sky and cloud constitutes an exception.

As concerns Jesus, His body could be divided into two distinct major areas, the left and the right side. On the left side of His body, the relief is intense and the paint was applied with the technique of impasto. On the right side, the relief is lower and the pattern of the canvas had become visible in some areas. Although, the area of the chest presents intense relief on both sides. Furthermore, there is a strong differentiation in the network of cracks (shape, size) from colour to colour (**Figure 5.24**). The cross had a relatively even cracking network, with the exception of three areas where a grouting treatment could be observed. These areas were located on the left, upper and right arm of the cross.

Figure 5.24 Statio VIII "Jesus meets the Women of Jerusalem", detail of the body of Jesus, where the intense relief of His garment is depicted (photo credit: Rompakis, Panagiotis, National Gallery – Greece).

The relief on the left soldier is smooth while an intense cracking network was found in the areas of the sleeve, face and left hand. The relief on the right soldier and the flag is uniform, while the crackle is characterized by small pieces. Additionally, on the left side of his tunic the pattern of the canvas becomes visible. As concerns the kneeling woman, the relief of her skirt differentiates on the bottom, where large pieces of crackle were presented. The blouse and the scarf of the woman had received applications of the technique of impasto, in contrast with her other parts. The female figure is characterized by the small and uniform size of her crackle. Moreover, the highlight on her right sleeve, which had been applied with the technique of impasto may be considered as a later addition. Finally, the relief of the three figures on the right of the painting presents intense differentiations. Right next to the left leg of the right soldier a very intense area is observed. Additionally, two spots where grouting treatment was applied were located in the same area.

The study of the painting "Station VIII" is completed through the technique of digital photography with the analysis of the photograph carried out using ultraviolet illumination (**Figure 5.25**). The study of the surface of the painting using UV radiation revealed hidden pictorial characteristics, the many later alterations or additions and the bad preservation state.

The painting does not present a uniform fluorescence coming from the varnish layer. On the contrary, the painting's fluorescence is associated with local characteristics; this results in the assumption that the varnish was removed either totally or partially. Fluorescence analysis of the individual forms will follow.

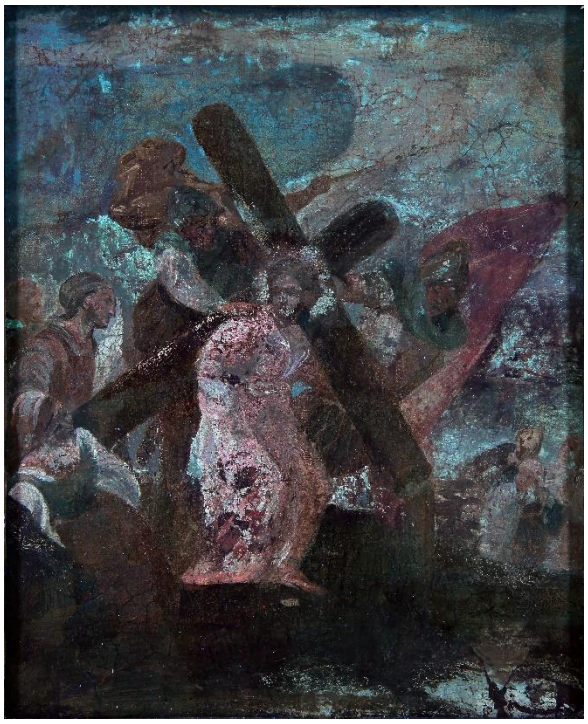

Figure 5.25 Statio VIII "Jesus meets the Women of Jerusalem", UV fluorescence photography at 45º (photo credit: Rompakis, Panagiotis, National Gallery - Greece).

The fluorescence of the sky is uneven. Starting from the edges, the areas which were depicted with a dark yellowish colour may be considered traces of remaining varnish. These areas of varnish were located in areas which were covered by the frame. This leads to the assumption that the removal of the varnish was made with the frame in position. Furthermore, through the comparison of the UVF image with that taken in the visible part of the spectrum, it is possible to detect five different colours associated with the blue pigments composing the sky's colour (**Figure 5.26**). Through the study of the ultraviolet image it is possible to discriminate that overpaintings or retouchings had been applied historically to the painting. There is no clear indication stating which, if any, of these colours constitutes the original part of the painting. As overpaintings/retouchings may be considered the dark areas of the sky, along with the areas observed as greenish and dark blue.

The fluorescence of the cloud, as in the case of the sky, is uneven. The area of the cloud had received many alterations due to overpaintings and retouchings, which were visible through observation with UV light.

VIS UVF

Figure 5.26 To the left: part of the sky in the visible part of the electromagnetic spectrum. To the right: part of the sky in the UV part of the electromagnetic spectrum. Fluorescence variations resulting from the presence of different blue pigments were observed (photo credit: Rompakis, Panagiotis, National Gallery - Greece).

To the left of the painting, on the area above the female and the male figures, three different types of overpaintings could be detected. As overpaintings may be considered the dark greyish and yellowish areas, as well as the area producing the intense greenish fluorescence. Continuing towards the right side of the painting, overpaintings may also be considered within the areas under and above the right hand of the right soldier, also the dark areas to the right of the flag. As concerns the rest of the cloud, it could be observed that the pink (yellowish in the visible areas) were overlapping a colour which is producing intense blueish fluorescence (**Figure 5.27**).

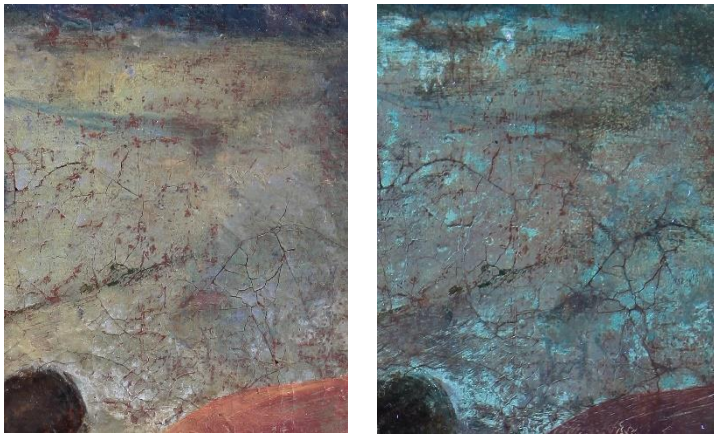

VIS UVF

Figure 5.27 To the left: part of the cloud above the flag in the visible part of the electromagnetic spectrum. To the right: part of the cloud above the flag in the UV part of the electromagnetic spectrum. Fluorescence variations resulting from the presence of different white pigments. Also, the overlapping of a colour producing intense fluorescence photo credit: Rompakis, Panagiotis, National Gallery - Greece).

Overpaintings/retouchings may additionally be considered within the dark yellow areas, mostly found on the upper part of the cloud. Finally, the red (on the visible spectrum) spot above the flag constitutes an area of interest. This spot, which

presented as very dark red in UV, absorbs differently to the other red areas (ground).

The ground in most of its entirety does not present fluorescence. The exception is the area on the bottom of the painting where an intense white fluorescence is observed (**Figure 5.28**). These areas cannot be linked with any specific surface characteristic observed in the visible part of the electromagnetic spectrum and may be associated with later additions. Moreover, the surface damage, depicted in red colour in the visible part of the spectrum, had become apparent. Furthermore, the upper part of the rock on the left of the painting and the area bellow the three figures on the right of the painting present linear areas of fluorescence, probably due to an underlying fluorescent layer.

VIS UVF

Figure 5.28 To the left: part of the ground in the visible part of the electromagnetic spectrum. To the right: part of the ground in the UV part of the electromagnetic spectrum. The right image has an area with intense fluorescence that corresponds to an area that in the visible part of the spectrum (left image) is displayed as pale yellow. Also, the black area is a point of later addition. Finally, in the upper part of the image there is a crack of the upper painting layer and the existence of a fluorescent underlying layer (photo credit: Rompakis, Panagiotis, National Gallery - Greece).

Jesus' body presents a great variety of different fluorescence hues. Through observation in UV, His halo is observed to extend beyond the observable halo in the visible part of the spectrum. Also, over His head, some lines with high UV absorbance could be observed. His face produces uneven fluorescence, with some parts (mostly the highlights) which produced intense fluorescence, in contrast with others. Continuing, the body of Jesus bore many different hues of fluorescence which abruptly alternate, leading to the conclusion that they were not done intentionally by the artist. Considering the results of UV photography there is no clear indication on which parts were original. However, the bark areas could be considered as overpaintings, as well as the purple (**Figure 5.29**). Concerning the cross, on its upper arm the transparency of the edges, as well as, the strokes of paint could be observed, while on the center of the arm some black lines were observed. The right arm presents no fluorescence, while dark areas on its bottom which may be considered as overpaintings. Continuing on the bottom arm of the cross, based on its fluorescence, it could be divided into four areas. The first is on the right side of the arm and presents similar fluorescence. The second is the black area on the contact of the cross with the kneeling woman which does not produce any fluorescence and may be considered as overpainting. The third produces weak fluorescence and is located right next to the black area. This third area is also suspected of being overpainted. The last and fourth area is the intense brown area which bore areas with intense white fluorescence.

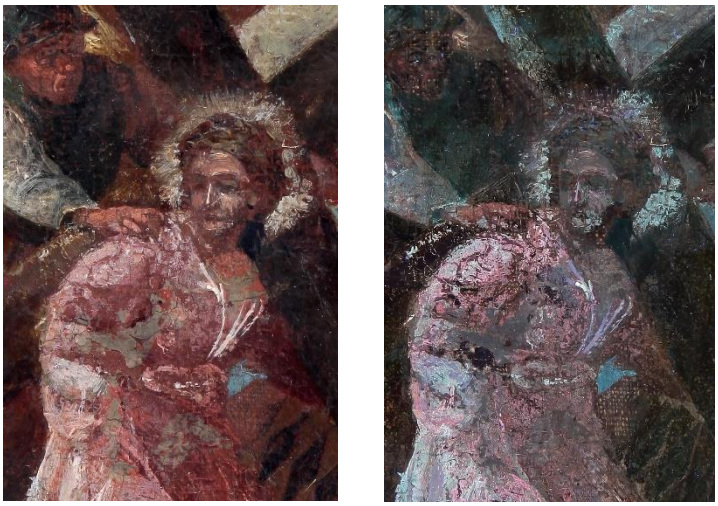

VIS UVF

Figure 5.29 Part of the body of Jesus on the visible part of the electromagnetic spectrum (on the left) and on the UV part of the electromagnetic spectrum. By the comparison between the two images the extended halo, the different fluorescence hues and the overpaintings of this area could be observed (photo credit: Rompakis, Panagiotis, National Gallery - Greece).

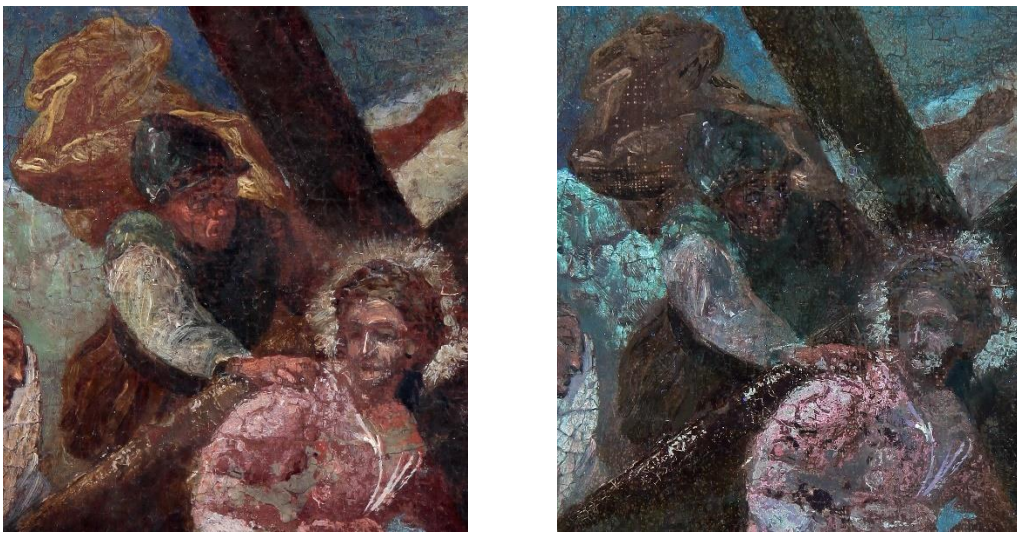

VIS UVF

Figure 5.30 To the left: the upper part of the left soldier in the visible part of the electromagnetic spectrum. To the right: the upper part of the left soldier in the UV part of the electromagnetic spectrum. The canvas pattern is observed, as well as the later interventions, such as the second left hand and the overpaintings on the cape (photo credit: Rompakis, Panagiotis, National Gallery - Greece).

The most important information, derived from the observation of the left soldier under UV light is the overpainting areas, presented with dark colours, on his face, cape, right hand and his “second” left hand. Furthermore, the pattern of the canvas becomes visible at various points of his cape, face and “second” left hand (**Figure 5.30**). On the left hand holding the sword, no fluorescence is observed, although on the external point of contact of the hand with the cross, a pink area is detected. This pink area seems to be part of the sleeve of the soldier. However, the right sleeve of the soldier is greenish, leaving the pink area without attribution to a person. The observation of the two left hands, along with the detection of the pink area lead to the assumption that a very extensive overpainting had taken place in this area.

Concerning the right soldier, after the observation under UV light, the assumption regarding the large overpainting on the area of the flag gets confirmed. In addition, it seems that overpainting could be considered within the area of the flag below the left leg of the soldier. Moreover, it is observed that the right part of the soldier had more intense fluorescence than the left side, maybe due to the presence of the fluorescent pigment used to highlight the armour and the helmet.

VIS UVF

Figure 5.31 To the left: the right soldier in the visible part of the electromagnetic spectrum. To the right: the right soldier in the UV part of the electromagnetic spectrum. The fluorescence of the flag varies from region to region, indicating the overpainting areas, and the intense fluorescence of the right side of the soldier is also observed (photo credit: Rompakis, Panagiotis, National Gallery - Greece).

Moreover, on the left side of the armour, as well as on the right part of the tunic the canvas pattern becomes visible, while overpaintings could be observed in various areas of the armour, the helmet and the scarf. Similarly, the left hand of the soldier is also an overpainting (**Figure 5.31**).

The observation of the kneeling woman reveals information not easily detectable in the visible part of the electromagnetic spectrum. Such information includes the differentiations of the fluorescence on the area of the face and the neck, where this area could be divided in three sub-areas (**Figure 5.32**).

The first is the face which is presented with dark colours, an indication of overpainting. The second area is the upper part of the neck which is characterized by its intense fluorescence. Finally, the third area is the area near the right shoulder of the woman which does not produce fluorescence. In regard to the white shirt of the woman, the right sleeve appears very different compared to the left sleeve. The right sleeve had a uniform fluorescence with only an area to be presented in a darker colour, while the left sleeve presents various fluorescence hues from white to dark purple, indications of later alterations. Furthermore, it could be observed that the vest was overpainted, since the blue areas on the edges of the vest had been overlapped by the brown paint.

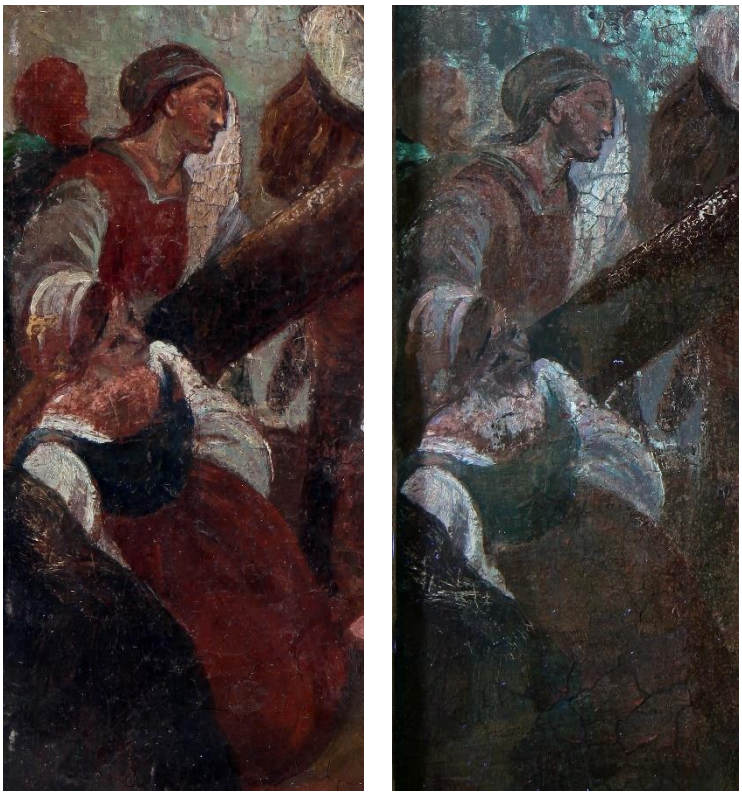

VIS UVF

Figure 5.32 To the left: the kneeling woman, the female and the male figure on the right side of the painting in the visible part of the electromagnetic spectrum. To the right: the kneeling woman, the female and the male figure on the right side of the painting in the UV part of the electromagnetic spectrum (photo credit: Rompakis, Panagiotis, National Gallery - Greece).

In the same way, the female figure on the left of the painting does not present uniform fluorescence (**Figure 5.32**). Starting from the face, many different tones could be observed. Similarly, the red shirt had a different response to the UV light in various parts, along with the grouting areas depicted in a purple colour.

The male figure behind the female with the red shirt under the UV light reveals the difference in tonality on the area of the head where the "unfinished" face presents a light-red colour on the areas where the eyes and the mouth of the figure would have been painted (**Figure 5.32**). This observation is important for a better understanding of the artist's technique. Moreover, his green garment produces intense green fluorescence, a feature that could help toward the identification of the pigment.

VIS UVF

Figure 5.33 To the left: the three figures on the visible part of the electromagnetic spectrum. To the right: the three figures in the UV part of the electromagnetic spectrum. On the right picture a child figure could be observed (photo credit: Rompakis, Panagiotis, National Gallery - Greece).

Finally, the three figures on the right of the painting constitute an area where extensive overpaintings had been performed. The most important contribution to a better understanding of this area through the observation under UV light is the detection of an additional figure that was not visible (**Figure 5.33**). This figure belongs to a child and is located in front of the frontal kneeling figure. The child appears to mourn, touching his head with one hand and turning his gaze from the scene as it unfolds.

5.1.2. Multispectral Imaging

Multispectral imaging provided detailed features of the painting, revealed underlying and hidden elements, identified subsequent and previous conservation treatments, and provided important information on the composition of materials, their chemical distribution, and manufacturing technology.

The study of the painting Statio VIII "Jesus and the Women of Jerusalem" would start with the analysis of the images taken on reflection mode (**Figure 5.34**). It was decided that the analysis would follow the previous methodology, in the

technique of digital photography, where each feature of the painting was analyzed separately. Thus, in the analysis of the images of the multispectral display, reference will be made to features that were found in all six selected wavelengths.

IRR 500 nm IRR 600 nm IRR 700 nm

IRR 800nm IRR 900 nm IRR 1000 nm

Figure 5.34 Statio VIII “Jesus and the Women of Jerusalem”. Multispectral images were taken on reflection configuration on the six selected bands of 500 nm, 600 nm, 700 nm, 800 nm, 900 nm and 1000 nm (photo credit: Dr. Moutsatsou, Anna P., National Gallery - Greece).

The observation of the sky through the multispectral images made apparent the many later additions or alterations applied in the past (**Figure 5.35**). In the false-colour infrared image, the different responses of the blue pigments to IR radiation could be observed. There seem to be four different IR responses corresponding to the blue pigments, an observation that agrees with the observation with the digital photography. Additionally, the areas where grouting had been detected with digital photography were confirmed.

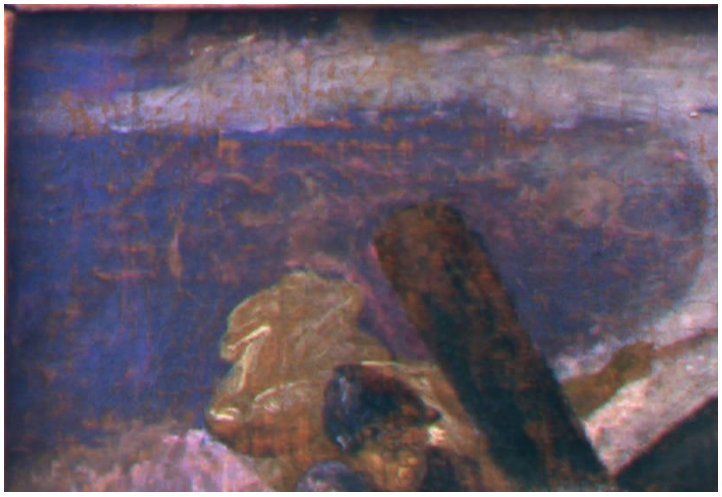

Figure 5.35 Statio VIII "Jesus and the Women of Jerusalem". Part of the sky. Composite FCIR picture of three spectral bands (Red: 900 nm, Green: 700 nm, Blue: 500 nm) (digital processing via Adobe Photoshop and ImageJ by Kesidis, Stelios).

Finally, above the right grouting area of the sky, the area depicted with white colour on the FCIR image corresponds to the yellow overpainting, detected also with digital photography.

In the cloud region, after 800 nm, areas with intense absorption were observed, which correspond to areas of the visible that were presented in intense white colour. In addition, at 1000 nm, there were points through linear absorption that cannot be attributed to some form (**Figure 5.36**). This observation leads to the hypothesis of the existence of an underlying layer. Furthermore, via the analysis of the false colour infrared image (**Figure 5.37**) the boundaries of the pale-yellow colour covering the big area of the cloud became apparent.

The area of the ground presents areas of great interest. The most important information gathered through the MSI technique is the disclosure of a stool with legs (**Figure 5.38**). This stool cannot be associated with any figure and strengthens the assumption that an extensive overpainting had occurred in the painting.

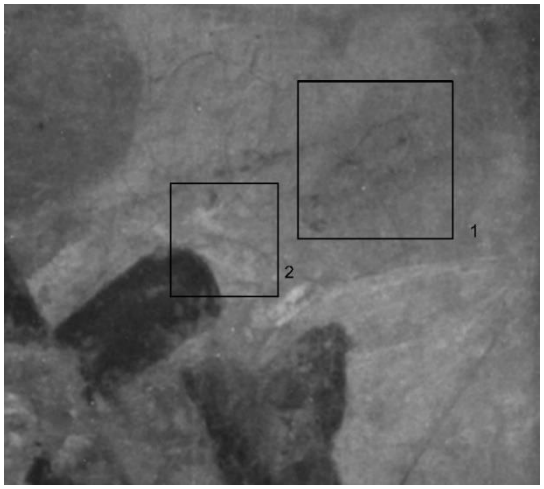

Figure 5.36 Statio VIII "Jesus and the Women of Jerusalem". Area of the sky. Multispectral image at IRR 1000 nm. 1st area: points of linear absorption. 2nd area: areas of intense absorption (digital processing via Adobe Photoshop by Kesidis, Stelios).

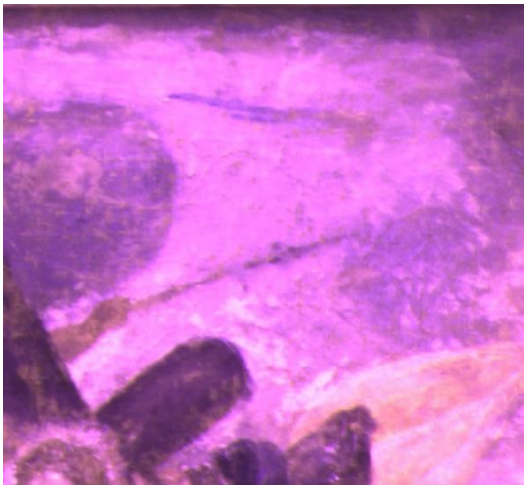

Figure 5.37 Statio VIII "Jesus and the Women of Jerusalem". Area of the sky. Composite FCIR picture of three spectral bands (Blue: 500 nm, Magenta: 700 nm, Yellow: 900 nm (digital processing via Adobe Photoshop and ImageJ by Kesidis, Stelios).

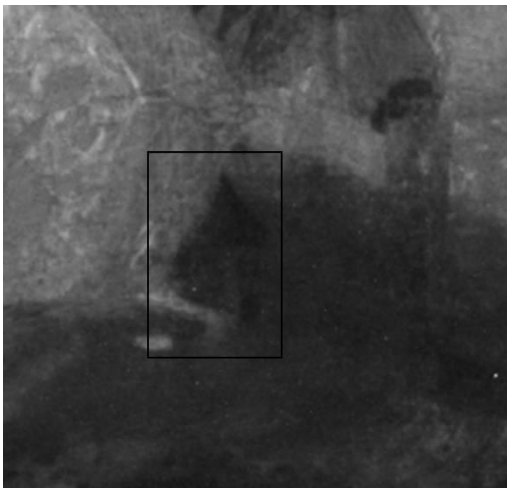

Figure 5.38 Statio VIII "Jesus and the Women of Jerusalem". Area of the ground. Multispectral image at IRR 1000 nm. Stool with legs besides the left leg of Jesus (digital processing via Adobe Photoshop by Kesidis, Stelios).

Moreover, on the bottom right corner of the painting there is an area which produces intense reflection, and may be considered as overpainting.

VIS IRR 500 nm IRR 900 nm

Figure 5.39 Statio VIII “Jesus and the Women of Jerusalem”. To the left: Jesus in the Visible part of the electromagnetic spectrum. To the middle: multispectral image of Jesus at 500 nm. To the right: multispectral image of Jesus at 900 nm (digital processing via Adobe Photoshop by Kesidis, Stelios).

During the analysis of the multispectral images of Jesus the many alterations and the fact that there is no indication on which if any part of His body and face were the original became apparent. In the (**Figure 5.39**) through the comparison between the images taken on the VIS, at 500 nm and at 900 nm, it could be observed that the left side of Jesus’ body reflects more intensely than the right side. This is due to the pigment used for the highlights of His garment. Additionally, after the 900 nm additional damages on the garment become visible, adding this way information on the bad preservation state of the painting. Also, the abrupt discontinuities of the reflection and absorption of the radiation strengthen the assumption of a large-scale intervention on the body of Jesus.

VIS IRR 1000 nm

Figure 5.40 Statio VIII "Jesus and the Women of Jerusalem. To the left: part of the cross in the visible part of the electromagnetic spectrum. To the right: part of the cross at 1000 nm (digital processing via Adobe Photoshop by Kesidis, Stelios).

In the same way, the cross bore large areas of later additions, which also had an effect on its shape. The overpaintings were located on all four arms of the cross, with the upper arm completely covered by overpainting.

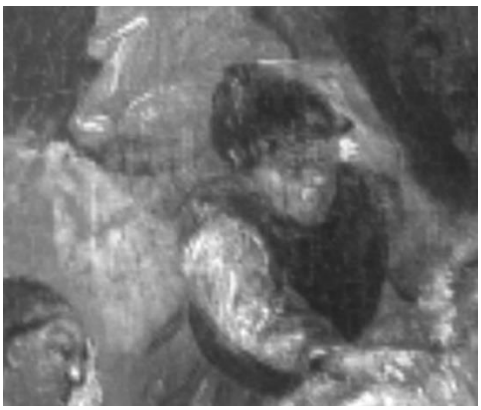

IRR 800 nm

Figure 5.41 Statio VIII "Jesus and the Women of Jerusalem. Multispectral image at 800 nm. The bottom part of the spear (digital processing via Adobe Photoshop by Kesidis, Stelios).

As concerns the left soldier, three important features were observed. First, is that the soldier with his left hand holds a spear rather a sword. This result leads to the detection of the bottom of the spear on the left of soldier's cape, which match with the "sword" in both width and orientation (**Figure 5.41**). Second is that the spear expands more to the right after the 1000 nm (**Figure 5.42**). Third, is that the "second" left hand could be observed only through its outline. However, this feature does not reveal whether this second hand is a result of later addition or a remnant of the original drawing (**Figure 5.41**).

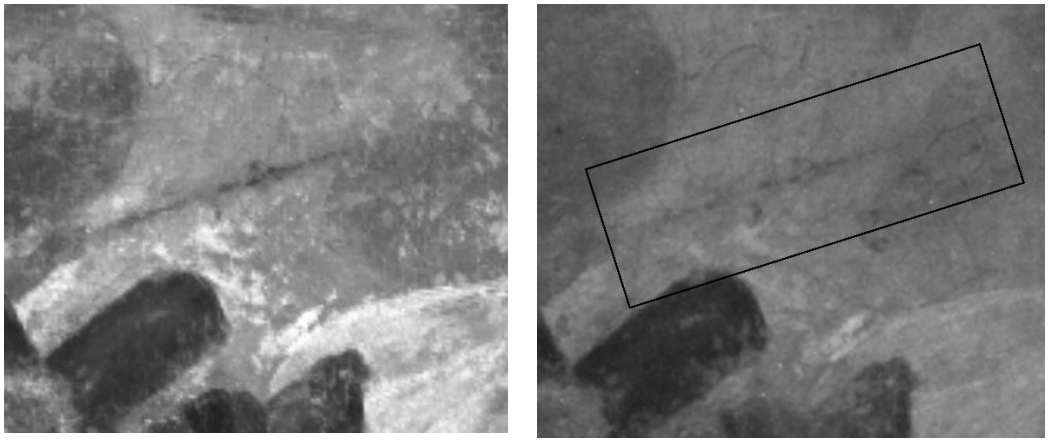

IRR 800 nm IRR 1000 nm

Figure 5.42 Statio VIII “Jesus and the Women of Jerusalem”. Part of the spear. To the left: multispectral image at the 800 nm. To the right: multispectral image at the 1000 nm. The contoured area on the right image delimits the extent of the spear’s lance (digital processing via Adobe Photoshop by Kesidis, Stelios).

The analysis of the kneeling woman revealed important information that was not visible. After 800 nm, spots appear on the woman's skirt that showed a very strong difference in reflection, which corresponds to the different shade of red that is observed in the visible spectrum. Thus, through the multispectral display, the area is demarcated, which seems to be an overpainting. Also, at 1000 nm, features of the woman's face were observed, such as the contour of the eyes, the nose, but also a point from her hair, points that seem to be overpaintings.(**Figure 5.43**).

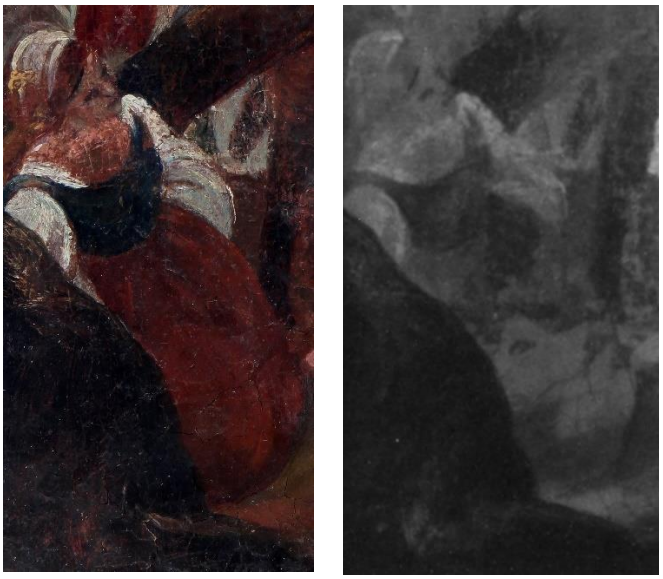

VIS IRR 1000 nm

Figure 5.43 Statio VIII “Jesus and the Women of Jerusalem”. To the left: the kneeling woman in the visible part of the electromagnetic spectrum. To the right: the kneeling woman at 1000 nm (digital processing via Adobe Photoshop by Kesidis, Stelios).

During the analysis of the multispectral images of the female figure on the left of the painting, the underdrawing of the right sleeve became visible. Furthermore, on the bottom right of her shirt spots of overpainting could be observed. (**Figure 5.44**)

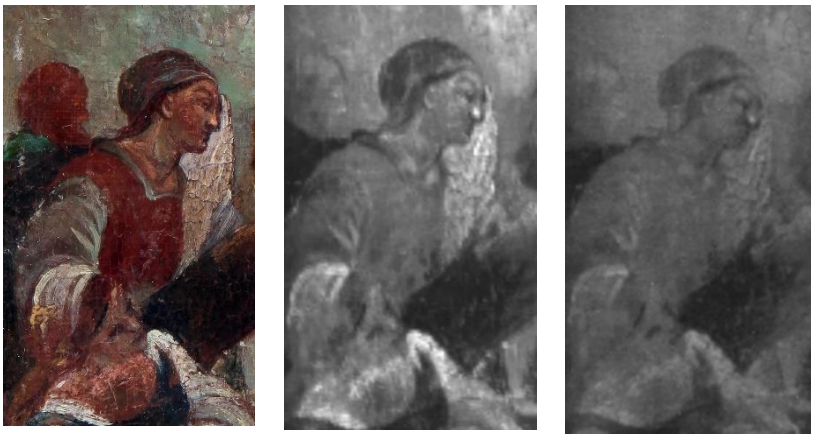

VIS IRR 800 nm IRR 1000 nm

Figure 5.44 Statio VIII "Jesus and the Women of Jerusalem. To the left: the female figure in the visible part of the electromagnetic spectrum. To the middle: the female figure at 800 nm. To the right: the female figure at 1000 nm (digital processing via Adobe Photoshop by Kesidis, Stelios).

The three figures to the right of the painting during the analysis showed areas of great interest. While up to 700 nm their contours were observed, after 800 nm the form on the right disappears, while at 1000 nm, their contours were indistinguishable (**Figure 5.45**).

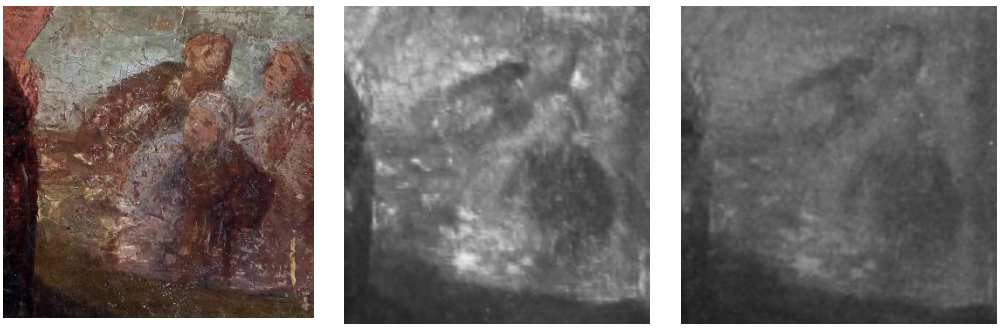

VIS IRR 800 nm IRR 1000 nm

Figure 5.45 Statio VIII "Jesus and the Women of Jerusalem. To the left: the three figures in the visible part of the electromagnetic spectrum. To the middle: the three figures at 800 nm. To the right: the three figures at 1000 nm (digital processing via Adobe Photoshop by Kesidis, Stelios).

The study of the painting Statio VIII “Jesus and the Women of Jerusalem” would continue with the analysis of the multispectral images been taken on transmission mode (**Figure 5.46**).

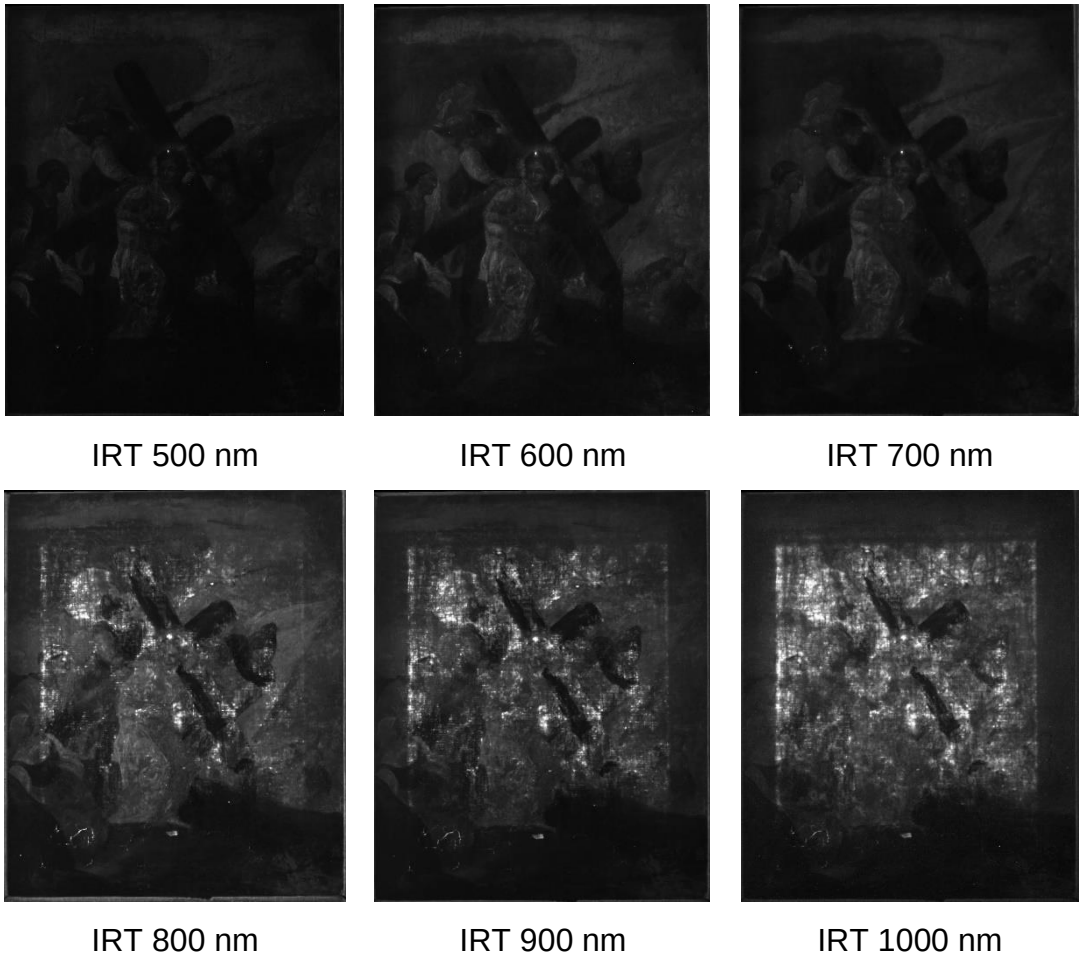

Figure 5.46 Statio VIII “Jesus and the Women of Jerusalem”. Multispectral images were taken on transmission configuration on the six selected bands of 500 nm, 600 nm, 700 nm, 800 nm, 900 nm and 1000 nm (photo credit: Dr. Moutsatsou, Anna P., National Gallery - Greece).

Taking multispectral photos on transmission configuration resulted in the appearance of the painting frame in the final result. Thus, the areas located in this area cannot be analyzed.

As seen in **Figure 5.46**, the radiation passes through the painting after 800 nm, in the infrared region. This observation leads to the conclusion that the work had a thick stratigraphy. The analysis of the multispectral photographs of transmitting radiation was a catalyst for the clarification of some hypotheses that had arisen

through the other techniques, and also provided important information about invisible elements of the painting, which could play a decisive role in drawing conclusions about the origin, but also the dating of the painting.

Through the observation of the photos at 900 nm and 1000 nm the areas where extensive overpaintings had taken place became visible. Such areas were the cross, the ground and big part of the cloud, which were depicted darker due to the thickness of the stratigraphy (**Figure 5.47**).

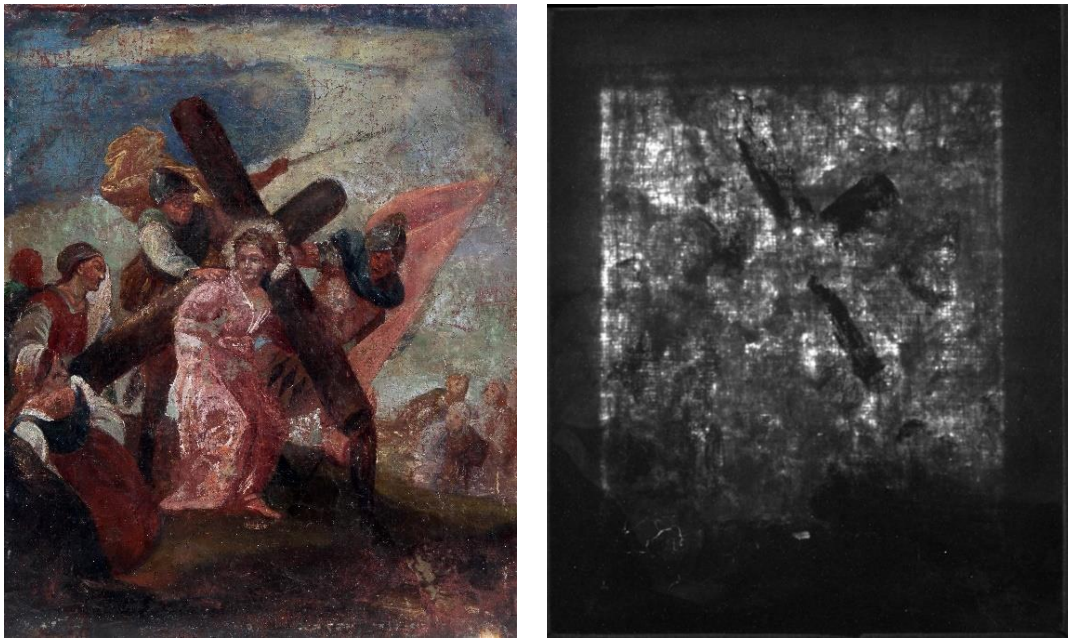

VIS IRT 1000 nm

Figure 5.47 Statio VIII “Jesus and the Women of Jerusalem”. To the right: the painting in the visible part of the electromagnetic spectrum. To the right: the painting at IRT 1000 nm.(digital processing via Adobe Photoshop by Kesidis, Stelios).

In addition, after extensive analysis and research of the left soldier, it was observed that his helmet had a feather (**Figure 5.48**).

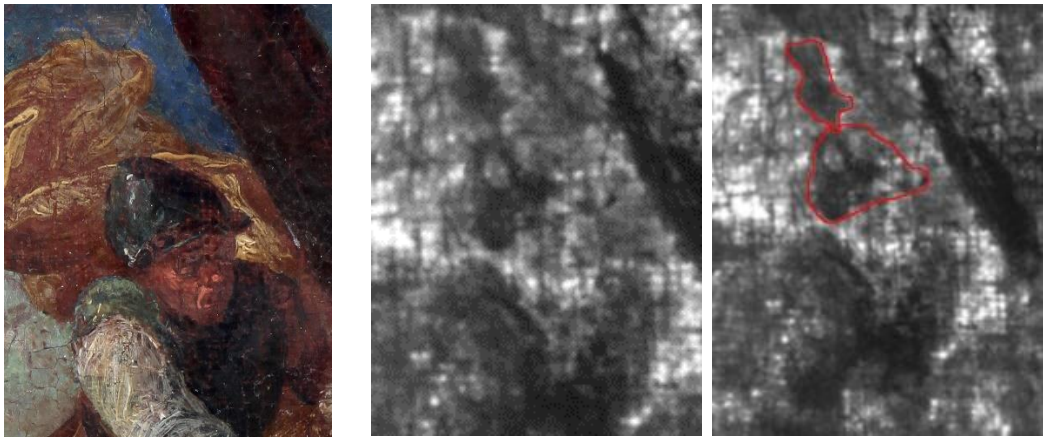

VIS IRT 1000 nm

Figure 5.48 Statio VIII “Jesus and the Women of Jerusalem”. To the left: part of the left soldier in the visible part of the electromagnetic spectrum. To the right: part of the left soldier at IRT 1000 nm. The area of the red border defines the boundaries of the feather on the soldier's helmet (digital processing via Adobe Photoshop by Kesidis, Stelios).

5.1.3. X-Ray Radiography

X-ray radiography provided valuable information on the invisible technical and artistic characteristics of the painting, shed light on the manufacturing techniques of the painting, lead to a better understanding of the preservation state and clarify the presence of later additions and past conservation treatments (**Figure 5.49**).

Figure 5.49 Statio VIII “Jesus and the Women of Jerusalem”. X-ray radiography. 60 kV high voltage, 6.3 mAs (digital processing via Adobe Photoshop by Kesidis, Stelios).

Considering this, the information obtained from the X-ray analysis would be reported layer by layer, starting from the frame and reaching the painting surface.

The information regarding the frame of the painting by the observation of the X-ray radiograph relates to the delimitation of its borders to the painting surface and the connection of related losses or damages. In addition, the nails used to fasten the canvas to the frame were observed around the perimeter, while the parts of the frame were joined with the mitre joint technique. The uniformity of the nails both in thickness and shape lead to the conclusion that they were industrially produced nails. A feature that limits the time of this operation.

Important information emerged regarding the canvas of the painting, information which is due to the negative imprint of the ground layer. The existence of two different canvases was observed, which is a clear indication of lining treatment. The edge of the authentic canvas could be observed to the bottom right corner, as well as to the left side of the painting. In addition, the holes, through which the nails that fastened the canvas to the frame, became distinct (**Figure 5.50**). It should be mentioned, that the authentic canvas had a smaller size than the frame, which meant that in its original form the painting had its sides painted. It also meant that since the present frame had a smaller size than the canvas, then it is verified that the frame is a later addition and is not the original. On the edges of the painting, a material, containing heavy elements, was used to connect the two canvases and to fill the void areas. The original canvas is made of fine yarn and had a dense weave. However, due to the lining treatment, it

XRR

Figure 5.50 Statio VIII “Jesus and the Women of Jerusalem”. X-ray radiography. Detail from the left side of the painting. The borders of the original canvas were observed, but also the holes through which the nails that supported the canvas in the frame passed (digital processing via Adobe Photoshop by Kesidis, Stelios).

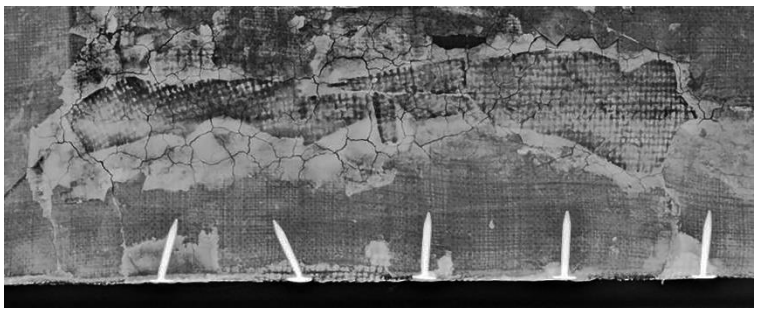

XRR

Figure 5.51 Statio VIII "Jesus and the Women of Jerusalem". X-ray radiography. Detail from the area of patch (digital processing via Adobe Photoshop by Kesidis, Stelios).

is not symmetrical. In contrast, the second canvas, which is observed on the top left corner of the painting, consisted of thick yarns, which were characterized by the many gaps between them. Of particular interest is the area of the painting below the feet of Christ, where a great loss is observed. The loss appears to be due to previous wear that led to tearing and hole formation. The area of loss is characterized by a canvas pattern of irregular layout, which is due to a patch treatment (**Figure 5.51**) (Hassell, 2005, pp. 114, 117).

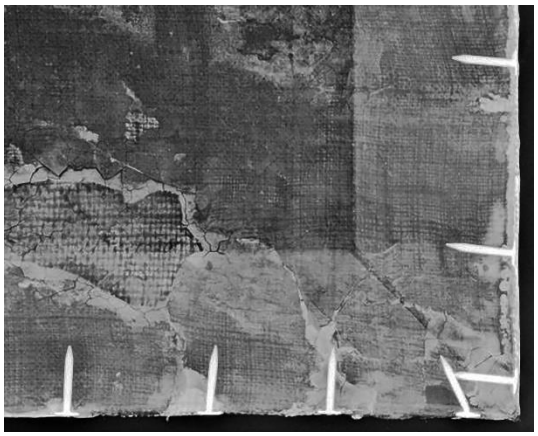

XRR

Figure 5.52 Statio VIII "Jesus and the Women of Jerusalem". X-ray radiography. Detail from the lower right corner of the painting, where grouting areas (areas of high X-ray absorption) could be observed (digital processing via Adobe Photoshop by Kesidis, Stelios).

Finally, around the perimeter of the original fabric (as in the lower right corner) there were areas of loss, where it was filled with grout. Grouting had also been applied in places around the area of patch (**Figure 5.52**).

Concerning the layer of preparation, no clear conclusions could be drawn. However, cracks and losses of the layer were observed.

From the study of the painting through the observation of the X-ray radiography, the poor state of preservation of the painting was better understood, with many losses being observed on the entire surface of the painting. However, in addition to information on the preservation state of the painting,

VIS XRR

Figure 5.53 Statio VIII “Jesus and the Women of Jerusalem”. X-ray radiography. Detail of the kneeling woman where in VIS her right hand is been covered by the rock, while in XRR the details of her arm could be clearly observed (digital processing via Adobe Photoshop by Kesidis, Stelios).

information was also extracted on later additions and subsequent restoration treatments. The x-ray radiography confirmed that the rock on the left side of the painting is a later addition, as the details of the right hand of the kneeling woman were observed, which, in the visible part of the spectrum, were covered by the rock (**Figure 5.53**).

In addition, areas that had received restoration treatments had been identified. Such areas were located on the left knee of Christ (**Figure 5.54**), where areas of cracks were observed to have been filled with grout (high absorption due to the content of heavy elements), but also on the skirt of the kneeling woman (**Figure 5.55**), where extensive filling had taken place.

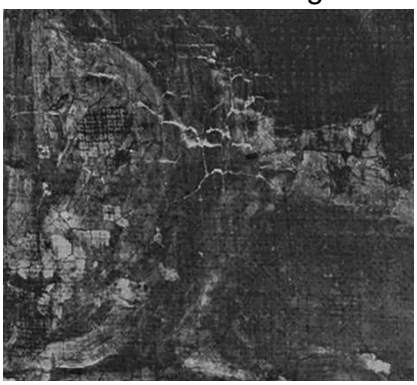

XRR

Figure 5.54 Statio VIII “Jesus and the Women of Jerusalem”. X-ray radiography. Detail of Jesus’ knee where filling could be observed (digital processing via Adobe Photoshop by Kesidis, Stelios).

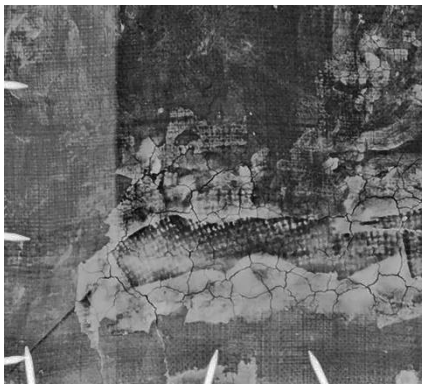

XRR

Figure 5.55 Statio VIII “Jesus and the Women of Jerusalem”. X-ray radiography. Detail of the kneeling woman where the extensive grouting could be observed (digital processing via Adobe Photoshop by Kesidis Stelios).,

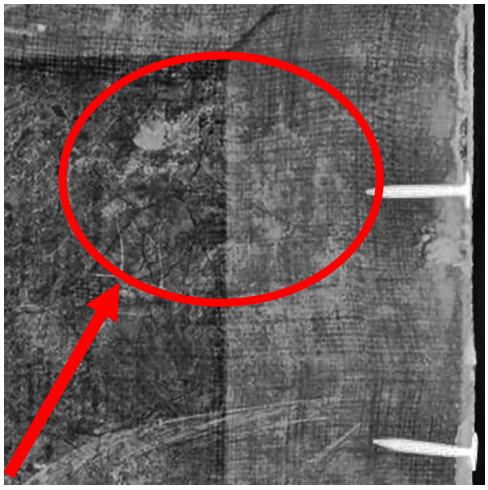

XRR

Figure 5.56 Statio VIII “Jesus and the Women of Jerusalem”. X-ray radiography. Detail of the demon on the upper right area of the painting (the red arrow point to the head of the demon) (digital processing via Adobe Photoshop by Kesidis, Stelios).

Finally, one of the most important pieces of information that X-ray radiography added to the knowledge of the painting, is the observation of a demon on the upper right area of the painting, which, due to the fact that it comes from an underlying layer, is not visible (**Figure 5.56**). During the thematic analysis of the work in comparison with other similar works, the bibliographic search on the correlation of the subject with demons, and also the comparison of the result of the radiography with those of the multispectral imaging, the hypothesis arose, that the soldiers accompanying Christ belong to the Order of the Lansquenets[3], a German-Austrian mercenary group of the Middle Ages. This conclusion, the confirmation of which goes beyond the scope of this dissertation and must be

Figure 5.57 A Lansquenet Standing by a Tree. 1520(Beham. Sebald derived from: link)

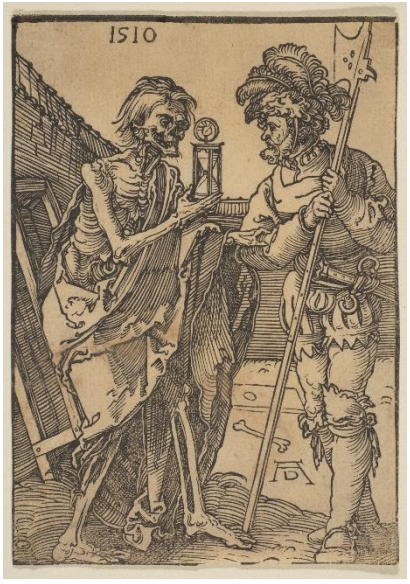

Figure 5.58 Death and the Lansquenet. 1510 (Dürer, Albrecht. Derived from: link).

[3] (Van Niwwegen, 2010, pp. 162-166)

made in collaboration with art historians, stems from the great resemblance of the costume of the soldiers accompanying Christ to that worn by the mercenaries of the lansquenets. The soldiers of this order wore various exuberant colourful uniforms, such as tight-fitting pants, large slashed sleeves and hats decorated with feathers (**Figure 5.48** and **Figure 5.57**). While their main weapon was the long pike (**Figure 5.42**) (Lepage, 2005, pp. 244-245; Richards, 2002, p. 46). Furthermore, according to Lepage (2005, p. 244) *"One said that they could not go to Heaven because they were too evil but were not accepted either in Hell because they frightened the Devil himself"* (**Figure 5.58**).

IRR 700 nm + XRR

Figure 5.59 Statio VIII "Jesus and the Women of Jerusalem". Detail of the area where the soldier's spear appears to either point to the "demon or death" or to pierce it. Composite picture of infrared reflectography at 700 nm and X-ray radiography (digital processing via Adobe Photoshop by Vedinoglou, Aggeliki).

Taking all the above under consideration resulted in the assumption that the devil may be a personification of death. The above hypothesis is reinforced by (**Figure 5.59**), where the soldier's spear appears to either point to the "demon or death" or to pierce it.

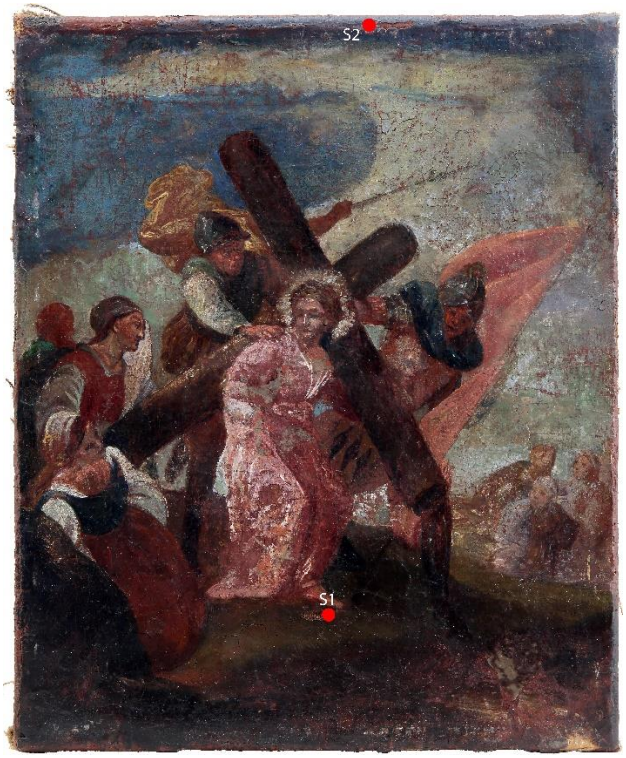

Figure 5.60 Statio VIII “Jesus and the Women of Jerusalem”. Sampling points for the performance of the microscopic techniques (digital processing via Adobe Photoshop by Kesidis, Stelios).

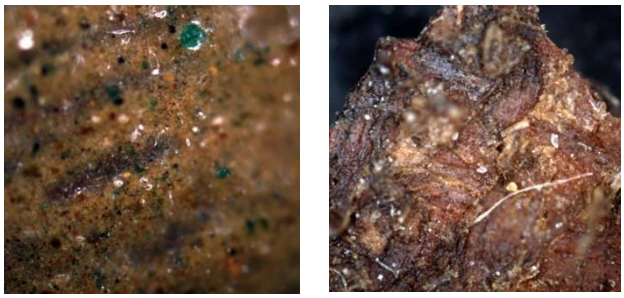

OM x200 OM x50

Figure 5.61 Sample’s (S1) surface observation before preparation for OM and SEM. To the left: detail of the surface of the sample at x200 magnification. To the right: detail of the back of the sample at x50 magnification (photo credit: Terlexi, Agni-Vasileia National Gallery - Greece) (digital processing via Adobe Photoshop by Kesidis, Stelios).

5.1.4. Optical Microscopy

Due to the requirements needed for performing the analysis through optical microscopy and scanning electron microscopy, it was necessary to take two (2) cross-sectional samples. Areas of wear on the painting that were representative of the area were selected as sampling points (**Figure 5.60**).

The first sampling area (S1) is in a loss area in the ground, just below Jesus' foot (**Figure 5.60**), where, the big area of loss, was observed with X-ray radiography. Observation of the front of the sample records the heterogeneity of the surface and the presence of various pigments in the upper colour layer. While, the back of the sample revealed the existence of brown colour preparation, which bore the imprint of the canvas (**Figure 5.61**).

The observation of the surface of the cross-sectional sample S1 with visible reflective light (**Figure 5.62**) revealed a complex multilayered stratification and presence of overpainting. In particular, starting from the lower layer, nine (9) layers were recorded.

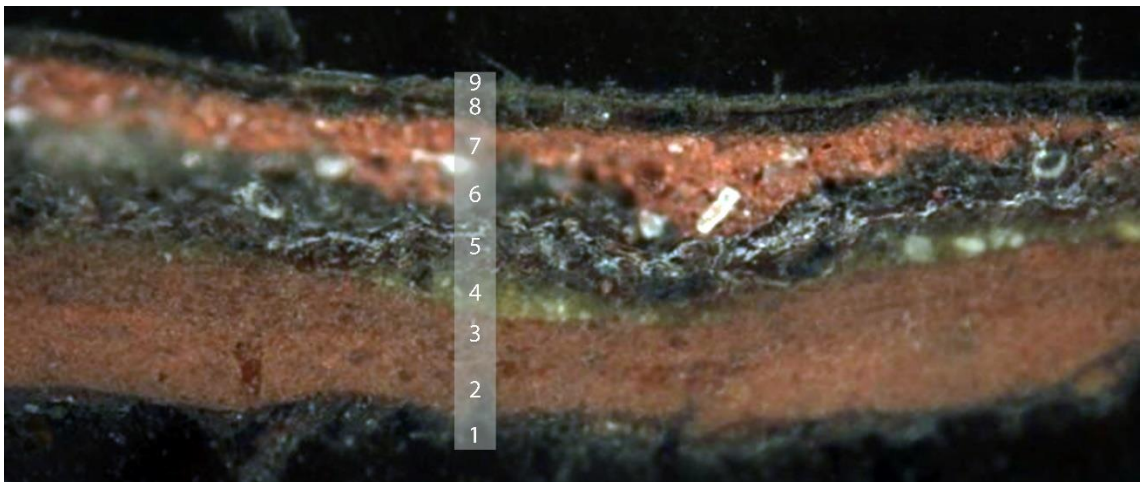

OM x100

Figure 5.62 Statio VIII “Jesus and the Women of Jerusalem”. Observation of the sample S1 with visible reflective light at x100 magnification (photo credit: Terlixi, Agni-Vasileia National Gallery - Greece) (digital processing via Adobe Photoshop by Kesidis, Stelios).

The first layer consisted of traces of organic coating. The second and third layers consisted of a brown-orange layer of preparation (ground layer). Between the second and third layers, slight colour differentiations are observed, while both of them were fine-grained. According to (Stols-Witlox, 2012, p. 172), reddish grounds were typical of the 16th to 18th century, leading thus to the assumption that the original preparation layer dates at least back to the 18th century. Next, is a light green layer, with grains indistinguishable in the resolution of the optical microscope, and some larger white grains. The fifth layer consisted of a dark coloured layer of organic, possibly, composition, which probably also contains some inorganic elements. The sixth layer is also a dark layer of organic composition that is visually separated from the underlying layer. The following layer is an inorganic layer of orange colour consisting of larger compared to the layer No.2 and 3 grains and probably had a role of preparation. After this layer, a fine dark coloured layer of indistinguishable texture is observed. And finally, the ninth layer consisted of a thin green colour layer. After the completion of the analysis of the sample, it arose that the later intervention at this point involved the deposition of several layers, including a preparation layer, over the initial layer of varnish.

This was followed by observation of the sample with UV illumination. The observation of sample S1 with UV light revealed features of the sample only visible

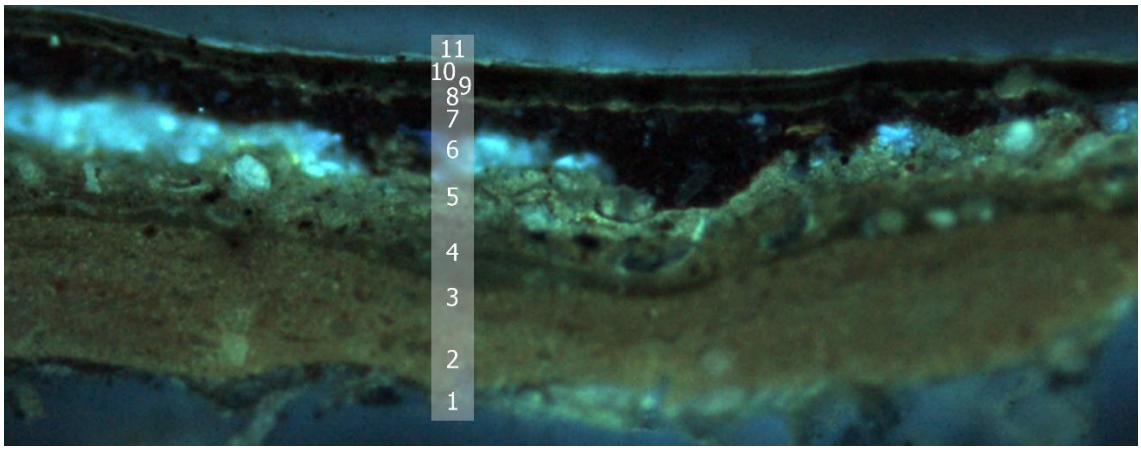

UVFM x100

Figure 5.63 Statio VIII “Jesus and the Women of Jerusalem”. Observation of the sample S1 with UV reflective light at x100 magnification (photo credit: Terlixi, Agni-Vasileia, National Gallery - Greece) (digital processing via Adobe Photoshop by Kesidis, Stelios).

under UV light, with the addition of two more layers compared to the visible reflective light (**Figure 5.63**). In particular, the distinction between the layers 5 and 6 becomes clear. They were of organic nature, of different composition and had the role of coatings of the original painting layers. From this observation arose the question of whether either of the two coatings had been applied in the same period or the second coating is a later addition. The aforementioned question gets even more significant after the observation that the sixth layer is interrupted and that these two layers had a non-horizontal arrangement. Moreover, the presence of a thin organic coating (layer 8) becomes visible, just above the second layer of preparation (layer 7). Finally, the presence of a thin surface organic coating on the surface of the upper colour layer, which records yellowish fluorescence, is noticeable.

The second area of sampling (S2) is from the upper edge of the painting, detached from the perimeter area of wear (**Figure 5.60**), wherein a grouting area is observed, through X-ray radiography. During the microscopic observation of the sample surface before the preparation for OM and SEM (**Figure 5.64**), the anisometric distribution of the surface blue layer was observed. On the back there is an orange layer that contains other heterochromatic grains. It is also noticeable that the blue colour layer is distributed on the side surfaces.

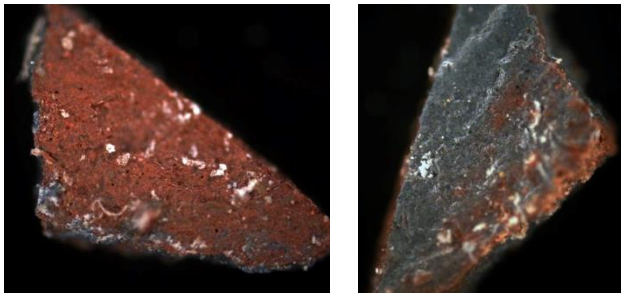

OM x100 OM x100

Figure 5.64 Sample's (S2) surface observation before preparation for OM and SEM. To the left: detail of the back of the sample at x100 magnification. To the right: detail of the surface of the sample at x100 magnification (photo credit: Terlixi, Agni-Vasileia, National Gallery - Greece) (digital processing via Adobe Photoshop by Kesidis, Stelios).

The observation of the surface of the cross-sectional sample S2 with visible reflective light (**Figure 5.64**) revealed that the stratification of the sample consisted of only two layers.

The first layer is an orange-coloured preparation layer containing other heterochromatic (white, black, etc.) grains. The second layer is a thin blue colour layer that is observed on the lateral edges of the section. The blue colour layer also contains a few black grains that become distinct at higher magnifications but also when observing the surface (**Figure 5.65**). Furthermore, the structure and the microscopic image of the preparation layer were similar to the second preparation layer, marked as layer 7, in sample S1. It is also discernible that the interface of the two layers of sample S2 is not flat and had microwaves.

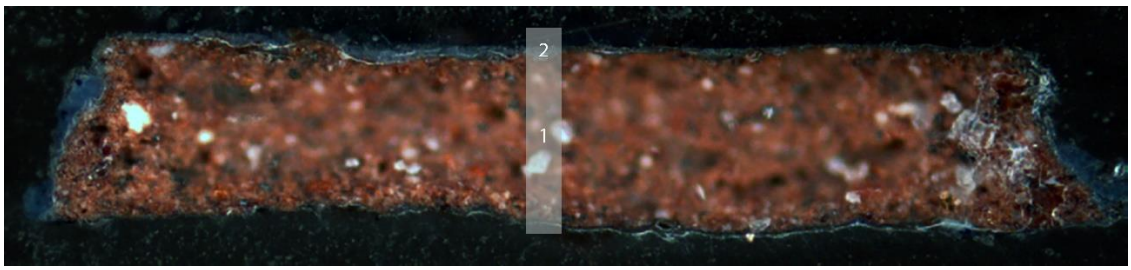

OM x100

Figure 5.65 Statio VIII "Jesus and the Women of Jerusalem". Observation of the sample S2 with visible reflective light at x100 magnification (photo credit: Terlixi, Agni-Vasileia , National Gallery - Greece) (digital processing via Adobe Photoshop by Kesidis, Stelios).

This was followed by the observation of the sample with UV illumination. The observation of sample S2 with UV light verified the observations within the visible light, while the observation of the sample under stimulation with UV radiation (**Figure 5.66**) records the intense blue-white fluorescence of the blue colour layer.

The underlying preparation layer generally does not record fluorescence, while off-white fluorescence is recorded only by some white (in visible) granules contained in this layer.

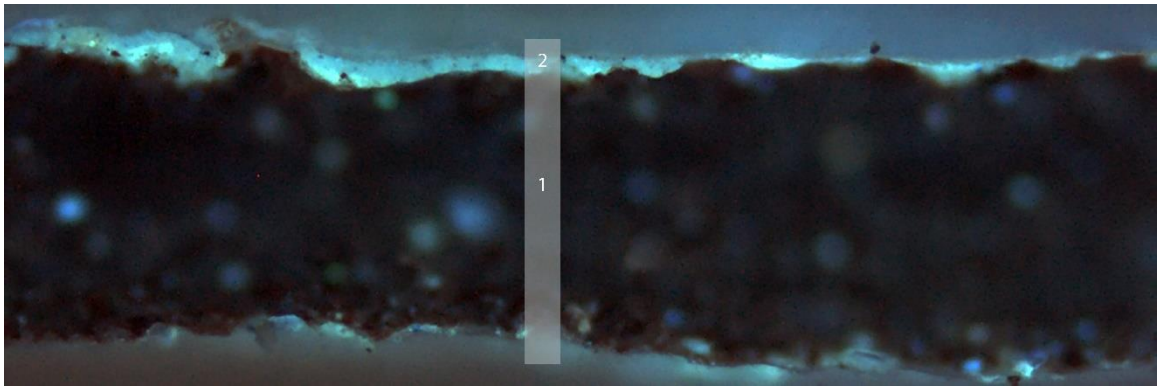

UVFM x100

Figure 5.66 Statio VIII “Jesus and the Women of Jerusalem”. Observation of the sample S2 with UV reflective light at x100 magnification (photo credit: Terlixi, Agni-Vasileia, National Gallery - Greece) (digital processing via Adobe Photoshop by Kesidis, Stelios).

5.1.5. Scanning Electron Microscopy – Energy Dispersive X-rays Spectroscopy

The application of the Scanning Electron Microscopy coupled with an Energy Dispersive X-rays Spectrometer provided valuable information on the stratigraphic composition of the painting samples, the elemental composition of all the sample layers, their preservation state, the detection of later additions, conservation treatments and the assessment of the dating of the two paintings, which led to safer conclusions through other non-invasive analysis techniques.

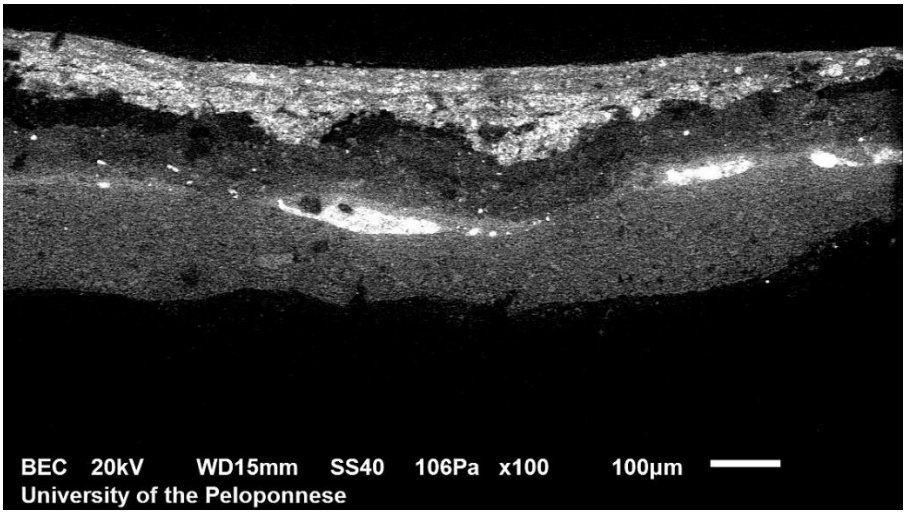

Figure 5.67 Statio VIII "Jesus and the Women of Jerusalem". Observation of the sample S1 with SEM at x100 magnification (photo credit: Dr. Palamara, Eleni - University of the Peloponnese, Greece) (digital processing via Adobe Photoshop by Kesidis, Stelios).

During the analysis of the first sample (S1) (**Figure 5.67** & **Figure 5.60**) through the backscattered images with higher magnifications (**Figure 5.68**) it was possible to select information regarding the granulometry of the layers, to distinguish the pigment layer, as well as to extract important information about the overpainting area. (**Table 5.1**)

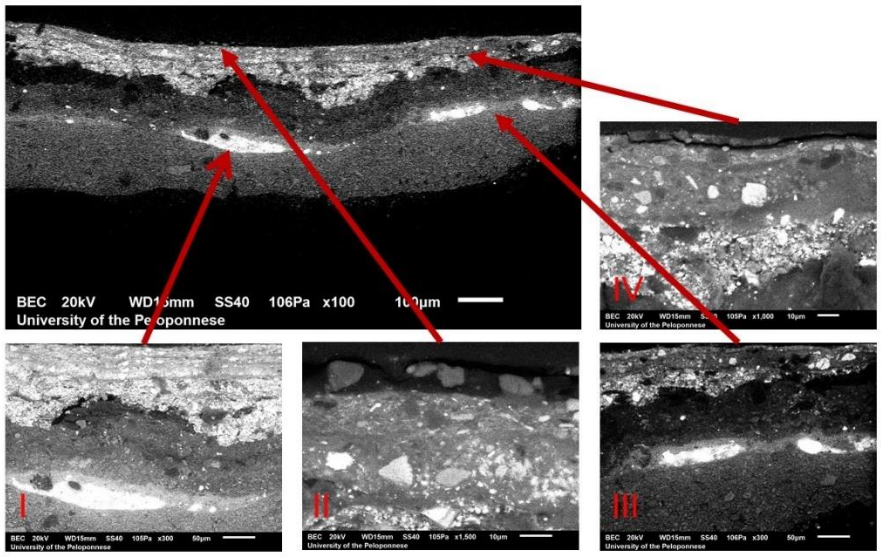

Figure 5.68 Statio VIII "Jesus and the Women of Jerusalem". Observation of the sample S1 and the four areas of interest with SEM (photo credit: Dr. Palamara, Eleni - University of the Peloponnese, Greece) (digital processing via Adobe Photoshop by Kesidis, Stelios).

Sample	Spot	OM Colour	SEM Observations	Layer	Elements Detected
S1	Coating			11th	
	Paint layer	Green	Very fine-grained with large grains	10th	Pb, Si, Fe, Al, Ca, Cu, Mg
	Ground layer	Dark	Fine-grained with large grains	9th	Pb, Si, Ca, Al, Fe, S, Ba, Mg
	Ground layer	Dark	Fine-grained with large grains	8th	Pb, Si, Ca, Al, Fe, S, Ba, Mg
	Ground layer	Orange	Coarse-grained with very large grains	7th	Si, S, Zn, Ba, Fe, Ca, Al, Mg
	Coating	Dark	Indistinguishable texture	6th	
	Coating	Dark	Indistinguishable texture	5th	
	Paint layer	Light green	Fine-grained with large grains	4th	Si, Pb, Fe, Al, Ca, Mg, Na, K
	Ground layer	Brown	Fine-grained with some large grains	3rd	Ca, Si, Mg, Al, Pb, Fe, K
	Ground layer	Brown	Fine-grained with some large grains	2nd	Ca, Si, Mg, Al, Pb, Fe, K

Table 5.1 Elemental Analysis of sample S1 by EDS

It was observed that the two layers of the original preparation were fine-grained, with the presence of some large grains. The EDS analysis showed that the layers contained: Calcium (Ca), Silicon (Si), Magnesium (Mg), Aluminum (Al), Lead (Pb), Iron (Fe) and Potassium (K). This led to the conclusion that it was a gesso layer based on dolomite ([Ca,Mg][CO3]2) and aluminum silicate (Al_2SiO_3), while the colour of the layer was achieved due to the presence of the red ochre (Fe_2O_3) (Eastaugh, et al., 2004, p. 320) and lead white ($(PbCO_3)_2 \cdot Pb(OH)_2$) (Eastaugh, et al., 2004, p. 233). This data confirms the previous dating estimation, stating that the original ground layer dates back at least to the 18th century. This was due to the materials used for the preparation layer. According to (Groen, 2011, p. 87), the main pigment used for grey grounds was the expensive lead white, while for

reddish or brown grounds red earth was used which was abundant in nature. The fourth layer of the sample was fine grained with large grains. The EDS analysis showed that the layer contained: Silicon (Si), Lead (Pb), Iron (Fe), Aluminum (Al), Calcium (Ca), Magnesium (Mg), Sodium (Na) and Potassium.

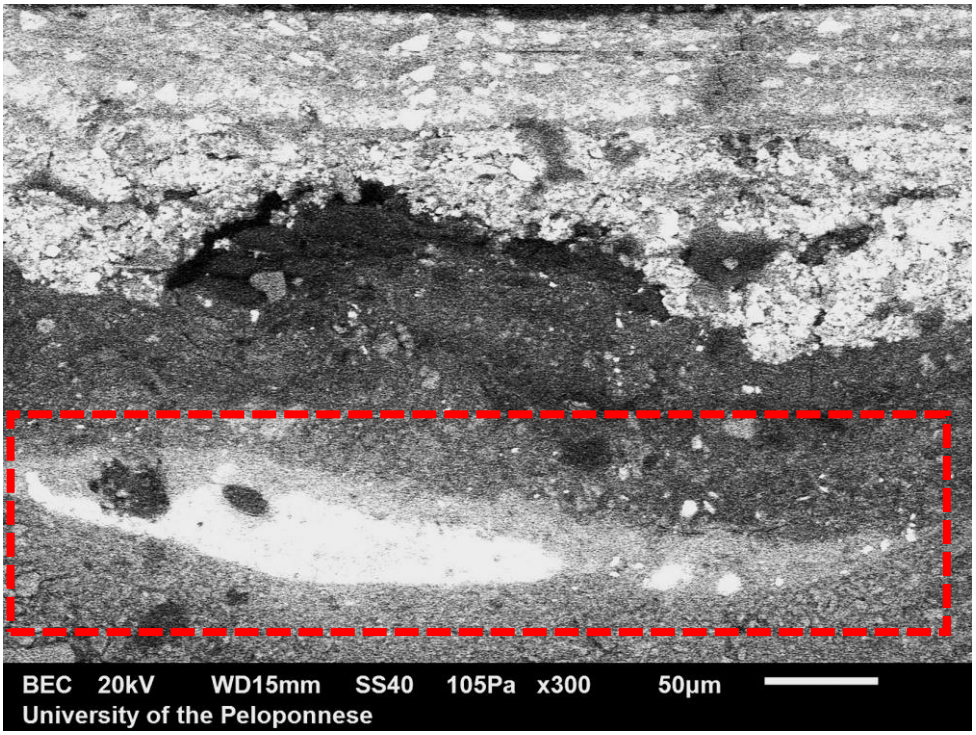

Figure 5.69 Statio VIII "Jesus and the Women of Jerusalem". Detail of the light green coloured layer of the sample S1 with SEM at x300 magnification (photo credit: Dr. Palamara, Eleni - University of the Peloponnese, Greece) (digital processing via Adobe Photoshop by Kesidis, Stelios).

This led to the conclusion that it was a layer of green earth $[(K,Na)(Fe,Al,Mg)_2(Si,Al)_4O_{10}(OH)_2]$ (Eastaugh, et al., 2004, p. 174) with the addition of white lead. **Figure 5.69** showed details of the fine-grained light green pigment, which contains large grains of white lead and others. The fifth and sixth layers of the sample constitute organic coatings of indefinite granulometry, thus no information gained from the analysis by SEM/EDS.

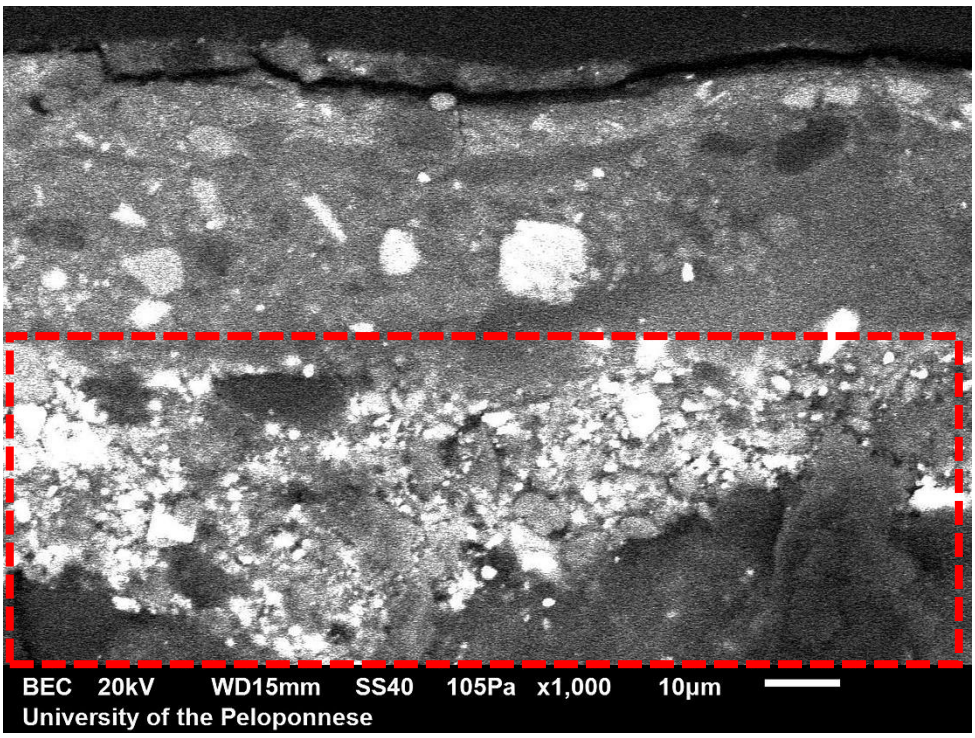

Figure 5.70 Statio VIII "Jesus and the Women of Jerusalem". Detail of the orange preparation layer of the sample S1 with SEM at x1000 magnification (photo credit: Dr. Palamara, Eleni - University of the Peloponnese, Greece) (digital processing via Adobe Photoshop by Kesidis, Stelios).

The seventh layer of the sample, attributed after the OM observation as the layer of preparation of the overpainting, was coarse-grained with large grains (**Figure 5.70**). The EDS analysis showed that the layer contained: Silicon (Si), Sulfur (S), Zinc (Zn), Barium (Ba), Iron (Fe), Calcium (Ca), Aluminum (Al) and Magnesium (Mg). This led to the conclusion that this layer was a mixture of pigments, and in particular, of lithopone ($BaSO_4 \cdot ZnS$) (Eastaugh, et al., 2004, p. 242), a white pigment discovered around 1850 by G.F. de Doubet, of red ochre (Fe_2O_3) (Eastaugh, et al., 2004, p. 320) and of silicon, which had the role of absorbent. The above results were significant as, thanks to lithopone, the overpainting was dated indirectly at the end of the 19th century and the beginning of the 20th. Furthermore, according to (Abendschein, 1906, p. 64), to counter the effect of excess oil on their works, painters by the end of the 18th and the beginning of the 19th century began to use grounds of higher absorbency, justifying, thus, the presence of silicon as an absorbent.

The ninth and tenth layers of the sample, attributed after the OM observation as a fine dark-coloured layer of indistinguishable texture, seems to be the second and

the third layers of the preparation layer belonging to the overpainting. By the observation of the two layers in (**Figure 5.71**) the differentiation within their granulometry showed that the eighth layer was coarser than the ninth, which acts as the top preparation layer. The EDS analysis showed that the layer contained: Lead (Pb), Silicon (Si), Calcium (Ca), Aluminum (Al), Iron (Fe), Sulfur (S), Barium (Ba) and Magnesium (Mg). This led to the conclusion that these two layers were mixtures of pigments, and in particular, of burnt sienna (SiO_2+Al_2O_3+Fe_2O_3) (Eastaugh, et al., 2004, p. 66) and of red lead (Pb_3O_4) (Eastaugh, et al., 2004, p. 229).

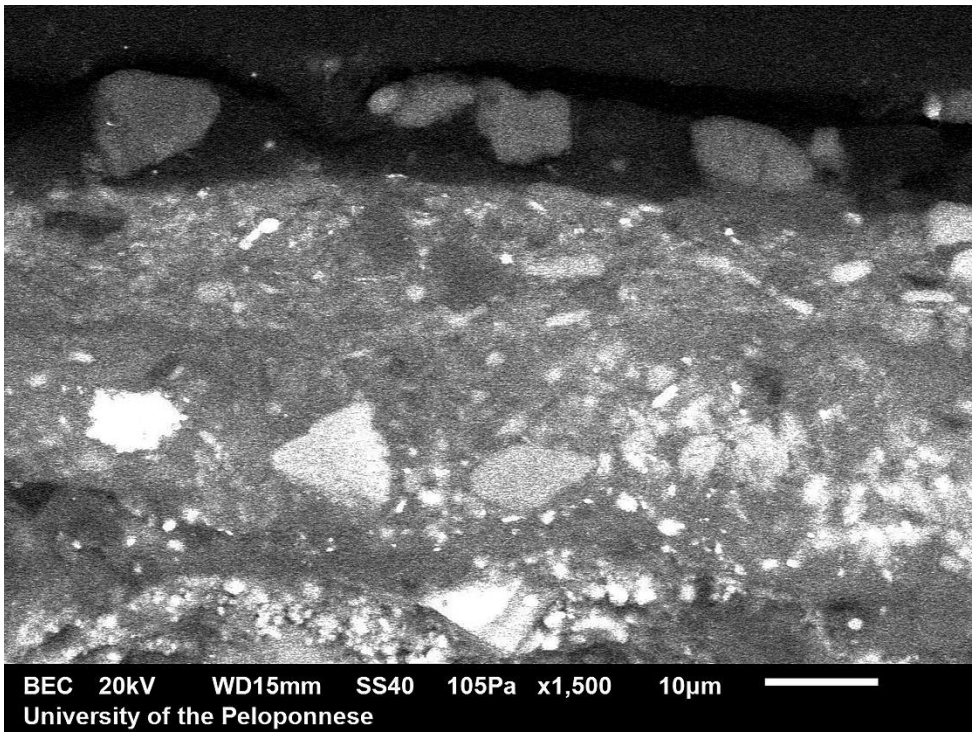

Figure 5.71 Statio VIII "Jesus and the Women of Jerusalem". Detail of the top layers of the sample S1 with SEM at x1500 magnification (photo credit: Dr. Palamara, Eleni - University of the Peloponnese, Greece) (digital processing via Adobe Photoshop by Kesidis, Stelios).

The eleventh layer was very fine-grained with some large grains. The observation of the BEC image (**Figure 5.71**) reveals that the paint layer was mainly composed by low atomic number elements with the addition of some higher atomic number elements in the form of grains. The EDS analysis showed that the layer contained: Lead (Pb), Silicon (Si), Iron (Fe), Aluminum (Al), Calcium (Ca), Copper (Cu) and Magnesium (Mg). The above led to the conclusion that this layer was a mixture of pigments, and in particular, of verdigris ($Cu(CH_3COO)_2.H_2O$) (Eastaugh, et al.,

2004, p. 385), of red (Fe_2O_3) or yellow ochre (α-FeOOH) (Eastaugh, et al., 2004, pp. 320, 401) and red lead (Pb_3O_4) (Eastaugh, et al., 2004, p. 229).

During the analysis of the second sample (S2) (**Figure 5.72**) through the backscattered images with higher magnifications (**Figure 5.73**) it was possible to select information regarding the granulometry of the layers and to distinguish the pigment layer (**Table 5.2**).

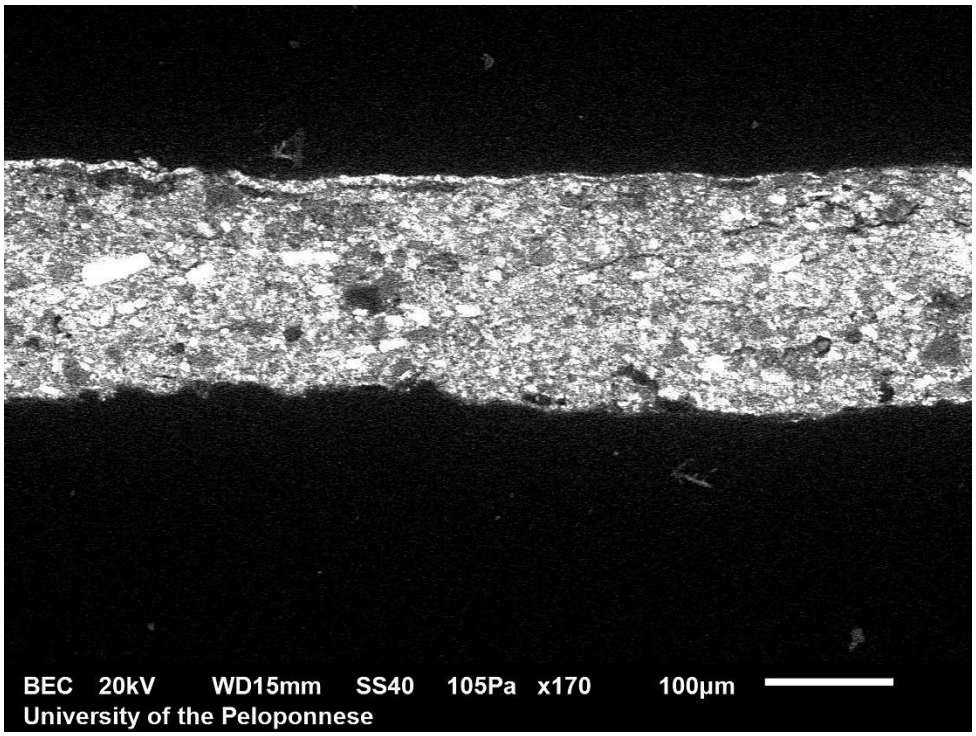

Figure 5.72 Statio VIII "Jesus and the Women of Jerusalem". Observation of the sample S2 with SEM at x170 magnification (photo credit: Dr. Palamara, Eleni - University of the Peloponnese, Greece) (digital processing via Adobe Photoshop by Kesidis, Stelios).

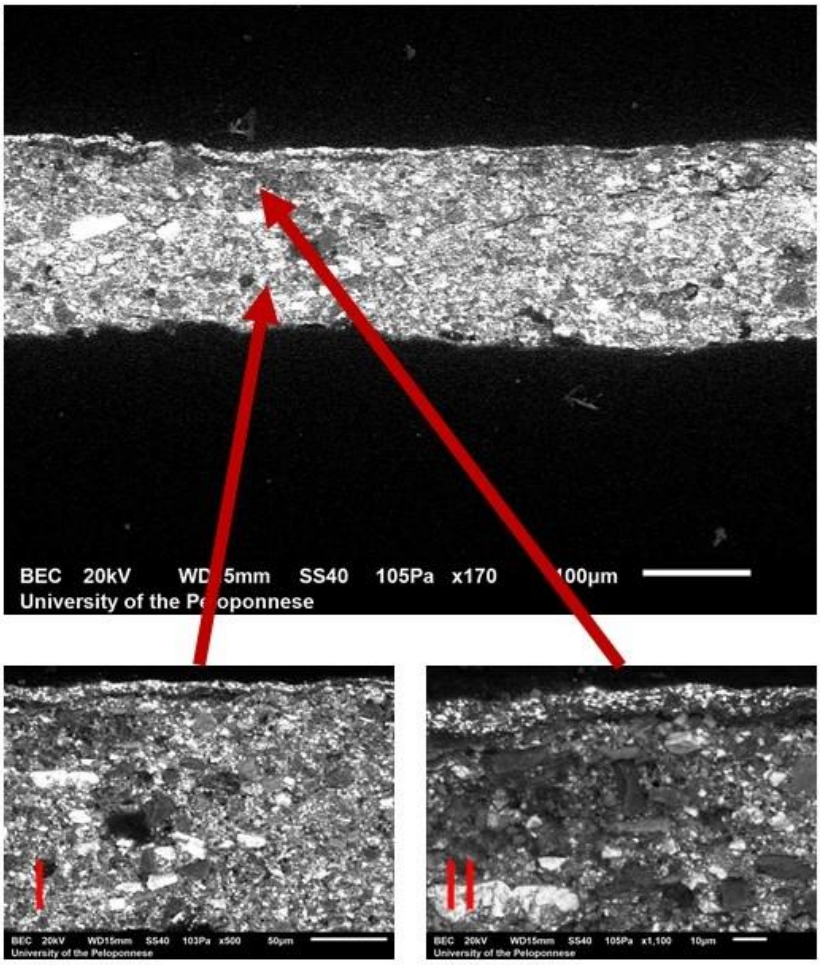

Figure 5.73 Statio VIII "Jesus and the Women of Jerusalem". Observation of the sample S2 and the two areas of interest with SEM (photo credit: Dr. Palamara, Eleni - University of the Peloponnese, Greece) (digital processing via Adobe Photoshop by Kesidis Stelios).

Sample	Spot	OM Colour	SEM Observations	Layer	Elements Detected
S2	Paint layer	Blue	Fine grained with small grains	2nd	Pb, Al, Fe, Co, Ba, Si, Zn, Ca, K
	Ground layer	Orange	Corse grained with very large grains	1st	Si, S, Zn, Ba, Fe, Ca, Al, Mg

Table 5.2 Elemental Analysis of sample S2 by EDS

The first layer of the sample S2 (**Figure 5.60**), attributed after the OM observation as the layer of preparation, was coarse-grained with large grains (**Figure 5.74**). The EDS analysis showed that the layer contained: Silicon (Si), Sulfur (S), Zinc (Zn), Barium (Ba), Iron (Fe), Calcium (Ca), Aluminum (Al) and Magnesium (Mg). This led to the conclusion that this layer was a mixture of pigments, and in particular, of lithopone ($BaSO_4 \cdot ZnS$) (Eastaugh, et al., 2004, p. 242), of red ochre (Fe_2O_3) (Eastaugh, et al., 2004, p. 320) and of silicon, which had the role of filler. This layer resembles totally to the seventh layer of the sample S1 (**Figure 5.70**). Taking this under consideration, reasoning emerges that, the two areas of sampling had been altered from their original form and composition and more specifically, the interventions had occurred in the same chronological framework, since both the composition and the texture of this layer were exactly the same with those of layer 7 of the sample S1.

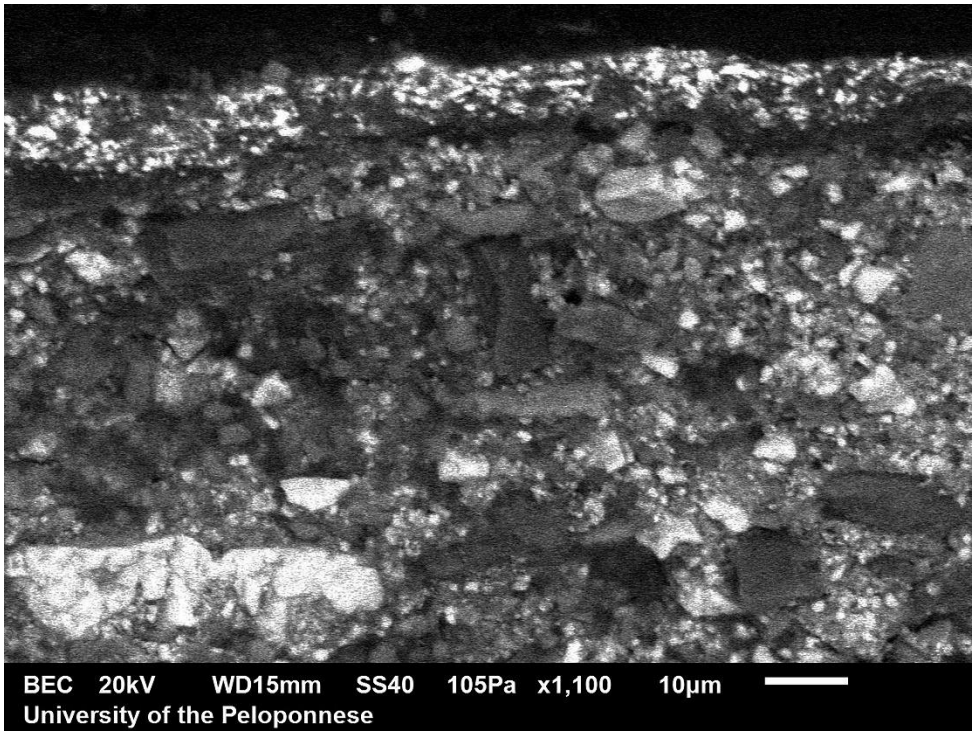

Figure 5.74 Statio VIII "Jesus and the Women of Jerusalem". Detail of the layers of the sample S2 with SEM at x1100 magnification (photo credit: Dr. Palamara, Eleni - University of the Peloponnese, Greece) (digital processing via Adobe Photoshop by Kesidis, Stelios).

The second layer of the sample was fine-grained with some small grains. The EDS analysis showed that the layer contained: Lead (Pb), Aluminum (Al), Iron (Fe),

Cobalt (Co), Barium (Ba), Silicon (Si), Zinc (Zn), Calcium (Ca) and Potassium (K). This led to the conclusion that the blue colour of the layer was achieved due to the presence of cobalt blue ($CoO.Al_2O_3$) and lead white ($(PbCO_3)_2 \cdot Pb(OH)_2$) (Eastaugh, et al., 2004, pp. 112, 233), while the presence of Iron (Fe), Barium (Ba), Silicon (Si), Zinc (Zn) and Calcium (Ca) was associated with the underlying layer.

After the completion of the analysis of the two samples from Statio VIII “Jesus and the Women of Jerusalem through scanning electron microscopy coupled with an energy dispersive spectrometer, the presence of overpaintings was confirmed, however, the most important revelation was the identification of the composition of the two layers of preparation in the samples taken from the painting. This helps towards establishing safer conclusions through other non-invasive analysis techniques, such as X-Ray Fluorescence Spectrometry.

5.1.6. X-Ray Fluorescence Spectrometry

The application of the X-Ray Fluorescence (XRF) Spectrometry on the Statio VIII “Jesus and the Women of Jerusalem” revealed the composition of the inorganic pigments and the ground layer, provided information for the indirect dating of the painting and finally, detected areas of later addition and past conservation treatments.

In the analysis of the painting, 53 point (**Figure 5.75**), 3 linear and 3 area scanning analyzes (**Figure 5.76**) were performed. Due to the large volume of data, it was decided that the analysis of the elemental results of XRF spectrometry would be done in colour.

The elemental analysis of the blue pigments by μ-XRF suggests the presence of the pigments: manganese blue, cobalt blue, Prussian blue and azurite (**Figure 5.77**).

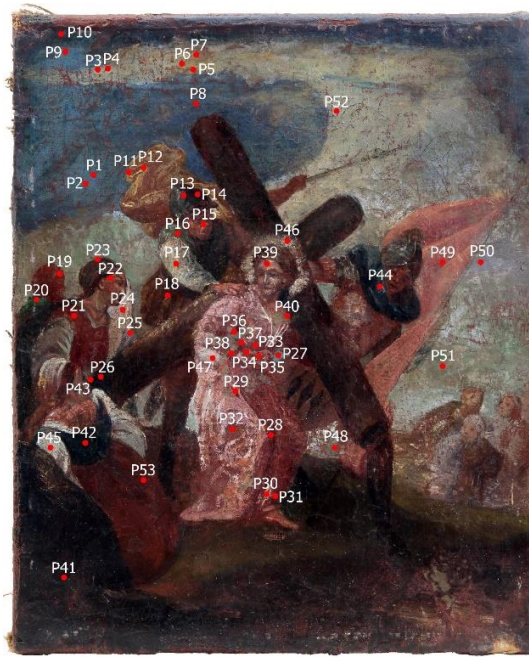

Figure 5.75 Statio VIII "Jesus and the Women Jerusalem". Positions of analysis by XRF (digi processing via Adobe Photoshop by Kesid Stelios).

Figure 5.76 Statio VIII "Jesus and the Women Jerusalem". Area & linear scanning analyz (digital processing via Adobe Photoshop Kesidis, Stelios).

Manganese blue ($xBaSO_4.yBaMnO_4$) (Eastaugh, et al., 2004, p. 37) was identified at the analysis position P1. Cobalt blue ($CoO.Al_2O_3$) (Eastaugh, et al., 2004, p. 112) was identified at the analysis positions: P5 to P10, at the analysis positions: P16, P17, P24, P25, P27, P34, P36, P44, P47, P48, P49, P50 and P52. Prussian blue ($[Fe(II)(CN)_6]_4$) (Eastaugh, et al., 2004, p. 308) was identified at the analysis positions: P20, P27 and P42. And finally, azurite ($Cu_3(CO_3)_2(OH)_2$) (Eastaugh, et al., 2004, p. 33) was identified at the analysis position P48 (**Table 5.3**).

From the previous analysis, it seems that cobalt blue, which was discovered in 1803 (Eastaugh, et al., 2004, p. 113), was the main blue pigment in the painting, with the complementary use of Prussian blue and azurite. Particularly interesting, however, was the identification of manganese blue, which was a modern pigment of the early 20th century (Eastaugh, et al., 2004, p. 38), leading to the conclusion that it may be a later addition. However, it had to be mentioned, that the identification of manganese blue contained doubts, due to the identification of this pigment only in one position of analysis but also due to the fact that XRF signal of sulfur were not easily detectable due to the fact that Auger yield was greater than the fluorescence (Donais & George, 2018, pp. 2-3; Janssens, 2013, p. 82).

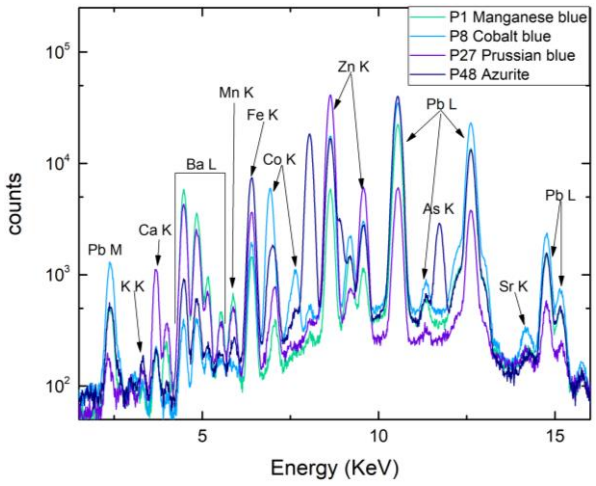

Figure 5.77 XRF spectra from the analysis positions: P1, P8, P27 and P48 of blue pigments of Statio VIII "Jesus and the Women of Jerusalem". Identification of: manganese blue, cobalt blue, Prussian blue and azurite (personal archive Karydas, Andreas-Germanos and Kesidis, Stelios).

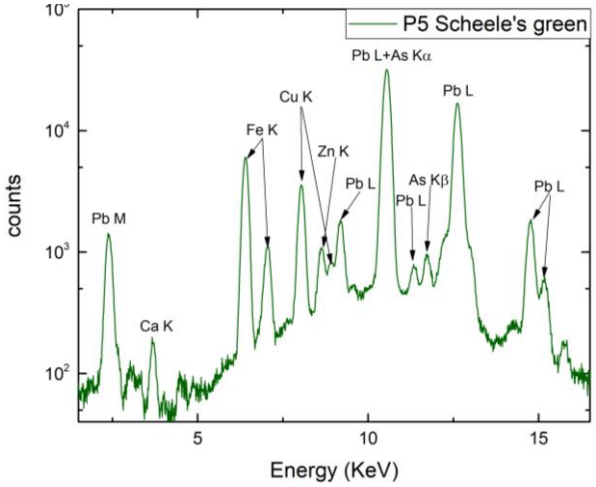

Figure 5.78 XRF spectra from the analysis position P5 of the green pigments of Statio VIII "Jesus and the Women of Jerusalem". Identification of: Scheele's green (personal archive Karydas, Andreas-Germanos and Kesidis, Stelios).

The elemental analysis of the green pigment by μ-XRF suggests the presence of the pigment Scheele's green (AsCuHO3) (**Figure 5.78**) (Eastaugh, et al., 2004, p. 335). However, it should be mentioned, that the detection of Scheele's green contains a margin of error, since the attribution was based on the presence of Cu and As K lines, not ruling out the possibility that it was emerald green ($Cu_4(OAc)_2(AsO_2)_6$) (Eastaugh, et al., 2004, p. 122). The pigment was identified at the analysis positions: P5 to P10 and at the analysis positions: P50 and P51. (**Table 5.3**).

The elemental analysis of the red pigments by μ-XRF suggests the presence of the pigments: cinnabar, red ochre, chrome orange and chrome red (**Figure 5.79**). Cinnabar (α-HgS) (Eastaugh, et al., 2004, p. 105) was identified at the analysis positions: P15 and P19. Red ochre (Fe_2O_3) (Eastaugh, et al., 2004, p. 279) was identified at the analysis positions: P15, P18, P19, P21, P22, P23, P28 to P35, P37 to 41, P47, P49 and P53. Chrome red and chrome orange ($PbCrO_4.PbO$) (Eastaugh, et al., 2004, p. 98) were identified at the analysis positions: P22, P24, P29 to P31, P34, P38, P40 and P53. (**Table 5.3**).

From the previous analysis, the conclusion arose that red ochre was the main red pigment in the painting, with the complementary use of cinnabar and orange chrome for the facial characteristics of some figures, while chrome red was identified only on the garment of Jesus. It should be mentioned, though, that some of the yields of iron peaked in red ochre and were due to the underlying layer.

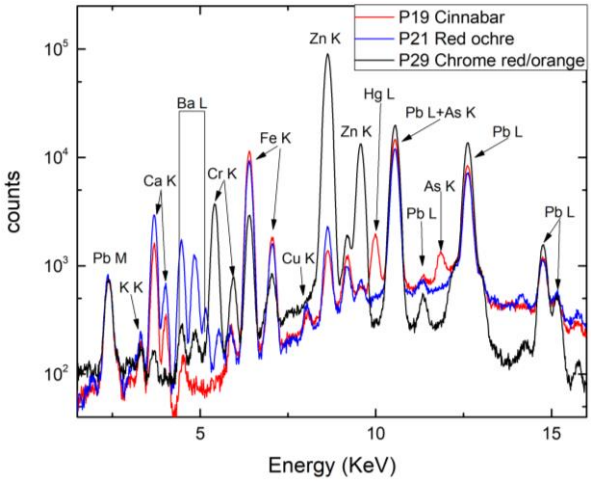

Figure 5.79 XRF spectra from the analysis positions: P19, P21 and P29 of the red pigments of Statio VIII "Jesus and the Women of Jerusalem". Identification of: cinnabar, red ochre, chrome red and chrome orange (personal archive Karydas, Andreas-Germanos and Kesidis, Stelios).

Furthermore, although cinnabar and red ochre had been used as pigments since antiquity (Eastaugh, et al., 2004, pp. 105, 279), chrome pigments were discovered in 1809 (Eastaugh, et al., 2004, p. 98), providing, this way, indirect information about the dating of the painting.

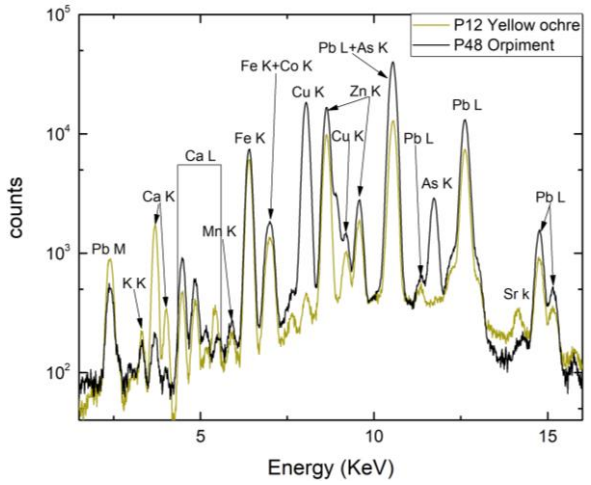

Figure 5.80 XRF spectra from the analysis positions: P12 and P48 of the yellow pigments of Statio VIII "Jesus and the Women of Jerusalem". Identification of: yellow ochre and orpiment (personal archive Karydas, Andreas-Germanos and Kesidis, Stelios).

The elemental analysis of the yellow pigments by μ-XRF suggests the presence of the pigments: yellow ochre and orpiment (**Figure 5.80**). Yellow ochre (γ-FeOOH) (Eastaugh, et al., 2004, p. 401) was identified at the analysis positions: P5 to P7, P11, P12, P18 and P51. Orpiment (As2S3) (Eastaugh, et al., 2004, p. 285; West FitzHugh, 1997, p. 47) was identified at the analysis positions: P20, P38 and P48. (**Table 5.3**). According to sources (Eastaugh, et al., 2004, p. 285; West FitzHugh, 1997, p. 50), orpiment was used until the end of the 19th century. Thus,

the identification of orpiment on the painting provides indirect information about the dating of the painting.

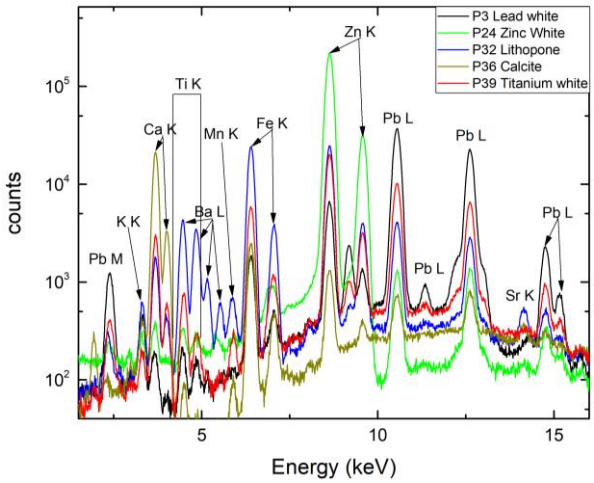

Figure 5.81 XRF spectra from the analysis positions: P3, P24, P32, P36 and P39 of the white pigments of Statio VIII "Jesus and the Women of Jerusalem". Identification of: lead white, zinc white, lithopone, calcite and titanium white (personal archive Karydas, Andreas-Germanos and Kesidis, Stelios).

The elemental analysis of the white pigments by μ-XRF suggests the presence of the pigments: lead white, calcite, zinc white, lithopone and titanium white (**Figure 5.81**). Lead white ($(PbCO_3)_2 \cdot Pb(OH)_2$) (Eastaugh, et al., 2004, p. 233) due to the high atomic number of lead (Pb) was identified in all analysis positions, however, due to the fact that XRF analysis provides elemental data, the discrimination between lead white and red lead (Pb_3O_4) (Eastaugh, et al., 2004, p. 229), component of the 8th and 9th layers of sample S1 (**Figure 5.71**) was not possible. Calcite ($CaCO_3$) (Eastaugh, et al., 2004, p. 74) was identified at the analysis positions: P18 and P36. Zinc white (ZnO) (Eastaugh, et al., 2004, p. 406) was identified at the analysis positions: P16, P17, P22, P23, P24, P27 to P31, P34, P38 to P40, P44 to P46, P51 and P53. Lithopone ($BaSO4 \cdot ZnS$) (Eastaugh, et al., 2004, pp. 242, 406) was identified at the analysis positions: P9, P11, P13, P20, P21, P27, P32, P37, P41, P42 and P52. Finally, titanium white (TiO_2) (Eastaugh, et al., 2004, p. 364) was identified at the analysis positions: P9, P23, P25, P27, P33, P36, P39 and P46 (**Table 5.3**).

The above analysis of the white pigments contributed important information about the history of the painting. While both lead white and calcite were used as pigments since antiquity, the identification of: zinc white, lithopone and titanium white on the painting, provide indirect information about the dating of the painting. Zinc white, which was discovered in 1803, and lithopone, which was discovered around the 1850 by G.F. de Doubet, were invented as alternatives for the replacement of the

toxic lead white, with the peak of their use being at the beginning of the 20th century (Eastaugh, et al., 2004, p. 406). Moreover, titanium oxide potentials as pigment were realized at the beginnings of the 20th century (Eastaugh, et al., 2004, p. 364). Finally, the fact that five white pigments were found in the painting reinforces the previous speculations of overpaintings.

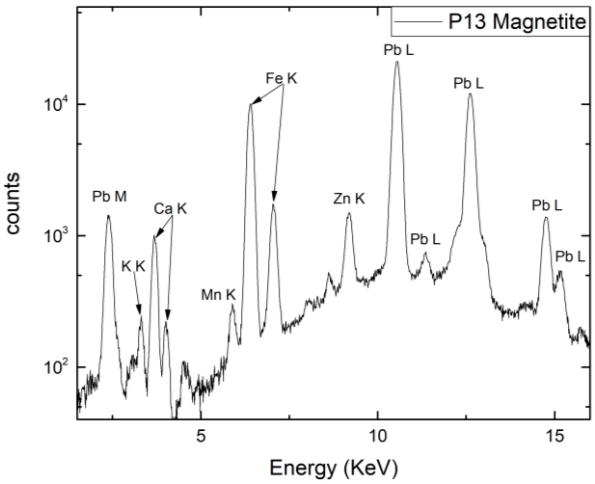

Figure 5.82 XRF spectra from the analysis position P13 of the black pigments of Statio VIII "Jesus and the Women of Jerusalem". Identification of magnetite (personal archive Karydas, Andreas-Germanos and Kesidis, Stelios).

The elemental analysis of the black pigments by μ-XRF suggests the presence of the pigment Magnetite (Fe_3O_4) (Eastaugh, et al., 2004, p. 248) (**Figure 5.82**). The pigment was identified at the analysis positions: P13, P14, P26 and P43 (**Table 5.3**).

Table 5.3 Elemental analysis of Statio VIII "Jesus and the Women of Jerusalem" by XRF

Spot	Colour	Elements Detected	Suggested Pigments
P1	Blue	Pb, Zn, Ba, Fe, Mn	Manganese blue, Lead white
P2	Red	Pb, Fe, Zn, Ca	Lead white
P3	Off-white	Pb, Zn, Fe, K	Lead white
P4	Red	Pb, Zn, Fe, Ca, Ba, K	Lead white
P5	Yellow	Pb, Fe, Cu, As, Zn, Co, Ca	Cobalt Blue, Scheele's green, Yellow ochre, Lead white
P6	Yellow	Pb. Fe, Zn, Cu, Ca, Co, As	Cobalt Blue, Scheele's green, Lead white
P7	Yellow	Pb, Fe, Cu, Zn, As, Co	Cobalt Blue, Scheele's green, Yellow ochre, Lead white
P8	Blue	Pb, Zn, Co, Fe, As, Cu, Ba,	Cobalt Blue, Scheele's green, Lead white
P9	Blue	Pb, Zn, Ba, Fe, Co, Ca, Ti, Cu, As, Mn	Cobalt Blue, Scheele's green, Lead white, Lithopone, Titanium white
P10	Dark blue	Pb, Fe, Cu, Co, Zn, As, Ca, Ba	Cobalt Blue, Scheele's green, Lead white

P11	Yellow	Pb, Fe, Zn, Ba, Ca, K, Ti	Yellow ochre, Lead white, Lithopone
P12	Light yellow	Pb, Fe	Yellow ochre, Lead white
P13	Grey	Pb, Fe, Ca, Zn, Mn, K	Lead white, Lithopone, Magnetite
P14	Dark grey	Fe, Ca, Pb, Zn, Ba, Mn	Lead white, Magnetite
P15	Brown	Pb, Fe, Ca, Hg, Cu, As, Mn	Cinnabar, Red ochre, Lead white
P16	Blue	Pb, Zn, Fe, Co, Ca, Ba, Cu,	Cobalt Blue, Lead white, Zinc white
P17	Pale yellow	Pb, Zn, Fe, Cu, Co	Cobalt Blue, Lead white, Zinc white
P18	Brown	Ca, Fe, Pb, Zn, Ba, Sr, Mn, As	Red ochre, Yellow ochre, Lead white, Calcite
P19	Red	Pb, Fe, Ca, Hg, Zn, Mn	Cinnabar, Red ochre, Lead white
P20	Green	Zn, Ba, Pb, Fe, As, Ca, Sr,	Prussian blue, Orpiment, Lead white, Lithopone
P21	Red	Pb, Fe, Ca, Zn, Ba, Cu, Mn	Red ochre, Lead white, Lithopone
P22	Pale brown	Zn, Pb, Fe, Mn, Cr, Ba, Ca	Red ochre, Chrome red/orange, Lead white, Zinc white
P23	Red	Pb, Fe, Ca, Zn, Cu, Ti, Ba, K	Red ochre, Lead white, Zinc white, Titanium white
P24	White	Zn, Fe, Pb, As, Co, Ca, Ba, Mn, Cr	Cobalt Blue, Chrome red/orange, Lead white, Zinc white
P25	Light blue	Pb, Fe, Zn, Ti, Co, Cu, Ca, Mn	Cobalt Blue, Lead white, Titanium white
P26	Black	Fe, Ca, Pb, Zn, Ba, K, Mn, Cu	Lead white, Magnetite
P27	Light blue	Zn, Pb, Ba, Fe, Ca, Co, Mn, Ti	Cobalt Blue, Prussian blue, Lead white, Zinc white, Lithopone, Titanium white
P28	Crimson red	Zn, Fe, Pb, Ca, K, Mn, Cr	Red ochre, Lead white, Zinc white
P29	Pink	Zn, Pb, Cr, Fe, Mn	Red ochre, Chrome red/orange, Lead white, Zinc white
P30	White	Zn, Fe, Pb, Ca, As, Cr, Mn	Red ochre, Chrome red/orange, Lead white, Zinc white
P31	Crimson red	Zn, Pb, Fe, Ba, Cr, Ca, Mn	Red ochre, Chrome red/orange, Lead white, Zinc white
P32	Dark crimson red	Zn, Fe, Ba, Pb, Ca, Mn, K, Sr, As	Red ochre, Lead white, Lithopone

P33	Dark crimson red	Fe, Pb, Zn, Ca, Ti, K	Red ochre, Lead white, Titanium white
P34	Pink	Zn, Pb, Fe, Cr, Ba, Ca, K, Co	Cobalt Blue, Red ochre, Chrome red/orange, Lead white, Zinc white
P35	Dark crimson red	Fe, Pb, Zn, Ca, Ti, K	Red ochre, Lead white
P36	Grey	Ca, Fe, Zn, Pb, K, Ti, Sn, Co	Cobalt Blue, Lead white, Calcite, Titanium white
P37	Dark crimson red	Fe, Zn, Ba, Ca, Sr, Mn, Pb, K	Red ochre, Lead white, Lithopone
P38	Crimson red	Zn, Pb, Fe, Ca, Cr, As, K, Sr	Red ochre, Chrome red/orange, Orpiment, Lead white, Zinc white
P39	Pale brown	Zn, Pb, Fe, Ca, Ti, Mn, K	Red ochre, Lead white, Zinc white, Titanium white
P40	Orange	Zn, Pb, Ca, Fe, Cr, K, Ti	Red ochre, Chrome red/orange, Lead white, Zinc white
P41	Dark brown	Fe, Pb, Zn, Ca, Ba, Cu, As, Mn, K	Red ochre, Lead white, Lithopone
P42	Dark blue	Zn, Pb, Fe, Ba, Ca, Sr, K	Prussian blue, Lead white, Lithopone
P43	Black	Fe, Ca, Pb, Zn, Ba, K, Ti	Lead white, Magnetite
P44	Blue	Pb, Fe, Zn, Co, Ca	Cobalt Blue, Lead white, Zinc white
P45	White	Pb, Zn, Fe, As	Lead white, Zinc white
P46	White	Pb, Fe, Zn, Ti, Ca	Lead white, Zinc white, Titanium white
P47	Pink	Zn, Pb, Ba, Fe, Ca, Co, Mn, Sr	Cobalt Blue, Red ochre, Lead white
P48	Blue	Pb, Cu, Zn, Fe, As, Co, Ba, Ca	Cobalt Blue, Orpiment, Lead white
P49	Red-orange	Pb, Fe, Zn, Co, Ba, Cu	Cobalt Blue, Red ochre, Lead white
P50	Blue-purple	Pb, Fe, Zn, Cu, Co, As	Cobalt Blue, Scheele's green, Lead white
P51	Green	Pb, Cu, Ca, Zn, As, Fe	Scheele's green, Yellow ochre, Lead white, Zinc white
P52	Grey	Zn, Pb, Ba, Fe, Ca, Co, Mn, Sr	Cobalt Blue, Lead white, Lithopone
P53	Red	Fe, Pb, Zn, Mn, Ba, Cr, Ca, Sr, K	Red ochre, Chrome red/orange, Lead white, Zinc white

5.1.7. Raman Spectroscopy

Figure 5.83 Statio VIII “Jesus and the Women of Jerusalem”. Positions of analysis by Raman spectroscopy (digital processing via Adobe Photoshop by Kesidis, Stelios).

The application of Raman spectroscopy on the Statio VIII “Jesus and the Women of Jerusalem” achieved to reveal important information about the composition of the pigments present in the painting. Moreover, Raman spectroscopy confirmed and specified the presence of pigments identified also by the other analytical techniques of the analytical protocol.

In the analysis of the painting, 9 point (***Figure 5.83***), analyzes were performed. It was decided that the analysis of the results of Raman spectroscopy would be done in colour.

Analysis of the blue coloured areas by Raman spectroscopy identified the existence of the pigment ultramarine ($Na_7Al_6Si_6O_{24}S_3$) (Eastaugh, et al., 2004, p. 375; Roy, 1993, p. 55) (**Figure 5.84**). The pigment was identified at the analysis position R2. The weak Raman signal of the other blue-coloured areas (R4, R5 and R6) did not provide any information on the pigment analyzed, possibly due to the lining treatment, which was performed with the glue-paste or the wax-resin techniques (Andersen & Fuster-Lopez, 2019, p. 17) **(Table 5.4)**.

Raman spectra, collected from brown-coloured areas (R9), were dominated by an intense broadband fluorescence emission and as such did not provide any information on the pigment present. **(Table 5.4)**.

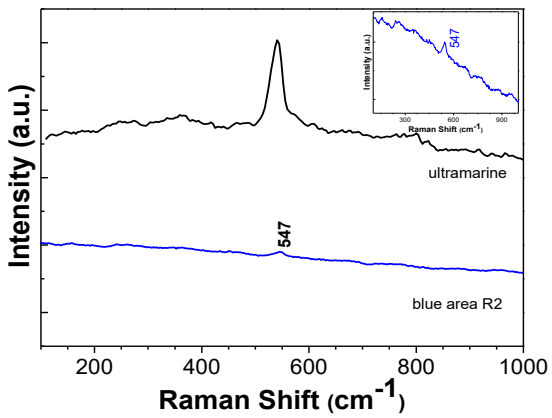

Figure 5.84 Raman spectrum collected from the analysis position (R2), showed a band corresponding to ultramarine. A spectrum from pure ultramarine was shown as a reference (black line). (In the inset, the Raman spectrum of the analysis position (R2) was presented enlarged) (personal archive of Dr. Filippidis, Aggelos and Kesidis, Stelios) (Burgio & Clark, 2001).

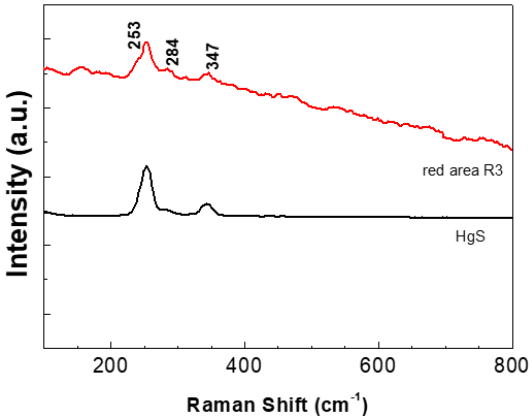

Figure 5.85 Raman spectrum collected from a red (R3) painted area, showed bands corresponding to cinnabar/vermilion (HgS). A spectrum from pure HgS was shown as a reference (black line) *(*personal archive of Dr. Filippidis, Aggelos and Kesidis, Stelios) (Burgio & Clark, 2001).

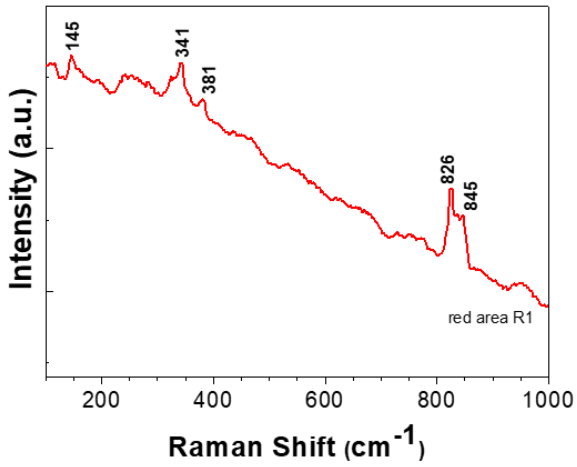

Figure 5.86 Raman spectrum collected from a red (R1) painted area, showed bands corresponding to chrome orange (PbCrO4.PbO) (personal archive of Dr. Filippidis, Aggelos and Kesidis, Stelios) (Burgio & Clark, 2001).

The intense fluorescence emission overwhelms the Raman scattering and for this reason, did not provide any information for the yellow-coloured areas (R7 and R8) **(Table 5.4)**.

Analysis of the red coloured areas by Raman spectroscopy identified the existence of the pigments: cinnabar and chrome orange. Cinnabar (α-HgS) (Eastaugh, et al., 2004, p. 105) was identified at the analysis position R3 (**Figure 5.85**). Chrome orange (PbCrO4.PbO) (Eastaugh, et al., 2004, p. 98) was identified at the analysis position R1 (**Figure 5.86**). (**Table 5.4**).

Table 5.4 Summary of the results obtained with mobile Raman micro-spectrometer for Statio VIII "Jesus and the Women of Jerusalem"

Spot	Colour	Pigment Identified
R1	Red	Chrome orange
R2	Blue	Ultramarine
R3	Red	Cinnabar
R4	Blue	Weak Raman signal
R5	Blue	Weak Raman signal
R6	Blue	Weak Raman signal
R7	Yellow	Intense fluorescence emission
R8	Yellow	Intense fluorescence emission
R9	Brown	Intense fluorescence emission

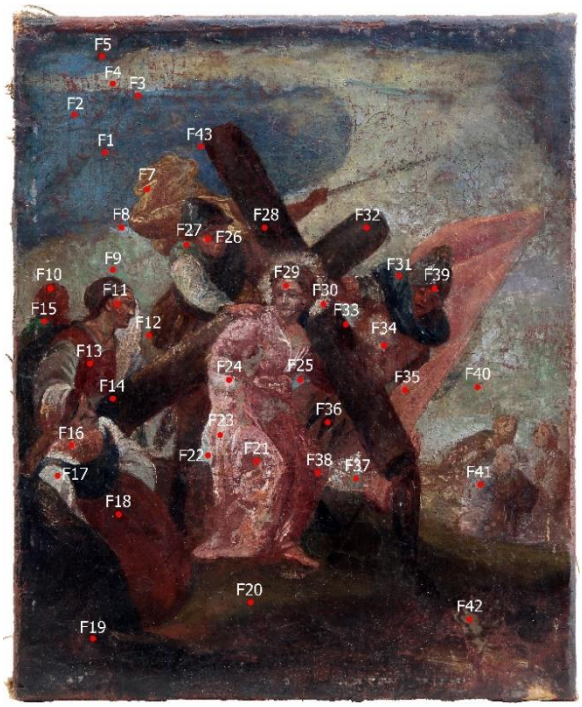

Figure 5.87 Statio VIII "Jesus and the Women of Jerusalem". Positions of analysis by laser induced fluorescence spectroscopy (digital processing via Adobe Photoshop by Kesidis, Stelios).

5.1.8. Laser Induced Fluorescence Spectroscopy

The application of laser induced fluorescence spectroscopy on the painting Statio VIII "Jesus and the Women of Jerusalem" identified the presence of fluorescent pigments

.

In the analysis of the painting, 43 point (**Figure 5.87**), analyzes were performed.

Examination of the painting with LIF showed mainly the presence of zinc white pigment (ZnO) in white, light red and light blue areas. Typical LIF spectra, indicative of ZnO, was recorded on the dress (light red and light blue areas), the forehead and the halo of Jesus Christ, as well as the guard's uniform. In **Figure 5.88**, **Figure 5.89**, **Figure 5.90** and **Figure 5.91**, LIF spectra, which were recorded at different areas of the painting, were present, in comparison with the (reference) LIF spectrum of pure ZnO. In the

spectra, two main fluorescence bands were observed: a strong band, at around 380 nm, and a weak one at around 510 nm, which were characteristic of pure ZnO (**Figure 5.90** and **Figure 5.91**). The weak fluorescence band was observed at around 500 nm (Fig. 2a) and at around 506 nm (**Figure 5.89**).

Zinc White (ZnO) (Eastaugh, et al., 2004, p. 406) was identified at the analysis

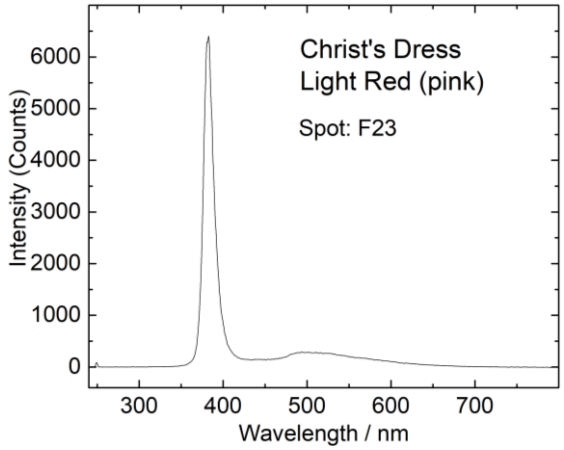

Figure 5.88 LIF spectrum recorded at point F23A (Christ's robe, light red) on STATIO VIII painting (personal archive of Dr. Kokkinaki, Olga and Kesidis, Stelios).

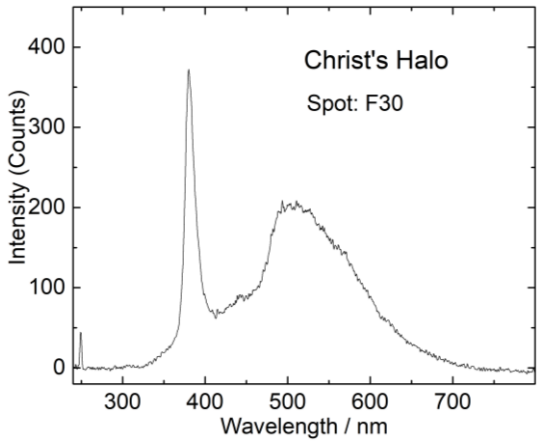

Figure 5.89 LIF spectrum at point F30 (halo, white) on STATIO VIII painting (personal archive of Dr. Kokkinaki, Olga and Kesidis, Stelios).

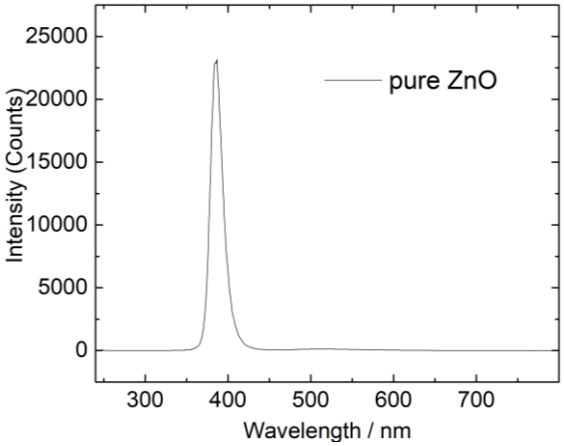

Figure 5.90 LIF spectrum of pure ZnO (personal archive of Dr. Kokkinaki, Olga and Kesidis, Stelios).

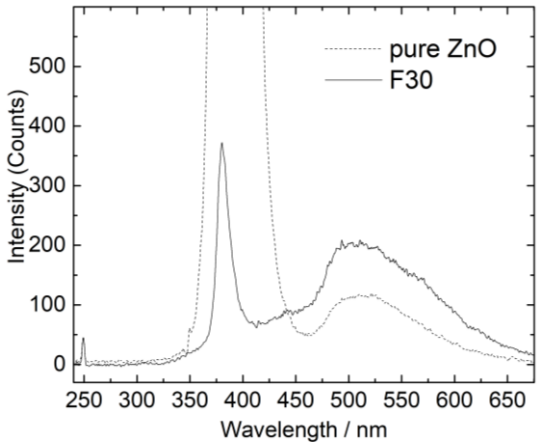

Figure 5.91 LIF spectrum at point F30 (halo, white) on STATIO VIII painting in comparison with pure ZnO reference spectrum (personal archive of Dr. Kokkinaki, Olga and Kesidis, Stelios).

positions: F8, F9, F11, F12, F22 to F25, F27, F29 to F31, F34, F37, F39 and F43.

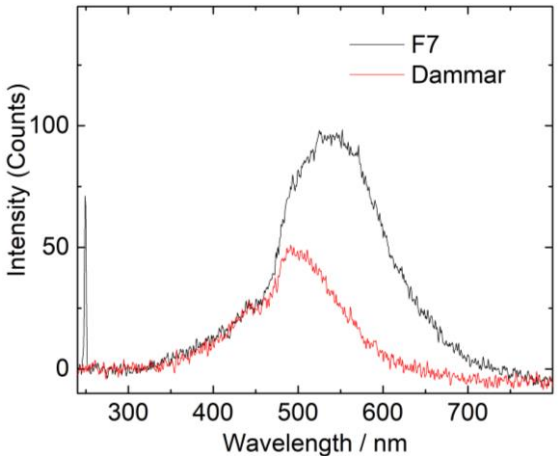

Figure 5.92 LIF spectra recorded at point F7 on STATIO VIII painting and on aged dammar varnish (reference sample) (personal archive of Dr. Kokkinaki, Olga and Kesidis, Stelios).

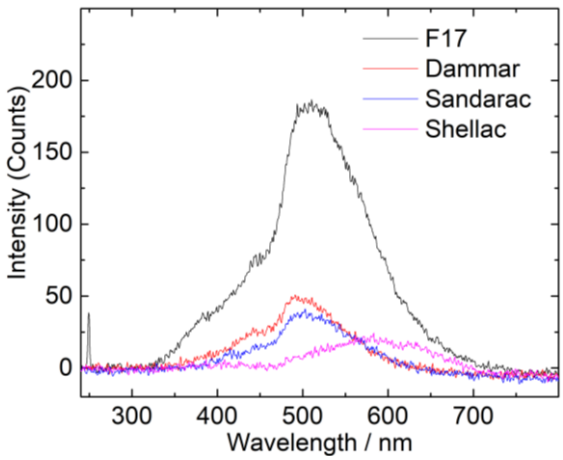

Figure 5.93 LIF spectra recorded at point F17A on STATIO VIII painting and on aged varnish (reference) samples (dammar, sandarac and shellac) (personal archive of Dr. Kokkinaki, Olga and Kesidis, Stelios).

In cases where no zinc white was observed, a broad band with a maximum in the region around 505-520 nm was observed. This band was probably indicative of varnish, however comparative examination of the spectra with spectra recorded from reference aged varnish films (e.g. dammar, mastic, shellac, etc.) did not show any correlation (**Figure 5.92**, **Figure 5.93**). Therefore, no varnish was identified.

5.1.9. Diffuse Reflectance Spectroscopy

The application of diffuse reflectance spectroscopy on the painting Statio VIII "Jesus and the Women of Jerusalem" provided valuable and important information on the pigments used by the artist on his painting.

In the analysis of the painting, 36 point analyzes were performed (**Figure 5.94**). It was decided that the analysis of the results of diffuse reflectance spectroscopy would be done in colour.

Analysis of the blue coloured areas by diffuse reflectance identified the existence of the pigments: ultramarine and cobalt blue. Ultramarine [$Na_{6\text{-}8}(AlSiO_4)_6S_{2\text{-}4}$] was identified

in the blue coloured area drblue14 (**Figure 5.*95***) while cobalt blue [$CoO.Al_2O_3$] was identified in drblue3 and drblue6 (**Figure 5.*96***). Spectra collected from blue coloured areas: drblue1, drblue2, drblue4, drblue5, drblue15 did not provide accurate information for pigment identification (**Figure 5.97**). Although spectra of blue areas: drblue1, drblue2, drblue4, drblue15 showed similar spectral profile which may be an indication of common chemical composition. (**Table 5.5**).

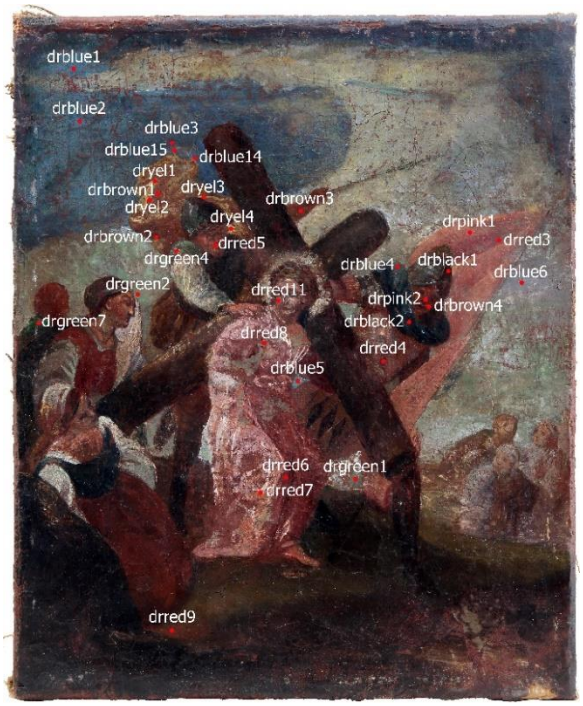

Figure 5.94 Statio VIII "Jesus and the Women of Jerusalem". Positions of analysis by diffuse reflectance spectroscopy (digital processing via Adobe Photoshop by Kesidis, Stelios).

Spectra collected from green coloured areas did not provide information for pigment identification. Spectra collected from areas: drgreen5 and drgreen7 showed similar spectral profile as well as spectra from areas: drgreen1 and drgreen3 (**Figure 5.98**).

The diffuse reflectance spectra collected from brown coloured areas display similar profile with a characteristic change in curvature between 590 nm (**Figure 5.99**), that could be attributed to red ochre (Fe_2O_3), although there was significant uncertainty to this assumption.

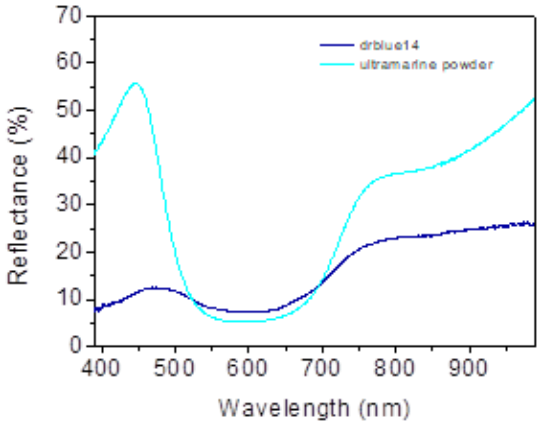

Figure 5.95 Diffuse reflectance spectra collected from blue area drblue14 and ultramarine powder for comparative analysis.

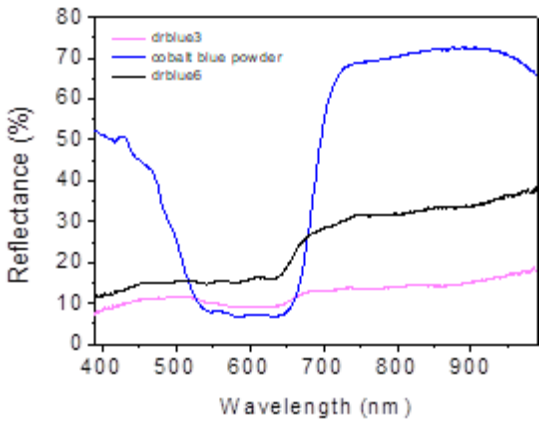

Figure 5.96 Diffuse reflectance spectra collected from blue areas: drblue3 and drblue6 and cobalt blue powder for comparative analysis.

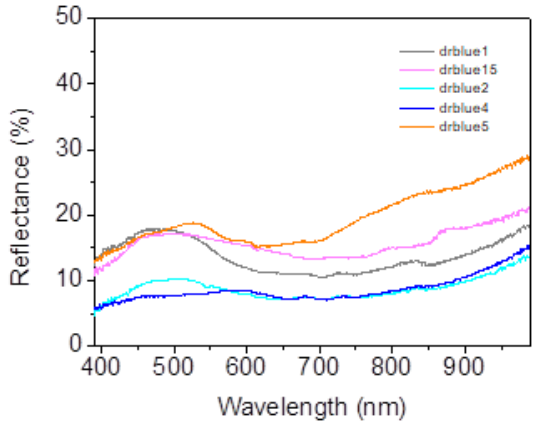

Figure 5.97 Diffuse reflectance spectra collected from blue areas: drblue1, drblue2, drblue4, drblue15 and drblue5.

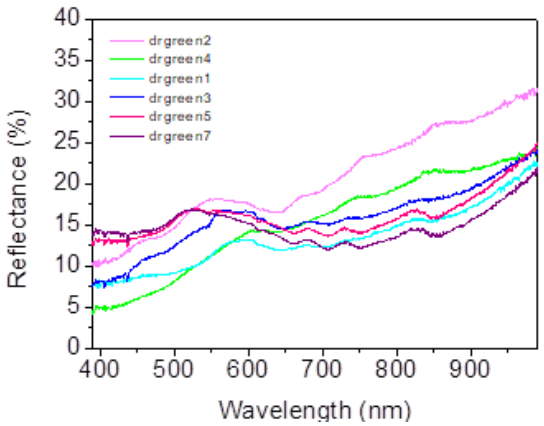

Figure 5.98 Diffuse reflectance spectra collected from green coloured areas: drgreen1, drgreen2, drgreen3, drgreen4, drgreen5 and drblue7.

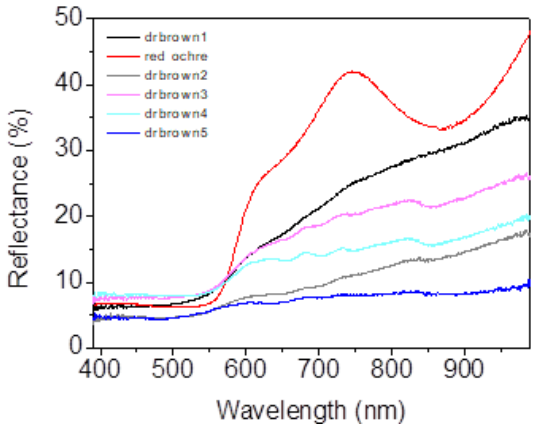

Figure 5.99 Diffuse reflectance spectra collected from brown coloured areas: drbrown1, drbrown2, drbrown3, drbrown4, drbrown5 and red ochre powder for comparative analysis.

The diffuse reflectance spectra collected from red coloured areas: drpink2, drpink3, drred11, drred5, drred7 and drred8 showed similar spectral profile (**Figure 5.100**) that could be attributed to a mixture of red ochre and cinnabar pigments. Diffuse reflectance spectrum of cinnabar pigment (HgS) showed a characteristic inflection point at 590 nm (2.1 eV) and high reflectance values in the near IR region. The spectrum of red ochre pigment (Fe_2O_3) showed a broad band with minimum at 872 nm, a second band at 654 nm and a broad band with minimum in the reflectance at 550 nm all attributed to electronic transition of the iron ion. The diffuse reflectance spectra collected from red areas: drred1, drred2, drred3, drred4, drred6, drred9, drpink1 (**Figure 5.101**) showed different spectral profiles similar to that of red ochre pigment. The main differences between the two groups of red areas were the abrupt incline of the spectra between 550 and 600 nm in the first group, due to cinnabar, and the appearance of a broad band at 872 nm, due to red ochre, in the second group which may have disappeared due to cinnabar in the first one. Differences in the reflectance values were attributed to the existence of some white compound. (**Table 5.5**).

Analysis of the diffuse reflectance spectra collected from the yellow coloured areas indicate the existence of both red and yellow ochre pigment. Diffuse reflectance spectrum of yellow ochre [FeO(OH).xH2O] showed a characteristic increase in the reflectance at 450 nm and an S-shape curve between 480 and 580 nm (**Figure 5.102**). The existence of red ochre shifts the spectrum to the red end (**Table 5.5**).

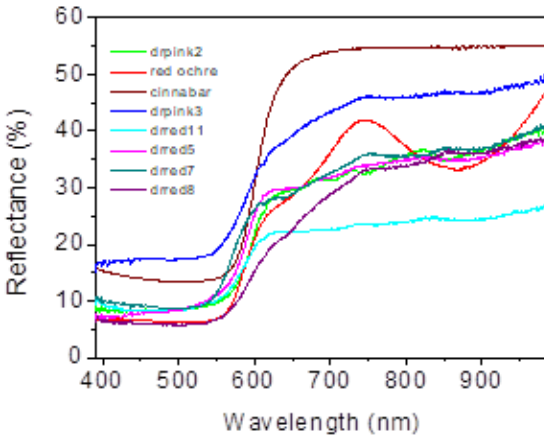

Figure 5.100 Diffuse reflectance spectra collected from red coloured areas: drpink2, drpink3, drred11, drred5, drred7, drred8 and red ochre and cinnabar powder for comparative analysis.

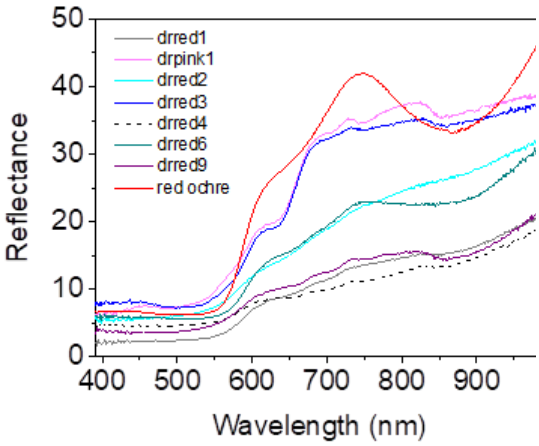

Figure 5.101 Diffuse reflectance spectra collected from red coloured areas: drred1, drpink1, drred2, drred3, drred4, drred6, drred9 and red ochre powder for comparative analysis.

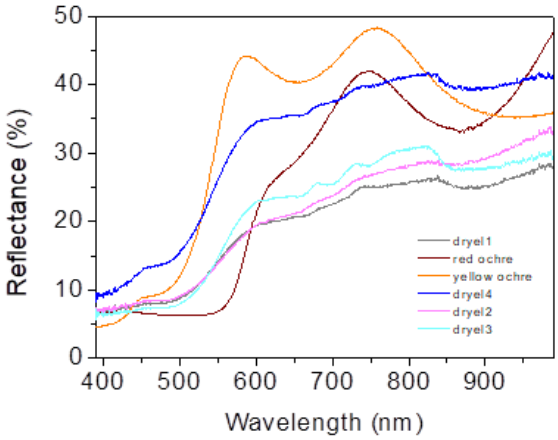

Figure 5.102 Diffuse reflectance spectra collected from yellow coloured areas: dryel1, dryel4, dryel2, dryel3 and red ochre and yellow ochre powder for comparative analysis.

Table 5.5 Summary of the results obtained with diffuse reflectance portable system for Statio VIII

Coloured Area Code	Pigment Identified	Coloured Area Code	Pigment Identified
Drblue1	-	**Drbrown5**	Possibly red ochre
Drblue15	-	**Drpink2**	Cinnabar and red ochre
Drblue2	-	**Drpink3**	Cinnabar and red ochre
Drblue4	-	**Drred11**	Cinnabar and red ochre

Drblue5	-	**Drred5**	Cinnabar and red ochre
Drblue14	Ultramarine	**Drred7**	Cinnabar and red ochre
Drblue3	Cobalt blue	**Drred8**	Cinnabar and red ochre
Drblue6	Cobalt blue	**Drred1**	Red ochre
Drgreen2	-	**Drpink1**	Red ochre
Drgreen4	-	**Drred2**	Red ochre
Drgreen1	-	**Drred3**	Red ochre
Drgreen3	-	**Drred4**	Red ochre
Drgreen5	-	**Drred6**	Red ochre
Drgreen7	-	**Drred9**	Red ochre
Drbrown1	Possibly red ochre	**Dryel1**	Red ochre and yellow ochre
Drbrown2	Possibly red ochre	**Dryel4**	Red ochre and yellow ochre
Drbrown3	Possibly red ochre	**Dryel2**	Red ochre and yellow ochre
Drbrown4	Possibly red ochre	**Dryel3**	Red ochre and yellow ochre

5.2. Statio XIII “Lamentation”

5.2.1. Digital Photography

Digital photography provided important and useful information regarding the study of the techniques of the artist and the surface characteristics of the painting which lead to a better understanding of its preservation state, with the detection of later additions or alterations.

Starting with the analysis of the picture taken in the visible part of the electromagnetic spectrum with illumination positioned at an angle of 45^{o} degrees to the painting (**Figure 5.103**) it was observed that the artist used a wide variety of colours as well as techniques in creating the painting. Moreover, the preservation state of the painting could be characterized as relatively poor, however there were indications of later additions, overpaintings and past conservation treatments. On the edges of the painting small areas of losses were observed, while on the top left corner two different types of canvases are observed (**Figure 5.104**). The key differences between them were the weave density, the fiber thickness and the colour. This led to the assumption that lining treatment was performed.

Figure 5.103 Statio XIII “Lamentation”, under VIS illumination at 45^{o} (photo credit: Rompakis, Panagiotis, National Gallery - Greece).

The sky, which occupied half of the painting, was black-coloured with a uniform hue. The paint seemed to have been applied evenly, while no brushstrokes were observed.

Figure 5.104 Statio XIII “Lamentation”. Detail from the top left corner of the painting, where two different canvases were observed (photo credit: Rompakis, Panagiotis, National Gallery - Greece).

Figure 5.105 Statio XIII “Lamentation”. Detail of the thorny wreath, where the underlying grey paint layer was observed (photo credit: Rompakis, Panagiotis, National Gallery - Greece).

The ground could be divided into three areas. The first was the one in which the figures were. It was brown-coloured with green and red details. The white inscription seems to have undergone alterations, since its lower right corner had a different texture from the rest of the object, it seems that this point was an authentic part of the object, while the rest was due to a later aesthetic restoration treatment. After careful observation, the suspicion arose that this level of the ground was completely overpainted. The red spots were part of the preparation layer, however there were scattered areas where a second layer of paint was clearly visible below the one shown in this brown-green colour. A characteristic point, where the underlaying layers was clearly visible, was the thorny wreath (**Figure 5.105**), at the top of which a gray layer with chiaroscuro could be seen, creating the impression of rock. After observing this point, others similar to it were searched, with positive results (left of the panel, and other small points). The second area was that of the main background, where rocky landscapes were represented in brown, while the third area was behind the second and appeared

as straight green lines, where the observation of this area requires careful observation.

Jesus who was the central figure of the painting seemed to have received extensive overpaintings and alterations. The white linen cloth appeared to have a white coating of overpainting with areas of the original cloth remaining visible. The “authentic” parts of the cloth had a more uniform appearance and whitish colour in relation to the rough touch of the overpainting and the intense white colour of the pigment. Upon careful observation, the body of Jesus appeared to have been almost completely covered by another pigment. This was inferred as the top layer left some points uncovered where the underlying original layer was visible. The underlying layer also matched in colour with the face of Jesus in which there were no clear subsequent interventions. The posterior layer was located all over the torso, the upper part of the legs and the entire part of the soles of the feet, in the hands and it was located mainly on the shoulders.

The Virgin Mary, who kneels and supports the dead body of Jesus, was also a central figure of the painting. After a detailed examination of the pictures taken, it arose that big parts of her body and face bore extensive overpaintings. In particular, her yellow shawl gets very bright in the front, while the paint in this area was applied with the technique of impasto. In some parts of the himation, such as directly below the right hand of the Virgin Mary, an area with a vivid blue pigment was located, which lays under the light-blue colour of himation and may be the original colour of the himation. This led to the conclusion that the robe of the Virgin Mary had also been overpainted. Finally, her face and hands also bore overpaintings. The right side of her face was assumed to be the original layer, while the bright area of the neck and perhaps a large part of the face were overpaintings. The Virgin's hands followed the same pattern as the face; the base of both hands was very different in colour (beige) while the palms were almost pink.

Figure 5.106 Statio XIII “Lamentation”. Under VIS illumination at 45º, rear view (photo credit: Rompakis, Panagiotis, National Gallery - Greece).

Figure 5.107 Statio XIII “Lamentation”. Detail from the rear view of the painting, where the third type of canvas was observed (photo credit: Rompakis, Panagiotis, National Gallery - Greece).

Lastly, Saint John's right shoulder had a warmer shade of lower artistic performance compared to the rest of the undertunic which had a softer shade and looked more homogeneous. The features of his face were very simplistic and without details in relation to the faces of Jesus and the Virgin Mary.

On the rear view of the painting (**Figure 5.106**) the frame and the backside of the canvas could be observed. The frame had a good preservation state with only some surface damage. The canvas was characterized by its dense weaving and its fine fibers. Upon closer observation of the rear of the painting the presence of one more type of canvas was revealed (**Figure 5.107**), apart from the two encountered to the front of the painting. Thereby, it could be assumed that a second lining treatment was performed.

Afterward, the picture taken in the visible part of the electromagnetic spectrum with illumination that was positioned at an angle of 5º degrees to the painting was studied (**Figure 5.108**). During the study of the painting under

tangentially incidental radiation the intense relief, the cracks and the poor preservation state of the surface became apparent.

After the analysis of the picture it was observed that the intensity of the relief was limited to the perimeter of the painting due to the stretcher that supported it. Due to the two lining treatments, the canvas pattern was strongly visible throughout the surface of the painting.

Figure 5.108 Statio XIII “Lamentation”. Under VIS illumination at 45º (photo credit: Rompakis, Panagiotis, National Gallery - Greece).

An area of interest was the sky, where cracking networks to the left of the cross were different to that on the right. On the left side crackings were divided in big parts on an uneven cracking network, while on the right side the relief had lower profile and was divided in smaller parts. Additionally, the paint on areas of the cross seemed to have been applied with the technique of impasto.

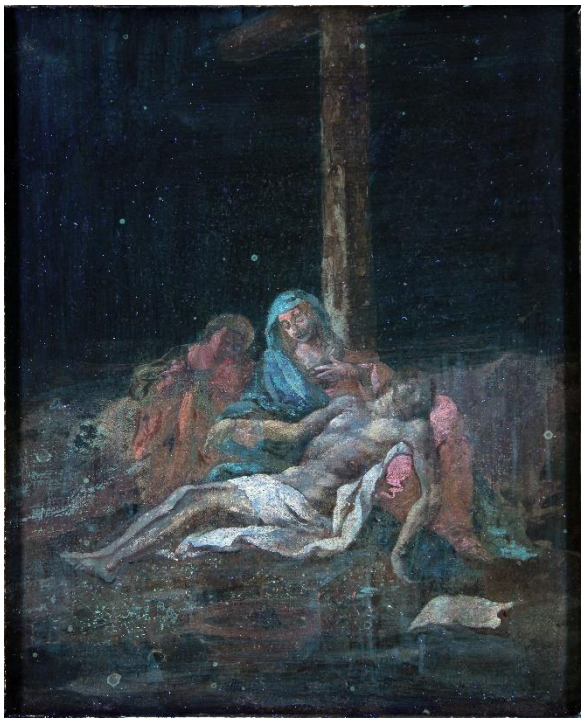

Figure 5.109 Statio XIII “Lamentation”. UV fluorescence photography at 45º (photo credit: Rompakis, Panagiotis, National Gallery - Greece).

The study of the painting "Station XIII" through the technique of digital photography was completed with the analysis of the photograph carried out using ultraviolet illumination (**Figure 5.109**). The study of the surface of the painting using UV

radiation revealed the hidden pictorial characteristics, the many later alterations or additions and the poor preservation state. The painting was generally covered by a blue fluorescent, for which the top layer of varnish should have been responsible.

The sky was characterized by blue fluorescence, while the direction of the brushstroke from the application of the varnish became apparent. In some areas, such as above the Virgin Mary and John, green-yellow spots were observed, perhaps remnants of wax.

The ground next to St. John in some places was fragmentarily blue fluorescent. This fluorescence cannot be matched to a visible feature of the painting. Thus, the hypothesis arose that it was a fluorescent pigment that was located under the upper paint layer. In this area there were also intensely dark spots that were overpaintings and may have been located above the fluorescent layer of varnish. Moreover, areas that showed small size, often in alignment, squares were assumed to belong to a layer of varnish that was removed, perhaps not completely. Also, in the outline of John's body there was a light-yellow area on which there were other dark areas and it should be considered as an overpainting. In the area just below Jesus' feet two different types of fluorescents were observed. The first was the one that appeared very fragmentary and was very intense, and corresponded to an area with white residues of fluorescent pigment. The second was the same as the one found next to the body of St. John, this part had less intense fluorescence and was located in areas where the upper layer of paint was missing due to wear.

On the area of the plate and its perimeter were located extensive overpaintings as dark areas. Specifically, at the left end of the plate was observed part of the original painting (**Figure 5.110**) (the pigment that covers the plate was an overpainting) observation that was possible only through UV lighting. The same sequence of fluorescent species previously attributed to the underlying paint layer was then observed. Such areas were located above and to the right of the plate, in the thorny wreath and in other scattered places. The specific points coincided with the areas, which during the observation with visible radiation, were also attributed to an underlying painting layer (**Figure 5.111**). The inscription, when observed with UV

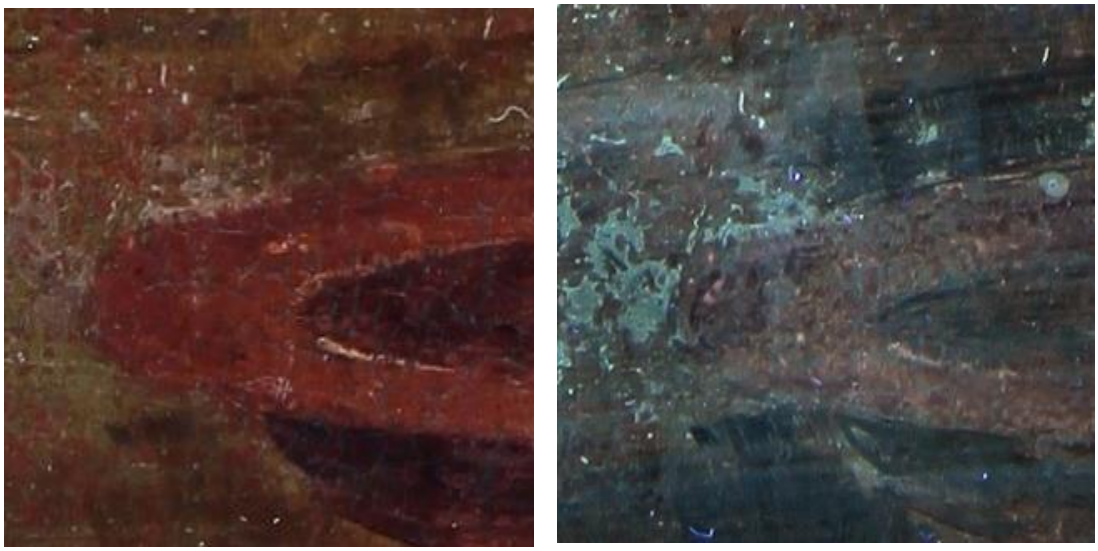

VIS UVF

Figure 5.110 To the left: detail of the plate in the visible part of the electromagnetic spectrum. To the right: detail of the plate in the UV part of the electromagnetic spectrum. Under UV lighting, part of the original painting was observed at the left end of the plate (photo credit: Rompakis, Panagiotis National Gallery - Greece).

VIS UVF

Figure 5.111 To the left: detail of the thorny wreath in the visible part of the electromagnetic spectrum. To the right: detail of the thorny wreath in the UV part of the electromagnetic spectrum. Under VIS lighting, the underlying grey paint layer was observed. Under UV lighting, the underlying fluorescent paint layer was observed (photo credit: Rompakis, Panagiotis, National Gallery - Greece).

radiation, appeared to consist of many different admixtures of pigments, the shadows observed in the visible part of the spectrum here turned brown, while a small part of the shading when observed in UV appeared as black, which confirmed suspicions of overpainting.

Regarding the body of Jesus, many overpainting treatments were found, as well as traces of old varnish. In particular, it seemed that a large part of His torso and parts of His head had overpaintings, which were observed thanks to their intense fluorescence, which was quite different from the fluorescence of the original parts of the painting. From the fluorescence variation of the paintings, it was concluded that at least three different pigments had been used (**Figure 5.112**).

UVF

Figure 5.112 Statio XIII "Lamentation". Detail of Jesus's body under UV lighting. The many overpainting treatments and the traces of old varnish were observed (photo credit: Rompakis, Panagiotis, National Gallery - Greece).

In the same way, Virgin Mary bore many overpaintings, while a different varnish covers areas of her body. In particular, various overpaintings were found on her face, arms and legs, which had similar fluorescence to areas identified as overpaintings on other parts of the object. Furthermore, the front side of the yellow shawl also constitutes an overpainting. The under tunic of the Virgin Mary located above Jesus' body was covered with old varnish, while the later aesthetical restoration treatment on the sleeve could be observed, with the same type of aesthetical restoration treatment also located at the knees of the Virgin (**Figure 5.113**). The attribution of this treatment as an aesthetical restoration was based on the fact that it could be traced only on areas where previous wear existed. As concerned the himation, there was extensive overpainting, perhaps by a painter. It seemed (from points of loss of the upper painting layer) that the overpainting

had followed the underlying pattern as far as the folds of the himation were concerned. While the existence of overpaintings should be considered certain in an attempt to restore the painting after the first stage of overpainting. The original colour of the himation could be seen in some fragmentary areas above the right hand of Jesus, in the bright part of the himation under the right hand of Jesus, and in the lower right corner of the himation, near the foot of the Virgin Mary (**Figure 5.113**). The characteristic that led to the assessment that this colour was the original, was initially that it was observed in areas of damage of the upper paint layer and that it was covered by a layer of highly oxidized varnish (in the lower right corner of the himation, near the Virgin Mary's foot, and the dark area above and below the right hand of Christ).

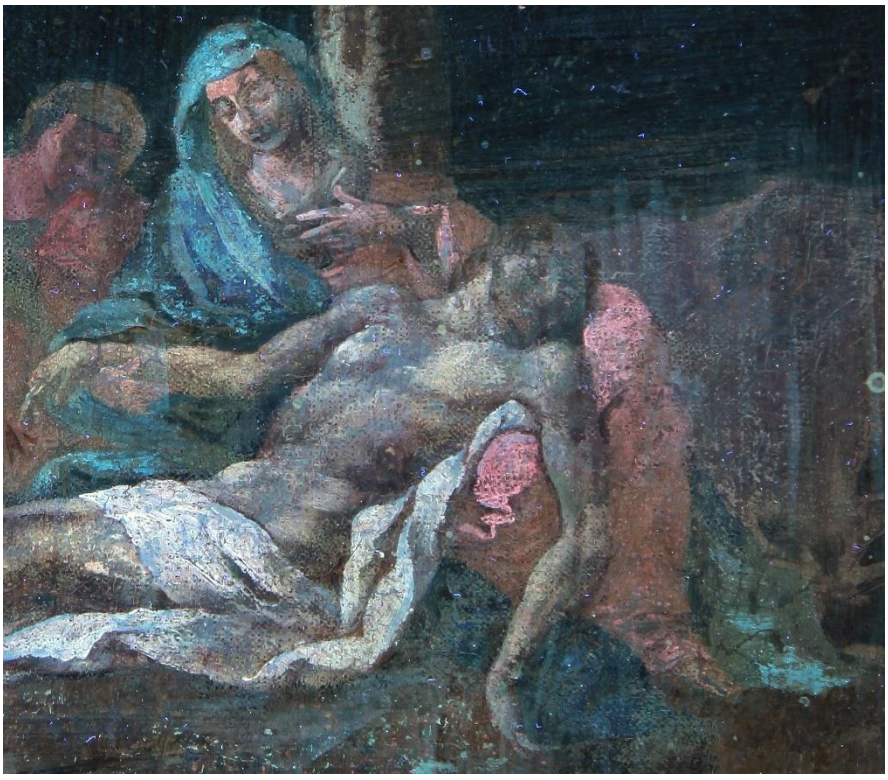

UVF

Figure 5.113 Statio XIII “Lamentation”. Detail of Virgin Mary’s body under UV lighting. The many overpainting treatments and the traces of old varnish were observed (photo credit: Rompakis, Panagiotis, National Gallery - Greece).

Regarding the colour of the extended overpainting, just above the forehead of the Virgin Mary, an area with a different blue shade was located. This point, after

careful observation of the VIS, showed sleekness and homogeneity, leading to the assessment that it was the colour used for the extended painting of the himation.

UVF

Figure 5.114 Statio XIII "Lamentation". Detail of St. John's body under UV lighting. The overpainting treatments and the traces of old varnish were observed (photo credit: Rompakis, Panagiotis, National Gallery - Greece).

Finally, St. John's body was also covered in its biggest part by an older varnish. While the face of St. John and the top right part of his undertunic could be considered as overpaintings (**Figure 5.114**). The reasons that lead to the conclusion that the face of St. John bore an overpainting were the uniformity of the pigments, their very different colour rendering in relation to the faces of the other two forms, the similarity of the illumination on the face and neck of John with that on the face and neck of the Virgin already assessed as an overpainting and the much inferior painting style used in relation to the other two faces (the details of the face but also the abrupt transition from the light side of the face to the dark, indicate an inexperienced painter).

5.2.2. Multispectral Imaging

Multispectral imaging provided detailed features of the painting, which revealed underlying and hidden elements, identified subsequent conservation treatments, and provided important information on the composition of materials, their chemical distribution, and manufacturing technology.

The study of the painting Statio XIII "Lamentation" started with the analysis of the images taken on reflection mode (**Figure 5.115**). It was decided that the analysis

would follow the previous methodology, in the technique of digital photography, where each feature of the painting was analyzed separately. Thus, in the analysis of the images of the multispectral display, reference would be made to features that were found in all six selected wavelengths.

IRR 500 nm IRR 600 nm IRR 700 nm

IRR 800 nm IRR 900 nm IRR 1000 nm

Figure 5.115 Statio XIII “Lamentation”. Multispectral images were taken on reflection configuration on the six selected bands of 500 nm, 600 nm, 700 nm, 800 nm, 900 nm and 1000 nm (photo credit: Dr. Moutsatsou, Anna P., National Gallery - Greece).

The dark sky at all wavelengths remained unaffected, with the original black colour appearing evenly everywhere. However, at 1000 nm to the right of the cross an area with very little reflection appeared, resembling a cloth wrapped around the cross (**Figure 5.116**). This would imply that since this area was not otherwise visible, this area was a painting. Also, to the right and above the head of John, two areas of small reflection also appeared at 1000 nm.

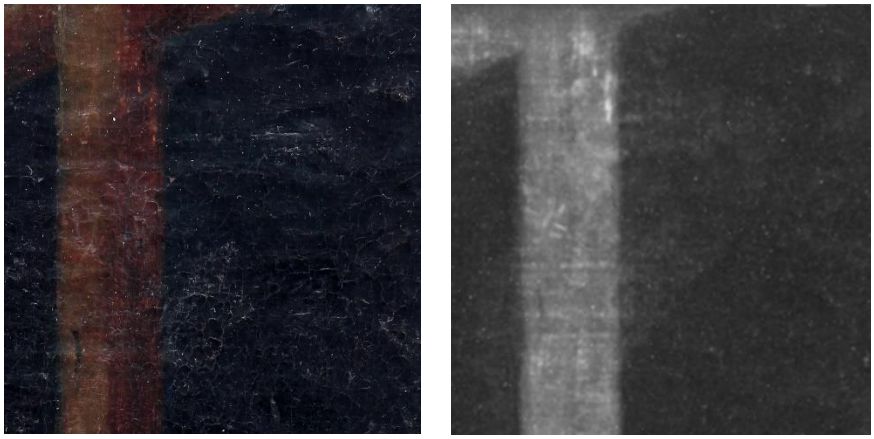

VIS IRR 1000 nm

Figure 5.116 Statio XIII “Lamentation”. To the left: part of the cross in the visible part of the electromagnetic spectrum. To the right: part of the cross at 1000 nm. A cloth wrapped around the cross was observed (digital processing via Adobe Photoshop by Kesidis, Stelios).

Observing the cross at 700 nm and above, the canvas pattern became apparent. This suggested that the stratigraphy of this area was delicate. Also, small areas of overpaintings and grouting treatments were observed.

As far as the ground was concerned, through the multispectral imaging the poor state of preservation of the object became apparent. The main reason for the state of preservation seemed to be the lining treatments, which had caused losses of paint but also resulted in a strong observation of the canvas pattern. Areas with loss of paint were observed with a greater degree of reflection. In addition, it was observed that the left edge of the plate had no clear boundaries. Also, to the right of the painting there was an area to the right of the Virgin Mary, in which no damage was caused, thus creating the assumption that this area was a later operation, as it was the only point in the painting where the canvas pattern was not observed.

Analysis of the body of Jesus confirmed hypotheses about the presence of overpaintings. Specifically, the areas that in the VIS and UV were indicated as overpaintings, in the infrared showed intense reflection, indicating that the pigments used for the painting were the ones that cause the difference in the reflection. A typical case of the above was the white cloth (**Figure 5.117**).

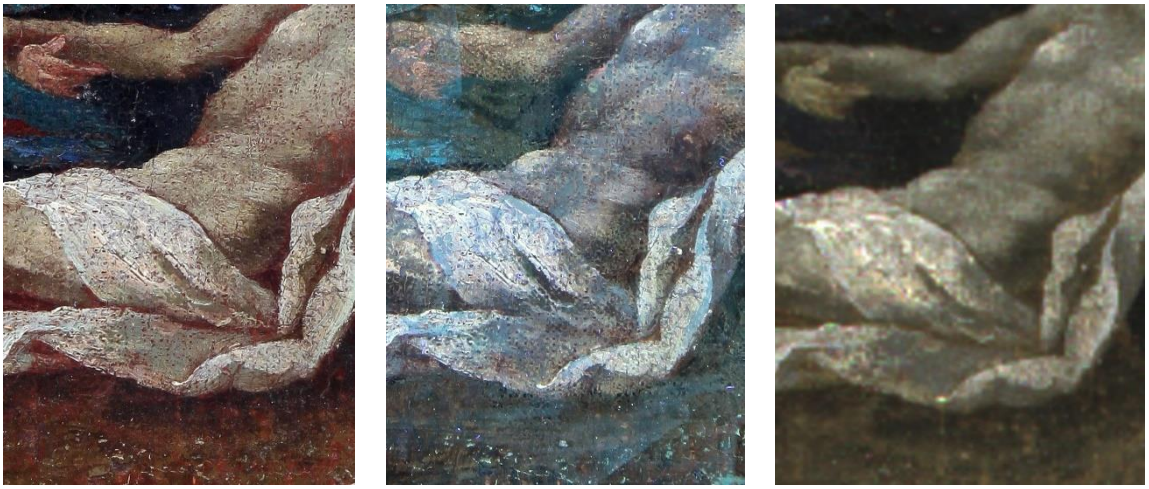

VIS UVF FCIR1

Figure 5.117 Statio XIII “Lamentation”. To the left: detail of the white cloth of Jesus in the visible part of the electromagnetic spectrum. To the middle: detail of the white cloth of Jesus in UV part of the electromagnetic spectrum. To the right: detail of the white cloth of Jesus on the false colour infrared (FCIR1) picture. On the false colour image, the yellow areas on the cloth were areas of overpainting (digital processing via Adobe Photoshop by Kesidis, Stelios).

During the analysis of the figure of the Virgin Mary, the signs of overpainting on her face and body became apparent. Specifically, on the face of the Virgin Mary the points could be observed that had an additional layer of painting (overpainting), such as the forehead, the right side of the face and a small spot on the left side of the face and almost the entire neck, except the left side. Also, the yellow shawl showed low reflection except for some points near the palm of the Virgin Mary. At these points the reflection was much higher, this area corresponded to the intense yellow observed in the visible part of the spectrum (possibly overpainting). The himation had a very high absorption, making it very difficult to observe differences. However, the part of the himation that covered the face of the Virgin Mary and reached up to her breast had an increased index of reflection. Also, there were some very small spots that were visible in different colours (bright blue) that had high reflection. Such a point was located under the right hand of the Virgin Mary (very bright blue), the same blue was observed at the end of the himation in its lower right corner. (**Figure 5.118**)

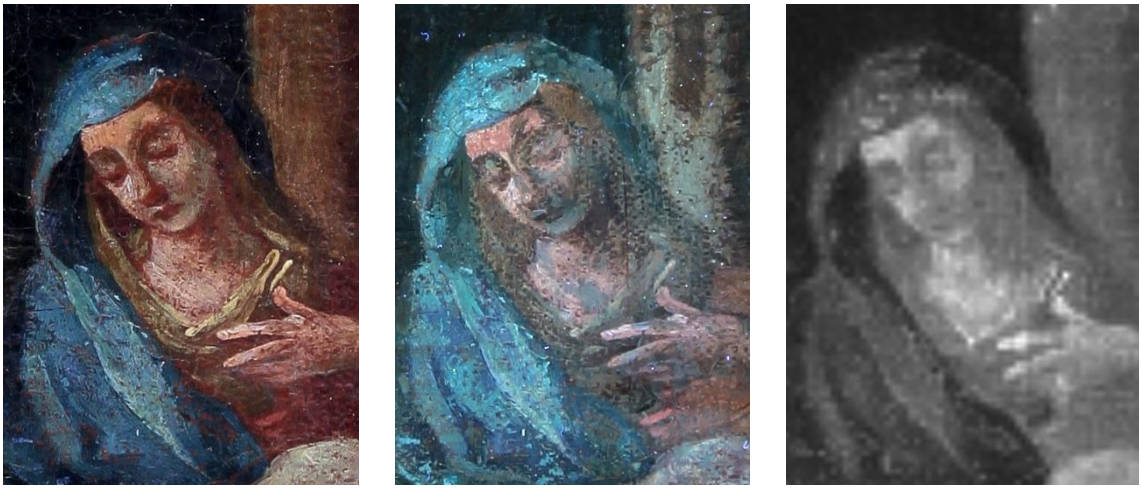

VIS UVF IRR 900 nm

Figure 5.118 Statio XIII “Lamentation”. To the left: detail of the Virgin Mary in the visible part of the electromagnetic spectrum. To the middle: detail of the Virgin Mary in UV part of the electromagnetic spectrum. To the right: detail of the Virgin Mary at the IRR 900 nm. The areas of overpainting on the face and body of Virgin Mary could be observed (digital processing via Adobe Photoshop by Kesidis, Stelios).

IRR 1000 nm

Figure 5.119 Statio XIII “Lamentation”. Detail of the himation of Virgin Mary, where with higher absorption were depicted the areas covered with varnish (digital processing via Adobe Photoshop by Kesidis, Stelios).

900 nm

Figure 5.120 Statio XIII “Lamentation”. Detail of St. John, where with higher absorption were depicted the areas of overpainting (digital processing via Adobe Photoshop by Kesidis, Stelios).

While, at 1000 nm the parts of the Virgin Mary’s himation that were covered with varnish had a higher absorption than the rest (**Figure 5.119**).

As concerned St. John, the presence of overpaintings on the himation and on the face was observed (**Figure 5.120**). In particular, from the observation at 900 nm

the conclusions could be drawn that the left eyebrow, a large part of the left sleeve and parts of the right sleeve were overpaintings.

The study of the painting Statio XIII “Lamentation” continued with the analysis of the multispectral images taken on transmission mode (**Figure 5.121**).

IRT 500 nm IRT 600 nm IRT 700 nm

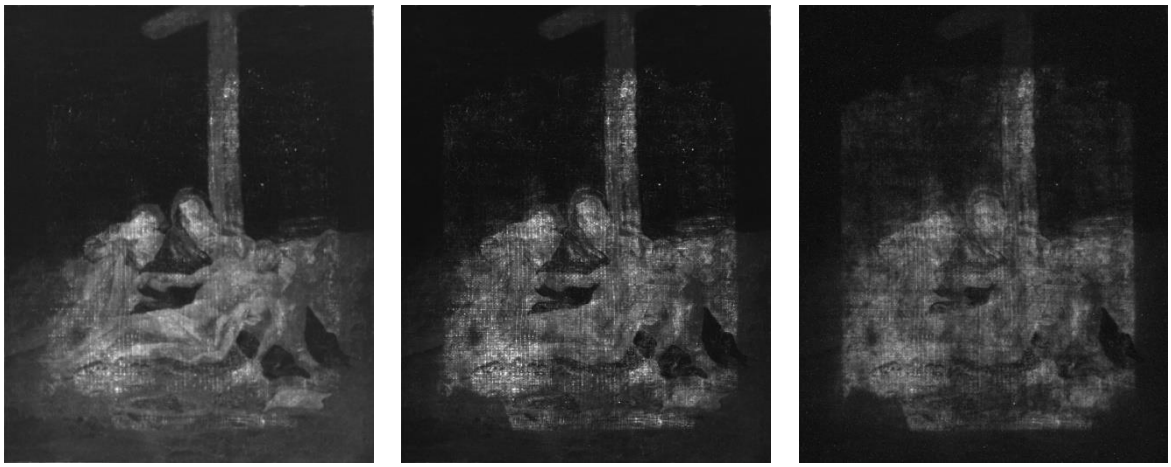

IRT 800 nm IRT 900 nm IRT 1000 nm

Figure 5.121 Statio XIII “Lamentation”. Multispectral images were taken on transmittance configuration on the six selected bands of 500 nm, 600 nm, 700 nm, 800 nm, 900 nm and 1000 nm (photo credit: Dr. Moutsatsou, Anna P., National Gallery - Greece).

Taking multispectral photos on transmission configuration resulted in the appearance of the painting frame in the final result. Thus, the areas located in this area cannot be analyzed.

As seen in **Figure 5.121**, the radiation passed through the painting after 800 nm, in the infrared region. This observation lead to the conclusion that the work had a thick stratigraphy.

The analysis of the multispectral photographs of transmitting radiation was a catalyst for the clarification of some hypotheses that had arisen through the other techniques, and also provided important information about invisible elements of the painting, which could play a decisive role in drawing conclusions about the origin, but also the dating of the painting.

During the analysis of the area of the sky, it was observed that some areas remain impenetrable to the radiation. These areas, which were located on the right of the cross, were either due to grouting (**Figure 5.122**) or to the assumption of the presence of an underlying paint layer, which stops the radiation. Moreover, above of the head of St. John an area with lower absorption relatively to her environment was observed, which could be due to a non-visible surface damage (**Figure 5.123**).

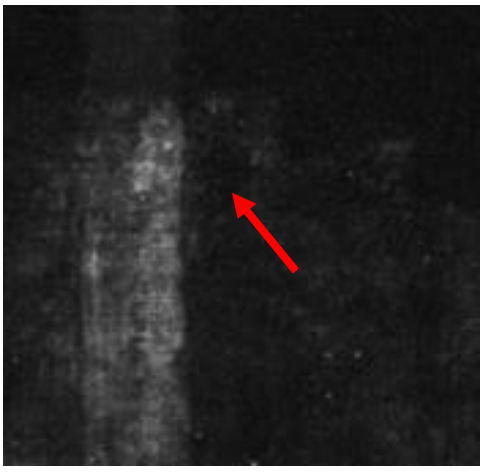

IRT 1000 nm

Figure 5.122 Statio XIII “Lamentation”. Detail of the sky. The red arrow points to area of grouting (digital processing via Adobe Photoshop by Kesidis, Stelios).

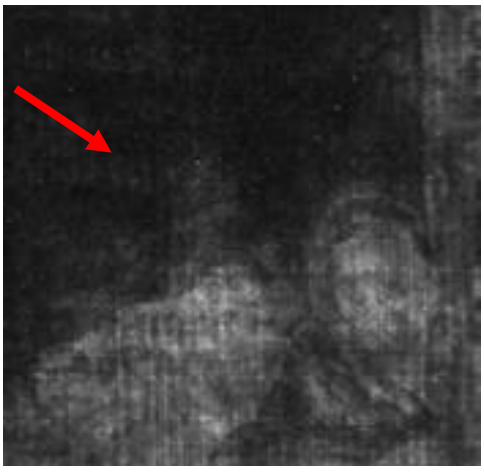

IRT 1000 nm

Figure 5.123 Statio XIII “Lamentation”. Detail of the sky. The red arrow points to area of possibly non-visible wear (digital processing via Adobe Photoshop by Kesidis, Stelios).

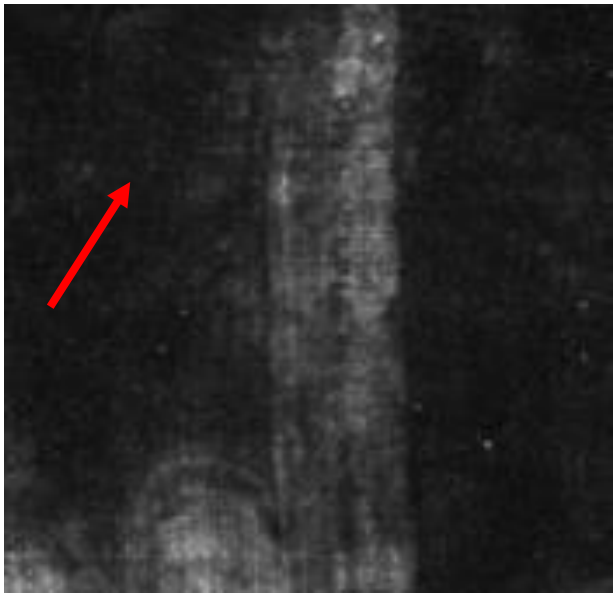

IRT 1000 nm

Figure 5.124 Statio XIII “Lamentation”. Detail of the cross. The red arrow points to the cloth wrapped to the cross (digital processing via Adobe Photoshop by Kesidis, Stelios).

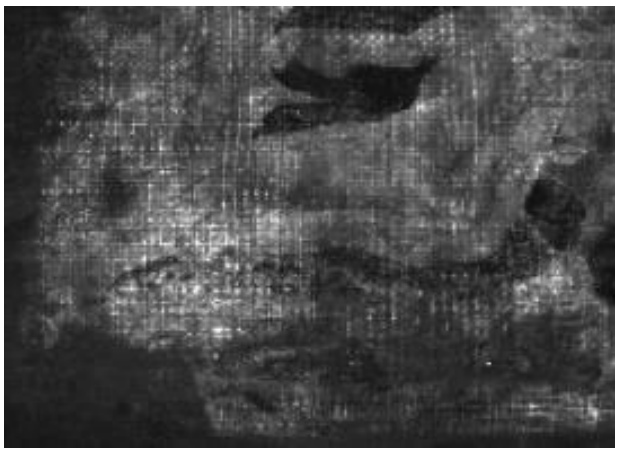

IRT 900 nm

Figure 5.125 Statio XIII “Lamentation”. Detail of the ground, where the impenetrable areas correspond to areas where overpainting had occurred (digital processing via Adobe Photoshop by Kesidis, Stelios).

As concerned the cross, it presented uniform transmission of the radiation, however, at the 900nm an area with low transmission was observed in the middle of the cross, leading to the assumption that was an overpainting. Furthermore, at the 1000 nm the assumption of the presence of a cloth wrapped around the cross was justified (**Figure 5.116** and **Figure 5.124**).

Starting from the left side, part of the ground to the left of St. John looked darker than its surroundings. This point corresponded to a part of the ground with blurred boundaries, leading to the assumption that this area was an overpainting. The same happened with a small area to the left of St. John's right knee. Furthermore, a large part of the left side of the ground was quite permeable to radiation, making the weave of the canvas visible. However, the points that showed impermeability may correspond to areas of the supposedly authentic paint layer that had been preserved (**Figure 5.110** and **Figure 5.125**). In these areas belong the plate, its perimeter, and some other

areas. While the permeable areas may correspond to parts of the painting that were completely lost and now there was only the painting. Also, during the analysis at the 1000 nm it arose that the thorny wreath was disappearing, while the edges of the plate were now clearly visible. In addition, to the right of the painting, starting from the point where the green hills were located (as seen in the infrared) there seemed to be two columns that continued downwards, passed through the feet of the Virgin Mary and ended a little further down (**Figure 5.126**). These columns were visible only at the highest wavelengths, indicating that they were located in an underlying layer. These data were justifying the extensive overpainting on the area of the ground.

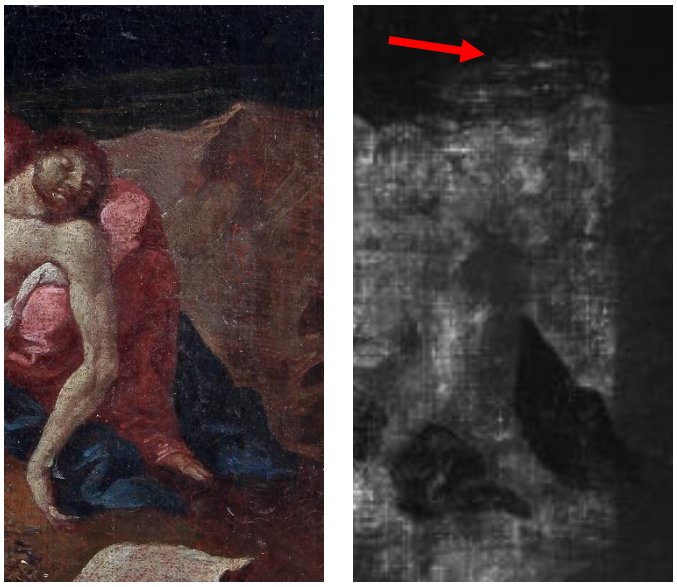

VIS IRT 900 nm

Figure 5.126 Statio XIII "Lamentation". Detail of the ground, where the two columns could be observed (red arrow) (digital processing via Adobe Photoshop by Kesidis, Stelios).

The cloth of Jesus showed some differences from the visible part of the spectrum. Firstly, under the armpit of Jesus, the pattern of the cloth in the visible part of the spectrum showed a smaller gap in the fold, and secondly, scattered variations (pentimenti) were observed (**Figure 5.127**). Also, Jesus' feet showed the outline of the left foot and not the right (this may confirm the observation that the right foot was an overpainting). Below Jesus, specifically at His feet, there were some spots (shadows of the foot in the visible part of the spectrum) that appeared darker and were probably paintings.

As far as Virgin Mary was concerned, an important element was the appearance of the sleeve of the undertunic in a different position and shape than in the visible part of the spectrum, also

VIS IRT 900 nm

Figure 5.127 Statio XIII “Lamentation”. Detail of Jesus. The red arrow points to the cloth of Jesus, showed the pentimenti of the painter (digital processing via Adobe Photoshop by Kesidis, Stelios).

the end from the sleeve was visible to the infrared, in contrast to the VIS (**Figure 5.128**). As for the Virgin Mary's himation, the part around her head had a very thin line of light. Also, different folds were observed around the head from those seen in the visible part of the spectrum. Especially in the lower right corner (next to the right shoulder of Jesus) there were traces of underdrawing. The difference in the folds

VIS IRT 900 nm

Figure 5.128 Statio XIII “Lamentation”. Detail of Virgin Mary, where the end of the sleeve (1) and the traces of underdrawing (2) could be observed (digital processing via Adobe Photoshop by Kesidis, Stelios).

continued to the right of the body of Christ, with the folds being observed as different from those of the visible spectrum being thinner and in different places.

During the analysis of St. John, it was realized that it was the figure from which the radiation passed the most, which was due to the fact that, apart from the previous paint areas attributed as overpaintings, it was an authentic part of the painting.

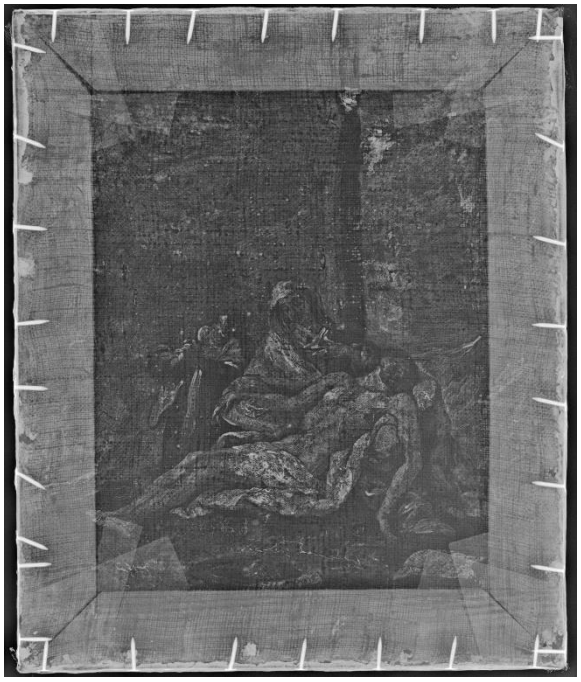

Figure 5.129 Statio XIII “Lamentation”. X-ray radiography. 60 kV high voltage, 7.1 mAs. (digital processing via Adobe Photoshop by Kesidis, Stelios).

5.2.3. X-Ray Radiography

X-ray radiography provided valuable information on the invisible technical and artistic characteristics of the painting, shed light on the manufacturing techniques of the painting, lead to a better understanding of the preservation state and clarified the presence of later additions and past conservation treatments (**Figure 5.129**).

Considering this, the information obtained from the X-ray analysis was d reported layer by layer, starting from the frame and reaching the painting surface.

The information regarding the frame of the painting by the observation of the X-ray radiograph related to the delimitation of its borders to the painting surface and the connection of related losses or damages. In addition, the nails used to fasten the canvas to the frame were observed around the perimeter, while the parts of the frame were joined with the mitre joint technique. The uniformity of the nails both in thickness and shape lead to the conclusion that they were industrially produced nails. A feature that limited the time of this operation.

Important information emerged regarding the canvas of the painting, information which was due to the negative imprint of the ground layer. The existence of two different canvases was observed, which was a clear indication of lining treatment.

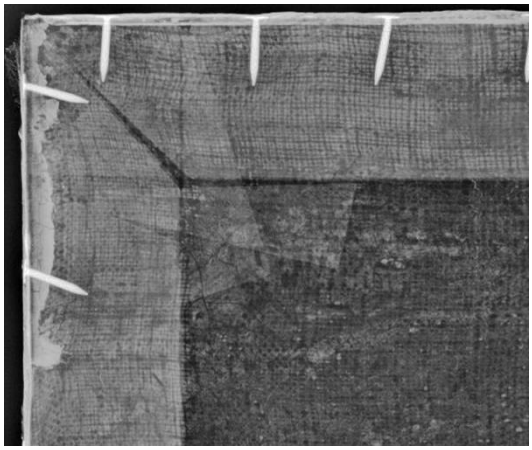

XRR

Figure 5.130 Statio XIII “Lamentation”. Detail from the top left corner of the painting. The borders of the original canvas were observed, but also the holes through which the nails that supported the canvas in the frame passed. (digital processing via Adobe Photoshop by Kesidis Stelios)

The edge of the authentic canvas could be observed to the top right corner of the painting. In addition, the holes, through which the nails that fastened the canvas to the frame, became distinct (**Figure 5.130**).

It should be mentioned that the authentic canvas had a smaller size than the frame, which meant that in its original form the painting had its sides painted. It also meant that since the present frame had a smaller size than the canvas, then it was verified that the frame was a later addition and was not the original. On the edges of the painting, a material, containing heavy elements, was used to connect the two canvases and to fill the void areas. The original canvas was made of fine yarn and had a dense weave. However, due to the lining treatment, it was not symmetrical. Finally, around the perimeter of the original fabric (as in the lower right corner) there were areas of loss, where it was filled with grout (**Figure 5.131**). Additionally, grouting was also located on the cross and the sky (**Figure 5.132**).

Concerning the layer of preparation, the image presented by the layer of preparation, with the uniform absorption, indicated that it was preserved in relatively good condition, without many subsequent interventions. However, cracks and losses of the layer were observed.

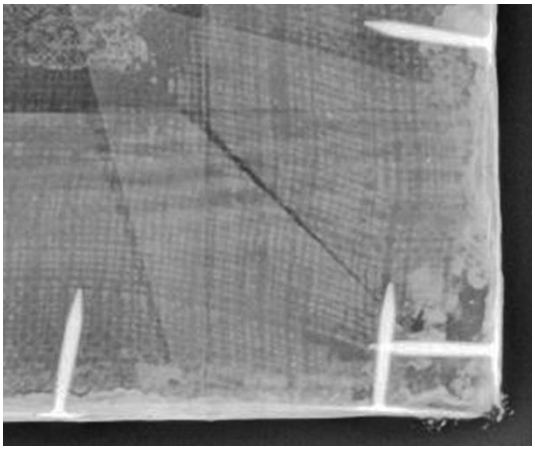

XRR

Figure 5.131 Statio XIII “Lamentation”. Detail of the bottom right corner of the painting, where areas of loss filled with grout could be observed (digital processing via Adobe Photoshop by Kesidis, Stelios).

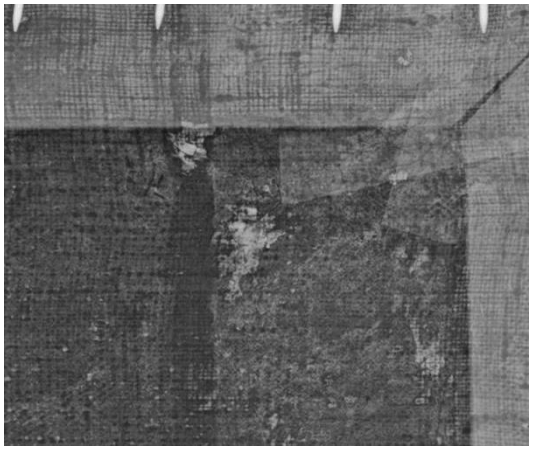

XRR

Figure 5.132 Statio XIII “Lamentation”. Detail of the cross and the sky of the painting, where areas of loss filled with grout could be observed (digital processing via Adobe Photoshop by Kesidis, Stelios).

XRR

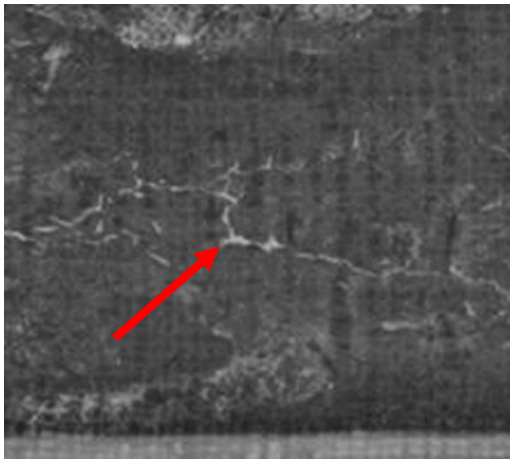

XRR

Figure 5.133 Statio XIII “Lamentation”. Details of the Virgin Mary’s palm and the ground of the painting, where filling treatments were performed (digital processing via Adobe Photoshop by Kesidis, Stelios).

From the study of the painting through the observation of the X-ray radiography, it was better understood the poor state of preservation of the painting, with many losses being observed on the entire surface of the painting. However, in addition

Figure 5.134 Statio XIII “Lamentation”. Sampling points for the performance of the microscopic techniques (digital processing via Adobe Photoshop by Kesidis, Stelios).

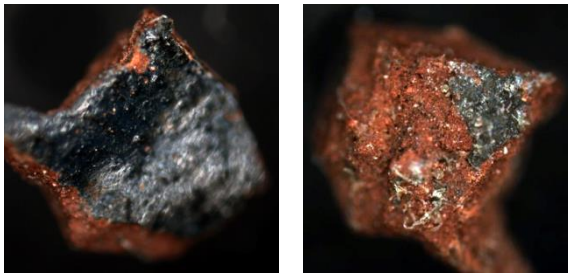

x50 x50

Figure 5.135 Sample’s (S3) surface observation before preparation for OM and SEM. To the left: detail of the surface of the sample at x50 magnification. To the right: detail of the back of the sample at x50 magnification (photo credit: Terlixi, Agni-Vasileia National Gallery - Greece) (digital processing via Adobe Photoshop by Kesidis, Stelios).

to information on the preservation state of the painting, information was also extracted on later additions and subsequent restoration treatments. In particular, areas where filling treatments was performed were located on the right palm and left knee of the Virgin Mary, and on various areas on the ground (**Figure 5.133**). The filling treatments were presented with bright colour, due to the heavy elements composing it.

5.2.4. Optical Microscopy

For the needs of performing the analysis through optical microscopy and scanning electron microscopy, it was necessary to take two (2) cross-sectional samples. Areas of wear on the painting that were representative of the area were selected as sampling points (**Figure 5.134**).

The first sampling area (S3) was in a loss area in the sky, on the top right corner of the painting (**Figure 5.134**). During the macroscopic observation of the area prior to the sampling process it was not possible to make absolutely clear whether the sample taken belonged to the original work or to layers deposited on the fabric of the first lining. However, it was probable that the sampling area consisted of subsequent layers of deposits on the fabric of the first lining (**Figure 5.135**). During the observation of the surfaces of the sample, the presence of a

dark blue colour layer deposited on a red preparation was recorded (**Figure 5.135**).

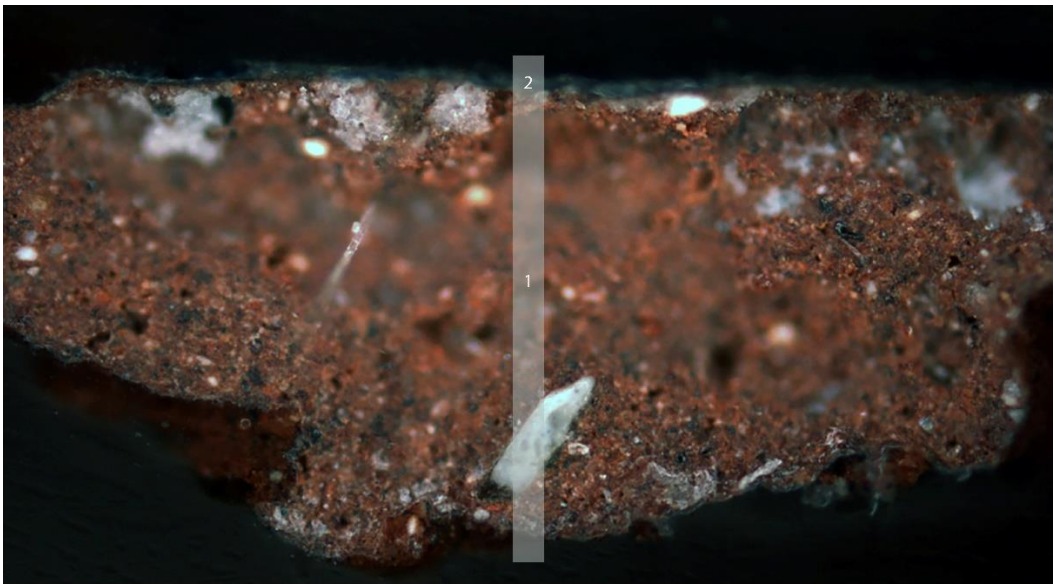

OM x100

Figure 5.136 Statio XIII “Lamentation”. Observation of the sample S3 with visible reflective light at x100 magnification (photo credit: Terlixi, Agni-Vasileia, National Gallery - Greece) (digital processing via Adobe Photoshop by Kesidis, Stelios.

When observing the stratigraphic section in the visible part of the spectrum it became clear that the sample consisted of only two layers, as recorded macroscopically (**Figure 5.136**). In particular it consisted of (1) a thick layer of orange-coloured preparation containing other heterochromatic (white, black, etc.) grains, and (2) a very thin layer of dark blue colour.

This was followed by observation of the sample with UV illumination. During the microscopic observation of the stratigraphic section under stimulation with ultraviolet illumination, the existence of another layer became distinct (**Figure 5.137**). This layer was located between its preparation layer and the dark blue colour layer, it was very thin discontinuous and possibly organic in nature. In addition, an agglomerate of zinc oxide granules was detected in the preparation layer, which recorded as yellow-green fluorescence.

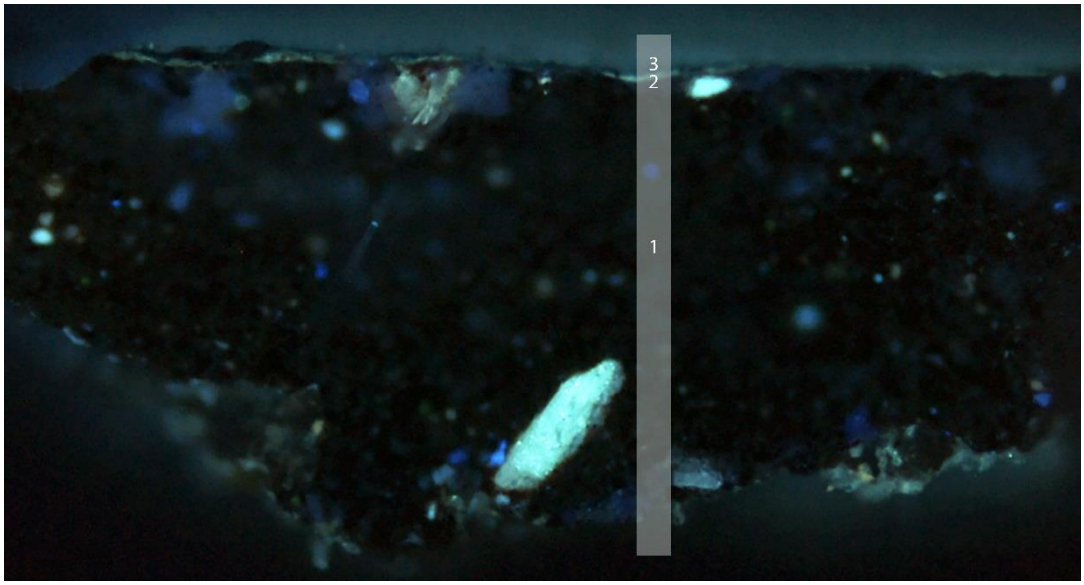

UVFM x100

Figure 5.137 Statio XIII “Lamentation”. Observation of the sample S3 with UV reflective light at x100 magnification (photo credit: Terlixi, Agni-Vasileia, National Gallery - Greece) (digital processing via Adobe Photoshop by Kesidis, Stelios).

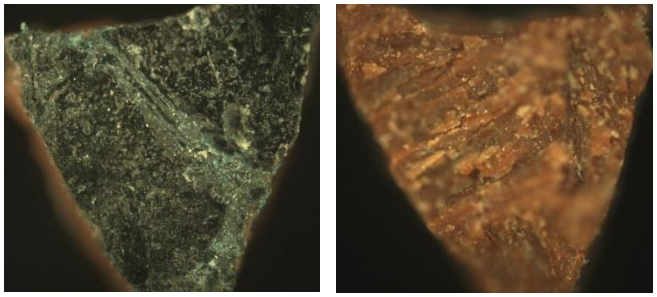

x50 x50

Figure 5.138 Sample’s (S4) surface observation before preparation for OM and SEM. To the left: detail of the surface of the sample at x50 magnification. To the right: detail of the back of the sample at x50 magnification (photo credit: Terlixi, Agni-Vasileia, National Gallery - Greece) (digital processing via Adobe Photoshop by Kesidis, Stelios).

The second area of sampling (S4) was also a loss area in the sky, located on the upper edge of the painting (**Figure 5.134**). When observing the surfaces of the sample, the existence of a dark paint layer was discernible, which had a coating. On the other hand, the existence of a red preparation was distinguished, which bore the imprint of the canvas (**Figure 5.138**).

Observing the stratigraphic section of the sample in visible reflection mode, the presence of orange preparation was discernible, which contained agglomerates of intense red granules and minimal black granules (**Figure 5.139**).

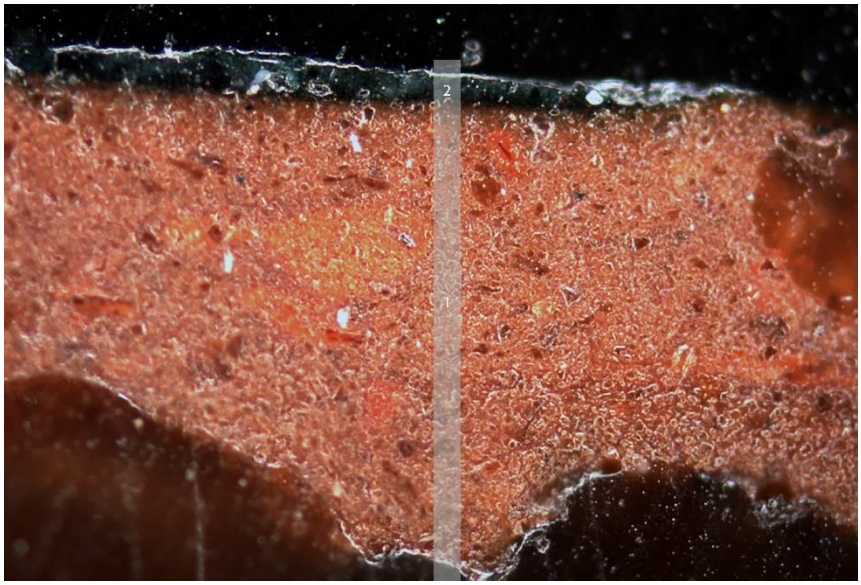

OM x200

Figure 5.139 Statio XIII “Lamentation”. Observation of the sample S4 with visible reflective light at x200 magnification (photo credit: Terlixi, Agni-Vasileia, National Gallery - Greece) (digital processing via Adobe Photoshop by Kesidis, Stelios).

This preparation captured a different visual image than the preparation of sample S3. Its grains, both chromatically and morphologically, bore no resemblance to that of the sample S3, reinforcing the hypothesis that the sample S3 was taken from an area where a preparation layer (and paint layers) was deposited directly on the first lining layer. A dark-coloured layer was deposited on top of the sample S4 preparation layer which contains black and green granules and possibly some white ones.

This was followed by observation of the sample with polarized light (**Figure 5.140**). In this mode the presence of one more layer was detected on the top of the sample, where a very thin black-coloured paint layer could be observed in fragments. Additionally, through the polarized light the granulometry of the other two layers was made clearer. In particular, the variety of the components, as well as their granulometry could be observed. Apart from the red and black granules observed in reflection mode, the presence of many small in size white granules could be seen. As for the second layer, the presence of small black-coloured granules was observed.

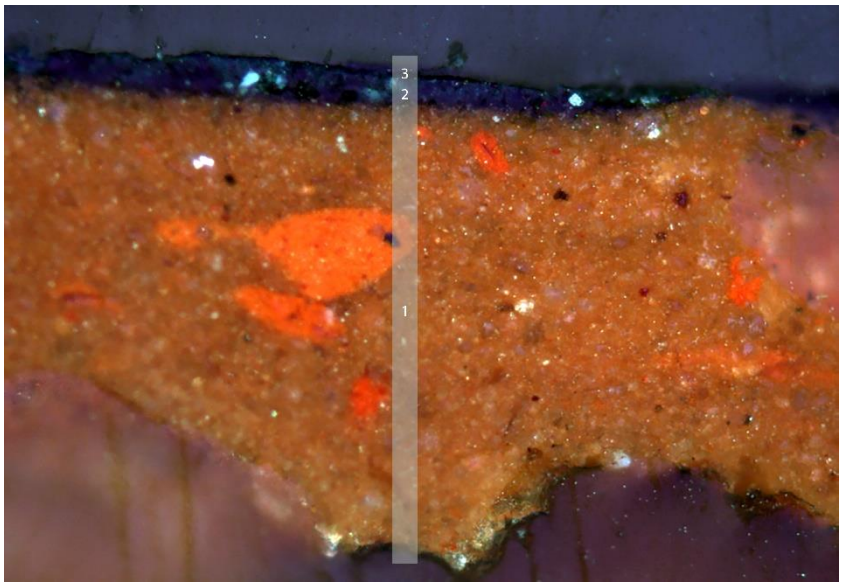

OM POL x200

Figure 5.140 Statio XIII “Lamentation”. Observation of the sample S4 with visible polarized light at x200 magnification (photo credit: Terlixi, Agni-Vasileia , National Gallery - Greece) (digital processing via Adobe Photoshop by Kesidis, Stelios).

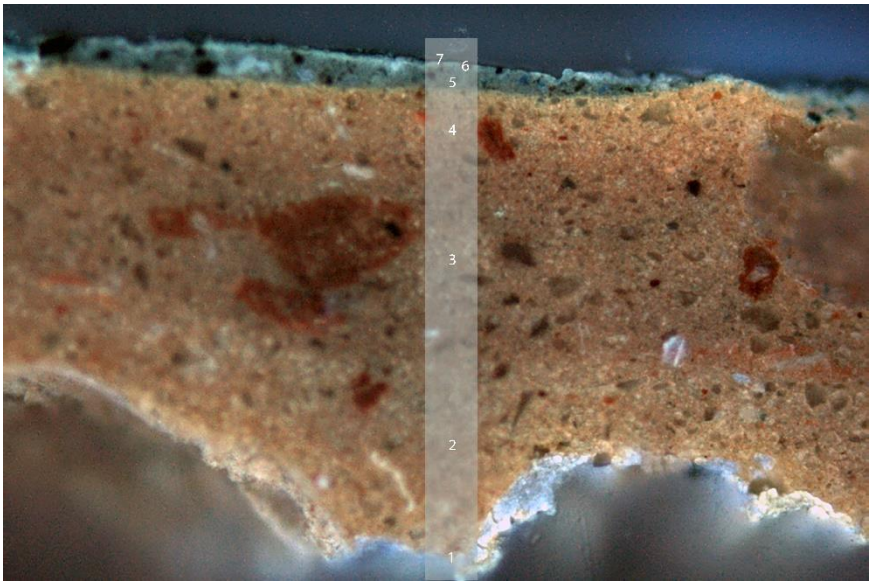

UVFM x200

Figure 5.141 Statio XIII “Lamentation”. Observation of the sample S4 with UV reflective light at x200 magnification (photo credit: Terlixi, Agni-Vasileia, National Gallery - Greece) (digital processing via Adobe Photoshop by Kesidis, Stelios).

This was followed by observation of the sample with UV light (**Figure 5.141**). Observing the same stratigraphic section under ultraviolet excitation made the sequence of layers even more distinct. Particularly, the presence of organic

material at the edges of the preparation layer - at the points of its interface with the fabric was distinguished. It was distinguished by the existence of three successive layers of preparation which were deposited successively and without time interval during their coating. These layers showed very good adhesion to each other and differed only in intensity and slightly in their fluorescent colour, which became distinct and their separation. Finally, it was discernible that the upper colour layer was not one in number but three successively deposited layers. A colour layer, a very thin layer of organic nature and a third, discontinuous, locally observed black.

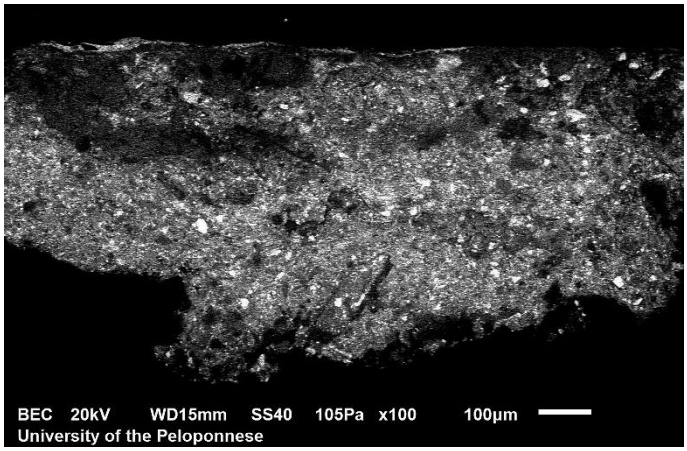

Figure 5.142 Statio XIII "Lamentation". Observation of the sample S3 with SEM at x100 magnification (photo credit: Dr. Palamara, Eleni - University of the Peloponnese, Greece) (digital processing via Adobe Photoshop by Kesidis, Stelios).

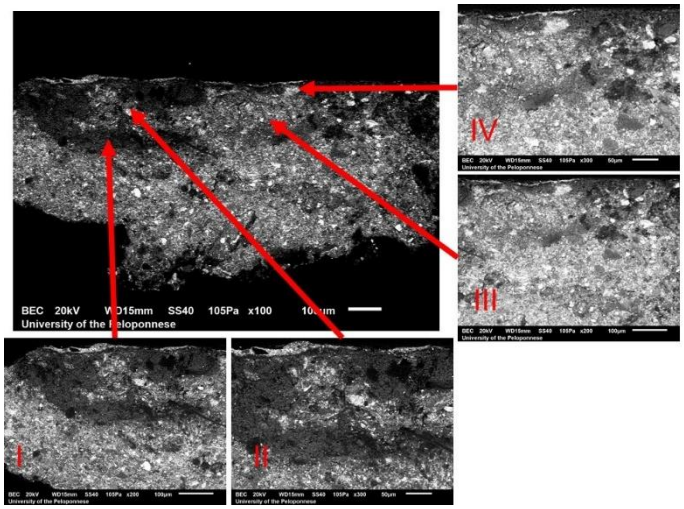

Figure 5.143 Statio XIII "Lamentation". Observation of the sample S3 and the four areas of interest with SEM (photo credit: Dr. Palamara, Eleni - University of the Peloponnese, Greece) (digital processing via Adobe Photoshop by Kesidis, Stelios).

5.2.5. Scanning Electron Microscopy – Energy Dispersive X-rays Spectroscopy

The application of the Scanning Electron Microscopy coupled with an Energy Dispersive X-rays Spectrometer provided valuable information on the stratigraphic composition of the painting samples, the elemental composition of all the sample layers, their preservation state, the detection of later additions and conservation treatments and the assessment of the dating of the two paintings, which led to safer conclusions through other non-invasive analysis techniques.

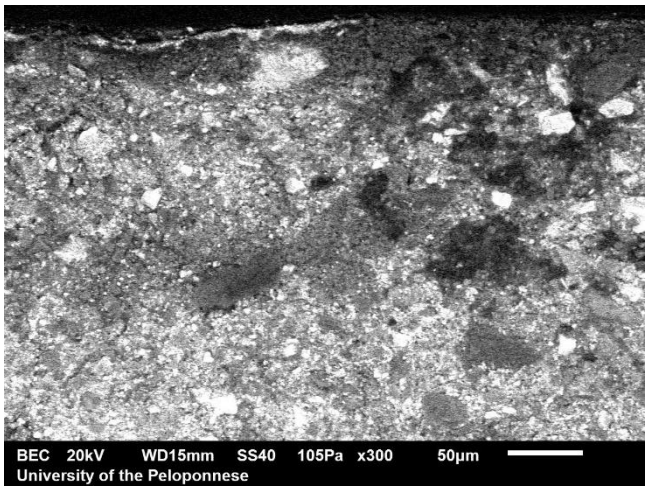

Figure 5.144 Statio XIII "Lamentation". Detail of the three layers of the sample S3 with SEM at x300 magnification (photo credit: Dr. Palamara, Eleni - University of the Peloponnese, Greece) (digital processing via Adobe Photoshop by Kesidis, Stelios).

During the analysis of the first sample (S3) (**Figure 5.142** & **Figure 5.135**) through the backscattered images with higher magnifications (**Figure 5.143**) it was possible to select information regarding the granulometry of the layers and to distinguish the composition of the preparation and the pigment layer. (**Table 5.6**) The first layer of the sample S3 (**Figure 5.142**), attributed after the OM observation as the layer of preparation, was coarse-grained with large grains (**Figure 5.144**). The EDS analysis showed that the layer contained: Silicon (Si), Sulfur (S), Zinc (Zn), Barium (Ba), Iron (Fe), Calcium (Ca), Aluminum (Al) and Magnesium (Mg).

Sample	Spot	OM Colour	SEM Observations	Layer	Elements Detected
S3	Paint layer	Black	Fine-grained	3rd	-
	Paint layer	Dark blue	Fine-grained with some large grains	2nd	Pb, Fe, Si, Ba, Zn, S, Al, Ca
	Ground layer	Brown-Orange	Coarse-grained with very large grains	1st	Si, S, Zn, Ba, Fe, Ca, Al, Mg

Table 5.6 Elemental Analysis of sample S3 by EDS

This led to the conclusion that this layer was a mixture of pigments, and in particular, of lithopone ($BaSO_4 \cdot ZnS$) (Eastaugh, et al., 2004, p. 242), of red ochre (Fe_2O_3) (Eastaugh, et al., 2004, p. 320) and of silicon, which had the role of filler. The second layer of the sample S3 were fine-grained with some large grains. The EDS analysis showed that the layer contained: Lead (Pb), Iron (Fe), Silicon (Si),

Barium (Ba), Zinc (Zn), Sulfur (S), Aluminum (Al) and Calcium (Ca). The data received, which probably originated from the first layer (preparation layer) did not give sufficient detail on the nature of this colour. However, the presence of Lead (Pb) had to be associated with the colour, as it was not encountered on the previous layer.

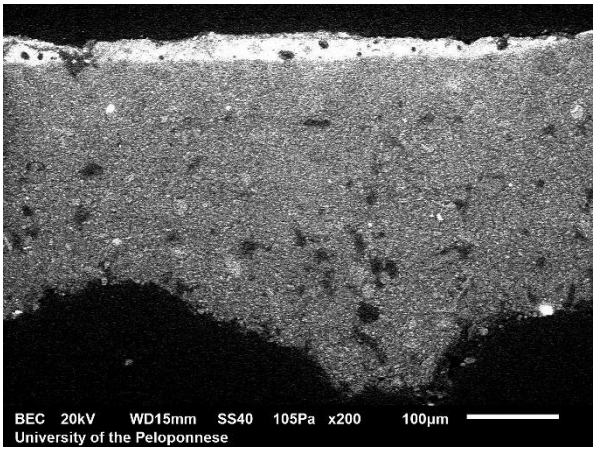

Figure 5.145 Statio XIII "Lamentation". Observation of the sample S4 with SEM at x200 magnification (photo credit: Dr. Palamara, Eleni - University of the Peloponnese, Greece) (digital processing via Adobe Photoshop by Kesidis, Stelios).

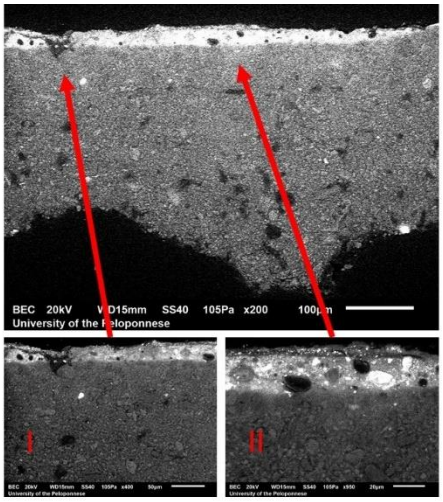

Figure 5.146 Statio XIII "Lamentation". Observation of the sample S4 and the two areas of interest with SEM (photo credit: Dr. Palamara, Eleni - University of the Peloponnese, Greece) (digital processing via Adobe Photoshop by Kesidis, Stelios).

During the analysis of the second sample (S4) (**Figure 5.145**) through the backscattered images with higher magnifications (**Figure 5.146**) it was possible to select information regarding the granulometry of the layers and to distinguish the pigment layer. (**Table 5.7)** The second, third and fourth layers of the sample S4 (**Figure 5.145**), attributed after the OM observation as the layers of preparation, were fine-grained with some large grains (**Figure 5.147**). The EDS analysis

showed that the layer contained: Calcium (Ca), Silicon (Si), Aluminum (Al), Magnesium (Mg), Lead (Pb), Iron (Fe) and Potassium (K). This led to the conclusion that it was a gesso layer based on dolomite ([Ca,Mg][CO3]2) and aluminum silicate (Al_2SiO_3), while the colour of the layer was achieved due to the presence of the red ochre (Fe_2O_3) (Eastaugh, et al., 2004, p. 320) and lead white ($(PbCO_3)_2 \cdot Pb(OH)_2$) (Eastaugh, et al., 2004, p. 233). This data confirmed the previous dating estimation, stating that

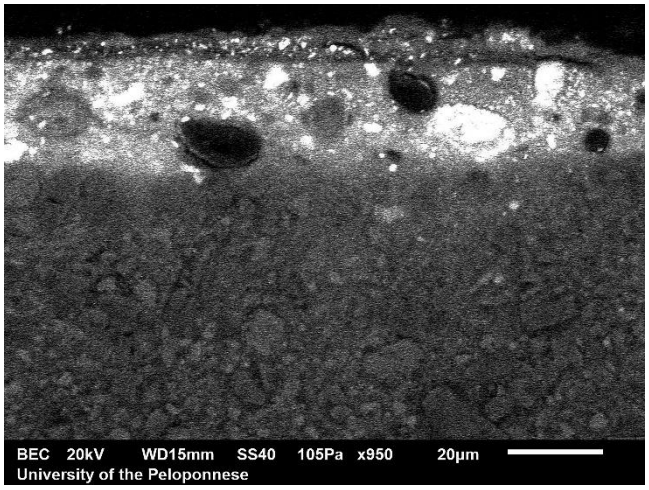

Figure 5.147 Statio XIII "Lamentation". Detail of the top layers of the sample S4 with SEM at x950 magnification (photo credit: Dr. Palamara, Eleni - University of the Peloponnese, Greece) (digital processing via Adobe Photoshop by Kesidis, Stelios).

the original ground layer dated back at least to the 18th century. This was due to the materials used for the preparation layer. According to (Groen, 2011, p. 87), the main pigment used for grey grounds was the expensive lead white, while for reddish or brown grounds red earth was used which was abundant in nature. The fifth layer of the sample S4 was fine-grained with some large grains. The EDS analysis showed that the layer contained: Lead (Pb), Calcium (Ca), Silicon (Si), Aluminum (Al), Iron (Fe), Magnesium (Mg), Potassium (K), Barium (Ba), Sodium (Na) and Sulfur (S). This led to the conclusion that this layer was a mixture of dyes. Specifically, taking into account the observation of the sample with OM that showed the presence of blue colour, as well as the detection of: sodium, silicon and aluminum, it seems that it could be ultramarine ($Na_7Al_6Si_6O_{24}S_3$) (Eastaugh, et al., 2004, p. 375; Roy, 1993, p. 55) with the presence of lead white ($(PbCO_3)_2 \cdot Pb(OH)_2$) (Eastaugh, et al., 2004, p. 233) and barite ($BaSO_4$) (Eastaugh, et al., 2004, p. 40). The identification of the ultramarine proves that the layers above it were overpainting. It also meant that since, as the data showed, the present colour was the original, the sky of the painting was originally blue. However, the identification of ultramarine had to be justified by the other analytical techniques applied. The detection of the remaining elements was due to the underlying layer of the preparation. Finally, the seventh layer of the sample S4

was very thin and fine-grained. The EDS analysis showed that the layer contained: Lead (Pb), Calcium (Ca), Silicon (Si), Iron (Fe), Aluminum (Al), Magnesium (Mg), Phosphorus (P) and Sodium (Na). This led to the assumption that it might be a layer of bone black ($Ca_5(OH)(PO_4)_3$)) (Eastaugh, et al., 2004, p. 57) with the detection of the remaining elements due to the underlying layer.

Sample	Spot	OM Colour	SEM Observations	Layer	Elements Detected
S4	Paint layer	Black	Fine-grained	7th	Pb, Ca, Si, Fe, Al, Mg, P, Na
	Organic coating	-	Indistinguishable texture	6th	-
	Paint layer	Blue	Fine-grained with some large grains	5th	Pb, Ca, Si, Al, Fe, Mg, K, Ba, Na, S
	Ground layer	Orange	Fine-grained with some large grains	4th	Ca, Si, Al, Mg, Pb, Fe, K
	Ground layer	Orange	Fine-grained with some large grains	3rd	Ca, Si, Al, Mg, Pb, Fe, K
	Ground layer	Orange	Fine-grained with some large grains	2nd	Ca, Si, Al, Mg, Pb, Fe, K
	Organic material	-	-	1st	-

Table 5.7 Elemental Analysis of sample S4 by EDS

5.2.6. X-Ray Fluorescence Spectrometry

The application of the X-Ray Fluorescence (XRF) Spectrometry on the Statio XIII "Lamentation" revealed the composition of the inorganic pigments and the ground layer, provided information for the indirect dating of the painting and finally, detected areas of later addition and past conservation treatments.

In the analysis of the painting, 44 point (**Figure 5.148**), 5 linear and 1 area scanning analyzes (**Figure 5.149**) were performed. Due to the large volume of

data, it was decided that the analysis of the elemental results of XRF spectrometry would be done in colour.

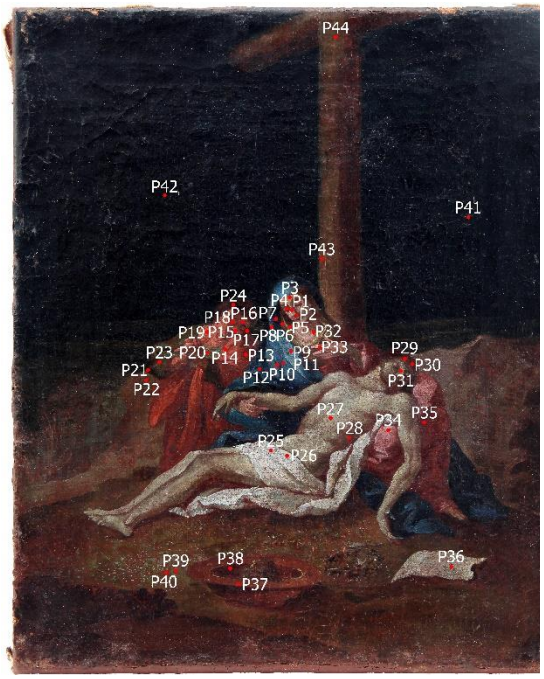

Figure 5.148 Statio XIII "Lamentation". Positions of analysis by XRF (digital processing via Adobe Photoshop by Kesidis, Stelios).

Figure 5.149 Statio XIII "Lamentation". Area & linear scanning analyzes (digital processing via Adobe Photoshop by Kesidis, Stelios).

The elemental analysis of the blue pigments by μ-XRF suggests the presence of the pigments: cobalt blue, Prussian blue and azurite (**Figure 5.150**). Cobalt blue ($CoO.Al_2O_3$) (Eastaugh, et al., 2004, p. 112) was identified at the analysis positions: P4, P5, P7, P10 to P15, P31, P41 and P42. Prussian blue ($[Fe(II)(CN)_6]_4$) (Eastaugh, et al., 2004, p. 308) was identified at the analysis positions: P7 to P12. And finally, azurite ($Cu_3(CO_3)_2(OH)_2$) (Eastaugh, et al., 2004, p. 33) was identified at the analysis positions: P7 to P12 and P39. (**Table 5.8**).

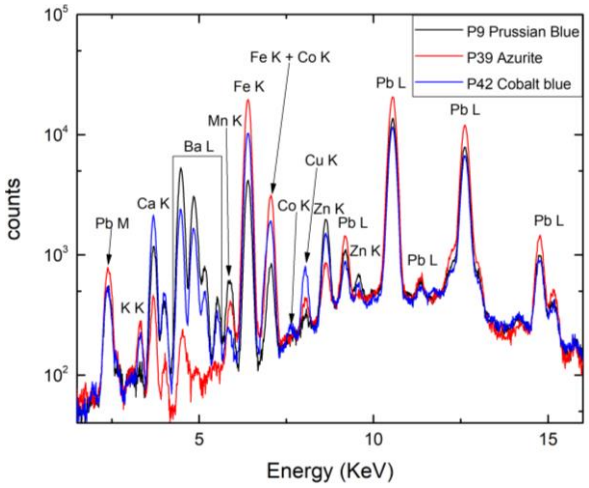

Figure 5.150 XRF spectra from the analysis positions: P9, P39 and P42 of blue pigments of Statio XIII "Lamentation". Identification of: cobalt blue, Prussian blue and azurite (personal archive Karydas, Andreas-Germanos and Kesidis, Stelios).

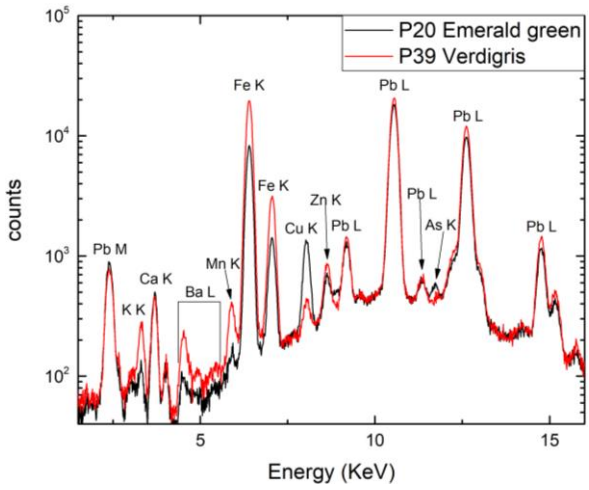

Figure 5.151 XRF spectra from the analysis positions: P20 and P39 of green pigments of Statio XIII "Lamentation". Identification of: emerald green and verdigris (personal archive Karydas, Andreas-Germanos and Kesidis, Stelios).

From the previous analysis, it seemed that cobalt blue, which was discovered in 1803 (Eastaugh, et al., 2004, p. 113), was the main blue pigment in the painting, with the complementary use of Prussian blue and azurite. However, it should be mentioned, that the detection of azurite contains a margin of error, since the attribution was based on the presence of Cu K line, not ruling out the possibility that it was verdigris ($Cu(CH_3COO)_2.H_2O$). (Eastaugh, et al., 2004, p. 385).

The elemental analysis of the green pigments by μ-XRF suggests the presence of the pigments: emerald green and verdigris (**Figure 5.151**). Emerald green ($Cu_4(OAc)_2(AsO_2)_6$) (Eastaugh, et al., 2004, p. 122) was identified at the analysis position P20. However, it should be mentioned, that the detection of emerald green contains a margin of error, since the attribution was based on the presence of Cu and As K lines, not ruling out the possibility that it was Scheele's green ($AsCuHO_3$) (Eastaugh, et al., 2004, p. 335). Verdigris

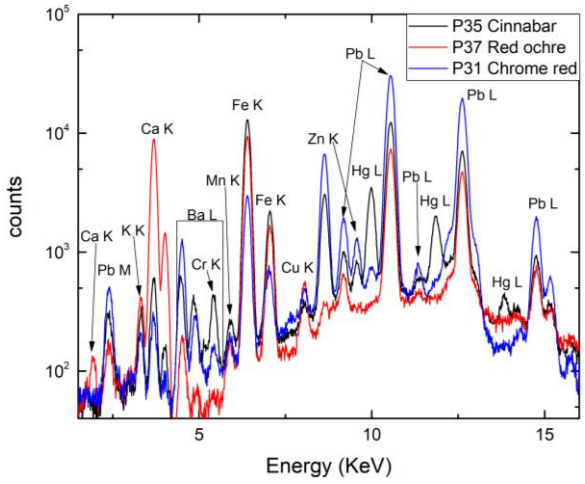

Figure 5.152 XRF spectra from the analysis positions: P31, P35 and P37 of red pigments of Statio XIII "Lamentation". Identification of: cinnabar, red ochre and chrome red (personal archive Karydas, Andreas-Germanos and Kesidis, Stelios

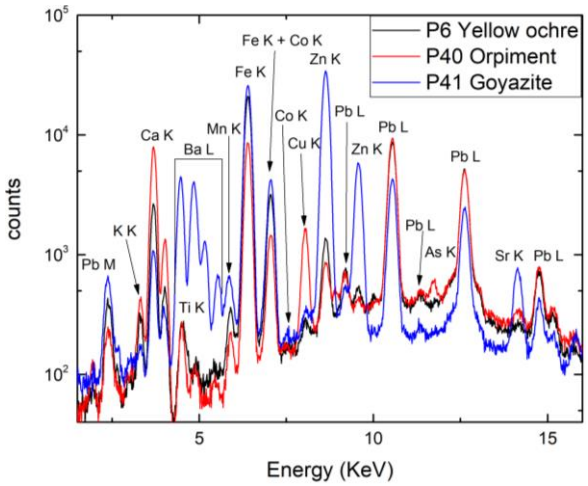

Figure 5.153 XRF spectra from the analysis positions: P6, P40 and P41 of yellow pigments of Statio XIII "Lamentation". Identification of: yellow ochre, orpiment and goyazite (personal archive Karydas, Andreas-Germanos and Kesidis, Stelios).

$(Cu(CH_3COO)_2.H_2O)$ (Eastaugh, et al., 2004, p. 385) was identified at the analysis positions: P23, P24, P29, P30, P37 to P40 and P42. The detection of verdigris had the same aforementioned issues as the detection of azurite. (**Table 5.8**).

The elemental analysis of the red pigments by μ-XRF suggests the presence of the pigments: cinnabar, red ochre, chrome orange and chrome red (**Figure 5.152**). Cinnabar (α-HgS) (Eastaugh, et al., 2004, p. 105) was identified at the analysis positions: P1 to P7, P9, P13 to P20, P24, P27 to P35, P37 and P38. Red ochre (Fe_2O_3) (Eastaugh, et al., 2004, p. 279) was identified in all analysis positions. It should be mentioned, though, that some of the yields of iron peaked in red ochre and were due to the underlying layer. Chrome red and chrome orange ($PbCrO_4.PbO$) (Eastaugh, et al., 2004, p. 98) were identified at the analysis position P31. (**Table 5.8**). From the previous analysis, arose the conclusion that red ochre was the main red pigment in the painting, with the complementary use of cinnabar and orange chrome for the facial characteristics of some figures, while chrome red was identified only on the face of Jesus. Furthermore, although cinnabar and red ochre were used as pigments since antiquity (Eastaugh, et al., 2004, pp. 105, 279), chrome pigments were discovered in 1809 (Eastaugh, et al., 2004, p. 98), providing, this way, indirect information about the dating of the painting.

The elemental analysis of the yellow pigments by μ-XRF suggests the presence of the pigments: yellow ochre, orpiment and goyazite (**Figure 5.153**). Yellow ochre (γ-FeOOH) (Eastaugh, et al., 2004, p. 401) was identified in all analysis positions. It should be mentioned, though, that some of the yields of iron peaked in yellow ochre and were due to the underlying layer. Orpiment (As2S3) (Eastaugh, et al., 2004, p. 285; West FitzHugh, 1997, p. 47) was identified at the analysis positions: P40, P43 and P44. According to sources (Eastaugh, et al., 2004, p. 285; West FitzHugh, 1997, p. 50), orpiment was used until the end of the 19th century. Thus, the identification of orpiment on the painting provides indirect information about the dating of the painting. Finally, goyazite ($SrAl_3(PO_4)_2(OH)_5.(H_2O)$) (Eastaugh, et al., 2004, p. 172) was identified at the analysis position P41. (**Table 5.8**).

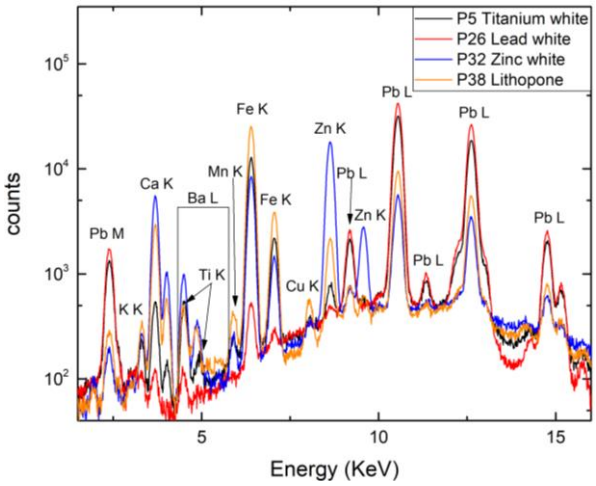

Figure 5.154 XRF spectra from the analysis positions: P5, P26, P32 and P38 of white pigments of Statio XIII "Lamentation". Identification of: lead white, zinc white, lithopone and titanium white (personal archive Karydas, Andreas-Germanos and Kesidis, Stelios).

The elemental analysis of the white pigments by μ-XRF suggests the presence of the pigments: lead white, zinc white, lithopone and titanium white (**Figure 5.154**). Lead white ($(PbCO_3)_2 \cdot Pb(OH)_2$) (Eastaugh, et al., 2004, p. 233) due to the high atomic number of lead (Pb) was identified in all analysis positions. Zinc white (ZnO) (Eastaugh, et al., 2004, p. 406) was identified at the analysis positions: P2, P4 to P6, P11, P13 to P15, P17, P18, P20 to P23, P25, P27, P28, P31, P32, P34, P37, P39, P40, P42 and P44. Lithopone (BaSO4 · ZnS) (Eastaugh, et al., 2004, pp. 242, 406) was identified at the analysis positions: P1, P3, P7 to P10, P12, P16, P19, P24, P29, P30, P33, P35, P38 and P41 to P43. And finally, titanium white (TiO_2) (Eastaugh, et al., 2004, p. 364) was identified at the analysis positions: P2, P4 to P6, P8, P9, P11, P13 to P16, P20 to P23, P25 to P28, P32, P34, P37, P39, P40 and P44. (**Table 5.8**).

The above analysis of the white pigments contributed important information on the history of the painting. While lead white was used as a pigment since antiquity, the

identification of: zinc white, lithopone and titanium white on the painting, provided indirect information about the dating of the painting. Zinc white, which was discovered in 1803, and lithopone, which was discovered around the 1850 by G.F. de Doubet, were invented as alternatives for the replacement of the toxic lead white, with the peak of their use being at the beginning of the 20th century (Eastaugh, et al., 2004, p. 406). Moreover, titanium oxides potential as a pigment were realized at the beginning of the 20th century (Eastaugh, et al., 2004, p. 364). Finally, the fact that five white pigments were found in the painting reinforced the previous speculations of overpaintings.

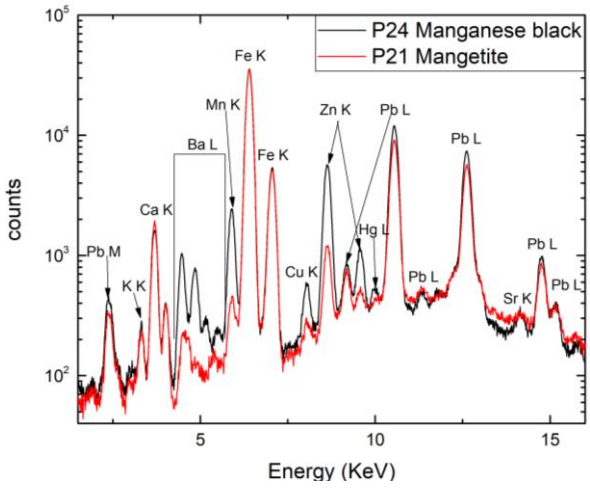

Figure 5.155 XRF spectra from the analysis positions: P21 and P24 of black pigments of Statio XIII "Lamentation". Identification of: manganese black and magnetite (personal archive Karydas, Andreas-Germanos and Kesidis, Stelios).

The elemental analysis of the black pigments by μ-XRF suggests the presence of the pigments: magnetite and manganese black (**Figure 5.155**). Magnetite (Fe_3O_4) (Eastaugh, et al., 2004, p. 248) was identified at the analysis positions: P21, P41 and P42. Manganese black (MnO_2) (Eastaugh, et al., 2004, p. 249) was identified at the analysis positions: P2, P4 to P9, P13 to P18, P20 to P24, P27 to P33, P35 to P40, P43 and P44. (**Table 5.8**).

Table 5.8 Elemental analysis of Statio XIII "Lamentation" by XRF

Spot	Colour	Elements Detected	Suggested Pigments
P1	White	Pb, Fe, Hg, Zn, Ba, K, Ca	Lead white, Red ochre, Yellow ochre, Cinnabar, Lithopone
P2	Brown-red	Fe, Ca, Pb, Zn, Ti, Hg, Mn	Lead white, Red ochre, Yellow ochre, Cinnabar, Zinc white, Titanium white, Manganese black
P3	Pink-orange	Pb, Fe, Hg, Zn, Cu, Ba, Ca, K	Lead white, Red ochre, Yellow ochre, Cinnabar, Lithopone

P4	Black	Pb, Fe, Ca, Zn, Hg, Ti, K, Mn, Cu	Lead white, Red ochre, Yellow ochre, Cobalt blue, Cinnabar, Zinc white, Titanium white, Manganese black
P5	Light yellow	Pb, Fe, Zn, Ti, Hg, Cu, Mn, Cu, Ca, K	Lead white, Red ochre, Yellow ochre, Cobalt blue, Cinnabar, Zinc white, Titanium white, Manganese black
P6	Yellow	Fe, Pb, Ca, Zn, Hg, Ti, K, Mn, Cu	Lead white, Red ochre, Yellow ochre, Cinnabar, Zinc white, Titanium white, Manganese black
P7	Blue	Pb, Fe, Zn, Ca, Ba, Hg, Mn, Cu, K	Lead white, Red ochre, Yellow ochre, Cobalt blue, Prussian blue, Azurite, Cinnabar, Lithopone, Manganese black
P8	Light Blue	Pb, Zn, Ba, Ti, Fe, Ca, Mn, K, Cu,	Lead white, Red ochre, Yellow ochre, Lithopone, Titanium white, Manganese black
P9	Light blue	Pb, Ba, Fe, Zn, Ti, Ca, Mn, Cu, Hg	Lead white, Red ochre, Yellow ochre, Cinnabar, Lithopone, Titanium white, Manganese black
P10	Blue	Pb, Fe, Zn, Co, Cu, Ba, Ca	Lead white, Red ochre, Yellow ochre, Cobalt blue, Lithopone
P11	Light Blue	Pb, Zn, Fe, Cu, Ca, Ti	Lead white, Red ochre, Yellow ochre, Cobalt blue, Zinc white, Titanium white
P12	Blue	Pb, Fe, Co, Zn, Ba, Ca, K, Cu	Lead white, Red ochre, Yellow ochre, Cobalt blue, Prussian blue, Azurite, Lithopone
P13	Red	Fe, Pb, Ca, Zn, Hg, K, Ti, Mn, Co, Cu	Lead white, Red ochre, Yellow ochre, Cobalt blue, Cinnabar, Zinc white, Titanium white, Manganese black
P14	Light red	Fe, Pb, Ca, Hg, Zn, Mn, Ti, K, Cu	Lead white, Red ochre, Yellow ochre, Cobalt blue, Cinnabar, Zinc white, Titanium white, Manganese black
P15	Brown-red	Fe, Ca, Pb, Hg, Zn, K, Mn, Ti, Cu	Lead white, Red ochre, Yellow ochre, Cobalt blue, Cinnabar, Zinc white, Titanium white, Manganese black
P16	Black	Fe, Ca, Zn, Pb, Mn, Hg, Ti, K, Ba, Cu	Lead white, Red ochre, Yellow ochre, Cinnabar, Lithopone, Titanium white, Manganese black
P17	Black	Fe, Ca, Pb, Zn, Mn, Ti, K, Cu, Hg,	Lead white, Red ochre, Yellow ochre, Cinnabar, Zinc white, Manganese black
P18	Black	Fe, Ca, Pb, Zn, Mn, Hg, K, Ti, Cu	Lead white, Red ochre, Yellow ochre, Cinnabar, Zinc white, Manganese black
P19	Pink	Pb, Fe, Hg, Zn, Ca, K, Ba, Mn	Lead white, Red ochre, Yellow ochre, Cinnabar, Lithopone
P20	Green	Pb, Fe, Cu, Zn, As, Ca, Mn, Hg, Ti	Lead white, Red ochre, Yellow ochre, Emerald green, Cinnabar, Zinc white, Titanium white, Manganese black
P21	Black	Fe, Pb, Ca, Zn, Mn, Ti, Cu	Lead white, Red ochre, Yellow ochre, Zinc white, Titanium white, Magnetite, Manganese black
P22	Brown	Pb, Fe, Zn, Ca, Mn, K, Ti, Cu	Lead white, Red ochre, Yellow ochre, Zinc white, Titanium white, Manganese black
P23	Green	Fe, Pb, Ca, Zn, Mn, Cu, Ti, K,	Lead white, Red ochre, Yellow ochre, Verdigris, Zinc white, Titanium white, Manganese black

P24	Brown	Fe, Pb, Zn, Mn, Ca, Ba, Cu, Co, Hg, K	Lead white, Red ochre, Yellow ochre, Verdigris, Cinnabar, Zinc white, Lithopone, Titanium white, Manganese black
P25	White	Pb, Zn, Ti, Fe,	Lead white, Red ochre, Yellow ochre, Zinc white, Titanium white
P26	White	Pb, Fe, Ti, Ca	Lead white, Red ochre, Yellow ochre, Titanium white
P27	Beige	Pb, Fe, Zn, Ti, Ca, K, Mn, Hg	Lead white, Red ochre, Yellow ochre, Cinnabar, Zinc white, Titanium white, Manganese black
P28	Brown	Pb, Fe, Ca, Zn, Mn, K, Ti, Hg	Lead white, Red ochre, Yellow ochre, Cinnabar, Zinc white, Titanium white, Manganese black
P29	Brown-red	Fe, Pb, Zn, Ca, Hg, Cu, Mn, Ba, K	Lead white, Red ochre, Yellow ochre, Verdigris, Cinnabar, Lithopone, Manganese black
P30	Dark brown	Fe, Pb, Ca, Zn, Ba, Mn, Cu, K, Sr	Lead white, Red ochre, Yellow ochre, Verdigris, Cinnabar, Lithopone, Manganese black
P31	White	Pb, Zn, Fe, Ti, Hg, Cu, Co, Mn, Cr, K	Lead white, Red ochre, Yellow ochre, Cobalt blue, Cinnabar, Chrome red/orange, Zinc white, Manganese black
P32	Pink	Zn, Fe, Ca, Pb, Ti, K, Mn, Hg, Cu	Lead white, Red ochre, Yellow ochre, Cinnabar, Zinc white, Titanium white, Manganese black
P33	White	Pb, Hg, Zn, Fe, Ba, Ca, K, Mn	Lead white, Red ochre, Yellow ochre, Cinnabar, Lithopone, Manganese black
P34	Pink	Pb, Fe, Zn, Hg, Ti, Ca, Cu	Lead white, Red ochre, Yellow ochre, Cinnabar, Zinc white, Titanium white
P35	Red	Fe, Pb, Hg!!, Zn, Ca, Ba, Mn,	Lead white, Red ochre, Yellow ochre, Cinnabar, Lithopone, Manganese black
P37	Brown	Fe, Ca, Pb, Cu, Zn, K, Ti, Mn, Hg	Lead white, Red ochre, Yellow ochre, Verdigris, Cinnabar, Zinc white, Titanium white, Manganese black
P38	Dark brown	Fe, Pb, Ca, Zn, Cu, Ba, Mn, Hg	Lead white, Red ochre, Yellow ochre, Verdigris, Cinnabar, Lithopone, Manganese black
P39	Green	Fe, Pb, Zn, Cu, Mn, Ca, Ti	Lead white, Red ochre, Yellow ochre, Azurite, Verdigris, Zinc white, Titanium white, Manganese black
P40	Red	Fe, Pb, Ca, Cu, Zn, K, Ti, Mn, As	Lead white, Red ochre, Yellow ochre, Verdigris, Orpiment, Zinc white, Titanium white, Manganese black
P41	Black	Zn, Fe, Ba, Pb, Ca, Sr, Ca, Cu, Co	Lead white, Red ochre, Yellow ochre, Cobalt blue, Goyazite, Lithopone, Magnetite
P42	Black	Fe, Pb, Ba, Ca, Zn, Co, Cu, K	Lead white, Red ochre, Yellow ochre, Cobalt blue, Verdigris, Zinc white, Lithopone, Magnetite
P43	Light brown	Fe, Pb, Zn, Ca, Mn, Ba, K, As, Cu,	Lead white, Red ochre, Yellow ochre, Orpiment, Lithopone, Manganese black
P44	Brown	Fe, Pb, Ca, Zn, Cu, Mn, K, Ti, As	Lead white, Red ochre, Yellow ochre, Orpiment, Zinc white, Titanium white, Manganese black

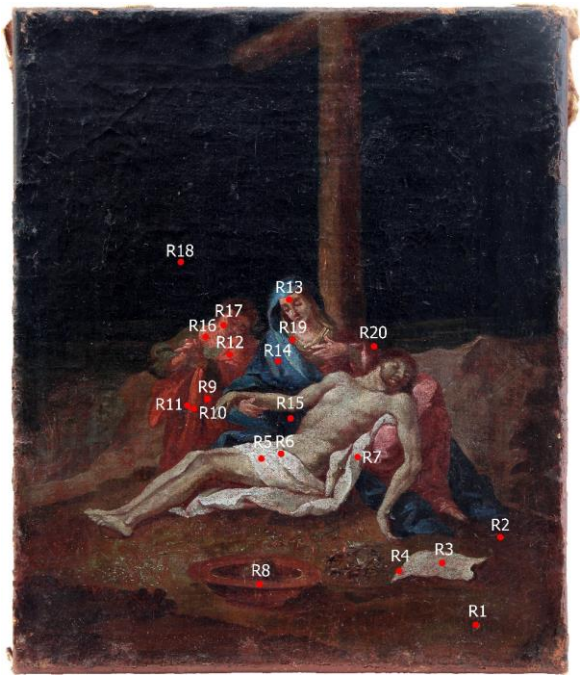

Figure 5.156 Statio XIII "Lamentation". Positions of analysis by Raman spectroscopy (digital processing via Adobe Photoshop by Kesidis, Stelios).

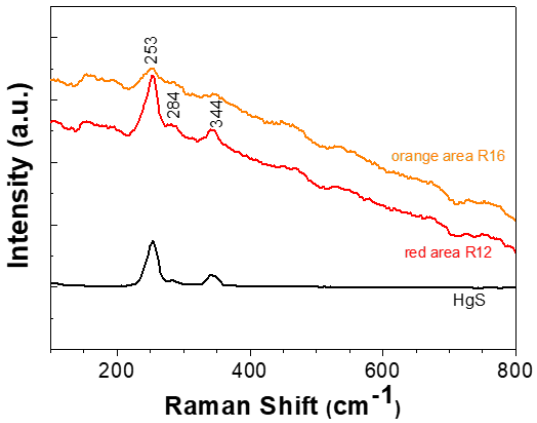

Figure 5.157 Raman spectra collected from a red (R12) and an orange (R16) painted area, showed bands corresponding to cinnabar. A spectrum from pure HgS was shown as a reference (black line).

5.2.7. Raman Spectroscopy

The application of Raman spectroscopy on the Statio XIII "Lamentation" revealed important information about the composition of the pigments present in the painting. Moreover, Raman spectroscopy confirmed and specified the presence of pigments identified also by the other analytical techniques of the analytical protocol.

In the analysis of the painting, 20 point (**Figure 5.156**), analyzes were performed. The application of μ-Raman on the analysis positions: R9 to R12, R16 and R17 confirmed the presence of cinnabar (α-HgS) (Eastaugh, et al., 2004, p. 105) (**Figure 5.157**). However, the majority of the analysis positions did not provide any information on the pigment analyzed, caused either by intense fluorescence emission or by weak Raman signal, possibly due to the lining treatment, which was performed with the glue-paste or the wax-resin techniques (Andersen & Fuster-Lopez, 2019, p. 17).

Table 5.9 Summary of the results obtained with mobile Raman micro-spectrometer for Statio XIII “Lamentation”

Spot	Colour	Pigment Identified
R1	Brown	Intense fluorescence emission
R2	Brown	Intense fluorescence emission
R3	White	Intense fluorescence emission
R4	White	Intense fluorescence emission
R5	White	Intense fluorescence emission
R6	White	Intense fluorescence emission
R7	White	Intense fluorescence emission
R8	Red	Weak Raman signal
R9	Red	Cinnabar
R10	Red	Cinnabar
R11	Red	Cinnabar
R12	Red	Cinnabar
R13	Green	Intense fluorescence emission
R14	Blue	Weak Raman signal
R15	Blue	Weak Raman signal
R16	Orange	Cinnabar
R17	Orange	Cinnabar
R18	Black	Weak Raman signal
R19	Yellow	Intense fluorescence emission
R20	Blossom	Intense fluorescence emission

5.2.8. Laser Induced Fluorescence Spectroscopy

The application of laser induced fluorescence spectroscopy on the painting Statio XIII “Lamentation” identified the presence of fluorescent pigments and the varnish coating of the painting.

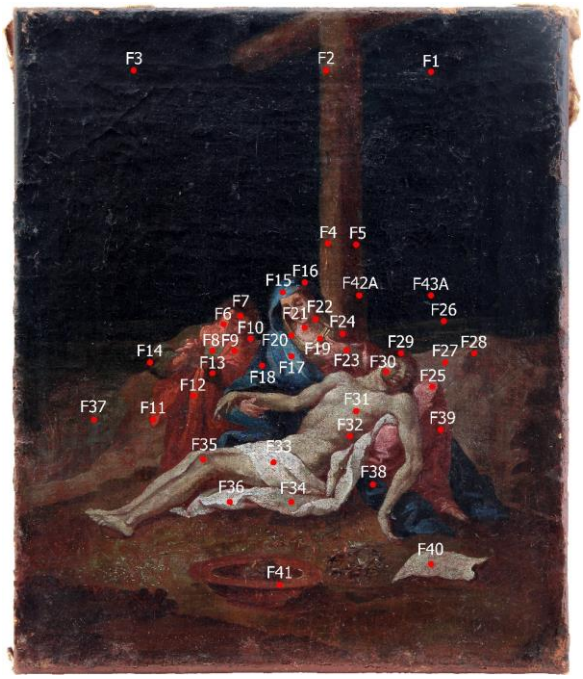

Figure 5.158 Statio XIII "Lamentation". Positions of analysis by laser induced fluorescence spectroscopy (digital processing via Adobe Photoshop by Kesidis, Stelios).

In the analysis of the painting, 43 point (**Figure 5.158**), analyzes were performed.

Examination of the Statio XIII painting revealed zinc white pigment fluorescence on white and light brown areas on the body of Virgin Mary (neck, chest, cheek) and on white and light blue areas on Jesus' cloth. Typical LIF spectra (**Figure 5.159**), similar to pure ZnO reference spectrum (**Figure 5.160**), were recorded. Zinc White (ZnO) (Eastaugh, et al., 2004, p. 406) was identified at the analysis positions: F6, F9, F10, F17, F19 to F25, F32 to F36 and F41.

In **Figure 5.161** reference fluorescence spectra of different aged varnishes, such as dammar, sandarac, mastic and shellac, were present. These spectra were very similar with each other, except for the spectrum corresponding to shellac resin. Therefore, LIF was not a straightforward method to identify the resin used as varnish on a painting. However, comparison of the spectra with the one corresponding to aged dammar varnish showed a very good correlation (**Figure 5.162**). Therefore, dammar was identified at the analysis positions: F1 to F5, F7, F8, F13 to F18 and F26 to F40.

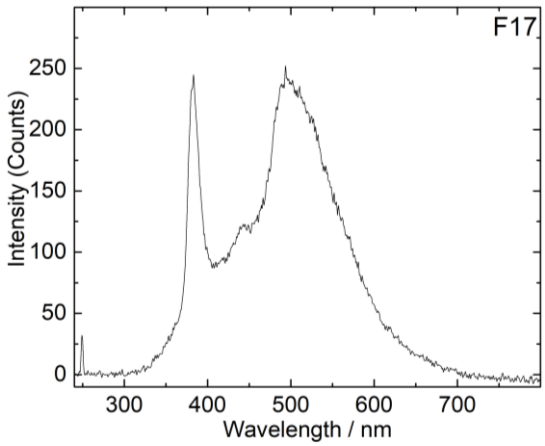

Figure 5.159 LIF spectrum on point F17 on painting STATIO XIII (personal archive of Dr. Kokkinaki, Olga and Kesidis, Stelios)

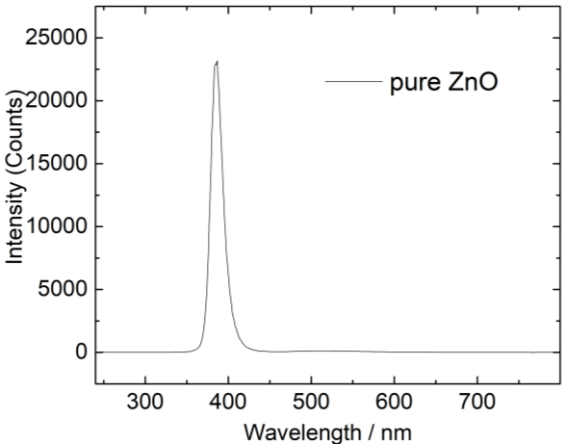

Figure 5.160 LIF spectrum of pure ZnO (personal archive of Dr. Kokkinaki, Olga and Kesidis, Stelios).

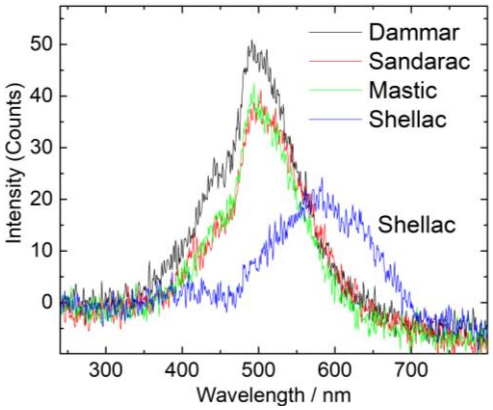

Figure 5.161 LIF spectra recorded from aged prototype films of resins deposited on quartz substrates (personal archive of Dr. Kokkinaki, Olga and Kesidis, Stelios).

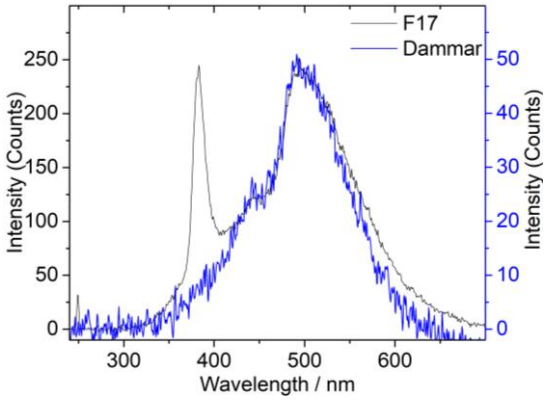

Figure 5.162 LIF spectrum on point F17A on painting STATIO XIII. The LIF spectrum of aged dammar was presented for comparison.

5.2.9. Diffuse Reflectance Spectroscopy

The application of diffuse reflectance spectroscopy on the painting Statio XIII “Lamentation” provided valuable and important information on the pigments used by the artist on his painting. (**Table 5.10**)

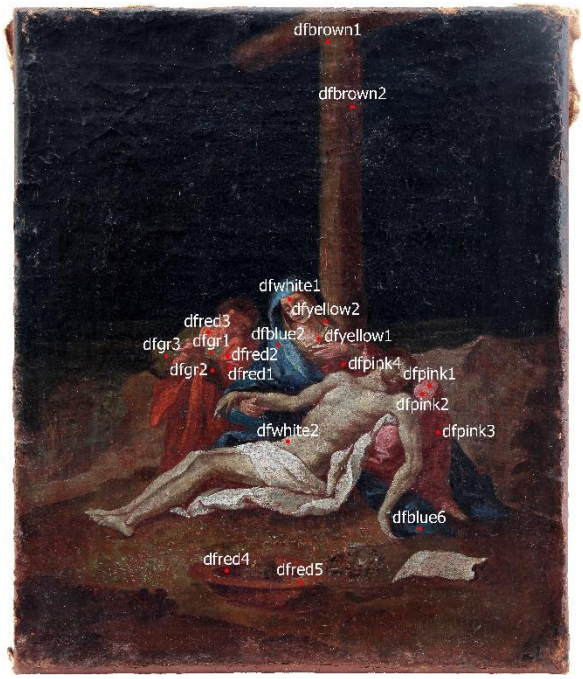

Figure 5.163 Statio XIII "Lamentation". Positions of analysis by diffuse reflectance spectroscopy (digital processing via Adobe Photoshop by Kesidis, Stelios).

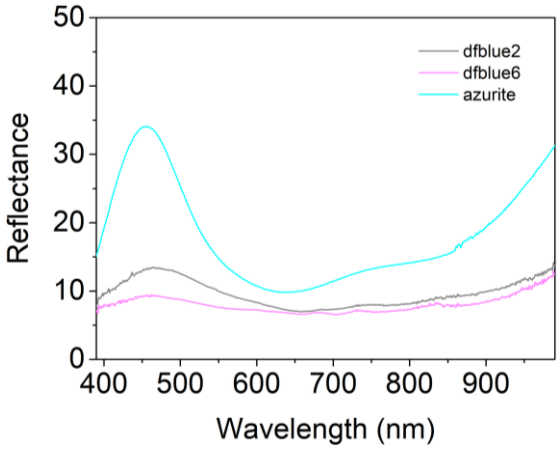

Figure 5.164 Diffuse reflectance spectra collected from blue coloured areas dfblue2, dfblue6 azurite powder for comparative analysis.

In the analysis of the painting, 18 point analyzes were performed (**Figure 5.163**). It was decided that the analysis of the results of diffuse reflectance spectroscopy would be done in colour.

The diffuse reflectance spectra collected from blue coloured areas: dfblue2 and dfblue6 display similar spectral profile (**Figure 5.164**) that indicated the existence of the same pigment. Diffuse reflectance spectrum of azurite pigment [$Cu_3(CO_3)_2(OH)_2$] showed a broad band in the same spectral region due to copper electronic transitions, although the assumption of azurite identification based only on the two collected diffuse reflectance spectra was impossible.

Analysis of the diffuse reflectance spectra collected from green coloured areas: dfgreen1 and dfgreen3 displayed similar spectral profile (**Figure 5.165**). An increase in the reflectance at 450 nm was observed in both spectra and was attributed to yellow ochre pigment. The greenish hue in the painting was probably a result of a mixture of yellow ochre with some blue pigment. Green coloured area dfgreen2, displayed different

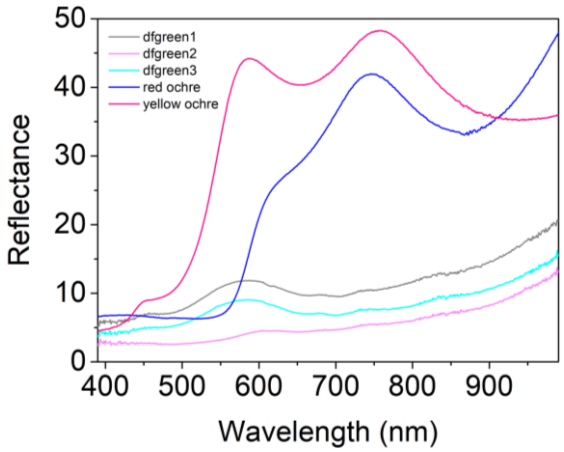

Figure 5.165 Diffuse reflectance spectra collected from green coloured areas: dfgreen1, dfgreen2, dfgreen3 and yellow ochre and red ochre powder for comparative analysis.

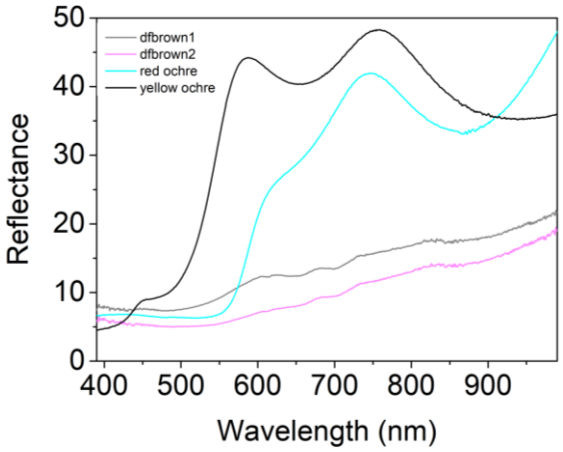

Figure 5.166 Diffuse reflectance spectra collected from brown coloured areas: dfbrown1, dfbrown2 and yellow ochre and red ochre powder for comparative analysis.

spectral profile (**Figure 5.165**) that was related to red ochre, although it cannot be accurately attributed to the pigment.

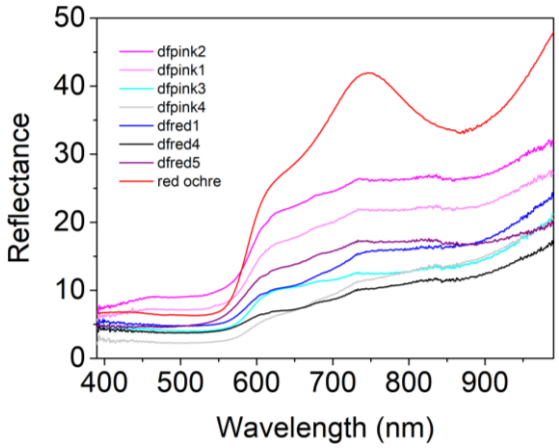

Figure 5.167 Diffuse reflectance spectra collected from red coloured areas: dfpink1, dfpink2, dfpink3, dfpink4, dfred1, dfred4, dfred5 and red ochre powder for comparative analysis.

The diffuse reflectance spectra collected from brown coloured areas: dfbown1 and dfbrown2 showed similar spectral profile to that of a mixture of red with yellow ochre (**Figure 5.166**).

Analysis of the red coloured areas identified the existence of cinnabar in areas: dfred1 and dfred2 and red ochre in areas: dfpink1, dfpink2, dfpink3, dfpink4, dfred1, dfred4 and dfred5 (**Figure 5.167**). Spectra collected from dfred1 and dfred2 present the characteristic S-shaped spectral profile of cinnabar with inflection point at 590 nm and high reflection values in the near IR spectral region. On the other hand, spectra from red coloured areas: dfpink1, dfpink2, dfpink3, dfpink4, dfred1, dfred4 and dfred5 showed lower

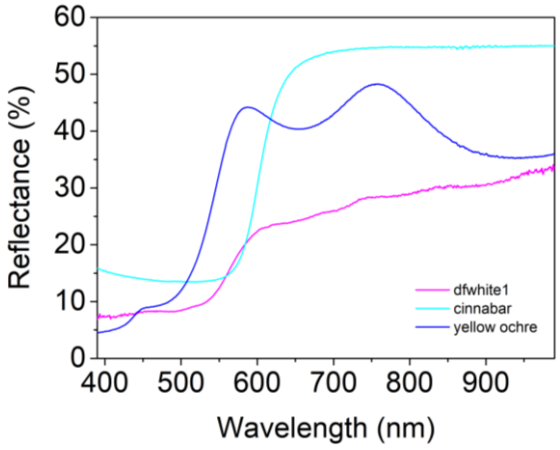

Figure 5.168 Diffuse reflectance spectrum collected from white coloured area dfwhite1 and yellow ochre and cinnabar powder for comparative analysis.

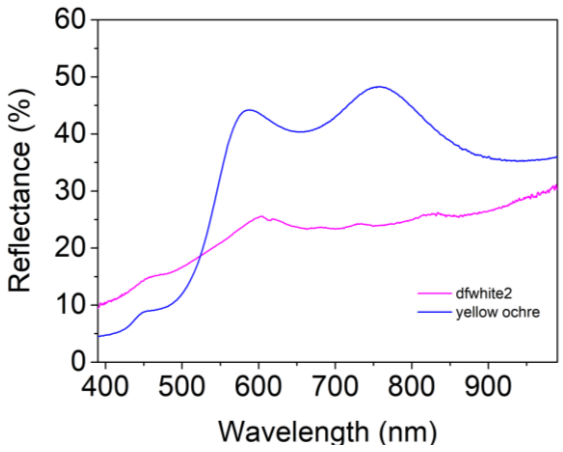

Figure 5.169 Diffuse reflectance spectrum collected from white coloured area dfwhite2 and yellow ochre powder for comparative analysis.

reflectance values and a broad band at between 870 nm that was attributed to electronic transitions of iron of red ochre. Variations in the reflectance values may be a result of the existence of some white compound.

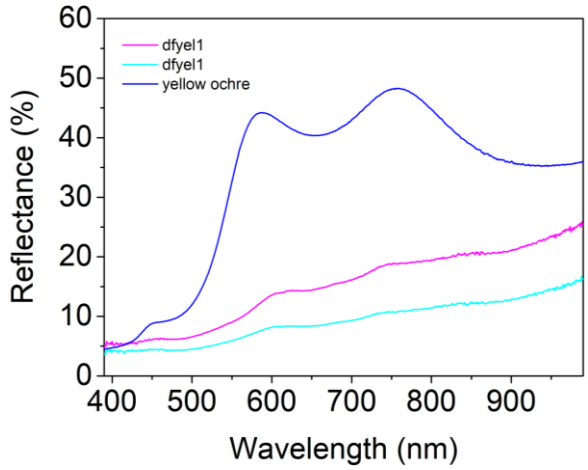

Figure 5.170 Diffuse reflectance spectra collected from yellow coloured areas: dfyel1, dfyel2 and yellow ochre powder for comparative analysis.

The diffuse reflectance spectra collected from white coloured areas: dfwhite1 and dfwhite2 displayed different spectral profiles. Spectrum from area dfwhite1 was probably a mixture of yellow ochre and cinnabar (**Figure 5.168**). The weak increment of reflectance at 450 nm and the blue shift of the S-shape curve were attributed to yellow ochre while the S-shape profile and the high reflectance value in the near IR region were attributed to cinnabar. The diffuse reflectance spectrum of white area dfwhite2 showed similar spectral profile to yellow ochre basically due to the peak at 450 nm attributed to the pigment (**Figure 5.169**).

Finally, analysis of the diffuse reflectance spectra collected from yellow coloured areas identified the existence of yellow ochre pigment (**Figure 5.170**).

Table 5.10 Summary of the results obtained with diffuse reflectance portable system for Statio XIII

Coloured Area code	Pigment Identified	Coloured Area code	Pigment Identified
Dfblue2	Possibly azurite	**Dfpink3**	Red ochre
Dfblue6	Possibly azurite	**Dfpink4**	Red ochre
Dfgreen1	Yellow ochre	**Dfred1**	Red ochre
Dfgreen2	Red ochre	**Dfred4**	Red ochre
Dfgreen3	Yellow ochre	**Dfred5**	Red ochre
Dfbrown1	Yellow ochre and red ochre	**Dfwhite1**	Cinnabar and yellow ochre
Dfbrown2	Yellow ochre and red ochre	**Dfwhite2**	Yellow ochre
Dfpink2	Red ochre	**Dfyel1**	Yellow ochre
Dfpink1	Red ochre	**Dfyel2**	Yellow ochre

5.3. Summary Results

Seeking the fulfillment of the research questions posed in Chapter 4 of this dissertation, namely the investigation of manufacturing technology, the assessment of the preservation state, but also the indirect dating of the two paintings (**Figure 5.171**), it was decided to use innovative and non-destructive methods. However, it becomes necessary to use invasive microscopic methods, which would clarify aspects of the research questions that made it difficult to interpret the analysis data correctly.

Statio VIII

"Jesus and the Women of Jerusalem"

Statio XIII

"Lamentation"

Figure 5.171 The paintings investigated (photo credits: Panagiotis Rompakis, National Gallery - Greece).

The implementation of the research protocol managed to answer all the research questions that were asked, providing a wealth of data. By applying different types of techniques, such as: imaging, stratigraphic and spectroscopic, in most cases, the intersection of conclusions was achieved. However, during the research, some parameters emerged that did not allow the expected amount of data to be extracted. In particular, due to the preservation state of the paintings, but also due to specific interventions, the application of molecular spectroscopic techniques had difficulty in identifying the data of some points of analysis, while the interpretation of data from the application of elemental techniques, in some cases contained margins of error.

Statio VIII "Jesus and the Women of Jerusalem"

Through the implementation of the research protocol on the painting Statio VIII "Jesus and the Women of Jerusalem", all the objectives of the research were fulfilled, as they were described in chapter §4 of this dissertation. Specifically, its manufacturing technology was examined, the state of its preservation was evaluated, and the date of its manufacture was indirectly determined.

In terms of manufacturing technology, the analysis of the painting with imaging techniques revealed evidence that lead to the conclusion that the work had undergone many changes throughout its history, also an attempt was made to interpret the data obtained, with some features of the painting, however, creating concern as to their interpretation. More specifically, it was observed that the painting was lined and that the frame of the object was not the original. These observations came from the observation of the work with X-rays, where the boundaries of the original canvas were observed, the holes from which the canvas was supported in the frame and finally the fact that the canvas wis smaller than the present frame. The parts of the present frame were joined with the mitre joint technique, while the nails that support the second canvas in the frame were of industrial production, a hypothesis based on their uniformity (**Figure 5.50**). It was also observed that for the unification of the two canvases, in addition to the lining, a substance was used at the boundaries of the object (**Figure 5.49**). In addition, through the observation of the work with transmitted infrared radiation, it was estimated that the object consisted of thick stratigraphy (**Figure 5.46**).

Regarding the painting, it was observed that the paint was applied with various techniques, as in some places the impasto technique was observed, while it was not possible to observe underdrawings, except on the shoulder of the female figure to the right of the painting (**Figure 5.44**). Characteristic of the painting were the intense colour differentiation, the fact that many figures had structural discontinuities and were not presented in detail and that in many cases it was not possible to distinguish between the authentic and non-authentic parts of the painting. In particular, at least five different blue pigments were observed through imaging techniques (**Figure 5.26**), an observation that was confirmed by spectroscopic analysis techniques. In addition, some figures were depicted with missing body parts, such as Jesus' right hand and sole, while the left soldier was depicted with two left hands (**Figure 5.16**). In addition, after careful observation, the presence of some elements that did not match the painting were noticed, such as the stool to the right of Jesus, the blue irregular shape below the right soldier (**Figure 5.19** &**Figure 5.38**) and the white irregular shape to the right of the standing female figure on the left of the painting (**Figure 5.20**). However,

information about previously invisible features of the painting also emerged. It was revealed that the left soldier holds a spear and not a sword, as could be seen from the observation in the visible part of the spectrum, which extends further to the right (**Figure 5.42**). It was also observed that the helmet of the left soldier had a decorative feather (**Figure 5.48**). Also, the observation with UV illumination revealed the presence of a child form, which was not otherwise visible (**Figure 5.33**). Finally, the most important information received through the x-ray radiography was the observation of a demon in the upper right corner of the painting, which was not previously visible. The combination of X-rays and multispectral imaging showed that the left soldier's spear appears to point to the demon, leading to the hypothesis that the soldiers accompanying Jesus belonged to the Lansquenets, which were associated with "demon/death" (**Figure 5.59**). Finally, it was observed that the object was not covered by a single layer of varnish, while there were indications of its partial removal (**Figure 5.15**).

Furthermore, as concerned the manufacturing technology, the stratigraphic techniques revealed the complex and multilayered stratification of the painting. In particular, on the sample S1 eleven layers were observed, while overpainting layers were also detected. Starting from the original ground layer was a red-coloured layer (**Figure 5.62**) based on dolomite ([Ca,Mg][CO3]2) and aluminum silicate (Al_2SiO_3), while the colour of the layer was achieved due to the presence of the red ochre (Fe_2O_3) (Eastaugh, et al., 2004, p. 320) with the addition of silicon (Si), which had the role of absorbent (**Table 5.1**), with this type of ground layer being typical of the 16th to 18th century when painters started to use light-coloured grounds. (Stols-Witlox, 2015, pp. 174-175) The original green paint layer was composed of green earth [$(K,Na)(Fe,Al,Mg)_2(Si,Al)_4O_{10}(OH)_2$] (Eastaugh, et al., 2004, p. 174) with the addition of lead white ($(PbCO_3)_2 \cdot Pb(OH)_2$) (Eastaugh, et al., 2004, p. 233), while after this layer two thick organic coatings followed. Moreover, the optical characteristics and composition of the overpainting were identified. It was revealed that the ground layer of the overpainting consisted of three sub-layers, with the first being red-coloured and the second and third layer being dark-coloured. The composition of the red-coloured layer was based on lithopone ($BaSO_4 \cdot ZnS$) (Eastaugh, et al., 2004, p. 242), red ochre (Fe_2O_3) (Eastaugh, et al., 2004, p. 320) and silicon (Si), which had the role of filler/absorbent. The two

dark-coloured layers' composition was based on burnt sienna (SiO_2+Al_2O_3+Fe_2O_3) (Eastaugh, et al., 2004, p. 66) and of red lead (Pb_3O_4) (Eastaugh, et al., 2004, p. 229). These results indicated that the overpainting had occurred after the second half of the 19th century, since lithopone was discovered around 1850 by G.F. de Doubet. Finally, the second paint layer was composed of verdigris ($Cu(CH_3COO)_2.H_2O$) (Eastaugh, et al., 2004, p. 385), red (Fe_2O_3) (Eastaugh, et al., 2004, p. 320) or yellow ochre (α-FeOOH) (Eastaugh, et al., 2004, pp. 320, 401) and red lead (Pb_3O_4) (Eastaugh, et al., 2004, p. 229). On the sample S2 two layers were observed. The first (ground layer) was identical with the seventh layer of the sample S1, thus suggesting that the sample S2 was taken from an area where overpainting was performed and that this also occurred at the second half of the 19th century.

The pigments of the painting were identified through the use of spectroscopic techniques of the research protocol (**Table 5.11**). Thus, it turned out that a total of five blue pigments were used with cobalt blue ($CoO.Al_2O_3$) (Eastaugh, et al., 2004, p. 112) as the main blue pigment, which was detected by XRF and the DFR. The detection of manganese blue ($xBaSO_4.yBaMnO_4$) (Eastaugh, et al., 2004, p. 37) was very important, as it was a modern pigment that was discovered in the 20th century. However, it should be noted that the pigment was identified only through XRF, thus leaving a margin for error, since the molecular spectroscopic techniques applied could not give information on the specific pigment, possibly due to the interference of the wax from the lining. The presence of azurite ($Cu_3(CO_3)_2(OH)_2$) (Eastaugh, et al., 2004, p. 33) was also detected, through XRF, on the blue irregular shape under the right soldier. This blue pigment was one of the most important blue pigments of the Middle Ages, with its use ceasing at the end of the 18th century. Prussian blue ($[Fe(II)(CN)_6]_4$) (Eastaugh, et al., 2004, p. 308), discovered in 1710, the fourth blue pigment was detected on the blue scarf of the right soldier. Finally, ultramarine ($Na_7Al_6Si_6O_{24}S_3$) (Eastaugh, et al., 2004, p. 375; Roy, 1993, p. 55) was detected through Raman and DRF on the upper arm of the cross.

As concerns red pigments, three red pigments were detected. Cinnabar (α-HgS) (Eastaugh, et al., 2004, p. 105), mostly detected on the faces of the figures, was

identified through XRF, Raman and DRF. Red ochre (Fe_2O_3) (Eastaugh, et al., 2004, p. 320), which was the main red pigment of the painting, was detected through XRF and DFR. And finally, chrome red/orange ($PbCrO_4$.PbO) (Eastaugh, et al., 2004, p. 98), which was discovered in the 19th century, was detected on the crimson-coloured garment of Jesus, through XRF and Raman.

Scheele's green (AsCuHO3) (Eastaugh, et al., 2004, p. 335), was detected on areas of overpainting, and was the only green pigment identified on the painting.

As concerned yellow pigments, two yellow pigments were identified. As the main yellow pigment of the painting, yellow ochre (α-FeOOH) (Eastaugh, et al., 2004, pp. 320, 401) was detected through XRF and DFR, with the second yellow pigment being orpiment (As2S3) (Eastaugh, et al., 2004, p. 285; West FitzHugh, 1997, p. 47), which was used until the end of the 19th century, identified through XRF.

The analysis of the painting detected the presence of five white pigments with lead white ($(PbCO_3)_2 \cdot Pb(OH)_2$) (Eastaugh, et al., 2004, p. 233) as the main white pigment. However, due to the fact lead white was detected only through XRF, it could not exclude the possibility of the presence of red lead (Pb_3O_4) (Eastaugh, et al., 2004, p. 229). Zinc white (ZnO) (Eastaugh, et al., 2004, p. 406), which was discovered in the 19th century, was also detected on the painting through XRF and LIF. The third white pigment detected was lithopone ($BaSO_4 \cdot ZnS$) (Eastaugh, et al., 2004, p. 242), discovered also at the 19th century. Also, the presence of calcite ($CaCO_3$) (Eastaugh, et al., 2004, p. 74) was detected on the painting, however due to the fact that pigment was tested only in one analysis position and also the fact that it was detected only through XRF leaves a margin of error. Finally, of great importance was the detention of titanium white (TiO_2) (Eastaugh, et al., 2004, p. 364). This pigment, which was identified through XRF, was a modern white pigment of the 20th century.

Pigment Colour	Pigment Type	Detected By
Blue	Cobalt blue	XRF, DFR
Blue	Manganese blue	XRF
Blue	Prussian blue	XRF
Blue	Azurite	XRF
Blue	Ultramarine	Raman, DFR
Red	Red ochre	XRF, DFR
Red	Cinnabar	XRF, Raman, DFR
Red	Chrome red	XRF, Raman
Green	Scheele's green	XRF
Yellow	Yellow ochre	XRF, DFR
Yellow	Orpiment	XRF
White	Lead white	XRF
White	Zinc white	XRF, LIF
White	Lithopone	XRF
White	Calcite	XRF
White	Titanium white	XRF
Black	Magnetite	XRF

Table 5.11 Summary of the results obtained with the spectroscopic analytic techniques

Lastly, magnetite (Fe_3O_4) (Eastaugh, et al., 2004, p. 248) was the only black colour identified on the painting.

The above information about the detection of specific pigments lead to conflicting conclusions, as the presence of some pigments was not chronologically consistent with the presence of others. In particular, azurite, which was used until the end of the 18th century, and orpiment and lead white, which were used until the end of the 19th century, were not consistent with the presence of manganese blue and titanium white, which were modern pigments of the 20th century. Thus, combining data from microscopy techniques and spectroscopic techniques, it appeared that the initial phase of the painting could be dated to the end of the 18th century (red preparation + presence of azurite), with the overpainting being carried out after the

second half of the 19th century (zinc white + lithopone) and possibly later 20th century interventions (manganese blue + titanium white).

As for the preservation state of the painting, the application of the imaging techniques established its poor preservation state. In particular, due to the lining treatment the canvas pattern was visible in most of the paintings surface, which led to many areas where paint loss was recorded (5.8). Furthermore, the patch treatment (5.37) along with the lining (5.36) denoted the bad preservation state of the painting during its history. Additionally, the presence of grouting (5.9) and filling (5.40) were also recorded, suggesting the application of conservation treatments. Finally, the extensive overpaintings (5.13, 5.18 and 5.32), recorded across the painting surface deteriorated the already poor preservation state of the painting.

Statio XIII "Lamentation"

Through the implementation of the research protocol on the painting Statio XIII "Lamentation", all the objectives of the research were fulfilled, as they were described in chapter §4 of this dissertation.

In terms of manufacturing technology, the analysis of the painting with imaging techniques revealed evidence that leads to the conclusion that the work has undergone many changes throughout its history. More specifically, it was observed that the painting was lined twice and that the frame of the object is not the original (**Figure 5.104** & **Figure 5.107**). These observations came from the observation of the object with X-rays and digital photography, where the boundaries of the original canvas were observed, the holes from which the canvas was supported in the frame and finally the fact that the canvas is smaller than the present frame. The parts of the present frame are joined with the mitre joint technique, while the nails that support the second canvas in the frame are of industrial production, a hypothesis based on their uniformity (**Figure 5.130**). It is also observed that for the unification of the two canvases, in addition to the lining, a substance was used at the boundaries of the object (**Figure 5.131**). In addition, through the observation of the work with transmitted infrared radiation, it was estimated that the object consists of thick stratigraphy (**Figure 5.121**).

Regarding the painting, it is observed that the paint was applied with different techniques, as in some places the impasto technique is observed and that a wide variety of colours were used (**Figure 5.108**). Through the careful observation of the object with the imaging techniques of the research protocol, it was revealed that the painting's surface has undergone extensive overpaintings. In particular, in small and scattered areas on the ground, a second underlying paint layer can be observed (**Figure 5.105**, **Figure 5.110** and **Figure 5.111**). The small thickness of the overpainting layer in these areas is consistent with the observation of the sample S4 with optical microscopy and SEM/EDS, where the overpainting layer is also very thin (**Figure 5.147**). Furthermore, a characteristic of the painting is that in many cases there are no clear indications of which part of the paint is authentic, as in the white linen cloth of Jesus, where many different colour tonalities and paint textures are found (**Figure 5.112**). Moreover, during the observation of the painting through multispectral imaging, the presence of some hidden features was revealed. Specifically, a cloth wrapped around the cross was observed, as it can be seen in figures **Figure 5.116** and **Figure 5.124**. While at 1000 nm, on the right of the painting starting from the point where the green hills are located (as seen visibly) there seem to be two columns that continue downwards. This feature was only visible through the IRT configuration, while the fact that it was visible only at the highest wavelengths indicates that they are located in an underlying layer (**Figure 5.126**). Additional to the hidden features of the painting, information on the presence of pentimenti by the artist also emerged. Namely, under the armpit of Jesus, where the pattern of the cloth in the VIS shows a smaller gap in the fold (**Figure 5.127**). Finally, during observation with UVF two different kinds of varnish were detected. The older, oxidized varnish located only in some areas of the painting (**Figure 5.113**), leading to the conclusion that some had been partially removed. The second varnish has applied evenly on the surface of the painting, with the brushstrokes from its application process being visible (**Figure 5.109**). The LIF analysis of the painting detected the presence of dammar, as one of the two varnishes of the painting (**Figure 5.162**).

Furthermore, as concerns the manufacturing technology, the stratigraphic techniques revealed the complex and multilayered stratification of the painting. In

particular, on the sample S3, which originates from the area of overpainting, three layers were observed (**Figure 5.136** and **Figure 5.142**). Starting from the first layer, which works as the ground layer, is a red-coloured layer based on lithopone ($BaSO_4 \cdot ZnS$) (Eastaugh, et al., 2004, p. 242), red ochre (Fe_2O_3) (Eastaugh, et al., 2004, p. 320) and silicon (Si), which has the role of filler/absorbent (**Table 5.6**). These results indicate that this layer was applied after the second half of the 19th century, since lithopone was discovered around 1850 by G.F. de Doubet. This layer is followed by two paint layers. The first paint layer is of a dark blue colour, with the EDS analysis not providing information on its nature. In the same way, the second black-coloured paint layer did not provide information that would lead to its identification. The lack of information on these two layers can be attributed either to the low-element composition of the pigments, or the overlapping of their peaks by the peaks of the ground layer. As regards the sample S4, seven layers where observed (**Figure 5.141**). The three layers of ground (layers 2 to 4) were red-coloured, based on dolomite ([Ca,Mg][CO3]2) and aluminum silicate (Al_2SiO_3), while the colour of the layer was achieved due to the presence of the red ochre (Fe_2O_3) (Eastaugh, et al., 2004, p. 320) with the addition of silicon (Si), which has the role of absorbent (**Table 5.7**), with this type of ground layer being typical of the 16th to 18th century when painters started to use light-coloured grounds (Stols-Witlox, 2015, pp. 174-175). Next followed a blue paint layer, with the EDS analysis to lead to the assumption that it might be a layer of ultramarine ($Na_7Al_6Si_6O_{24}S_3$) (Eastaugh, et al., 2004, p. 375; Roy, 1993, p. 55) with the presence of lead white ($(PbCO_3)_2 \cdot Pb(OH)_2$) (Eastaugh, et al., 2004, p. 233) and barite ($BaSO_4$) (Eastaugh, et al., 2004, p. 40). The sixth layer was an organic coating, with the last layer of the stratigraphy being a black paint layer, revealing this way the presence of overpainting. The EDS analysis detected the presence of phosphorus (P), leading to the assumption that it is a layer of bone black ($Ca_5(OH)(PO_4)_3$)) (Eastaugh, et al., 2004, p. 57). (**Table 5.7**).

The pigments of the painting were identified through the use of the spectroscopic techniques from the research protocol (**Table 5.11**). Thus, it turns out that a total of three blue pigments were used with cobalt blue ($CoO.Al_2O_3$) (Eastaugh, et al., 2004, p. 112) as the main blue pigment, which was detected by XRF. The detection of cobalt blue on the analysis positions on the dark black sky was very important,

indicating the presence of the pigment on an underlying layer. Thus, after taking under consideration the identification of ultramarine by SEM/EDS on the area of sky, the fact arises that the sky was originally blue and that it was a mixture of cobalt blue and ultramarine. The presence of azurite [$Cu_3(CO_3)_2(OH)_2$] (Eastaugh, et al., 2004, p. 33) was also detected, through XRF and DRF, on the himation of the Virgin Mary, with its identification providing indirect dating information, since its use ceased at the end of the 18th century. Prussian blue [[Fe(II)$(CN)_6]_4$] (Eastaugh, et al., 2004, p. 308), discovered in 1710, was also detected on the himation of the Virgin Mary.

As concerns the red pigments, three red pigments were detected. Cinnabar (α-HgS) (Eastaugh, et al., 2004, p. 105), mostly detected on the faces and bodies of the figures, was identified through XRF, Raman and DRF. Red ochre (Fe_2O_3) (Eastaugh, et al., 2004, p. 320), which is the main red pigment of the painting, was detected through XRF and DFR. Finally, chrome red ($PbCrO_4$.PbO) (Eastaugh, et al., 2004, p. 98), which was discovered in the 19th century, was detected on the face of Jesus, through XRF. (**Table 5.11**).

The analysis of the painting showed the presence of emerald green and verdigris. Emerald green [$Cu_4(OAc)_2(AsO_2)_6$] (Eastaugh, et al., 2004, p. 122), was detected on the himation of St. John, through XRF. However, it has to be mentioned, that the detection of emerald green contains a margin of error, since the attribution was based on the presence of Cu and As K lines, not ruling out the possibility that it is Scheele's green ($AsCuHO_3$) (Eastaugh, et al., 2004, p. 335). Verdigris [$Cu(CH_3COO)_2.H_2O$] (Eastaugh, et al., 2004, p. 385) was also identified through XRF. However, it has to be mentioned, that the detection of verdigris contains a margin of error, since the attribution was based on the presence of a Cu K line, not ruling out the possibility that it is [$Cu_3(CO_3)_2(OH)_2$] (Eastaugh, et al., 2004, p. 33). (**Table 5.11**).

Regarding the yellow pigments on the painting, the analysis showed the presence of: yellow ochre, orpiment and goyazite. Yellow ochre (γ-FeOOH) (Eastaugh, et al., 2004, p. 401), identified by XRF and DRF, was the main yellow pigment on the painting. Orpiment (As2S3) (Eastaugh, et al., 2004, p. 285; West FitzHugh, 1997,

p. 47) was identified on the cross and the ground of the painting through XRF spectroscopy. According to sources (Eastaugh, et al., 2004, p. 285; West FitzHugh, 1997, p. 50), orpiment was used until the end of the 19th century. Thus, the identification of orpiment on the painting provides indirect information about the dating of the painting. Finally, goyazite ($SrAl_3(PO_4)_2(OH)_5.(H_2O)$) (Eastaugh, et al., 2004, p. 172) was identified through XRF spectroscopy on the sky of the painting. Thus, after the revelation that the sky was originally blue-coloured, the addition of a yellow pigment strengthens the suspicions of an underlying layer, which differs radically from the present state of the painting. However, the identification of goyazite contains margins of error, since the attribution of the pigment was based on the intense strontium (Sr K line) peak. (**Table 5.11**).

The analysis of the painting showed the presence of four different white pigments, specifically: lead white, zinc white, lithopone and titanium white. Lead white ($(PbCO_3)_2{\cdot}Pb(OH)_2$) (Eastaugh, et al., 2004, p. 233), due to the high atomic number of lead, was identified in all analysis positions through XRF, with a proportion of the attributed peaks which originated from underlying layers. Zinc white (ZnO) (Eastaugh, et al., 2004, p. 406) which was discovered in the 19th century, was also detected on the painting through XRF and LIF. Lithopone $BaSO4 \cdot ZnS$) (Eastaugh, et al., 2004, pp. 242, 406) was the third white pigment detected.it was also discovered during the 19th century. Finally, of great importance was the detection of titanium white (TiO_2) (Eastaugh, et al., 2004, p. 364). This pigment, which was identified through XRF, is a modern white pigment of the 20th century. (**Table 5.11**).

Finally, two different black pigments were detected on the painting. Magnetite (Fe_3O_4) (Eastaugh, et al., 2004, p. 248) was identified through XRF. Manganese black (MnO_2) (Eastaugh, et al., 2004, p. 249), which is the main black pigment was detected through XRF. (**Table 5.11**).

Pigment Colour	Pigment Type	Detected By
Blue	Cobalt blue	XRF
Blue	Prussian blue	XRF
Blue	Azurite	XRF, DRF
Red	Red ochre	XRF, DFR
Red	Cinnabar	XRF, Raman, DFR
Red	Chrome red	XRF
Green	Emerald green	XRF
Green	Verdigris	XRF
Yellow	Yellow ochre	XRF, DFR
Yellow	Orpiment	XRF
Yellow	Goyazite	XRF
White	Lead white	XRF
White	Zinc white	XRF, LIF
White	Lithopone	XRF
White	Titanium white	XRF
Black	Magnetite	XRF
Black	Manganese black	XRF

Table 5.12 Summary of the results obtained with the spectroscopic analytic techniques.

The above information regarding the detection of specific pigments leads to conflicting conclusions, as the presence of some pigments is not chronologically consistent with the presence of others. In particular, azurite, which was used until the end of the 18th century, and orpiment and lead white, which were used until the end of the 19th century, are not consistent with the presence of titanium white, which is a modern pigment of the 20th century. Thus, combining data from microscopy techniques and spectroscopic techniques, it appears that the initial phase of the painting can be dated to the end of the 18th century (red preparation + presence of azurite), with the overpainting being carried out after the second half of the 19th century (zinc white + lithopone) and possibly later 20th century interventions (titanium white).

As for the preservation state of the painting, the application of the imaging techniques establishes its relatively poor preservation state. In particular, due to the two lining treatments, the canvas pattern is visible on most of the painting surface, which led to many areas where paint loss is recorded (**Figure 5.131**). Additionally, the presence of grouting and filling (**Figure 5.132** and **Figure 5.133**) were also recorded, suggesting the application of conservation treatments. The conservation/restoration treatments were also tracked in the form of aesthetical restoration treatments, since retouching was recorded on the knee of the Virgin Mary (**Figure 5.113**). Finally, the extensive overpaintings (**Figure 5.114**, **Figure 5.117** and **Figure 5.118**),), recorded across the painting surface deteriorate the already poor preservation state of the painting.

5.3.1. Comparison of The Two Paintings

At the end of the presentation of the results, it was considered useful to list the main similarities and differences between the two paintings (**Figure *5.171***), which may lead to some conclusions about the correlation of the two paintings in terms of manufacturing technology, preservation state and dating, but also about their attribution to the same artist and artistic ensemble.

The two paintings have several similarities, both in terms of manufacturing technology and preservation state, as well as in terms of their dating. Both works have lining operations (Statio VIII → 1 lining and 1 patch, Statio XIII → 2 lining), while the frame of both paintings is not the original. The frames have similarities both visually and in terms of their manufacturing technology (mitre joint technique). While for the unification of the two canvases, in addition to the lining, a substance was used at the boundaries of the object. This substance was identified on the first layer of the samples S2 from Statio VIII and S3 from Statio XIII.

Regarding the painting techniques in the two paintings, the abrupt colour differentiations found in Statio VIII are not found in Statio XIII. However, in both paintings there are places where the impasto technique was used, which are associated with overpainting areas. A common feature is also the presence of underlying painting layers, as well as the extensive painting. It should be noted

that Statio VIII, unlike Statio XIII, has problems with the composition of the painting, with structural discontinuities and objects or elements of the painting that cannot be interpreted.

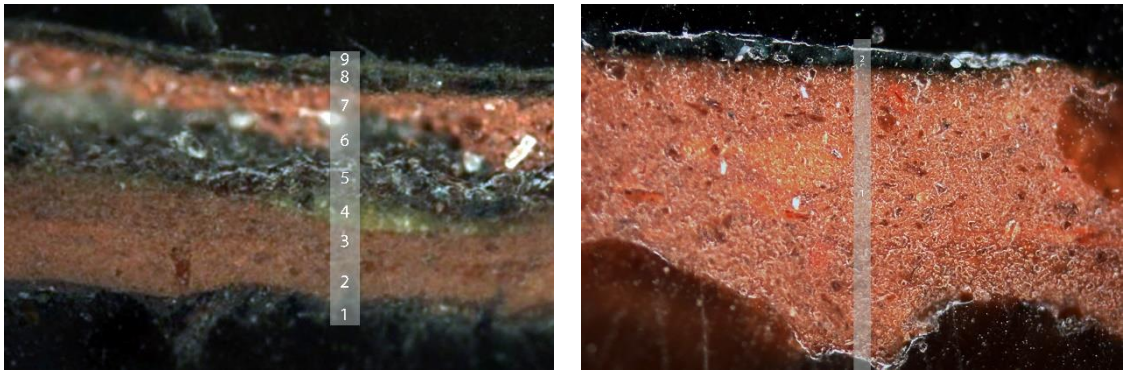

Statio VIII - Sample S1 (OM) Statio XIII - Sample S4 (OM)

Figure 5.172 The stratigraphy of the samples S1 from Statio VIII and S4 from Statio XIII observed through optical microscopy. (Photo Credits: Terlixi, Agni-Vasileia, National Gallery - Greece) (digital processing via Adobe Photoshop by Kesidis, Stelios).

Concerning their stratigraphy, both paintings have thick, multilayered stratification (**Figure 5.172**). The authentic preparation layer, visually and compositionally identical in both paintings, is a fine-grained, red-coloured preparation, rendered chronologically in the late 18th century. A small differentiation on the preparation layers is the presence of three sub-layers on the Statio XIII, compared to the two sub-layers on the Statio VIII. Furthermore, data showed that the phase of overpainting occurred in both paintings after the second half of the 19th century, since the substance used for the unification of the two canvases contained lithopone (Sample S1 → layer 7, sample S2 → layer 1, sample S3 → layer 1). An important finding was the fact that the overpainting in sample S4 had no preparation, compared to the overpainting of the sample S1, where a stratification of three preparation layers was found. Moreover, the presence of some modern pigments suggests that interventions have occurred also in the 20th century.

As concerns the preservation state of the painting, it is relatively similar, where the paintings deal with the same type of pathology and conservation treatments. The exception is the aesthetical restoration treatment found on Statio XIII.

All the above contribute to the assumption that the paintings shared the same history. Both the facts that they present similarities on their manufacturing technology and dating, and that they bear similar interventions and conservation treatments lead to the assumption that maybe the two paintings derived from the same place and that maybe they were altered/conserved by the same people. Connecting this way, the two paintings with the same artistic ensemble.

6. Conclusions

The present work aimed to investigate two paintings from a group of an important type of objects that have not received adequate attention. Studying two works from the series "Stations of the Cross", the eighth station "Jesus and the Women of Jerusalem" and the thirteenth station "Lamentation", research questions arose about their construction technology, their state of preservation and chronological placement.

In order to achieve the abovementioned objectives, a detailed review of the history of the typology, as well as the methods, techniques and materials used historically in similar objects was carried out. Leading in this way to the formation and adoption of the research methodology.

The primary goal of the research methodology was to extract the richest and most complete information possible, with as a priority the least possible intervention on the paintings using innovative non-invasive methods of analysis. However, the complexity of the objects necessitated the application of certain invasive methods of analysis as well, which nevertheless provided very important information, elucidating many, until then inaccessible, aspects of the objects.

Current research has shown that the two works, which belong to the same artistic ensemble, belong to the late 18th century, following the practices of the time, such as the red preparation. The great variety and the choice of high-quality pigments indicate the importance of these objects. Of great interest are the indication of the existence of underlying painting layers, which differ greatly from the present state of the objects. Such an example is the revelation that the sky in Statio XIII it was blue instead of black, radically changing the image of the painting.

The relatively poor state of preservation of the paintings became clear, with the main factors leading to this conclusion being the lining and patching operations identified in both panels, and the extensive painting interventions, which are either of a general nature or are operations performed for restoration purposes. Finally,

indirect dating via selected pigments occured, which recorded operations of the 19th and the 20th century.

All the above testify to the importance of the study of these two paintings, as their investigation shed light on this category of objects, highlighting their intense history over the centuries.

6.1. Future Research

The present research investigated and answered many key questions about the two paintings from the series "Stations of the Cross", but there is room for future research.

After the application of the research protocol, the hypotheses regarding the existence of underlying painting layers emerged, which greatly differentiate the painting representation of the two paintings. Aiming to reveal these layers, it was proposed to perform a series of non-invasive state-of-the-art analysis techniques. Specifically, after taking the four samples used to perform the microscopy techniques, it emerged that the samples, which come even from the same painting, show strong differences. Thus, the use of Terahertz (THz) Imaging (Janssens , et al., 2010, p. 823) and Optical Coherence Tomography (OCT) (Janssens , et al., 2010, p. 822; Alfeld & Broekaert, 2013, p. 223) was recommended. These techniques identified paint interfaces, identified secondary layers, and overpaintings, as well as study the build-up of paint layers. While for the revelation of the underlying painting layers, the use of Macroscopic X-Ray Fluorescence (MA-XRF) spectrometry (Alfeld & de Viguerie, 2017, p. 87) was suggested, where the revelation of the underlying painting layers was be done through the creation of chemical maps. In addition, the use of a multi-spectrum camera capable of exploiting most of the infrared radiation, such as InGaAs multi-spectrum cameras, would answer important questions about the invisible elements of the two paintings (Alexopoulou, et al., 2018, p. 444).

In addition, the use of Synchrotron Radiation X-ray Absorption Spectroscopy (SR-XAS) (Bardelli, et al., 2011, p. 3148) was recommended to verify the results of the

identification of the pigments used, which played a very important role in drawing conclusions about the technology of making the objects, but also their dating. By locating the local chemical environment will provide quantitative information about the dyes used. The application of Macroscopic X-ray Powder Diffraction Scanning (MA-XRPD) (Alfeld & Broekaert, 2013, p. 219; Vanmeert, et al., 2019, p. 7154) would offer an additional advantage for the clarification of the presence or not of the pigments but also for the identification of the areas in which they have been applied. This was e achieved by the direct identification and visualization of crystalline compounds in the painting layers.

Finally, the use of Fourier Transform Infrared (FTIR) spectroscopy was proposed to investigate the binder of the pigments, an element that could provide even more information about the technology of construction of the objects but also to expand the field of comparison between them. Also, through Fourier Transform Infrared (FTIR) spectroscopy it was proposed to study the traces of varnish found in both works, in order to verify the dammar varnish detected in the painting Statio XIII "Lamentation", and to identify the rest (Kouloumpi, et al., 2012, pp. 375-376; Stuart, 2007, pp. 126-128; Prati, et al., 2017, p. 130).

Bibliography

- Abendschein, A., 1906. *The secrets of old masters.* New York: D. Appleton and Company.
- Aceto, M. et al., 2014. Characterisation of colourants on illuminated manuscripts by portable fibre optic UV-visible-NIR reflectance spectrophotometry. *Analytical Methods*, Volume 6, pp. 1488-1500.
- Adriaens, A., 2005. Non-destructive analysis and testing of museum objects: An overview 5 years of research. *Spectrochimica Acta Part B*, Volume 60, pp. 1503-1516.
- Adriaens, A. & Dowsett, M. G., 2004. Electron microscopy and its role in cultural heritage studies. In: *Non-Destructive Microanalysis of Cultural Heritage Materials.* Amsterdam: Elsevier, pp. 73-128.
- Akhtar, K., Khan, S. A., Khan, S. B. & Asiri, A. M., 2018. Scanning Electron Microscopy: Principle and Applications in Nanomaterials Characterization. In: S. K. Sharma, et al. eds. *Handbook of Materials Characterization.* Cham: Springer, pp. 113-145.
- Alexopoulou - Agoranou, A. & Xrysoulakis, J., 1993. *Θετικές Επίστήμες και Έργα Τέχνης (Physical Sciences and Works of Art).* Athens: Γκόνη.
- Alexopoulou, A., Kaminari, A. A. & Moutsatsou, A., 2018. *Multispectral and Hyperspectral Studies on Greek Monuments, Archaeological Objects and Paintings on Different Substrates. Achievements and Limitations.* Athens, Springer, pp. 443-461.
- Alfeld, M. & Broekaert, J. A. C., 2013. Mobile depth profiling and sub-surface imaging techniques for historical paintings—A review. *Spectrochimica Acta Part B: Atomic Spectroscopy*, Volume 88, pp. 211-230.
- Alfeld, M. & de Viguerie, L., 2017. Recent developments in spectroscopic imaging techniques for historical paintings - A review. *Spectrochimica Acta Part B: Atomic Spectroscopy*, Volume 136, pp. 81-105.
- Amanatiadis, S., Apostolidis, G. & Karagiannis, G., 2018. *Fusion of the Infrared Imaging and the Ultrasound Techniques to Enhance the Sub-surface Characterization.* Athens, Springer, pp. 472-481.

- Analytical Methods Committee AMCTB No 75, 2016. UV-visible-NIR reflectance spectrophotometry in cultural heritage: Background paper. *Analytical Methods*, Volume 8, pp. 5894-5896.
- Andersen, C. K. & Fuster-Lopez, L., 2019. Insight into canvas paintings' stability and the influence of structural conservation treatments. In: *The Mechanics of Art Materials and its Future in Heritage Science.* s.l.:Smithsonian Contributions to Museum Conservation, pp. 13-20.
- Anglos, D., Couris, S. & Fotakis, C., 1997. Laser Diagnostics of Painted Artworks: Laser-Induced Breakdown Spectroscopy in Pigment Identification. *Applied Spectroscopy*, 51(7), pp. 1025-1030.
- Anglos, D., Georgiou, S. & Fotakis, C., 2009. Lasers in the Analysis of Cultural Heritage Materials. *Journal of Nano Research*, Volume 8, pp. 47-60.
- Anglos, D. et al., 1996. Laser-Induced Fluorescence in Artwork Diagnostics: An Application in Pigment Analysis. *Applied Spectroscopy*, 50(10), pp. 1331-1334.
- Anon., 1993. *New Testament, Today's New International Version.* s.l.:Harper Torch.
- Antonopoulou-Athera, N. et al., 2017. *Investigation of laser cleaning procedures for the restoration of burnt paintings.* Sozopol, Bulgaria, Proc. SPIE 10226, 19th International Conference and School on Quantum Electronics: Laser Physics and Applications.
- Artioli, G., 2010. *Scientific Methods and Cultural Heritage.* New York: Oxford University Press .
- Artioli, G., 2017. X-Ray Diffraction, Studies of Inorganic Compounds and Minerals. In: J. Lindon, G. Tranter & D. Koppenaal, eds. *Encyclopedia of Spectroscopy and Spectrometry.* San Diego: Academic Press, pp. 676-683.
- Atanassova, V. et al., 2014. Laser-Induced Fluorescence Spectroscopy – a Contemporary Approach to Cultural Heritage. *Advances in Bulgarian Science*, pp. 5-10.
- Bardelli, F. et al., 2011. Combined non-destructive XRF and SR-XAS study of archaeological artefacts. *Analytical and Bioanalytical Chemistry*, Volume 399, pp. 3147-3153.

- Bastidas, D. M. & Cano, E., 2018. *Advanced Characterization Techniques, Diagnostic Tools and Evaluation Methods in Heritage Science.* s.l.:Springer.
- Beck, L., Jeynes, C. & Barradas, N. P., 2008. Characterization of paint layers by simultaneous self-consistent fitting of RBS/PIXE spectra using simulated annealing. *Nuclear Instruments and Methods in Physics Research B*, Volume 266, pp. 1871-1874.
- Berrie, B. H. & Thoury, M., 2019. Examination of Luminescence of Cross Sections (Fluorescence Microscopy). In: *UV-Vis Luminescence Imaging Techniques.* Valencia : Editorial Universitat Politècnica de València, pp. 119-138.
- Bouvier, M. J. B., 1848. *A Treatise on Indulgences.* London: James Burns.
- Brandon, D. & Kaplan, W. D., 2008. *Microstructural Characterization of Materials.* 2 ed. Chichester: John Wiley & Sons Ltd.
- Britannica, T. E. o. E., 2019. *Industrial Revolution,* s.l.: s.n.
- Brown, B., 2003. Stations of the Cross. In: *The New Catholic Encyclopedia.* Second Edition ed. Washington, D.C.: Gale, pp. 499-501.
- Brunetti, B. et al., 2017. Non-invasive Investigations of Paintings by Portable Instrumentation: The MOLAB Experience. In: R. Mazzeo, ed. *Analytical Chemistry for Cultural Heritage.* Cham: Springer, pp. 41-75.
- Burgio, L. & Clark, R., 2001. Library of FT-Raman spectra of pigments, minerals, pigment media and varnishes, and supplement to existing library of Raman spectra of pigments with visible excitation.. *Spectrochimica Acta Part A,* Volume 57, pp. 1491-1521.
- Burgio, L. et al., 2000. Pigment Identi® cation in Painted Artworks: A Dual Analytical Approach Employing Laser-Induced Breakdown Spectroscopy and Raman Microscopy. *Applied Spectroscopy*, 54(4), pp. 463-469.
- Calligaro, T., Gonzalez, V. & Pichon, L., 2015. PIXE analysis of historical paintings: Is the gain worth the risk?. *Nuclear Instruments and Methods in Physics Research B*, Volume 363, pp. 135-143.
- Calvo Del Castillo, H. & Strivay, D., 2012. X-Ray Methods. In: H. Edwards & P. Vandenabeele, eds. *Analytical Archaeometry Selected Topics.* Cambridge: The Royal Society of Chemistry Publishing, pp. 59-113.

- Carlyle, L., 1990. British nineteenth-century oil painting instruction books: A survey of their recommendations for vehicles, varnishes and methods of paint application. *Studies in Conservation*, 35(1), pp. 76-80.
- Carlyle, L., 1993. Authenticity and adulteration: what materials were 19th century artists really using?. *The conservator*, 17(1), pp. 56-60.
- Carlyle, L., 1999. Paint Driers Discussed in 19th-Century British Oil Painting Manuals. *Journal of the American Institute for Conservation*, 38(1), pp. 69-82.
- Casadio, F., Daher, C. & Bellot-Gurlet, L., 2017. Raman Spectroscopy of cultural heritage Materials: Overview of Applications and New Frontiers in Instrumentation, Sampling Modalities, and Data Processing. In: R. Mazzeo, ed. *Analytical Chemistry for Cultural Heritage.* Cham: Springer, pp. 161-211.
- Casoli, A., Mirti, P. & Palla, G., 1995. Characterization of medieval proteinaceous painting media using gas chromatography and gas chromatography-mass spectrometry. *Fresenius' Journal of Analytical Chemistry*, Volume 352, pp. 372-379.
- Cheilakou, E., kastronaki, M., Koui, M. & Callet, P., 2009. A nondestructive study of the identification of pigments on monuments by colorimetry. *International Journal of Microstructure and Materials Properties*, 4(1), pp. 112-127.
- Cheilakou, E., Troullinos, M. & Koui, M., 2014. Identification of pigments on Byzantine wall paintings from Crete (14th century AD) using non-invasive Fiber Optics Diffuse Reflectance Spectroscopy (FORS). *Journal of Archaeological Science*, Volume 41, pp. 541-555.
- Church, A. H., 1890. *The Chemistry of Paint and Paintings.* London: Seeley and Co. Limited.
- Colombini, M. P. & Modungo, F., 2009. Organic Materials in Art and Archaeology. In: *Organic Mass Spectrometry in Art and Archaeology.* Pisa: John Wiley & Sons, pp. 1-36.
- Cosentino, A., 2014. FORS spectral database of historical pigments in different binders. *e-conservation journal*, Volume 2, pp. 54-65.

- Cotte, M., Genty-Vincent, A., Janssens, K. & Susini, J., 2018. Applications of synchrotron X-ray nano-probes in the field ofcultural heritage. *Comptes Rendus Physique*, Volume 19, pp. 575-588.
- Daffara, C. & Fontana, R., 2011. Multispectral Infrared Reflectography to Differentiate Features in Paintings. *Microscopy And Microanalysis*, Volume 17, pp. 691-695.
- Delaney, J. K. et al., 2016. Visible and infrared imaging spectroscopy of paintings and improved reflectography. *Heritage Science*, 4(6).
- Delaney, J. K. et al., 2010. Visible and Infrared Imaging Spectroscopy of Picasso's Harlequin Musician: Mapping and Identification of Artist Materials in Situ. *Applied Spectroscopy*, 64(6), pp. 584-594.
- Domenech-Carbo, A., Domenech-Carbo, M. T. & Costa, V., 2009. *Electrochemical Methods in Archaeometry, Conservation and Restoration.* Heidelberg: Springer.
- Donais, M. K. & George, D. B., 2018. *X-Ray Fluorescence Spectrometry and its Applications to Archaeology.* New York: Momentum Press®, LLC.
- Dupuis, G. & Menu, M., 2005. Quantitative evaluation of pigment particles in organic layers by fibre-optics diffuse-reflectance spectroscopy. *Applied Physics A*, Volume 80, pp. 667-673.
- Eastaugh, N., Nadolny, J. & Lowengard, S., 2012. Pigments in western easel paintings. In: *The conservation of easel paintings.* Oxon: Routledge, pp. 189-207.
- Eastaugh, N. & Walsh, V., 2012. Optical microscopy. In: *The Conservation of Easel Paintings.* Oxon: Routledge, pp. 306-317.
- Eastaugh, N., Walsh, V., Chaplin, T. & Siddall, R., 2004. *The Pigment Compendium A Dictionary of Historical Pigments.* Oxford: Elsevier Butterworth-Heinemann.
- Eastaugh, N., Walsh, V., Chaplin, T. & Siddall, R., 2004. *The Pigment Compendium A Dictionary of Historical Pigments.* Oxford: Elsevier Butterworth-Heinemann.
- Edwards, H. G. M. & Vandenabeele, P., 2012. Vibrational Spectroscopy: Theoretical Basis Relevant to Archaeometry and Archaeological Applications. In: H. Edwards & P. Vandenabeele, eds. *Analytical*

Archaeometry Selected Topics. Cambridge: The Royal Society of Chemistry, pp. 49-58.

- Elias, M., Mas, N. & Cotte, P., 2011. Review of several optical non-destructive analyses of an easel painting. Complementarity and crosschecking of the results. *Journal of Cultural Heritage*, Volume 12, pp. 335-345.
- Fantoni, R. et al., 2013. Laser-induced fluorescence study of medieval frescoes by Giusto de' Menabuoi. *Journal of Cultural Heritage*, 14(3), pp. S59-S65.
- Faries, M., 2005. Analytical Capabilities of Infrared Reflectography: An Art Historian's Perspective. In: *Scientific Examination of Art: Modern Techniques in Conervation and Analysis.* Washington D.C.: The National Academic Press, pp. 87-104.
- Fischer, C. & Kakouli, I., 2006. Multispectral and hyperspectral imaging technologies in conservation: current research and potential applications. *Review in Conservation*, 51(1), pp. 3-16.
- Forth-Photonics, n.d. *MuSIS MS Operation Manual.* Athens: s.n.
- Fotakis, C. et al., 2007. *Lasers in the Preservation of Cultural Heritage Principles and Applications.* Florida: Taylor & Francis Group.
- Gavrilov, D., Maev, R. G. & Almond D. P. , 2014. A review of imaging methods in analysis of works of art: Thermographic imaging method in art analysis. *Canadian Journal Of Physics*, Volume 92, pp. 341-364.
- Genestar, C. & Pons, C., 2005. Earth pigments in painting: characterisation and differentiation by means of FTIR spectroscopy and SEM-EDS microanalysis. *Analytical and Bioanalytical Chemistry*, Volume 382, pp. 269-274.
- Gigante, G. E. & Ridolfi, S., 2013. X-Ray Techniques and X-Ray Fluorescence with Portable Systems. In: *Conservation Science for the Cultural Heritage Applications of Instrumental Analysis.* Heidelberg: Springer, pp. 92-105.
- Gillman, J., 2011. *Stations of the Cross.* [Online] Available at:

https://onlinelibrary.wiley.com/doi/10.1002/9780470670606.wbecc1314 [Accessed 20 October 2019].

- Glascock, M. D., 2011. Comparison and Contrast Between XRF and NAA: Used for Characterization Of Obsidian Sources in Central Mexico. In: *X-Ray Fluorescence Spectrometry (XRF) in Geoarchaeology.* New York: Springer, pp. 161-192.
- Goffer, Z., 2007. *Archaeological Chemistry.* 2nd Edition ed. New Jersey: John Wiey & Sons.
- Groen, C. M., 2011. *Paintings in the laboratory: scientific examination for art history and conservation.,* s.l.: s.n.
- Grygar, T. et al., 2003. Analysis of earthy pigments in grounds of Baroque paintings. *Analytical and Bioanalytical Chemistry*, Issue 375, pp. 1154-1160.
- Gulmini, M. et al., 2013. Identification of dyestuffs in historical textiles: Strong and weak points of a non-invasive approach. *Dyes and Pigments*, Volume 98, pp. 136-145.
- Hassell, C., 2005. Paintings. In: *Radiography of Cultural Material.* Oxford: Elsevier Butterworth-Heinemann, pp. 112-.
- Hazzikostas, D., 1998. Grieving/Lamentation. In: *Encyclopedia of Comparative Iconography.* Chicago: Fitzroy Dearborn Publishers, pp. 363-372.
- Hermens, E. & Townsend, J., 2012. Binding media. In: *The conservation of easel paintings.* Oxon: Routledge, pp. 207-213.
- Hiller, H., 1945. *The painter's pocket book of methods and materials.* Los Angeles: Research Publishing Company.
- Inkson, B. J., 2016. Scanning electron microscopy (SEM) and transmission electron microscopy (TEM) for materials characterization. In: *Materials Characterization Using Nondestructive Evaluation (NDE) Methods.* Duxford : Elsevier, pp. 17-43.
- Ioakimoglou, E. E., 2004. *Τα οργανικά Υλικά στη Τέχνη και την Αρχαιολογία (Organic Materials in Art and Archaeology).* Athens: ION.
- Iwanicka, M., Sylwestrzak, M. & Targowski, P., 2018. Optical Coherence Tomography (OCT) for Examination of Artworks. In: *Advanced*

Characterization Techniques, Diagnostic Tools and Evaluation Methods in Heritage Science. Cham: Springer, pp. 49-59.

- Janssens , K., Dik, J., Cotte, M. & Susini, J., 2010. Photon-Based Techniques for Nondestructive Subsurface Analysis of Painted Cultural Heritage Artifacts. *Accounts of Chemical Research*, 43(6), pp. 814-825.
- Janssens, K., 2013. *Modern Methods for Analysing Archaeological and Historical Glass.* Chichester: John Wiley & Sons, Ltd.
- Janssens, K. et al., 2013. The Use of Synchrotron Radiation for the Characterization of Artists' Pigments and Paintings. *The Annual Review of Analytical Chemistry*, Volume 6, pp. 399-425.
- Janssens, K. et al., 2016. Non-Invasive and Non-Destructive Examination of Artistic Pigments, Paints, and Paintings by Means of X-Ray Methods. In: *Analytical Chemistry for Cultural Heritage.* Cham: Springer, pp. 77-128.
- Janssens, K. & van Grieken, R., 2004. *Non-Destructive Microanalysis of Cultural Heritage Materials.* Amsterdam: Elvesier.
- Jutras, M., 2017. *Way of the Cross.* [Online] Available at: http://www.newadvent.org/cathen/15569a.htm [Accessed 1 10 2019].
- Kantarelou, V. et al., 2011. X-ray Fluorescence analytical criteria to assess the fineness of ancient silver coins: Application on Ptolemaic coinage. *Spectrochimica Acta Part B*, Volume 66, pp. 681-690.
- kantarelou, V. et al., 2015. In situ scanning micro-XRF analyses of gilded bronze figurines at the National Museum of Damascus. *Journal of Analytical Atomic Spectrometry*, Volume 30, pp. 1787-1798.
- Karydas , A. G. et al., 2005. Importance of in-situ EDXRF Measurements in the Preservation and Conservation of Material Culture. In: *X-rays for Archaeology.* Dordrecht: Springer, pp. 27-53.
- Karydas , A. G., Padilla-Alvarez, R., Drozdenko, M. & Moreno Guzman, M., 2014. Handheld XRF analysis of the old Mexican feather headdress in the Weltmuseum Vienna. *X-Ray Spectrometry*, Volume 43, pp. 138-145.
- Karydas, A. G., 2007. Appication of a Portable XRF Spectrometer for the Non-Invasive Analysis of Museum Metal Artefacts. *Annali di Chimica*, Volume 97, pp. 419-432.

- Koch, R., 1955. *The Book of Signs.* New York: Dover Publications.
- Kokiasmenou, E., 2018. *Portable XRF analysis and MA-XRF Imaging of Mycenaean Wall-Painting Pigments from the Palace of Nestor at Pylos,* Thessaloniki: s.n.
- Kouloumpi, E., 2007. *Western-European Influences on the Post-Byzantine icon Painting Technique of Crete & the Islands of Ionion,* Leicester: s.n.
- Kouloumpi, E., Moutsatsou, A. P. & Terlixi , A.-V., 2012. Canvas and Panel Paintings: Techniques and Analyses. In: *Analytical Archaeometry Selected Topics.* s.l.:The Royal Society of Chemistry Publishing, pp. 361-398.
- Kouloumpi, E., Moutsatsou, A. P. & Terlixi, A.-V., 2012. Canvas and the Panel Paintings: Techniques and Analyses. In: H. Edwards & P. Vandenabeele, eds. *Analytical Archaeometry Selected Topics.* Cambridge: The Royal Society of Chemistry Publishing, pp. 361-398.
- Kouloumpi, E. et al., 2007. Analysis of post-Byzantine icons from the Church of the Assumption in Cephalonia, Ionian Islands, Greece: A multi-method approach. *Analytica Chimica Acta*, Volume 598, pp. 169-179.
- Kozaris, I. A., 2013. Imagine Techniques. In: *Conservation Science for the Cultural Heritage Applications of Instrumental Analysis.* Heidelberg : Springer, pp. 38-47.
- Kubic, M., 2007. Hyperspectral Imaging: A New Technique for the Non-Invasive Study of Artworks. In: *Physical Techniques in the Study of Art, Archaeology and Cultural Heritage.* Amsterdam: Elvesier, pp. 199-259.
- Kushel, D. A., 1985. Applications of transmitted infrared radiation to the examination of artifacts. *Studies in Conservation*, 30(1), pp. 1-10.
- Kvick, A., 2017. X-Ray Diffraction, Materials Science Applications. In: J. Lindon, G. Tranter & D. Koppenaal, eds. *Encyclopedia of Spectroscopy and Spectrometry.* San Diego: Academic Press, pp. 648-655.
- Lahanier, C., 1991. Scientific Methods Applied to the Study of Art Objects. *Mikrochimica Acta*, Issue 2, pp. 245-254.
- Larkin, P., 2011. *Infrared and Raman Spectroscopy Principles and Spectral Interpretation.* Waltham: Elvesier.
- Laurie, A. P., 1926. *The Painter's Methods & Materials.* London: Seeley, Service & Co. .

- Laver, J., 1969. *The Concise History of Costume and Fashion.* New York: Harry N. Abrams, INC.
- Leng, Y., 2008. *Materials Characterization introduction to Microscopic and Spectroscopic Methods.* Singapore: JohnWiley & Sons (Asia) Pte Ltd.
- Lepage, J. D., 2005. *Medieval Armies and Weapons in Western Europe an illustrated history.* North Carolina: McFarland &. Company, Inc., Publishers.
- Lepage, J. D., 2005. *Medieval Armies and Weapons in Western Europe, An Illustrated History.* Carolina: McFarland & Company.
- Liang, H., 2012. Advances in Multispectral and Hyperspectral Imaging for Archaeology and Art Conservation. *Applied Physics A*, Volume 106, pp. 309-323.
- Liritzis, I. & Zacharias, N., 2011. Portable XRF of Archaeological Artifacts: Current Research, Potentials and Limitations. In: *X-Ray Fluorescence Spectrometry (XRF) in Geoarchaeology.* New York: Springer, pp. 109-142.
- MacBeth, R., 2012. The technical examination and docomentation o easel paintings. In: *The Conservation of Easel Paintings.* Oxon: Routledge, pp. 291-305.
- Mairinger, F., 2000. The ultraviolet and fluorescence study of paintings and manuscripts. In: *Radiation in Art and Archeometry.* Amsterdam: Elvesier, pp. 56-75.
- Mairinger, F., 2004. UV-, IR- and X-ray imaging. In: *Non-Destructive Microanalysis of Cultural Heritage Materials.* Amsterdam: Elvesier, pp. 15-71.
- Martin-Ramos, J. D., Zafra-Gómez, A. & Vílchez, J. L., 2017. Non-destructive pigment characterization in the painting Little Madonna of Foligno by X-ray Powder Diffraction. *Microchemical Journal*, Volume 134, pp. 343-353.
- Mastrotheodoros, G. P., 2016. *Χρωστικές Κονίες και άλλα Υλικά Μεταβυζαντινής Ζωγραφικής (Pigments and Various Materials of Post - Byzantine Painting),* Ioannina: s.n.
- Mayer, L. & Myers, G., 1993. Understanding the Techniques of American Tonalist and Impressionist Painters. *Journal of the American Institute for Conservation,* 32(2), pp. 129-139.

- Mayer, R., 1970. *The Artist's Handbok of Materials and techniques.* 3rd ed. New York: The Viking Press.
- Mills, J. S. & White, R., 1987. *The Organic Chemistry of Museum Objects.* London: Butterworths.
- Moura, C. C., Tare, R., Oreffo, R. & Mahajan, S., 2016. Raman spectroscopy and coherent antiStokes Raman scattering imaging:. *Journal of the Royal Society Interface*, Volume 13, p. 20160182.
- Nadolny, J., 2003. The first century of published scientific analyses of the materials of historical painting and polychromy, circa 1780-1880. *Reviews in Conservation*, Issue 4, pp. 39-51.
- Nadolny, J., 2012. A history of early scientific examination and analysis of painting materials ca. 1780 to the mid-twentieth century. In: *The Conservation of Easel Paintngs.* Oxon: Rutledge, pp. 336-340.
- National Gallery of Victoria, n.d. *Artists' Colourmen.* [Online] Available at: https://www.ngv.vic.gov.au/explore/collection/conservation/colourmen/ [Accessed 03 05 2020].
- Nevin, A., Spoto, G. & Anglos, D., 2012. Laser spectroscopies for elemental and molecular analysis in art and archaeology. *Appied Physics A*, Volume 106, pp. 339-361.
- O'Neill, J. P., 1986. *Gothic and Renaissance Art in Nuremberg 1300-1550.* New York: The Metropolitan Museum of Art.
- Ormsby, B. & Gottsegen, M., 2012. Grounds in the twentieth century and beyond. In: *The conservation of easel paintings.* Oxon: Routledge, pp. 185-188.
- Pavlidou, E., 2013. The Role of Microscopy Techniques in the Study of Cultural Heritage Materials. In: *Conservation Science for the Cultural Heritage Applications of Instrumental Analysis.* Heidelberg: Springer, pp. 47-65.
- Phenix, A. & Townsend, J., 2012. A brief survey of historical varnishes. In: *The Conservation of Easel Paintings.* Oxon: Routledge, pp. 252-263.
- Picollo, M., Fukunaga, K. & Labaune, J., 2015. Obtaining noninvasive stratigraphic details of panel paintings using terahertz time domain

spectroscopy imaging system. *Journal of Cultural Heritage*, 16(1), pp. 73-80.

- Polland, A. M. & Heron, C., 2008. *Archaeological Chemistry.* Cambridge: The Royal Society of Chemistry.
- Prati, S., Sciutto, G. & Mazzeo, R., 2017. New Frontiers in Application of FTIR Microscopy for Characterization of Cultural Heritage Materials. In: R. Mazzeo, ed. *Analytical Chemistry for Cultural Heritage.* Cham: Springer, pp. 129-160.
- Rai, P. & Dubey, S. K., 2018. Raman Spectroscopy: A Potential Characterization Tool for Carbon Materials. In: S. K. Sharma, et al. eds. *Handbook of Materials Characterization.* Cham: Springer, pp. 405-434.
- Richards, J., 2002. *Landsknechts Soldier 1486-1560.* Oxford: Osprey Publishing.
- Roy, A., 1993. *Artists´ Pigments A Handbook of Their History and Characteristics VOLUME 2.* Washington: National Gallery of Art.
- Salzer, R., 2013. Infrared and Raman Spectroscopy. In: *Conservation Science for the Cultural Heritage Applications of Instrumental Analysis.* Heidelberg: Springer, pp. 65-79.
- Saverwyns, S. & Vanden Berghe, I., 2012. Separation Techniques in Archaeometry. In: H. Edwards & P. Vandenabeele, eds. *Analytical Archaeometry Selected Topics.* Cambridge: The Royal Society of Chemistry, pp. 132-162.
- Schlotz, R. & Uhlig, S., 2000. *Introduction to X-ray Fluorescence (XRF).* Karlruhe: Bruker AXS GmbH.
- Schneider, M., 1990. Microanalysis for the study of materials and objects of art and archaeology. *Fresenius Journal of Analytical Chemistry*, Volume 337, pp. 715-720.
- Sciutto, G. et al., 2018. From macro to micro: An advanced macro X-ray fluorescence (MA-XRF) imaging approach for the study of painted surfaces. *Microchemical Journal*, Volume 137, pp. 277-284.
- Shackley, M. S., 2011. An Introduction to X-Ray Fluorescence (XRF) Analysis in Archaeology. In: *X-Ray Fluorescence Spectrometry (XRF) in Geoarchaeology.* New York: Springer, pp. 7-44.

- Shefer, E., 1998. Death. In: *Encyclopedia of Comparative Iconography.* Chicago: Fitzroy Dearborn Publishers, pp. 221-233.
- Siozos, P., Phillippidis, A. & Anglos, D., 2017. Portable laser-induced breakdown spectroscopy/diffuse reflectance hybrid spectrometer for analysis of inorganic pigments. *Spectrochimica Acta Part B*, Volume 137, pp. 93-100.
- Smith , G. D. & Clark, R. J. H., 2001. Raman microscopy in art history and conservation science. *Reviews in Conservation*, Volume 2, pp. 92-106.
- Smith, G. D. & Clark, R. J. H., 2004. Raman Microscopy in Archaeological Science. *Journal of Archaeological Science*, Volume 31, pp. 1137-1160.
- Sokaras, D. et al., 2009. Combined elemental analysis of ancient glass beads by means of ion beam, portable XRF, and EPMA techniques. *Analytical and Bioanalytical Chemistry*, Volume 395, pp. 2199-2209.
- Sole, V. A. et al., 2007. A multiplatform code for the analysis of energy-dispersive X-ray fluorescence spectra. *Spectrochimica Acta Part B*, Volume 62, pp. 63-68.
- Speed, H., 1873. *Oil Painting Techniques and Materials.* New York: Dover Publications.
- Spizzichino, V., Bertani, L., Caneve, L. & Caso, M. F., 2020. Rapid analysis of marble treatments by laser induced fluorescence. *Optical and Quantum Electronics*, 52(117).
- Stols-Witlox, M., 2012. Grounds, 1400-1900. In: *The conservation of easel paintings.* Oxon: Routledge, pp. 161-185.
- Stols-Witlox, M., 2012. Grounds, 1400-1900. In: *The Conservation of Easel Paintings.* Oxon: Routledge, pp. 161-185.
- Stols-Witlox, M., 2015. ‘By no means a trivial matter’. The influence of the colour of ground layers on artists' working methods and on the appearence of oil paintings, according to historical recipes from North West Europe, c. 1550-1900. *Oud Holland*, 4(128), pp. 171-186.
- Stuart, B. H., 2007. *Analytical Techniques in Materials Conservation.* s.l.:John Wiley & Sons Ltd.
- Swicklik, M., 1993. French Painting and the Use of Varnish, 1750-1900. *Studies in the History of Art,* Volume 41, pp. 156-174.

- Taft, S. W. & Mayer, J. W., 2000. *The Science of Paintings.* New York: Springer.
- Tambroni, S., 1821. *A treatise on painting written by Cennino Cennini.* London: Edward Lumley.
- Telle, H. H. & Ureña, A. G., 2018. *Laser Spectroscopy and Laser Imaging An Introduction.* Boca Raton: CRC Press.
- Terlixi, A. V. et al., 2010. *Diagnostic and analytical investigation of the famous painting of Iakovos Rizos: "The Athenian Night".* Thessaloniki, Proceeding of the International Symposium "Works of art and Conservation Science today".
- The Editors of Encyclopaedia Britannica, 2018. *Stations of the Cross.* [Online]
  Available at: https://www.britannica.com/topic/Stations-of-the-Cross [Accessed 01 10 2019].
- Thurston, H., 1914. *The Stations of the Cross - An Account of their History and Devotional Purpose.* London: Burns & Oates.
- Torrent, J. & Barron, V., 2002. Diffuse Reflectance Spectroscopy of Iron Oxides. In: M. Dekker, ed. *Encyclopedia of Surface and Colloid Science.* s.l.:s.n., pp. 1438-1446.
- Townsend, J. & Boon, J., 2012. Research and instrumental analysis in the materials of easel paintings. In: *The Conservation of Easel Paintings.* Oxon: Routledge, pp. 341-365.
- Townsend, J. H., 1994. The materials and techniques of J. M. W. Turner: primings and supports. *Studies in Conservation*, 3(39), pp. 145-153.
- Tserevelakis, G. J. et al., 2019. Non-invasive photoacoustic detection of hidden underdrawings in paintings using air-coupled transducers. *Ultrasonics*, Volume 98, pp. 94-98.
- Tserevelakis, G. J. et al., 2017. Photoacoustic imaging reveals hidden underdrawings in paintings. *Scientific Reports*, 07 April, 7(1), pp. 1-11.
- Van der Goltz, M. et al., 2012. Varnishing as Part of the Conservation Treatment of Easel Paintings. In: *Conservation of Easel Paintings.* Oxon: Routledge, pp. 635-658.

- Vandenabeele, P., 2013. *Practical Raman Spectroscopy - An Introduction.* Chichester: John Wiley & Sons, Ltd.
- Vandenabeele, P., Edwards, H. G. M. & Moens, L., 2007. A Decade of Raman Spectroscopy in Art and Archaeology. *Chemical Reviews*, 107(3), pp. 678-686.
- Vandenabeele, P. et al., 2019. Pigments and Colourants. In: P. Vandenabeele & H. Edwards, eds. *Raman Spectroscopy in Archaeology and Art History.* Croydon: The Royal Society of Chemistry, pp. 61-67.
- Vanderlip de Carbonnel, K., 1981. A Study of French Painting Canvases. *Journal of the American Institute for Conservation*, 20(1), pp. 3-20.
- Vanmeert, F. et al., 2019. Transmission and Reflection Mode Macroscopic X-ray Powder Diffraction Imaging for the Noninvasive Visualization of Paint Degradation in Still Life Paintings by Jan Davidsz. de Heem. *Analytical Chemistry*, Volume 91, pp. 7153-7161.
- Varella, E. A., 2013. General Considerations. In: *Conservation Science for the Cultural Heritage.* Thessaloniki: Springer, pp. 1-14.
- Vieillescazes, C., Sierra, I. & Morante-Zarcero, S., 2013. Separation Techniques. In: E. Varella, ed. *Conservation Science for the Cultural Heritage.* Heidelberg: Springer, pp. 15-25.
- West FitzHugh, E., 1997. *Artists´ Pigments A Handbook of Their History and Characteristics VOLUME 3.* Washington: National Gallery of Art.
- Westlake, P. et al., 2012. Studying pigments on painted plaster in Minoan, Roman and Early Byzantine Crete. A multi-analytical technique approach. *Analytical and Bioanalytical Chemistry*, Volume 402, pp. 1413-1432.
- Wolbers, R. C., Buck, S. L. & Olley , P., 2013. Cross-section microscopy analysis and fluorescent staining. In: *The Conservation of Easel Paintings.* Oxon: Routledge, pp. 326-335.
- Young, C., 2012. History of Fabric Supports. In: *The Conservation of Easel Paintings.* Oxon: Routledge, pp. 116-147.